HABILITATION À DIRIGER DES RECHERCHES

Rodrigo Prado Martins

HABILITATION À DIRIGER DES RECHERCHES

en Sciences de la vie et de la Santé

Année universitaire : 2020 / 2021

présentée et soutenue publiquement par :

Rodrigo PRADO MARTINS

le 17/12/2020

JURY :
(Par ordre alphabétique)

Prénom	NOM	Grade	Établissement d'exercice
- M. Marc	BLONDEL	Professeur des universités	UBO, Brest
- Mme. Isabelle	DIMIER-POISSON	Professeur des universités	Université de Tours
- M. Gilles	FOUCRAS	Professeur des universités	ENVT, Toulouse
- Mme. Sonia	LACROIX-LAMANDÉ	Chargée de Recherche, HDR	INRAE Centre Val de Loire
- Mme. Sabine	RIFFAULT	Directrice de Recherche	INRAE, Jouy-en-Josas

Remerciements

Je tiens tout d'abord à remercier les membres du jury pour leur présence, pour leur lecture attentive de ce mémoire ainsi que pour leur contribution à la suite de mon projet professionnel.

Je remercie tous les collègues de l'équipe IBIR pour leur accueil et leur gentillesse.

Je remercie aussi Franck Biet pour son soutien et son encouragement pour la poursuite de mon HDR et de ma carrière.

Je souhaite remercier particulièrement Florence Gilbert pour la révision de ce mémoire et surtout pour toujours venir à mon aide en cas de difficultés (scientifiques ou pas) et Patricia Cunha pour son excellence, sa motivation et sa patience ! (le Français à la brésilienne, les manips de 100 tubes… ce n'est pas rien).

Je remercie les collègues du service d'appui et des plateaux techniques pour leur assistance quotidienne.

A mes enseignants

Aos meus professores

Sommaire

1. Avant-propos

Devenir un scientifique pour lutter contre des maladies a été mon ambition depuis mes études secondaires. Dès ma première année à la Faculté de Médecine Vétérinaire en 2003, j'ai réalisé un stage au sein d'un laboratoire de microbiologie médicale. Cette expérience fut mon premier contact avec la recherche, la démarche scientifique et un laboratoire de recherche. En 2005 et 2006, j'ai obtenu une bourse du programme brésilien d'initiation scientifique du Conseil National de Développement Scientifique et Technologique (CNPq) pour mettre en place, avec l'aide d'enseignants-chercheurs de la faculté, des projets dans les domaines de la reproduction animale et de la microbiologie. Mon activité en tant qu'apprenti-chercheur a renforcé mon goût pour la science et ma préférence pour la recherche sur les différents aspects de la microbiologie et de l'immunologie. En 2007, j'ai obtenu une bourse du Programme Santander Universidades pour étudier à l'étranger. J'ai ainsi eu l'opportunité de m'inscrire à l'Université d'Évora au Portugal pour mon deuxième stage de fin d'études. J'ai alors été formé à la médecine des animaux de compagnie à l'Hôpital Vétérinaire Universitaire et, parallèlement, j'ai appris les techniques de clonage moléculaire dans un laboratoire du Département de Biologie. Pendant ce séjour à Évora, j'ai été en contact avec un milieu académique international et multiculturel qui a éveillé mon intérêt pour la formation postuniversitaire et la recherche en Europe.

En 2008, diplômé vétérinaire, j'ai posé ma candidature au programme de bourses de la Fundación Carolina (Espagne). J'ai ainsi intégré le master en santé animale de l'Université de Cordoue et je me suis intéressé à l'application des techniques d'imagerie et de biologie moléculaire pour étudier la réponse immunitaire aux infections. J'ai réalisé mon stage sous la direction du Pr. Juan José Garrido dans l'unité de recherche AGR231 du département de Génétique de l'Université de Cordoue. J'ai appris les techniques de fixation de tissus, les analyses histopathologiques, les extractions d'ADN et d'ARN et les analyses d'expression génique par PCR quantitative à partir d'échantillons de tissus provenant de porcs infectés par *Salmonella*. À la fin du master, j'ai reçu une bourse de doctorat du Ministère Espagnol de l'Éducation qui m'a permis de poursuivre mon doctorat dans la même équipe (2009-2013).

Mon projet de thèse de doctorat avait pour but d'étudier le rôle du tissu lymphoïde du tube digestif pendant les infections par *Salmonella enterica* serovar Typhimurium (*Salmonella* Typhimurium). Nous avons ainsi mis en place un modèle porcin de salmonellose pour décrypter la réponse tissulaire aux niveaux morphologique et moléculaire. Ma thèse a été l'occasion de nombreuses collaborations qui m'ont donné l'opportunité de réaliser des expériences au sein d'autres laboratoires en Espagne (équipe du Pr. Concha Gil, Département de Microbiologie II, Université Complutense de Madrid), aux Etats-Unis (équipe du Pr. James Graham, École de Médecine, Département de Microbiologie et Immunologie, Université de Louisville) et en Irlande (équipe du Pr. Jarlath Nally, École Vétérinaire, University College

Dublin). Cela m'a permis de développer mes compétences en langues étrangères et de me former aux différentes techniques de la protéomique et de la transcriptomique.

Mon doctorat a renforcé mon intérêt pour l'immunologie et j'ai fait le choix de poursuivre mes activités dans ce domaine de recherche sous la direction du Dr. Robin Fåhraeus (UMR 1162 - Inserm, Université Paris Descartes-Paris Diderot-Paris 13), en collaboration avec le Dr. Sébastien Apcher (UMR 1015 - Inserm, Institut Gustave Roussy, Université Paris-Sud). Ainsi, entre avril 2014 et décembre 2018, j'ai étudié les sources de peptides antigéniques pour la voie du CMH-I et d'autre part, j'ai travaillé sur les stratégies établies par le virus d'Epstein-Barr (EBV) pour entraver la production de ces peptides.

En 2019, j'ai intégré INRAE en tant que chargé de recherche au sein de l'UMR1282 ou Infectiologie et Santé Publique (ISP), dans l'équipe Infections Bactériennes et Immunité des Ruminants (IBIR). Dans le cadre de mes travaux, j'étudie les mécanismes de la réponse immunitaire à médiation cellulaire, dans le but de mettre en place des vaccins innovants pour les espèces de ruminants de rente. Je m'intéresse notamment au processus de présentation croisée d'antigènes bactériens, ainsi que l'activation et la polarisation des lymphocytes T chez le bovin. Un bilan de mon parcours est montré dans la **Figure 1**.

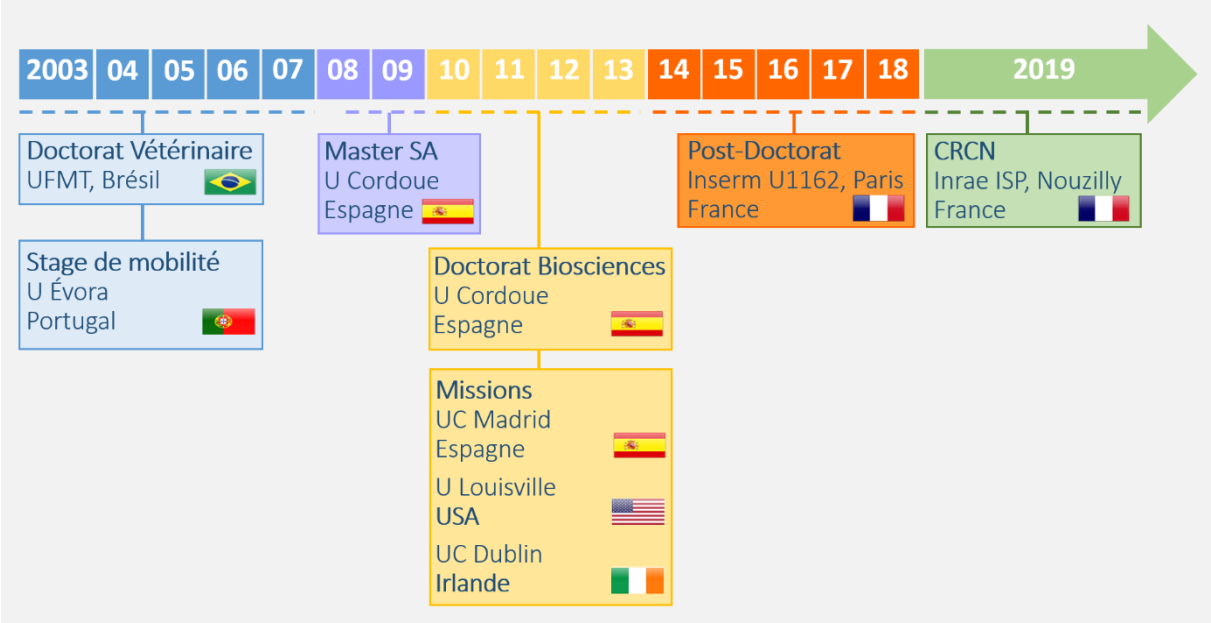

Figure 1 – Schéma décrivant mon parcours professionnel:

2. *Curriculum Vitae*

2.1 Etat civil

Nom de famille: Prado Martins **Prénom :** Rodrigo
Nationalité: Brésilienne **Date de naissance:** 01-05-1984
Téléphone: +33 782827058 **E-mail:** rodrigo.prado-martins@inrae.fr
Adresse: 85 rue Marcel Cachin 37700 St. Pierre des Corps, France

2.2 Education

2009-2013 **Doctorat en Biosciences.** Université de Cordoue (Espagne)

2008-2009 **Master en Santé Animale.** Université de Cordoue (Espagne)

2003-2008 **Doctorat Vétérinaire**. Universidade F. de Mato Grosso (Brésil, Espagne)

2.3 Expérience professionnelle

Depuis 01/2019 **Chargé de Recherche,** Institut national de recherche pour l'agriculture, l'alimentation et l'environnement - INRAE UMR Infectiologie et Santé Publique, Nouzilly (France).

04/2014-12/2018 **Chercheur post-doctorant,** Institut National de la Santé et de la Recherche Médicale - Inserm UMR 1162 – Equipe Robin Fahraeus, Institut de Génétique Moléculaire, Paris (France).

2009-2013 **Doctorant,** Département de Génétique, Université de Cordoue. Équipe AGR-231, Cordoue (Espagne). Bourse FPU du Ministère Espagnol de l'Éducation.

2008 **Enseignant,** Département d'Elevage Animal, Université Fédérale de Mato Grosso (Brésil)

10/2007-01/2008 **Stagiaire,** Médecine des animaux de compagnie. Hôpital Vétérinaire, Université d'Évora (Portugal)

04-08/2007 **Stagiaire,** Microbiologie, Immunologie et Biologie Moléculaire. Université d'État de Campinas (Brésil)

2005-2007 **Stagiaire d´initiation scientifique,** Département d'Elevage Animal, Université Fédérale de Mato Grosso (Brésil). Bourse du Conseil National de développement scientifique et technologique (CNPq).

2.4 Projets de recherche

14- UMR ISP, INRAE, Nouzilly (France). CelBoVax: Novel comprehensive approach to shape cattle cell-mediated immunity. Financement ANR Jeune Chercheuse Jeune Chercheur, France. 2020. **Coordinateur**, *sélectionné pour l'étape 2 d'évaluation*.

13- UMR ISP, INRAE, Nouzilly (France). Étude de la polarisation et plasticité des lymphocytes bovins. Département Santé Animale, INRAE, France. **Coordinateur**, depuis 01/2020.

12- UMR ISP, INRAE, Nouzilly (France). Présentation croisée d'antigènes : une nouvelle piste pour lutter contre les infections bactériennes persistantes – PagBac. UMR ISP, INRAE, France. **Co-coordinateur**, depuis 10/2019

11- UMR ISP, INRAE, Nouzilly (France). Caractérisations phénotypiques et fonctionnelles des cellules somatiques du lait impliquées dans la réponse des vaches laitières aux mammites – Masticells. APIS-GENE, France. Depuis 10/2019. **Animateur de *work package***

10- UMR ISP, INRAE, Nouzilly (France). Réduire le nombre d'animaux en recherche : Développement de modèles alternatifs ex-vivo - Animalt. Région Centre-Val de Loire APR-IA, France. Depuis 10/2019. **Animateur de *work package***

9- UMR1162, Inserm, Paris (France) : Identification de facteurs de la cellule hôte impliqués dans l'échappement immunitaire de l'oncovirus d'Epstein-Barr : caractérisation des mécanismes et exploitation comme cibles thérapeutiques. INCa_10683. Institut National du Cancer, France. Septembre 2016 – Décembre 2018.

8- UMR1162, Inserm, Paris (France) : Le rôle de l'exportation et de la maturation de l'ARN messager dans la production des produits pionniers de traduction (PTPs) dans la voie du CMH de classe I. ANR-12-BSV3-0016. Agence Nationale de la Recherche, France. Avril 2014 – Août 2016.

7- AGR231, UCO, Cordoue (Espagne) : COST action FA1020: Farm animals proteomics. European Cooperation in Science and Technology. (EU). 2011 – 2013.

6- AGR231, UCO, Cordoue (Espagne): Inmunogénomique appliquée à l'analyse moléculaire de la réponse intestinale aux infections chez le porc. Identification de gènes de résistance à la salmonellose. AGL2008-00400/GAN. Ministère Science et Technol., Espagne. 2012 – 2014.

5- AGR231, UCO, Cordoue (Espagne): EADGENE. Strengthening the implementation of durable integration of EADGENE KBBE.2010.4-0. European Union. 2011 – 2013.

4- AGR231, UCO, Cordoue (Espagne): Résistance génétique aux maladies chez les porcins. Analyse génomique de l'interaction hôte-pathogène et identification des gènes impliqués dans la réponse aux infections par *Salmonella*. AGL2008-00400/GAN. Ministère de la Science et Technologie, Espagne. 2009 – 2011.

3- AGR231, UCO, Cordoue (Espagne): SABRE. Genomics and epigenetics to develop sustainable animal breeding strategies for improved long/term product quality and safety (Integrated Project). FP6.2004-FOOD.3-016250-2. European Union. 2006 – 2010.

2- UFMT, Cuiabá-MT (Brésil): Étiologie de la mammite bovine dans la région Centre-Sud de MT. Conseil National de développement scientifique et technologique, Brésil. 2006 – 2007

1- UFMT, Cuiabá-MT (Brésil): Influence du stress thermique sur la fertilité de porcs élevés dans la région de Cuiabá-MT. Conseil National de développement scientifique et technologique, Brésil. 2005 – 2006

2.5 Activités d'enseignement

4- Vacataire. Licence de Sciences de la Vie. **Université de Versailles St-Quentin-en-Yvelines** - UFR de Sciences, Département de Biologie. Versailles, France.

2018/2019, Du gène à la protéine, L1, TP, 32h
2017/2018, Du gène à la protéine, L1, TP, 24h

3- Vacataire. Licence de Sciences de la Vie. **Université de Cergy-Pontoise** - UFR Sciences et Techniques, Département de Biologie. Cergy-Pontoise, France.

2017/2018, Structure et bases fonctionnelles des molécules du vivant, L1, TD, 19.5h

2- Vacataire. Diplôme de Docteur Vétérinaire. **Université de Cordoue** - Faculté de Vétérinaire, Département de Génétique. Cordoue, Espagne.

2011/2012, Nouvelles techniques en amélioration génétique des animaux, 4 et 5ème année, TD, 20h
2011/2012, Élevage et santé des animaux, 3ème année, TD, 20h
2011/2012, Amélioration génétique des animaux, 2ème année, TP, 25h
2010/2011, Génétique, 1ère et 2ème année, TP, 40h
2010/2011, Nouvelles techniques en amélioration génétique des animaux, 4 et 5ème année, TD, 10h
2009/2010, Génétique, 2ème année. TP, 25h

1- Remplaçant. Diplôme de Docteur Vétérinaire. **Université Fédérale de Mato Grosso** - Faculté d'Agronomie et Vétérinaire, Département de Sciences Fondamentales et Production animale. Cuiabá-MT, Brésil.

2008, Cytologie et histologie animale, 1ère année, CM, 60h
2008, Physiologie animale, 1ère année, CM, 40h
2008, Technologie des produits d'origine animale, 3ème année, CM, 20h

2.6 Formations

12- **École technique Ethologie et bien-être en expérimentation animale.** INRAE, France (2019)

11- **Réglementation relative à l'utilisation des animaux à des fins scientifiques**. Charles River, France (2018)

10- **Ethique et Bien-être des rongeurs.** Charles River, France (2018)

9- **Microscopie confocale et à haute résolution**. Institut Curie, France (2016)

8- **Expérimentation Animale - niveau concepteur de projet**. UPMC, France (2015)

7- **1st European Ingenuity Pathway Analysis Training.** Andaluzian Platform of Bioinformatics, Espagne (2013).

6- **Farm Animals proteomics**. Centre de Recherche Public - Gabriel Lippmann, Luxembourg (2011).

5- **Infection meets immunity**. University of Utrecht, Pays Bas (2011).

4- **Microarray Analysis**. Andaluzian Platform of Bioinformatics, Espagne (2010).

3- **Handling of Experimental Animals**. Animal Experimentation Facility. Université de Cordoue, Espagne (2009).

2- **How to analyse 2D gels**. Université de Cordoue, Espagne (2009).

1- **Food Microbiology**. University of Evora, Portugal (2008).

2.7 Missions

3- School of Veterinary Medicine, University College Dublin, **Irlande** (Octobre/2012). Competence en "Hydrophobic Antigen Tissue Triton Extraction (HATTREX)".

2- Department of Microbiology and Immunology, School of Medicine, University of Louisville, **États-Unis** (Février-Mars/2012). Compétence en "Selective Capture of Transcribed Sequences (SCOTS)".

1- Departamento de Microbiología II, Universidad Complutense de Madrid, **Espagne** (Mai-Juin/2010). Competence en "2D-DIGE and Mass Spectrometry".

2.8 Langues

Anglais: Lu, écrit, parlé.
Espagnol: Lu, écrit, parlé.
Français: Lu, écrit, parlé.
Portugais: Maternelle.

2.9 Prix

4- Outstanding doctoral thesis award *(Premio Extraordinario de Tesis Doctoral).* Université de Cordoue. Cordoue, 2015 (Espagne).

3- Premier de la promotion 2008 du Diplôme de Vétérinaire, Université Fédérale de Mato Grosso, Cuiabá (Brésil).

2 - Best oral presentation on Proteomics and Animal Health. 3rd Meeting of Working Groups 1, 2 & 3 of COST Action FA1002. Kosice, 2013 (Slovaquie).

1- Prêmio Prof. Dr. Vangi Pinto – Second prize for the Best oral presentation. I Jornada Científica do ENIPEC, FAMATO. Cuiabá, 2004 (Brésil)

.

3. Activité scientifique

3.1 Initiation scientifique et doctorat vétérinaire

Pendant mon premier stage, j'ai été formé au diagnostic des mammites et aux techniques de collecte et d'analyse microbiologique de lait, dans le but d'étudier les microorganismes responsables des cas de mammite bovine dans les fermes de la microrégion de Cuiabá-MT, Brésil. Les mammites représentent l'une des contraintes majeures pour le développement durable de l'industrie laitière. En plus de son impact sur la santé des animaux et sur l'économie de l'exploitation laitière, les mammites engendrent des retombées négatives importantes sur la santé publique et le bien-être animal [1].

En tant qu'apprenti-chercheur du programme brésilien d'initiation scientifique du Conseil National de Développement Scientifique et Technologique (*CNPq*), j'ai eu l'opportunité mettre en place une étude comprenant cinq fermes laitières bovines représentatives de la microrégion Centre-Sud de Cuiabá. Nous avons constaté que 5,8 et 65% des quartiers mammaires analysés étaient atteints de mammite clinique et subclinique, respectivement ([2], *ci-joint*). Nous avons aussi identifié les bactéries des genres *Staphylococcus* et *Corynebacterium* comme les principaux microorganismes responsables des mammites subcliniques et cliniques dans la microrégion étudiée (**Figure 2**).

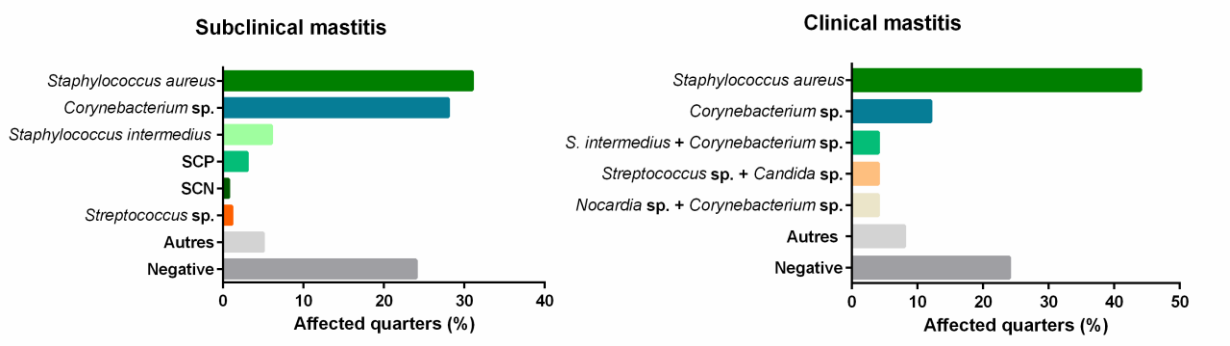

Figure 2 – Microorganismes isolés de cas de mammite subclinique et clinique chez la vache, dans la microrégion centre Sud de Cuiabá-MT, Brésil. Adapté de Martins et al. (2010) Ci. Anim. Bras. [2].

Ces résultats ont mis en évidence une prévalence élevée des mammites contagieuses, malgré le fait que les mesures de prévention des mammites, comme la désinfection des trayons par trempage après la traite, étaient adoptées sur la totalité des exploitations analysées. Cependant, une analyse plus approfondie de chaque exploitation nous a permis de constater des défauts d'hygiène pendant la traite ainsi qu'une mauvaise prise en charge des mammites cliniques. En collaboration avec mes enseignants et des vétérinaires praticiens, nous avons ensuite mis en place des stratégies de contrôle des mammites adaptées à chaque ferme. Ce projet m'a permis ainsi de développer des compétences en lien avec le terrain en intervenant auprès des éleveurs pour expliciter le bien fondé des mesures proposées.

Mon expérience en tant qu'apprenti-chercheur et stagiaire a donné naissance à deux articles de vulgarisation [3, 4] et sept articles scientifiques [2, 5-10], dont trois publiés dans des journaux internationaux [7-9].

3.2 Doctorat en Biosciences

Salmonella est la cause la plus fréquente des foyers épidémiques d'origine alimentaire dans l'UE. En 2018, 91.857 cas de salmonellose chez l'homme ont été rapportés par les États membres et entre plus de 2500 sérotypes, *S.* Typhimurium est le second le plus impliqué dans ces infections [11]. Chez le porc, les infections par *S.* Typhimurium entrainent une entérocolite localisée que souvent évolue vers un cadre de portage asymptomatique [12]. Cette particularité représente un risque pour la santé publique, étant donné que les infections par *S.* Typhimurium chez l'homme sont associées à la consommation de viande de porc et de volaille contaminée [11]. De plus, la salmonellose entraine des pertes économiques importantes pour la totalité de la filière porcine [13].

Suite à son ingestion et une fois dans la lumière de l'intestin grêle, *Salmonella* adhère et pénètre les cellules épithéliales pour ensuite coloniser la lamina propria et les plaques de Peyer. De l'intestin, *Salmonella* est sensée migrer vers les ganglions lymphatiques mésentériques régionaux par l'intermédiaire de phagocytes ou libre dans le milieu extracellulaire [14]. Il convient de noter que jusqu'aux années 2000, la plupart des informations concernant la physiopathologie de la salmonellose étaient issues d'observations chez la souris. Cependant, déjà à cette époque, il a été suggéré que les modèles murins n'étaient pas représentatifs des infections par *S.* Typhimurium chez l'homme et les animaux de rente [15, 16]. En effet, les souris infectées par *S.* Typhimurium développent une maladie systémique comparable à la fièvre typhoïde chez l'homme, très différente des entérocolites localisées.

Les similarités entre les systèmes immunitaires humain et porcin, ainsi que les manifestations cliniques communes de la salmonellose chez ces deux espèces suscitent l'intérêt du porc comme modèle biomédical pour cette maladie. L'étude de la salmonellose chez le porcin engendrerait donc des retombées significatives sur la santé animale et la rentabilité de la filière porcine, mais également pour la prise en charge de cette maladie chez l'homme.

Pendent ma thèse j'ai utilisé une infection expérimentale chez le porc pour étudier la réponse du tissu lymphoïde du tube digestif aux infections par *Salmonella enterica* serovar Typhimurium (*Salmonella* Typhimurium). Ce modèle a été combiné à différentes approches de génomique fonctionnelle afin de mieux comprendre les mécanismes et les interactions moléculaires mis en place dans les ganglions lymphatiques mésentériques et les plaques de Peyer (PP) suite à l'infection.

3.2.1 Analyse de ganglions lymphatiques mésentériques suite à l'infection par *Salmonella Typhimurium*

Dans la première étude de ma thèse ([17], ci-joint), j'ai analysé l'expression différentielle de gènes impliqués dans la réponse immunitaire, les altérations morphologiques et la charge bactérienne dans les ganglions à 1, 2 et 6 jours après l'infection (jpi). Nos résultats ont mis en évidence la présence de *Salmonella* dans ces organes, principalement à l'intérieur de cellules polynucléaires localisées dans la région médullaire, autour des trabécules (**Figure 3A**). Une analyse par PCR quantitative en temps réel a confirmé que *Salmonella* est déjà détectée dans les ganglions 1 jour après l'infection et que sa charge tissulaire culmine au 2ème jour après l'infection, avant de devenir indétectable au 6ème jour (**Figure 3B**).

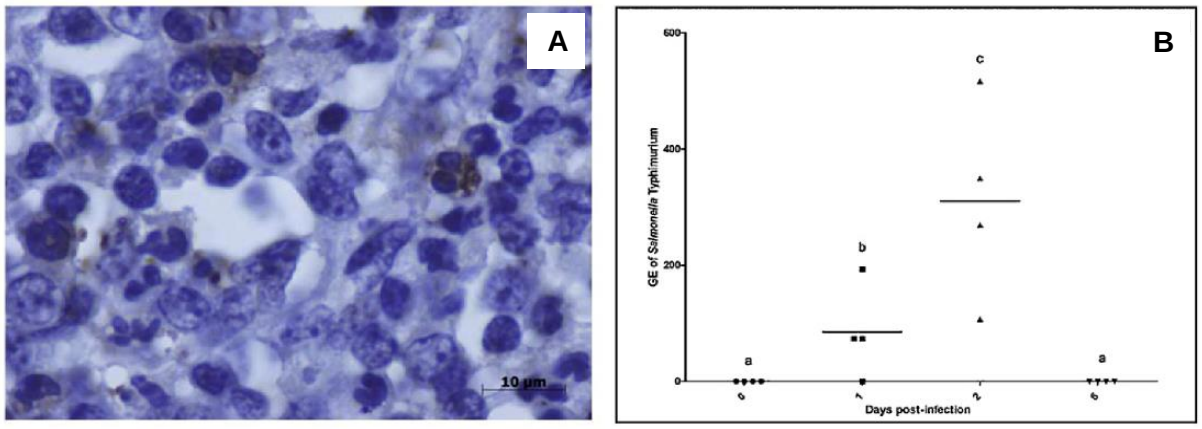

Figure 3 – Détection de *Salmonella* Typhimurium dans les ganglions lymphatiques mésentériques de porcs expérimentalement infectés. **A:** marquage de *Salmonella* par immunohistochimie. **B:** Quantification de la charge bactérienne par PCR en temps réel. Les résultats sont exprimés en équivalent-génome (GE) de *S.* Typhimurium. Des lettres différentes indiquent des différences significatives ($p<0.05$) entre les groupes. Adaptée de Martins et al. (2013) Comp Immunol Microbiol Infect Dis [17].

L'infiltration de neutrophiles et macrophages, principalement dans la région médullaire des ganglions, s'est avérée la modification histologique la plus remarquable suite à l'infection (**Figure 4A-B**). La présence de ces cellules a culminé au 2ème jour après l'infection, puis leur nombre a baissé pour atteindre un niveau comparable à celui observé dans le groupe contrôle (**Figure 4C-D**). La même tendance a été constatée pour l'expression de gènes codant pour différents médiateurs de la réponse pro-inflammatoire [17].

Ces résultats ont démontré que d'une façon similaire aux observations chez les modèles murins, *Salmonella* est capable d'atteindre, peu de temps après l'infection, les ganglions lymphatiques mésentériques porcins. Cependant, la présence du pathogène à l'intérieur de phagocytes polynucléaires ainsi que la réduction de la charge bactérienne suite à l'infiltration de phagocytes indiquerait que, en plus de leur rôle comme organes lymphoïdes secondaires, la réponse innée mise en place dans les ganglions mésentériques leur

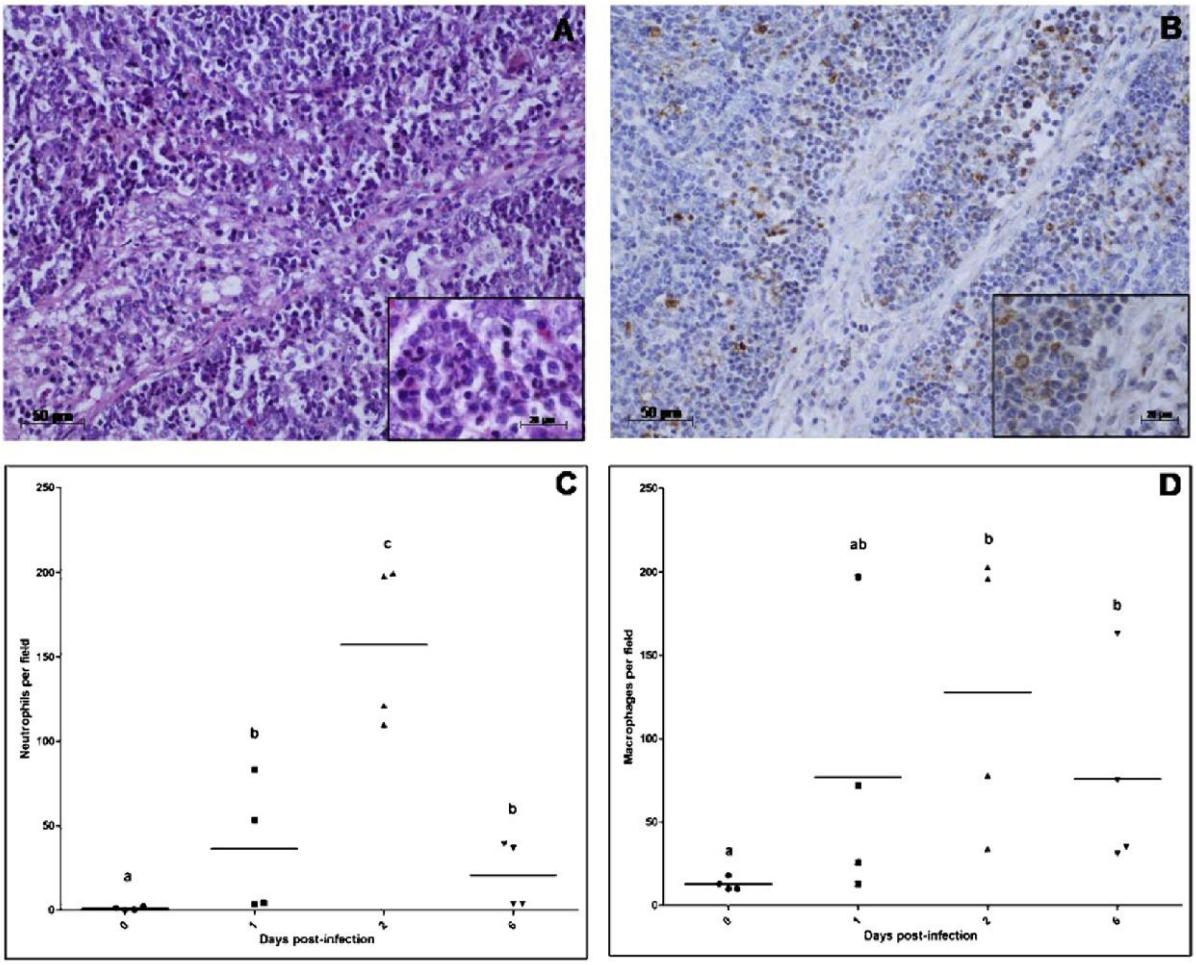

Figure 4 – Analyse histologique de ganglions lymphatiques de porcs infectés par *Salmonella* Typhimurium**. A :** Coloration HE montre l'infiltration de neutrophiles autour de trabécules. B : Marquage de macrophages par immunohistochimie avec l'anticorps 4E9/11. La présence de macrophages est démontrée dans la région médullaires des ganglions. C-D : Comptage de neutrophiles et macrophages dans les tissus. Des lettres différentes indiquent des différences significatives ($p<0.05$) entre les groupes. D'après Martins et al. (2013) Comp Immunol Microbiol Infect Dis [17].

permettrait d'agir comme une barrière à la dissémination systémique de *Salmonella* chez le porc. A la différence de l'infection systémique décrite chez la souris, les porcs infectés lors de cette expérience ont présenté une rémission complète des symptômes au 6ème jour.

Dans le but d'approfondir ces observations, nous avons mis en place une analyse de la réponse globale des ganglions par deux approches à haut débit. Lors de ma deuxième étude, j'ai utilisé la technologie 2D-DIGE (*two dimensional difference gel-electrophoresis*) pour étudier la réponse protéomique de ces organes à *Salmonella* Typhimurium ([18], ci-joint). L'interprétation des données protéomiques par des outils bioinformatiques a indiqué l'induction de processus comme la motilité cellulaire, la phagocytose et le remodelage du cytosquelette dans les tissus infectés, en cohérence avec les résultats de nos analyses histologiques. Curieusement, nos résultats ont montré une augmentation de la réponse anti-apoptotique, contrairement à l'induction d'apoptose décrite dans les modèles murins de salmonellose. J'ai

également observé la surexpression de protéines impliquées dans les différentes étapes de la présentation d'antigènes par le CMH de classe I (CMH-I) (**Figure 5**).

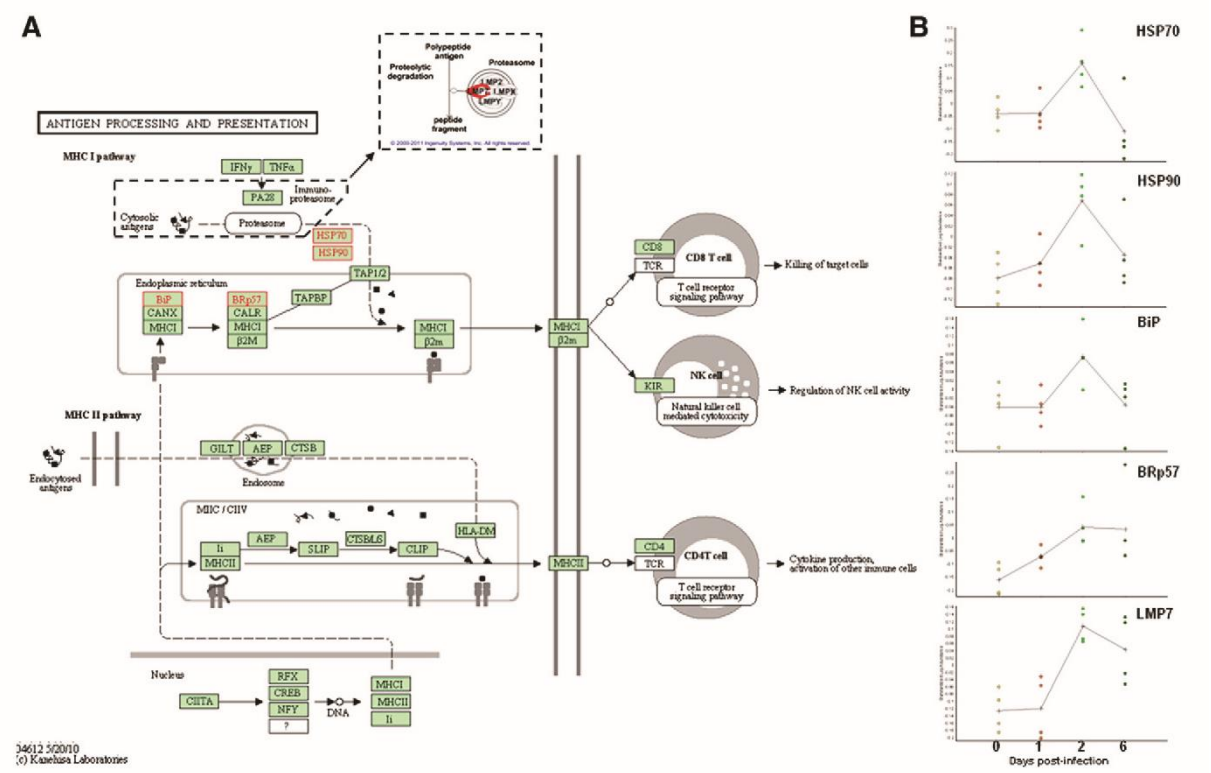

Figure 5 –Voies de présentation d'antigènes par le CMH-I et CMH-II. **A :** Schéma produit sur les plateformes Kegg pathways and Ingenuity Pathway Analysis. Les protéines différentiellement exprimées sont marquées en rouge. **B :** Quantité relative des protéines différentiellement exprimées à 1, 2 et 6 jours après l'infection. D'après Martins et al. (2012) J. Proteomics [18].

Pendant longtemps, la présentation d'antigènes d'origine exogènes, comme ceux provenant des bactéries, champignons et parasites, a été attribuée à la voie du CMH-II, tandis que la voie du CMH-I était associée à la présentation de peptides issus de la dégradation de protéines endogènes d'origine tumorale et virale. Néanmoins, des travaux récents ont démontré que des peptides d'origine exogène peuvent aussi être présentés dans le contexte du CMH-I par les cellules dendritiques par un mécanisme nommé "présentation croisée d'antigènes" (*antigen cross-presentation*). Pour la première fois, notre étude protéomique a fourni des indices suggérant l'occurrence de ce phénomène pendant la salmonellose non-typhique.

Dans ma troisième étude ([19], ci-joint), j'ai analysé la réponse transcriptionnelle globale des ganglions par la technologie des puces à ADN et des outils bioinformatiques. Par ailleurs, j'ai analysé l'expression de gènes codant pour des protéines effectrices de *Salmonella* dans les tissus infectés, afin de préciser les mécanismes moléculaires déclenchés suite à l'infection, du point de vue de l'hôte et du pathogène.

Les résultats de cette analyse ont indiqué que l'apoptose des cellules infectées est inhibée lors de l'infection, en accord avec les résultats issus de notre analyse protéomique. De plus, nous avons montré l'induction de la mort cellulaire par pyroptose dans les ganglions (**Figure 6**), 1 jour après l'infection et précédant l'augmentation de la charge bactérienne, l'infiltration de cellules phagocytaires et le déclanchement de l'inflammation observées au 2ème jour dans les tissus.

La pyroptose, comme l'apoptose, induit la fragmentation et la condensation nucléaire, entrainant une réaction positive au marquage TUNEL (*terminal deoxynucleotidyl transferase dUTP nick end labeling*). Néanmoins, la pyroptose est caractérisée par la libération du contenu intracellulaire dans le milieu extracellulaire, ce qui provoque une importante réaction inflammatoire dans les tissus affectés contrairement à l'apoptose, qui est décrite comme une mort cellulaire programmée et « immunologiquement silencieuse » [20].

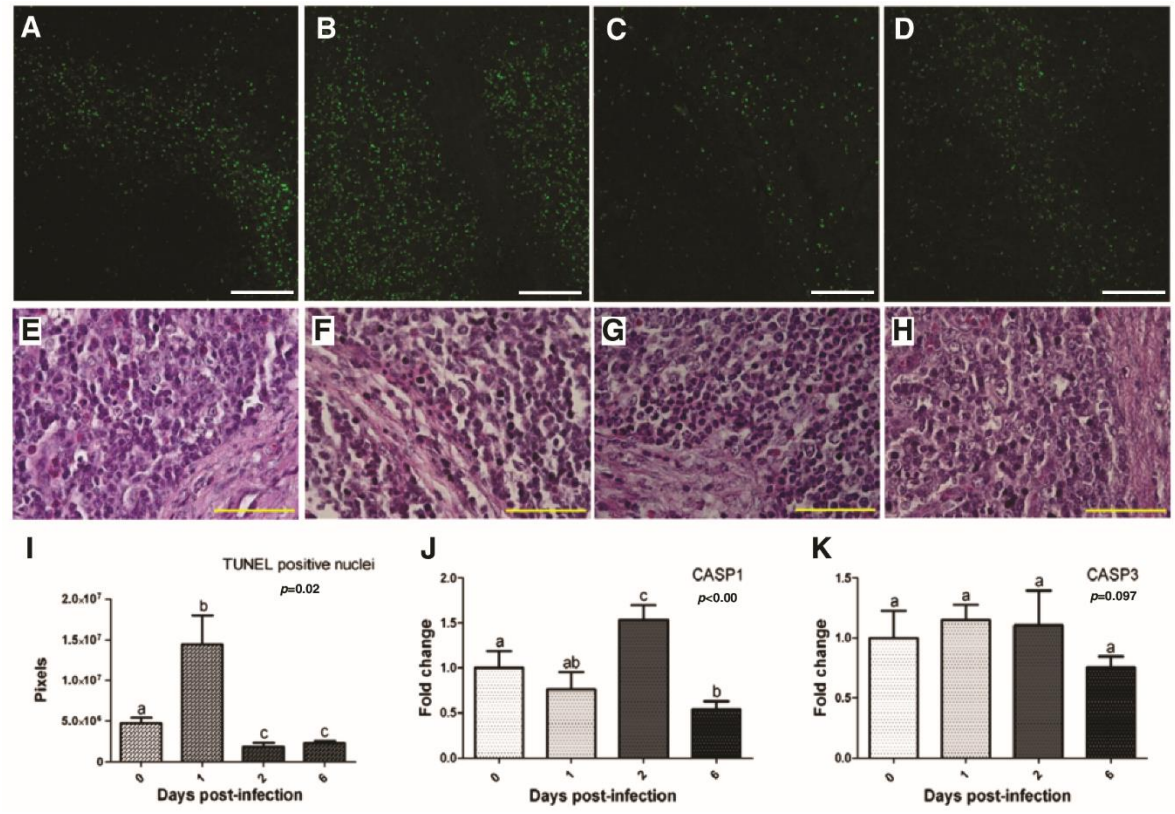

Figure 6 – Analyse de la mort cellulaire dans les ganglions lymphatiques mésentériques de porcs expérimentalement infectés avec *Salmonella* Typhimurium**. A-D :** Marquage TUNEL (*Terminal deoxynucleotidyl transferase dUTP nick end labeling*) à 0 (A), 1 (B), 2 (C) et 6 (D) jours après l'infection. Les noyaux des cellules subissant la pyroptose ou apoptose sont marqués en vert. **E-H :** Afin de différentier ces deux types de mort cellulaire, l'analyse histopathologique des mêmes échantillons sont montrés. La forte infiltration de cellules polynucléaires indique l'occurrence de pyroptose. **I :** La quantification de cellules TUNEL-positives indique l'augmentation de la pyroptose au 1er jour après l'infection. **J-K :** la surexpression du principal médiateur de la pyroptose (CASP1) et l'absence de régulation du principale médiateur d'apoptose (CASP3) suggère la prédominance de la pyroptose. D'après Martins et al. (201 3) Vet .Res. [19].

Chez la souris, l'induction de l'apoptose a été rapportée comme un mécanisme employé par *Salmonella* pour éviter la réponse de l'hôte [14]. En effet, la mort des cellules infectées par pyroptose jouerait en défaveur du pathogène, étant donné que celui-ci se trouverait exposé aux médiateurs de la réponse innée dans le milieu extracellulaire et pourrait pourtant y être facilement éliminé. Il est important de souligner que l'observation de *Salmonella* dans les tissus par microscopie confocale a montré la présence de bactéries à l'intérieur de vésicules intracellulaires et a également dévoilé un marquage suggérant la présence de cellules bactériennes libres dans le milieu extracellulaire (**Figure 7**).

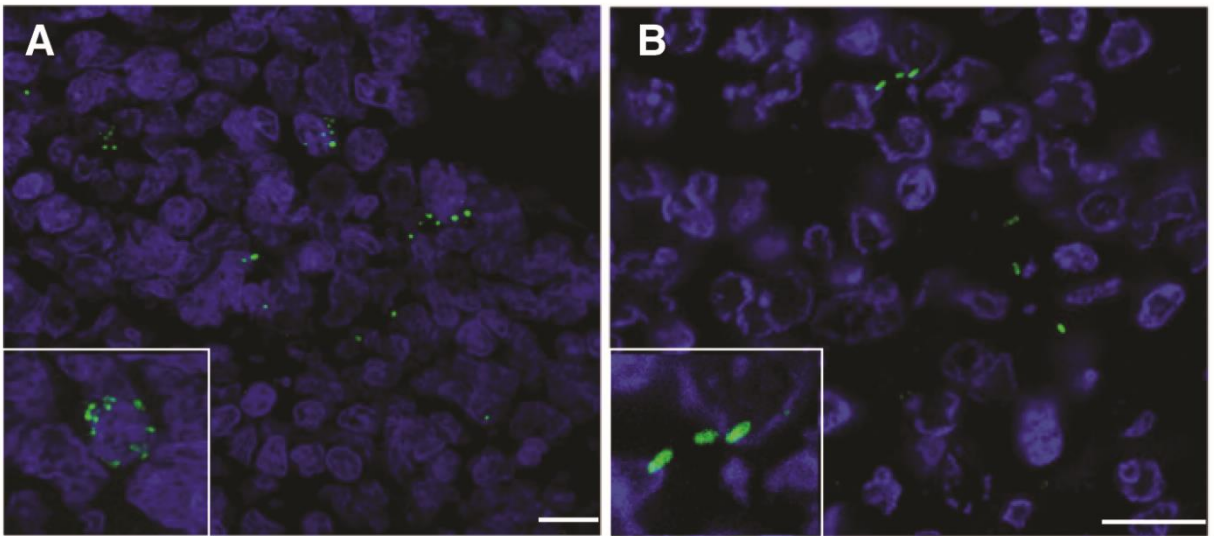

Figure 7 – Détection de Salmonella Typhimurium dans les ganglions lymphatiques mésentériques de porcins par microscopie confocale**. A-B :** Les marquages observés suggèrent la présence du pathogène à l'intérieur de vésicules intracellulaires (A) et libre dans le milieu extracellulaire (B). Les bactéries et les noyaux sont marqués en vert et bleu, respectivement. Barres d'echèle = 10µm. Adapté de Martins et al. (201 3) Vet .Res. [19].

Nous avons aussi étudié l'expression *in vivo* de facteurs de virulence de *Salmonella* impliqués dans la régulation de l'apoptose. Malgré le fait que le pathogène exprime ces médiateurs chez les ganglions porcins, la réponse immunitaire semble avoir un avantage dans la tension entre les mécanismes déclenchés par l'hôte et le pathogène. Chez la souris, *Salmonella* entrave l'induction de la pyroptose en supprimant l'expression de la flagelline et de l'effecteur de type III prgJ [21]. Curieusement, nous avons constaté l'expression des gènes codant pour ces deux molécules chez le porc.

L'ensemble de ces résultats nous a mené à déduire que chez le porc, *Salmonella* est incapable d'exploiter l'apoptose des cellules infectées comme une voie d'échappement à la réponse immunitaire. Cela entraine sa libération dans le milieu extracellulaire par pyroptose et son élimination par la réponse immunitaire innée. De plus, nos observations ont suggéré que la présentation croisée de peptides antigéniques bactériens contribue à l'élimination des cellules infectées par les lymphocytes T cytotoxiques. Un schéma de ses résultats est montré dans la **Figure 8**.

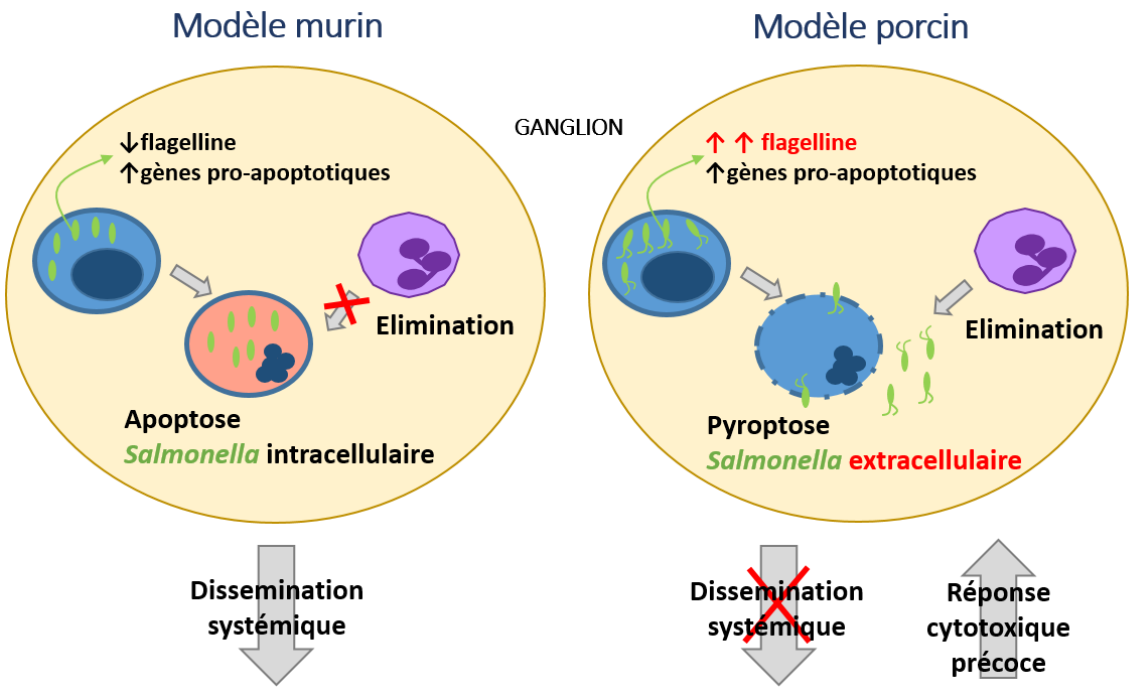

Figure 8 – Différences entre les mécanismes mis en place dans les ganglions lymphatiques mésentériques suite à l'infection par Salmonella Typhimurium chez la souris et chez le porc.

3.2.2 Réponse des follicules lymphoïdes des plaques de Peyer à l'infection par *Salmonella* Typhimurium

Lors de mes quatrième ([22], ci-joint) et cinquième études (manuscrit, ci-joint), j'ai analysé les altérations morphologiques et la réponse transcriptionnelle des follicules lymphoïdes des PP suite à l'infection par *Salmonella.* Ces organes, situés majoritairement dans la partie terminale de l'iléon, sont des amas de follicules lymphoïdes séparés de la lumière intestinale par un épithélium spécialisé dans la capture d'antigènes. Chaque follicule est à son tour composé d'un agrégat de lymphocytes B, lymphocytes T et cellules dendritiques folliculaires [23]. Les PP jouent un rôle majeur dans la physiopathologie des salmonelloses non-typhiques en tant que porte d'entrée pour le pathogène. Avant ma thèse, ces organes avaient été étudiés dans le cadre de la salmonellose chez le porc par des approches chirurgicales consistant à injecter le pathogène directement dans les anses intestinales d'animaux sous anesthésie [24]. Cependant, cette technique ne reproduit que partiellement l'infection, étant donné que l'influence du tractus gastro-intestinal sur le pathogène avant son arrivée à l'iléon n'est pas prise en compte.

Nous avons ainsi mise en place une stratégie innovante, basée sur la microdissection laser, pour étudier les mécanismes mis en place par les PP en réponse à *Salmonella*. La

microdissection laser a été traditionnellement appliquée à l'oncologie pour caractériser avec précision des populations tumorales d'intérêt. Dans nos analyses, nous avons utilisé cette technique pour prélever exclusivement les cellules composant les follicules lymphoïdes des PP et ensuite étudier leur transcriptome (**Figure 9A-C**).

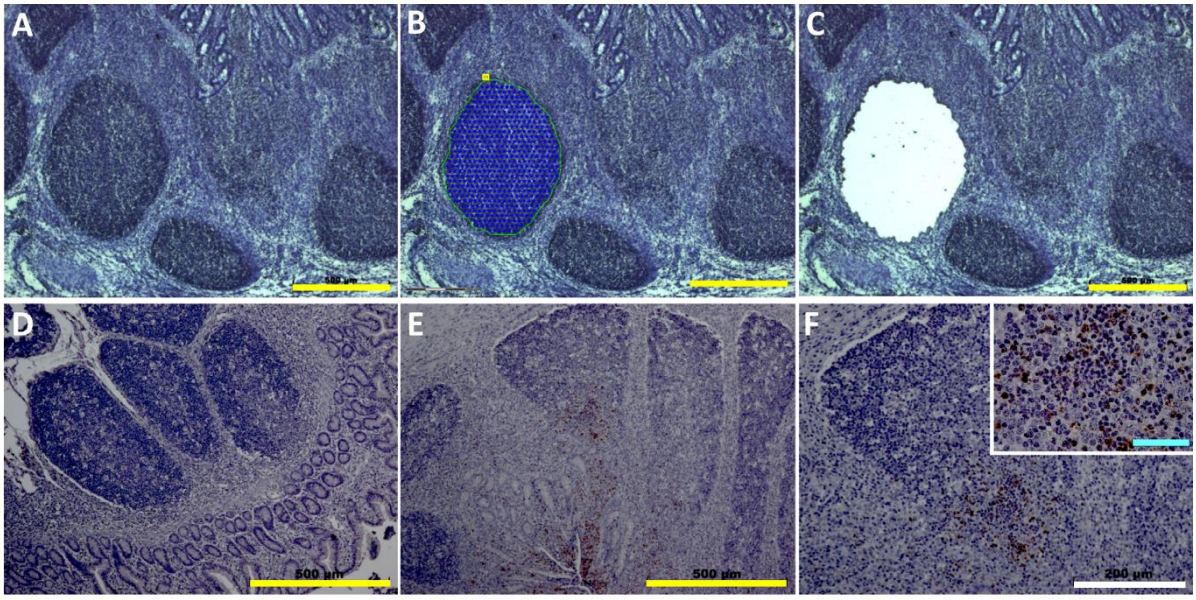

Figure 9 – Analyse des plaques de Peyer de porcs expérimentalement infectés avec *Salmonella* Typhimurium par microsdissection laser. **A-C:** Identification (A), selection (B) et prélèvement des follicules lymphoides par *Auto-Laser pressure catapulting mode* (C). **D-F:** Marquage de *Salmonella* par immunohistochimie dans les tissus du groupe contrôle (D) et infecté (E, F). Adapté de Martins et al. (2013) Dev Comp Immunol [22].

Le marquage *in situ* du pathogène a confirmé que chez porc *Salmonella* traverse l'épithélium associé aux PP afin d'envahir la muqueuse intestinale et atteindre les follicules lymphoïdes (**Figure 9D-F**).

L'analyse préliminaire du transcriptome des cellules folliculaires par PCR quantitative a mis en évidence la surexpression de gènes codant pour des récepteurs de reconnaissance de motifs moléculaires (*Pattern Recognition Receptors - PRR*), cytokines pro-inflammatoires et molécules impliquées dans l'activation de cellules dendritiques [22]. L'activation de la réponse Th1 au détriment des voies Th2 et Th17 a été également observée, en accord avec les observations chez les modèles murins de salmonellose.

Dans ma dernière étude, j'ai élargi notre analyse transcriptionnelle en utilisant la technique de puces à ADN combinée à des outils bioinformatiques. Cette approche a montré l'activation des PP en tant qu'organes secondaires suite à l'infection, traduite par la formation de centres germinatifs et l'induction de mécanismes de l'immunité humorale. Curieusement, nos analyses ont dévoilé, de la même façon que dans les ganglions lymphatiques mésentériques, la surexpression de gènes codant pour des molécules impliquées dans diverses étapes du processus de présentation antigénique par la voie du CHM-I. Ce processus serait majoritairement régulé par le récepteur NLRC5 (**Figure 10**).

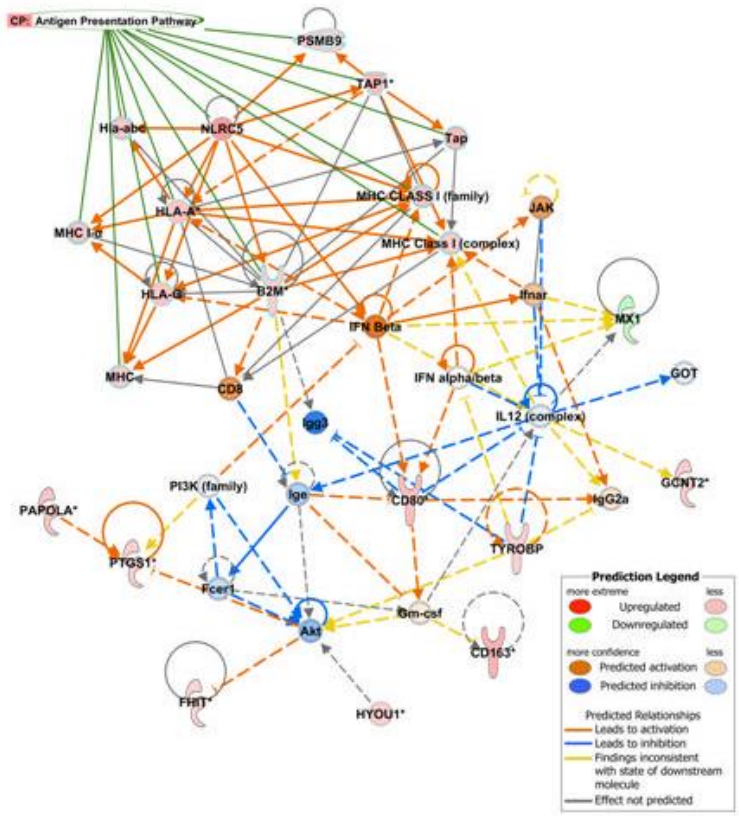

Figure 10 – Réseau moléculaire généré par le logiciel *Ingenuity Pathway Analysis (IPA).* L'activation de la voie du CMH-I suite à l'infection par *Salmonella* Typhimurium serait régulée par la surexpresion du récepteur NLRC5.

L'analyse des tissus par *western-blot* (**Figure 11**) a confirmé que la surexpression des ARNm de NLRC5 et CMH-I entraine leur augmentation au niveau protéique. Il est important de souligner que des niveaux élevés de NLRC5 ont été constaté dans le cytoplasme de phagocytes polynucléaires (**Figure 12**). Cette observation et le lien entre NLRC5 et la présentation d'antigènes nous a mené à déduire que les neutrophiles, en plus de contribuer à élimination du pathogène, pourraient jouer un rôle important dans la régulation de la réponse à médiation cellulaire contre *Salmonella.*

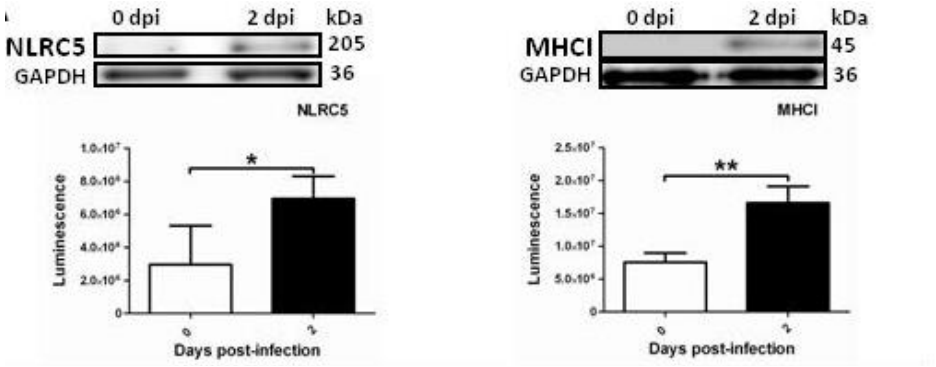

Figure 11 – Quantification par *western-blot* de NLRC5 et CMH-I (*MHC-I*) dans les follicules lymphoides de plaques de Peyer porcines suite à l'infection (*2 days post-infection: dpi*) par *Salmonella* Typhimurium.

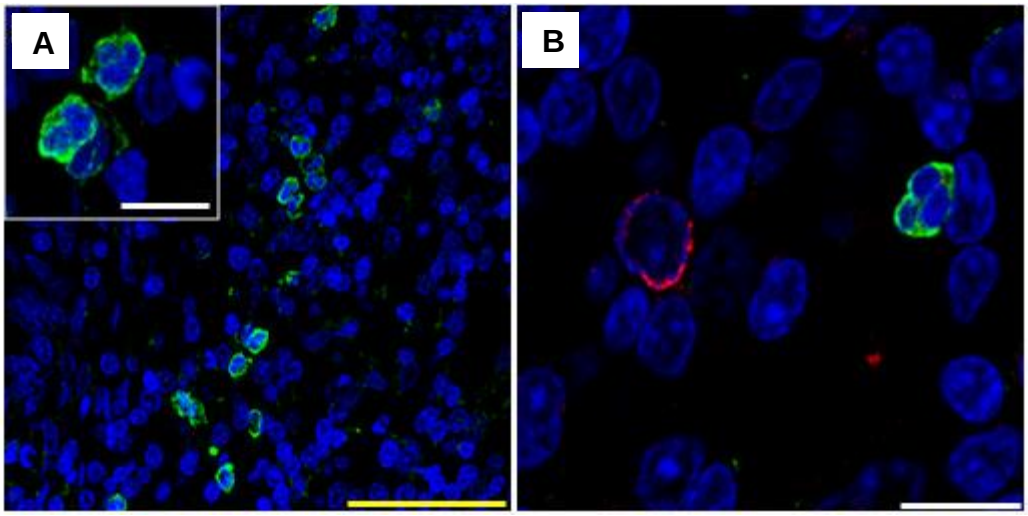

Figure 12 – Marquage de NLRC5 dans les plaques de Peyer de porcs expérimentalement infectés avec *Salmonella* Typhimurium. **A**: la présence de NLRC5 (vert) a été observée à l'intérieur de phagocytes polynucléaires. **B**: NLRC5 n'a pas été réperé chez les macrophages (4E9/11, rouge). Bleu: DAPI. Barres d'échèlle: blanche (10 µm), jaune (50 µm).

L'activation de lymphocytes T suite à leur interaction avec des cellules dendritiques ayant acquis des antigènes transportés et transférés par des polynucléaires neutrophiles a été rapporté dans le cadre des infections par *Mycobacterium bovis* chez la souris et chez l'homme [25].

Ces résultats ont ainsi démontré que *Salmonella* utilise les PP pour franchir la barrière épithéliale intestinal porcine et qu'une réponse inflammatoire a lieu dans ces organes suite à l'infection. Cependant, la présence de *Salmonella* dans les ganglions lymphatiques mésentériques a montré que, chez le porc, cette réponse est insuffisante pour éliminer le pathogène et empêcher sa dissémination par la voie lymphatique, comme décrit chez la souris. Fait intéressant, cette absence de différences remarquables au niveau des PP renforce l'hypothèse que l'espèce porcine a développé des mécanismes spécifiques lui permettant d'utiliser les ganglions lymphatiques mésentériques comme une dernière barrière contre la dissémination de *Salmonella* Typhimurium. Les différents mécanismes mis en place dans les follicules lymphoïdes joueraient ainsi un rôle crucial dans la coordination de la réponse humorale et à médiation cellulaire. Il est à souligner que les observations indiquant la présentation d'antigènes par le CMH-I dans deux organes lymphoïdes différents suggèrent un rôle majeur de la réponse cytotoxique dans le contrôle des infections par *Salmonella.* Cependant, ce mécanisme reste très peu étudié dans le cadre de la salmonellose et d'autres infections bactériennes.

En résumé, ma thèse de doctorat a permis de mettre en évidence un rôle majeur du tissu lymphoïde dans le contrôle des infections par *Salmonella* chez le porc. Mes résultats sont relatés dans quatre articles scientifiques [17-19, 22] qui font l'objet de plus de 100 citations et contribuent ainsi à la lutte contre une problématique importante de santé animale et publique. Un dernier manuscrit (ci-joint) sera complémenté avec des observations résultantes d'une collaboration effectuée pendant mon post-doc qui sera détaillée dans la prochaine section de ce mémoire. J'ai également participé à deux articles scientifiques [26, 27] dans le domaine de l'infectiologie en tant que co-auteur.

3.2.3 Articles et manuscrit en pièce jointe

Martins, R. P., Collado-Romero, M., Arce, C., Lucena, C., Carvajal, A., Garrido, J. J. (2013). Exploring the immune response of porcine mesenteric lymph nodes to *Salmonella enterica* serovar Typhimurium: an analysis of transcriptional changes, morphological alterations and pathogen burden. Comparative Immunology, Microbiology and Infectious Diseases, 36 (2), 149-160.

Martins, R. P., Collado-Romero, M., Martínez-Gomáriz, M., Carvajal, A., Gil, C., Lucena, C., Moreno, Á., Garrido, J. J. (2012). Proteomic analysis of porcine mesenteric lymph-nodes after *Salmonella typhimurium* infection. Journal of Proteomics, 75 (14), 4457-4470.

Martins, R. P., Aguilar, C., Graham, JE., Carvajal, A., Bautista, R., Claros, MG., Garrido, J. J. (2013). Pyroptosis and adaptive immunity mechanisms are promptly engendered in mesenteric lymph-nodes during pig infections with *Salmonella enterica* serovar Typhimurium. Veterinary Research, 44, 1-14.

Martins, R. P., Lorenzi, V., Arce, C., Lucena, C., Carvajal, A., Garrido, J. J. (2013). Innate and adaptive immune mechanisms are effectively induced in ileal Peyer's patches of *Salmonella typhimurium* infected pigs. Developmental and Comparative Immunology, 41 (1), 100-104.

Martins, R.P., Aguilar, C., Lorenzi, V., Jiménez-Marín, A., Zaldívar-López, S., Argüello, H., Herrera-Uribe, J., Carvajal A., Bautista, R., Claros, M.G., Garrido J.J. *Salmonella* Typhimurium elicits specific humoral and cell mediated immune responses in porcine Peyer's patches. *En preparation.*

Comparative Immunology, Microbiology and Infectious Diseases 36 (2013) 149–160

Contents lists available at SciVerse ScienceDirect

Comparative Immunology, Microbiology and Infectious Diseases

journal homepage: www.elsevier.com/locate/cimid

Exploring the immune response of porcine mesenteric lymph nodes to *Salmonella enterica* serovar Typhimurium: an analysis of transcriptional changes, morphological alterations and pathogen burden

Rodrigo Prado Martins[a], Melania Collado-Romero[a], Cristina Arce[a], Concepción Lucena[a], Ana Carvajal[b], Juan J. Garrido[a,*]

[a] *Grupo de Genómica y Mejora Animal, Departamento de Genética, Universidad de Córdoba, Campus de Rabanales, Edificio Gregor Mendel C5, 14071 Córdoba, Spain*
[b] *Departamento de Sanidad Animal, Facultad de Veterinaria, Universidad de León, 24071 León, Spain*

ARTICLE INFO

Article history:
Received 22 May 2012
Received in revised form
14 November 2012
Accepted 19 November 2012

Keywords:
Pig
Mesenteric lymph-node
Immune response
Salmonella enterica serovar Typhimurium

ABSTRACT

Infections caused by *Salmonella* enterica serovar Typhimurium (*S. typhimurium*) cause important economic problems in the swine industry and threaten the integrity of a safe and healthy food supply. Controlling the prevalence of *Salmonella* in pig production requires a thorough knowledge of the response processes that occurs in the gut associated immune tissues. To explore the *in vivo* porcine response to *S. typhimurium*, MLN samples from four control pigs and twelve infected animals at 1, 2 and 6 days post infection (dpi) were collected to quantify the mRNA expression of gene coding for 42 innate immune-related molecules. In addition, the presence of *S. typhimurium* in MLN was examined and its effect on tissue micro-anatomy. Higher *S. typhimurium* loads were observed at 2 dpi, triggering an innate immune response, marked by a substantial infiltration of phagocytes and up-regulation of pro-inflammatory genes. Such response resulted in a significant decrease in pathogen burden in MLN at 6 dpi, although *Salmonella* could not be completely eliminated from tissue. Furthermore, our results suggest that in porcine infections, *S. typhimurium* might interferes with dendritic cell–T cell interactions and this strategy could be involved in the conversion of *Salmonella* infected pigs to a carrier state.

1. Introduction

Salmonella is one of the most frequent causes of food-borne outbreaks in Europe, with 108,614 confirmed cases of human salmonellosis in 2009 [1]. Worldwide, *Salmonella* causes 94 million cases of acute gastroenteritis, including 155,000 that are fatal, with children in particular falling victim to the disease [2]. Among more than 2500 serovariants, the host-generalist *Salmonella enterica* serovar Typhimurium (herein *S. typhimurium*) is reported as the serovar most frequently associated with human illness, with *S. typhimurium* cases mostly associated with the consumption of contaminated pig and poultry meat [3].

Infections by *S. typhimurium* in pigs lead to a localized enterocolitis and, in general, infected swine evolve into healthy carriers in which bacteria are able to persist without triggering clinical signs [3]. The existence of asymptomatic carriers is a major threat to public health

* Corresponding author at: Grupo de Genómica y Mejora Animal, Departamento de Genética, Facultad de Veterinaria, Universidad de Córdoba, Campus de Rabanales, Edificio Gregor Mendel C5, 14071 Córdoba, Spain. Tel.: +34 957 212692; fax: +34 957 212072.
E-mail address: ge1gapaj@uco.es (J.J. Garrido).

0147-9571/$ – see front matter © 2012 Elsevier Ltd. All rights reserved.
http://dx.doi.org/10.1016/j.cimid.2012.11.003

given that such animals cannot be detected easily and thus serves as source of contamination in food industry [4]. In addition to its importance as zoonotic disease, salmonellosis has an important impact in porcine health and negative implications in the efficiency and economy of the porcine production systems [5].

As a result of food poisoning, *Salmonella* enters the body through the gastrointestinal tract. After location in intestinal lumen and attachment in epithelial cells, *Salmonella* actively invade intestinal cells, colonize the lamina propria and Peyer's patches and rapidly invade host cells, especially macrophages, but also dendritic cells and neutrophils [6]. Consequently, these innate immune cells produce and release chemoattractant cytokines to recruit additional inflammatory cells into the site of invasion and initiate a T helper 1 (Th1) response [7]. From intestine, *Salmonella* reaches mesenteric lymph nodes (MLN), can enter the bloodstream and spread to internal organs [8]. To prevent systemic infection, MLN form a life-saving firewall that protects the host from rapid pathogen dissemination beyond the intestine to others organs, such as liver and spleen [9].

One way to learn about the molecular interactions during *Salmonella* infection is to analyze the host response. To this end, infection experiments using isolated primary cells or cell lines have been carried out to generate most of the knowledge currently available on the molecular events during *Salmonella*–host interaction [10–12]. However, although these *in vitro* models can provide valuable information, it is clear that this approach does not enable the interaction of pathogens with a multitude of different interacting cells involved in the invasion process *in vivo* [13]. Moreover, in mammals, studies on the host mechanisms against *Salmonella* have been largely focused on mice infection models [14,15], although accumulating evidences suggest differences in virulence mechanisms, pathogen colonization and disease susceptibility in food-producing animals infections compared to the murine model of systemic disease [16]. Thus, while in mice *S. typhimurium* moves into the mesenteric lymph nodes, and from there bacteria spread *via* the efferent lymph to the circulatory system, causing a systemic disease [17], in pigs usually causes a self-limiting intestinal disease enterocolitis which is similar to gastroenteritis in humans [6]. Factors that could cause these differences have not been sufficiently clarified, but make the pig an ideal model for investigating enteric salmonellosis in humans.

In swine, *in vitro* and *in vivo* studies have generated valuable insight in the crosstalk between *Salmonella* and porcine tissues and cells [18–20]. Nevertheless, few studies have addressed the requirements for the gut-associated lymph nodes in the development of immune responses, their effect on the protective immunity against *Salmonella* infection and the relationship between changes in MLN transcriptome, tissue cellularity and level of pathogen invasion. In order to contribute to improved knowledge on the role of porcine MLN on *S. typhimurium* infection, in the current study we use a model of *in vivo* experimental challenge to evaluate changes in gene expression and tissue morphological alterations that occur in this organ following infection.

2. Materials and methods

2.1. Experimental infection

The experimental infection design was described elsewhere [19]. Briefly, sixteen weaned piglets of approximately 4 weeks of age and fecal-negative for *Salmonella* were penned in an environmentally controlled isolation facility at 25 °C with *ad libitum* access to feed and water. All the animals were randomly allocated to control group (4 piglets) or infected group (12 piglets). The four non-infected pigs were necropsied 2 h before the experimental infection. The animals belonging to the infected group were orally challenged with 10^8 CFU of *S. typhimurium* phagetype DT104. Afterwards, four infected pigs were randomly sampled and necropsied at 1, 2 and 6 days post infection (dpi). Fecal samples from the infected group were cultured for *Salmonella* to ensure the effectiveness of the experimental challenge. Furthermore, rectal temperature and clinical signs were daily recorded for each animal to observe the evolution of the infection. All procedures involving animals were performed in accordance with the European regulations regarding the protection of animals used for experimental and other scientific purposes.

2.2. Histopathology and immunohistochemistry

Samples of MLN from all experimental animals were fixed in 10% neutral buffered formalin for 24 h and embedded in paraffin-wax for histological processing. Afterwards, 5 μm tissue sections were routinely processed as previously described [21], and stained with hematoxylin and eosin (H&E). Presence of bacteria in the tissue samples was demonstrated by using an anti-*Salmonella* polyclonal antibody raised by immunization of a New Zealand rabbit with a formalin fixed bacterial suspension. Quantification of tissue infiltration of macrophages was carried out by using a monoclonal antibody specific for porcine macrophages (clone 4E9/11) [22]. Immunohistochemical staining of formalin-fixed, paraffin-embedded sections of porcine MLN samples, subjected to heat-mediated antigen retrieval in 0.01 M citric acid, with *Salmonella* antiserum and 4E9 monoclonal antibody was performed by using the immunoperoxidase method as has been described elsewhere [21]. Neutrophils identify by morphology and immunolabeled macrophages were counted in 50 randomly selected high magnification fields (400×) in sections of two different MLN samples from each infected and control animal. Results were expressed as the mean number of cells per field.

2.3. Nucleic acids purification

Samples of MLN from control and infected animals were aseptically collected after necropsies and immediately frozen in liquid nitrogen for DNA and RNA isolation. Then, after treatment with RNA*later*-ICE (Ambion), a volume of 0.6 ml of RLT buffer (Qiagen) was added per 30 mg of tissue followed by disruption in a rotor–stator homogenizer. DNA and RNA were isolated by using the AllPrep DNA/RNA/Protein Mini Kit (Qiagen) and eluted RNA was

Table 1
List of genes and primer sequences for quantitative PCR analysis.

Gene name	Forward primer (5′ → 3′)	Reverse primer (5′ → 3′)	GenBank Accession number
β-Actin	CAGGTCATCACCATCGGCAACG	GACAGCACCGTGTTGGCGTAGAGGT	U07786
CASP1	CTCTCCACAGGTTCACAATC	GAAGACGCAGGCTTAACTGG	NM_214162
CCL2	ACCAGCAGCAAGTGTCCTAAAG	GTCAGGCTTCAAGGCTTCGG	NM_214214
CCL3	TCTCGCCATCCTCCTCTG	TGGCTGCTGGTCTCAAAATA	AY643423
CCL4	CAGCACCAATGGGCTCAGA	TTCCGCACGGTGTATGTGA	EF107667
CCL5	CCAGCAGCAAGTGCTCCAT	ACACCTGGCGGTTCTTTCTG	NM_001129946.1
CCL28	AACATCACAGCAAGAGGAACAG	TGGCACAAAGGAACATTCACC	NM_001024695
CD11b	GCGAGGACTCCCACGGAACTC	GAAGATGGGGTGGTTTATGC	Y11618.1
CD14	ACCACCCTCAGACTCCGTAATG	TTGCGCCACTTTCAGTACCTT	EF051626
CD40	TGGTTTCCAGAGTCGGATGAG	ACAGGATCCCCAGCGTGAT	NM_214194.1
CD40L	CAACACCCACAGTTCCTCCAA	AGACTCCGCCCAAGTGAATG	AB040443.1
CD209	CTGACTTGGCCCCTCCTTCT	GAGACTGGTGGATCCTGGAAAC	NM_001129972.1
CXCL2	GGATAGCACGCTGTACCATC	ACTGTCTCAATAAATAACAACCGAC	AY578786
CXCL8	TTCGATGCCAGTGCATAAATA	CTGTACAACCTTCTGCACCCA	M86923
Cyclophilin-A	CCTGAAGCATACGGGTCCT	AACTGGGAACCGTTTGTGTTG	AY266299
DEFB1	ACCGCCTCCTCCTTGTATTC	GGTGCCGATCTGTTTCATCT	NM_213838
DEFB2	CTGTCTGCCTCCTCTCTTCC	CAGGTCCCTTCAATCCTGTT	NM_214442
IFNγ	CAAAGCCATCAGTGAACTCATCA	TCTCTGGCCTTGGAACATAGTCT	X53085
IL1β	GGCCGCCAAGATATAACTGA	GGACCTCTGGGTATGGCTTTC	NM_214055
IL4	TTGCTGCCCCAGAGAAC	TGTCAAGTCCGCTCAGG	AY294020
IL5	TGGTGGCAGAGACCTTGACA	CCATCGCCTATCAGCAGAGTT	NM_214205.1
IL6	TGGCTACTGCCTTCCCTACC	CAGAGATTTTGCCGAGGATG	NM_214399
IL10	CAGATGGGCGACTTGTTG	ACAGGGCAGAAATTGATGAC	L20001
IL12p40	GGAGTATAAGAAGTACAGAGTGG	GATGTCCCTGATGAAGAAGC	U08317
IL13	AAGTGGCCCAGTTCGTAAAAGA	ACCCGTGGCGAAAAATCA	NM_213803.1
IL18	AGGGACATCAAGCCGTGTTT	CGGTCTGAGGTGCATTATCTGA	EU118362.1
IL23p19	GCTTGCAAAGGATCCACCAA	GGCTCCCCTGTGAAAATGTC	NM_001130236.1
MyD88	TGGTGGTGGTTGTCTCTGATGA	TGGAGAGAGGCTGAGTGCAA	NM_002468
NFκB1	CTCGCACAAGGAGACATGAA	ACTCAGCCGGAAGGCATTAT	DQ834921
NOD1	ACCGATCCAGTGAGCAGATA	AAGTCCACCAGCTCCATGAT	AB187219
NOD2	CCTTTTGAAGATGCTGCCTG	GATTCTCTGCCCCATCGTAG	NM_001105295
SELL	CGCTTCCCTTCAGTCGTAG	CCACACAGTCCTCCTTAGTC	NM_001112678
SLC11A1	CCAAAGCAGAGCAGAAC	GGTCCAGGTAAGCAATG	AF132037
TLR1	TGCTGGATGCTAACGGATGTC	AAGTGGTTTCAATGTTGTTCAAAGTC	AB219564
TLR2	TCACTTGTCTAACTTATCATCCTCTTG	TCAGCGAAGGTGTCATTATTGC	AB085935
TLR3	AGTAAATGAATCACCCTGCCTAGCA	GCCGTTGACAAAACACATAAGGACT	DQ266435
TLR4	GCCATCGCTGCTAACATCATC	CTCATACTCAAAGATACACCATCGG	AB188301
TLR5	CAGCGACCAAAACAGATTGA	TGCTCACCAGACAGACAACC	NM_001123202
TLR6	AACCTACTGTCATAAGCCTTCATTC	GTCTACCACAAATTCACTTTCTTCAG	AB085936
TLR7	TCAGTCAACCGCAAGTTCTG	GATGGATCTGTAGGGGAGCA	NM_001097434
TLR8	AAGACCACCACCAACTTAGCC	GACCCTCAGATTCTCATCCATCC	AB092975
TLR9	CACGACAGCCGAATAGCAC	GGGAACAGGGAGCAGAGC	AY859728
TLR10	CCTGTCCAACTGCCTCATTTG	CTAAGTGTTCTAAGGATGTGTTTCTG	AB219565
TNFα	CCTCTTCTCCTTCCTCCTG	CCTCGGCTTTGACATTGG	NM_214022

treated with RNase-Free DNase Set (Qiagen) according to manufacturer instructions. Afterwards, purified RNA and DNA were routinely precipitated with ethanol. RNA and DNA quality was checked by agarose gel electrophoresis before being quantified using a Nanodrop ND-1000 spectrophotometer (Thermo Scientific).

2.4. Quantitative real-time PCR

Real-time quantitative PCR (qPCR) technology was used to determine the relative expression of 42 immune-related genes along the time course of infection (1, 2 and 6 dpi). Total RNA (1.5 μg) from infected and control animals was reverse transcribed to cDNA using the iScript cDNA Synthesis kit (Biorad) in a total volume of 30 μl. cDNA solutions were diluted by adding 70 μl of UHQ water and stored at −20 °C. The qPCR assays were performed on an iQ5 Thermo Cycler (BioRad) using 96 well PCR plates. All samples were amplified in duplicate in the same PCR plate and plates were repeated at least twice. Twenty microliters qPCR reactions were prepared using 2 μl of cDNA as template and iQ SYBR® Green Supermix (BioRad) according to manufacturer's instructions. Final concentration of the primers in the PCR reactions was 0.4 μM. Primers (Table 1) were designed using Beacon Designer (Biosoft International) as previously described [19]. The qPCR conditions were as follows: 95 °C for 5 min, 35 cycles of 94 °C for 30 s, 57 °C for 30 s and 72 °C for 45 s. After amplification, a melting program was run to ensure correct amplification of the expected amplicons.

2.5. Salmonella quantification assay

TaqMan qPCR assays were used for quantifying the *S. typhimurium* load in MLN samples, following the method previously described by Park et al. [23]. DNA from the *Salmonella* strain employed in the experimental infection was extracted using DNeasy Blood & Tissue Kit

(Qiagen) and subsequently diluted to final concentrations of 1.0×10^4, 5.0×10^3, 1.0×10^3, 5.0×10^2, 2.5×10^2, 1.0×10^2, 5.0×10^1 and 0 genome equivalents (GE) per 1 μl. One genome equivalent of *S. typhimurium* corresponded to 5.46904 fg of DNA [23]. A 19-mer forward primer (5′-GCGCACCTCAACATCTTTC-3′), a 22-mer reverse primer (5′-CGGTCAAATAACCCACGTTCA-3′) and a fluorogenic probe (FAM ATCATCGTCGACATGC MGB/NFQ) were used in the quantification assays. Each 25 μl PCR reaction contained 12.5 μl IQ Supermix 2× (Biorad), 0.4 μM of each primer, 0.2 μM probe, 1 μM $MgCl_2$, 1 μl DNA (at 800 ng/μl for porcine samples) and 10 μl UHQ water. PCR amplifications were performed on an iQ5 Thermo Cycler (Biorad) under the following conditions: 95 °C for 10 min and 35 cycles of 95 °C for 15 s and 60 °C for 1 min. Each MLN sample was tested by triplicate in three independent assays. Number of genome equivalents was deduced from the standard curve employing the quantification cycle (Cq) obtained for each sample. Results were shown as the number of genome equivalents of *S. typhimurium* per 800 ng of MLN DNA (GE/800 ng DNA).

2.6. Isolation of S. typhimurium from MLN samples

In order to verify the presence of live *S. typhimurium* in MLN samples, 1 g of tissue was drenched in 9 ml of buffered peptone water (Oxoid) and disrupted with sterile mortars and pestles. Tissue suspensions were transferred to sterile tubes and incubated at 37 °C with shaking at 200 rpm for 12 h. Afterwards, 10 μl of the resulting culture was streaked on XLD agar (Oxoid) plates and incubated at 37 °C for 24 h. The identification of the suspected colonies was confirmed by PCR assays. For this, 20 colonies with typical *Salmonella* morphology were collected from each plate, mixed in 300 μl of UHQ water and their DNA extracted by boiling. PCR was carried out in a final volume of 20 μl, containing 2 μl of DNA template, 400 nM of each primer, 200 nM of each dNTP, 2 mM $MgCl_2$, 2 μl of 10× reaction buffer and 0.75 U *Tth* DNA polymerase (Biotools). Primers employed in this assay were the same used in the procedure of *S. typhimurium* quantification by TaqMan qPCR. PCR cycling protocol consisted of a denaturing step at 94 °C for 5 min, followed by 35 cycles of 94 °C for 30 s, 60 °C for 30 s, 72 °C for 30 s, and a final step of 6 min at 72 °C.

2.7. Data analysis

The relative gene expression was assessed by the $2^{-\Delta\Delta Cq}$ method [24] as previously described [19]. Afterwards, fold change values ($2^{-\Delta\Delta Cq}$) were standardized by a series of sequential corrections proposed by Willems et al. [25], which included log transformation, mean centering and autoscaling. A fold change of 1 denoted no change in gene expression. Values lower than 1 and higher than 1 denoted up and down-regulation, respectively. Standardized data were analyzed using the software SPSS 15.0 for Windows® (SPSS, Inc). Data were tested for normality and variance homogeneity by Shapiro–Wilk and Levene's tests, respectively. Those data assumed to be from a normal distribution and which within-group variances were constant across groups were analyzed by one-way ANOVA and Duncan *post hoc* test. Remaining data were analyzed by Kruskal–Wallis and Mann–Whitney tests. Differences in the rectal temperature among groups were assessed by ANOVA and Duncan *post hoc* test. Data from *S. typhimurium* quantification as well as neutrophil and macrophage count were analyzed by Kruskal–Wallis and Mann–Whitney tests. Spearman's rank correlation test was used to examine the association among *S. typhimurium* load, neutrophil and macrophage count and gene expression. A *p*-value below 0.05 was considered statistically significant.

3. Results

3.1. Experimental infection

Animals experimentally infected were observed daily for development of clinical disease. The analysis of *S. typhimurium* fecal carriage revealed that all animals were positive after the bacterial challenge. In addition, infected pigs manifested clinical signs characterized as lethargy, weight loss and diarrhea. Rectal temperature changed significantly among groups ($p = 0.000$), fever began at 1 dpi (40.58 ± 0.17) and peaked at 2 dpi (40.88 ± 0.46 °C). However, at 6 dpi the rectal temperature declined to normal values (39.15 ± 0.35 °C), not significantly different from those observed in control animals.

3.2. Histopathology and immunohistochemistry

Lymphadenitis, marked by a strong infiltration of inflammatory cells was observed at 2 dpi (Fig. 1A). Similar pathological alterations were observed at 1 and 6 dpi, although to a lesser extent than those seen at 2 dpi. Significant changes in neutrophil count were observed along the time course of the infection ($p = 0.005$). Thus, the number of neutrophils peaked at 2 dpi (Fig. 1C) and a broad infiltration of these cells around trabeculae was uncovered at this time point. Immunohistochemistry revealed that the presence of macrophages in MLN also changed significantly after *S. typhimurium* infection ($p = 0.036$). As shown in Fig. 1D, macrophages count peaked at 2 dpi, being predominantly found in lymph nodes capsule and within the T-cell area near trabeculae (Fig. 1B).

Immunohistochemistry was also carried out to verify the level of tissue invasion by *S. typhimurium*. As shown in Fig. 2A–C, bacterial labeling was observed in the cytoplasm of mononuclear cells. In addition, infiltrated neutrophils were located in the diffuse lymphatic tissue around trabeculae. Again, our results demonstrated that labeled cells were more prevalent in lymph nodes at 2 dpi than in groups of animals infected at 1 and 6 dpi.

3.3. Expression of immune-related genes during S. typhimurium infection

In order to evaluate the porcine MLN response to *S. typhimurium*, qPCR expression profiling was performed on a panel of 42 immune-related genes encoding pattern recognition receptors, immune cells markers, innate/inflammatory and T cell response mediators.

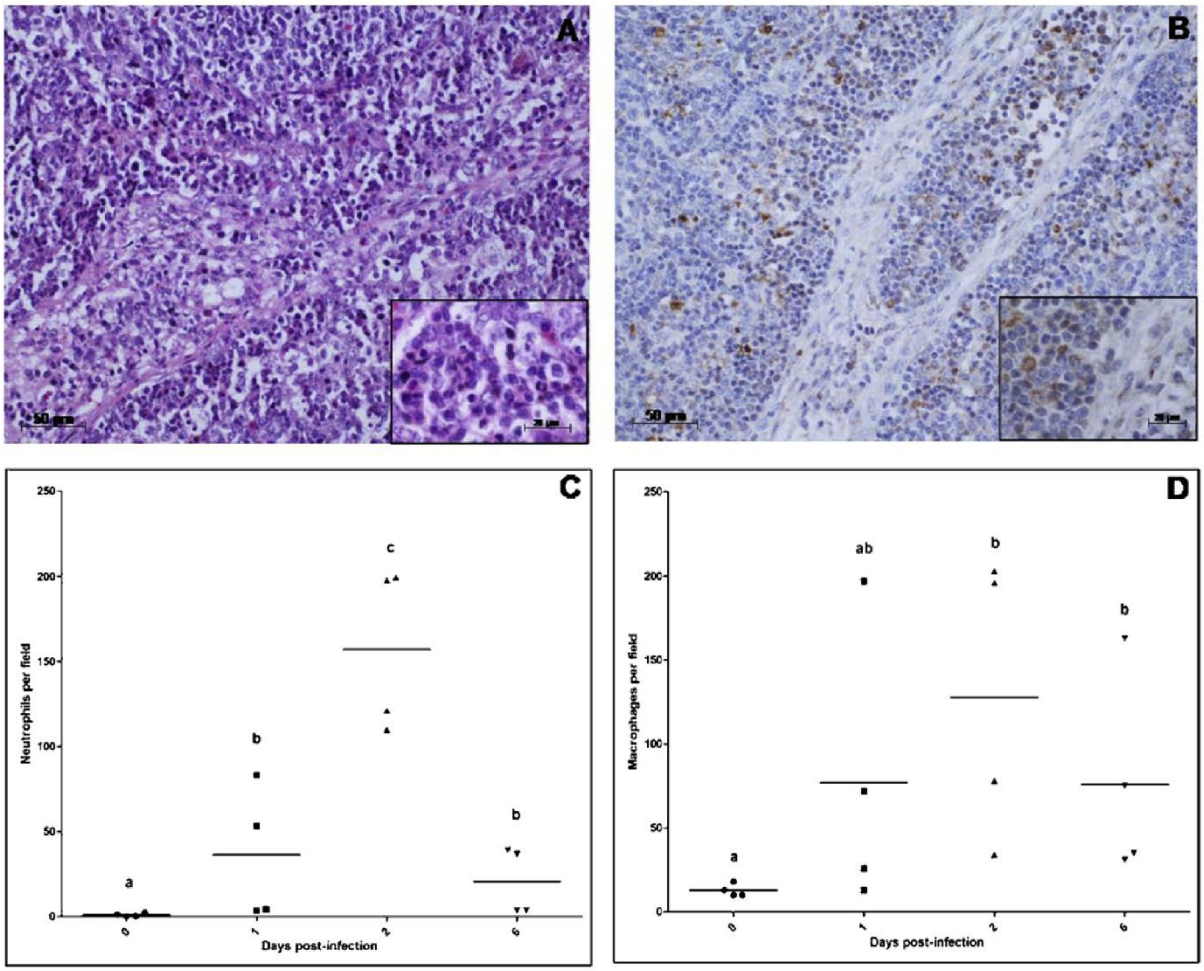

Fig. 1. Histological analysis of MLN from *S. typhimurium* infected pigs. (A) Tissue-infiltrating phagocytes were visualized around trabeculae by H&E staining at 2 dpi. (B) 4E9/11 labeling shows the presence of macrophages within the lymph nodes T-cell area at 2 dpi. (C and D) Quantification of neutrophils and macrophages in tissue, respectively. Data are shown as the number of neutrophils or macrophages per microscope field. Different letters mean significant difference among groups ($p < 0.05$).

Statistically significant expression changes were observed in 26 genes along the time course analyzed (Table 2). Overall, the higher number of differentially expressed genes was observed at 2 and 6 dpi (20 and 14 genes, respectively) whereas only 6 genes had their expression changed at 1 dpi. Interestingly, all the significant observed changes at 6 dpi consisted in down-regulation of gene transcripts (Fig. 3).

Changes in expression of genes coding for different innate/inflammatory response mediators were uncovered mainly at 2 dpi. Thus, significant mRNA up-regulation of IL1β, CXCL2, CXCL8, CASP1, SLC11A and DEFB2 was observed at this time point, whereas expression of CCL28 and SELL resulted down-regulated. Moreover, mRNA expression of IL1β and CXCL2 were also significantly up-regulated at 1 dpi whereas CXCL8 and CASP1 showed down-regulation at 6 dpi. In spite of the absence of significant difference in mRNA expression at 1 or 2 dpi compared to control, genes coding for TNFα and CCL2 showed down-regulation at 6 dpi. Many of the proinflammatory mediators up-regulated at 1 and 2 dpi have their mRNA expression under the control of the transcription factor NFκB. However, NFκB mRNA expression was significantly down-regulated at 2 and 6 dpi.

A down-regulation of genes coding for cytosolic and transmembrane pattern-recognition receptors (PRR) was asserted in our study, except for TLR8 and NOD2, which were up-regulated at 2 dpi.

Expression of genes coding for other cell surface proteins described as phenotype markers of swine immune cells was checked to estimate changes in MLN cellularity after infection. Changes in gene expression were not found out for CD14 or CD40. However, genes coding for CD11b and CD209 showed significant down-regulation at 2 dpi and CD40L at 1 and 2 dpi.

Finally, a diverse mRNA expression profile was observed among Th1 related genes. Although an up-regulation of IFNγ mRNA could be observed at 2 dpi, statistically significant changes in expression were not observed for IL12p40 and IL18 was down-regulated during the infection period studied. Concerning to Th2 response, down-regulation was verified for IL4 transcripts at 2 and 6 dpi and IL13 at 2 dpi. Furthermore, IL5 did not exhibited changes in expression after infection. Other genes encoding T cell costimulatory molecules were also studied. Thus, changes in IL23p19 mRNA expression were not detected and IL10 showed down-regulation at 6dpi.

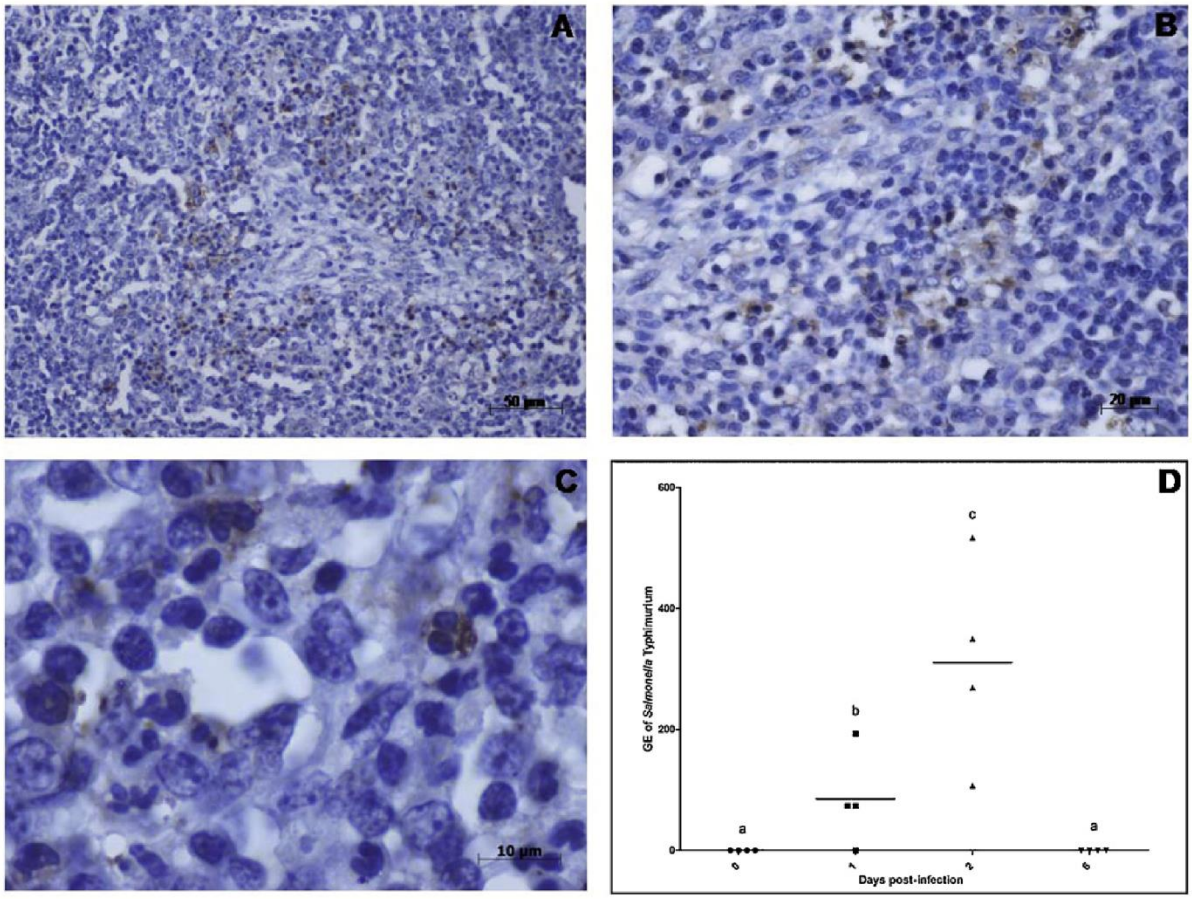

Fig. 2. *S. typhimurium* labeling in MLN of infected pigs. (A) 100×, (B) 400× and (C) 1000×. (D) Quantification of *S. typhimurium* by TaqMan real-time PCR assay. Data are shown as the number of genome equivalents (GE) of *S. typhimurium* per 800 ng of MLN genomic DNA. Different letters mean significant difference among groups ($p < 0.05$).

3.4. Isolation and quantification of S. typhimurium in MLN of infected pigs

TaqMan real-time PCR technology was employed to quantify the presence of *S. typhimurium* in MLN at different times after infection. As shown in Fig. 2D, *S. typhimurium* burden changed significantly ($p = 0.005$) along the time course of infection. Pathogen load could be quantified at 1 dpi (85.4 ± 79.7 GE/800 ng DNA), peaked at 2 dpi (310.5 ± 171.1 GE/800 ng DNA), and decreased to unquantifiable levels at 6 dpi (0 GE/800 ng DNA), indicating the efficient clearance of most of bacteria from the tissue. Although *Salmonella* was not detected at 6 dpi or in one animal necropsied at 1 dpi, the screening by microbiological methods allowed us to determine the presence of live *S. typhimurium* in MLN of all animals belonging to groups 1, 2 and 6 dpi. Nevertheless, the presence of bacteria was not detected in control animals, confirming their previously established *Salmonella* free status.

3.5. Conjunctive analysis of S. typhimurium burden, phagocyte count and immune-related genes expression

Spearman's rank correlation indicated a strong positive association between *Salmonella* burden and neutrophil count (Table 3 and Supplementary data file 1). Transcripts level of IFNγ, CXCL2, IL1β, CCL3 and SLC11a was also positively associated with the pathogen load in infected MLN, at a high level of significance ($p < 0.01$). Among genes which expression was negatively associated with *Salmonella* burden, TLR3, IL18, CD40L and CD11b could be highlighted. Expression of IFNγ, CXCL2 and IL1β was also positively associated with neutrophil count, whereas, mRNA levels of CD40L, IL4 and TLR3 were negatively associated. Differently from *Salmonella* load and neutrophil count, macrophages count showed a higher frequency of significant negative associations. Interleukin 13, CD209 and CD11b should be cited as genes which expression showed the most significant associations with macrophages count.

4. Discussion

MLN are important sites for the induction of immune response against invading pathogens in the gut [26]. In this work, we applied an *in vivo* approach to obtain insight into the response of porcine MLN to *S. typhimurium*. The effectiveness of the performed bacterial challenge was confirmed by the manifestation of typical clinical signs of pig salmonellosis by infected animals. Moreover, the presence of *S. typhimurium* in MLN at 1, 2 and

Table 2
Changes in gene expression relative to uninfected controls (0 dpi) in porcine MLN at 1, 2 and 6 days after *S. typhimurium* infection. Fold change (FC) values with the same letters above are not significantly different ($p < 0.05$).

Gene	0 dpi		1 dpi		2 dpi		6 dpi	
	FC	SD	FC	SD	FC	SD	FC	SD
CASP1	1.00^{a}	0.19	0.76^{ab}	0.19	1.53^{c}	0.17	0.54^{b}	0.09
CCL2	1.00^{a}	0.14	1.17^{ab}	0.42	1.23^{a}	0.27	0.62^{b}	0.12
CCL3	1.00	0.29	1.06	0.20	1.64	0.22	1.05	0.24
CCL4	1.00	0.26	1.35	0.22	1.23	0.22	0.77	0.24
CCL5	1.00	0.24	0.95	0.18	0.89	0.12	1.26	0.34
CCL28	1.00^{a}	0.25	0.74^{ab}	0.24	0.35^{b}	0.08	1.16^{a}	0.14
CD11b	1.00^{a}	0.17	0.69^{ab}	0.23	0.43^{b}	0.11	0.76^{a}	0.16
CD14	1.00	0.24	1.32	0.36	1.79	0.56	0.92	0.33
CD40	1.00	0.14	0.95	0.24	1.26	0.20	0.82	0.14
CD40L	1.00^{a}	0.18	0.71^{b}	0.04	0.53^{c}	0.03	0.90^{ab}	0.16
CD209	1.00^{a}	0.28	0.72^{a}	0.36	0.13^{b}	0.02	0.46^{a}	0.22
CXCL2	1.00^{a}	0.20	3.11^{b}	1.22	2.85^{b}	1.17	1.34^{ab}	0.55
CXCL8	1.00^{a}	0.20	1.18^{a}	0.15	2.84^{b}	0.41	0.49^{c}	0.09
DEFB1	1.00	0.38	2.06	0.49	0.78	0.24	1.70	0.81
DEFB2	1.00a	0.14	0.98^{a}	0.26	2.52^{b}	0.59	1.05^{a}	0.41
IFNγ	1.00^{a}	0.31	1.91^{ab}	0.66	3.50^{b}	1.32	1.08^{a}	0.41
IL1β	1.00^{a}	0.20	6.85^{b}	3.36	10.07^{b}	4.43	1.03^{a}	0.28
IL4	1.00^{a}	0.27	0.50^{ab}	0.12	0.23^{b}	0.05	0.42^{b}	0.11
IL5	1.00	0.20	0.66	0.23	0.61	0.14	0.84	0.22
IL6	1.00	0.35	0.97	0.42	0.93	0.32	0.62	0.10
IL10	1.00^{ab}	0.16	0.76^{bc}	0.18	1.14^{a}	0.15	0.63c	0.09
IL12p40	1.00	0.24	0.63	0.22	0.37	0.17	0.47	0.17
IL-13	1.00^{a}	0.28	0.55^{ab}	0.27	0.24^{b}	0.03	0.39^{ab}	0.17
IL-18	1.00^{a}	0.08	0.76^{b}	0.11	0.51^{c}	0.10	0.53^{c}	0.08
IL-23p19	1.00	0.19	0.93	0.22	0.94	0.06	0.84	0.24
MyD88	1.00	0.15	0.85	0.17	0.80	0.14	0.67	0.07
NFkB1	1.00^{a}	0.17	1.00^{a}	0.24	0.62^{b}	0.16	0.61^{b}	0.13
NOD1	1.00	0.26	0.89	0.30	1.19	0.21	0.60	0.20
NOD2	1.00^{ab}	0.24	1.16^{bc}	0.32	1.70^{c}	0.26	0.68^{a}	0.17
SELL	1.00^{a}	0.23	0.76^{ab}	0.18	0.56^{b}	0.10	0.58^{b}	0.12
SLC11A1	1.00^{a}	0.43	1.80^{a}	0.58	8.40^{b}	1.22	0.90^{a}	0.37
TLR1	1.00	0.10	0.69	0.15	0.75	0.15	0.75	0.10
TLR2	1.00^{a}	0.09	1.01^{a}	0.27	1.07^{a}	0.21	0.59^{b}	0.08
TLR3	1.00^{a}	0.07	0.73^{ab}	0.18	0.51^{b}	0.13	0.61^{b}	0.16
TLR4	1.00^{a}	0.06	0.93^{a}	0.22	0.82^{ab}	0.22	0.58^{b}	0.08
TLR5	1.00	0.29	0.45	0.19	0.64	0.15	0.57	0.23
TLR6	1.00^{a}	0.12	0.58^{b}	0.10	0.75^{ab}	0.15	0.73^{b}	0.11
TLR7	1.00^{a}	0.04	0.55^{b}	0.08	0.58^{b}	0.06	0.56^{b}	0.08
TLR8	1.00^{a}	0.12	0.78^{a}	0.12	1.30^{b}	0.08	0.77^{a}	0.15
TLR9	1.00	0.22	1.22	0.22	0.97	0.21	1.11	0.16
TLR10	1.00	0.14	0.73	0.17	0.71	0.15	0.78	0.14
TNFα	1.00^{a}	0.23	1.41^{a}	0.36	1.14^{a}	0.23	0.65^{b}	0.09

6 dpi was demonstrated employing microbiological and DNA based techniques. Higher *S. typhimurium* loads were observed at 2 dpi, when a peak of corporal temperature was recorded and most of changes in gene expression were observed. In addition, histological analysis confirmed the existence of bacteria in the tissue and detected changes in MLN cellularity as a consequence of the infection.

Consistent with the latter, we observed that infection led to a strong infiltration of macrophages and neutrophils in MLN, which was highly correlated with *S. typhimurium* burden in the tissue. The recruitment of monocytes and neutrophils from blood to infected tissues is a requirement for controlling pathogens replication and ensuring host survival to infection [27]. L-Selectin (SELL), a glycoprotein constitutively expressed by porcine leucocytes [28], was down-regulated at 2 and 6 dpi. Negative correlations observed between the level of SELL transcripts and neutrophil/macrophage count in MLN confirms previous reports of SELL down-regulation by recruited monocytes [27] and neutrophils [29].

Chemokines are the main mediators involved in the recruitment and migration of leukocytes to and within tissues [30]. According with previously reported data [31,32], our experimental infection produced an up-regulation of chemokines in MLN. Moreover, significant correlations were observed between mRNA levels of CXCL8, CXCL2, and tissue neutrophil count. However, changes in expression of these chemokines were not significantly correlated to macrophages count. Interestingly, changes in expression of SLC11A1 showed positive correlations with mRNA levels of most of pro-inflammatory genes, such as CXCL2, CXCL8, IFNγ, IL1β and CASP1 (Supplementary data file 1). SLC11A1 is an important innate host resistance factor to *S. typhimurium*, specially expressed in phagocytic cells, such as dendritic cells (DC) [33], macrophages and neutrophils [34]. In mice, the impact of SLC11A1 on the severity and outcome of *S. typhimurium* infection is determined

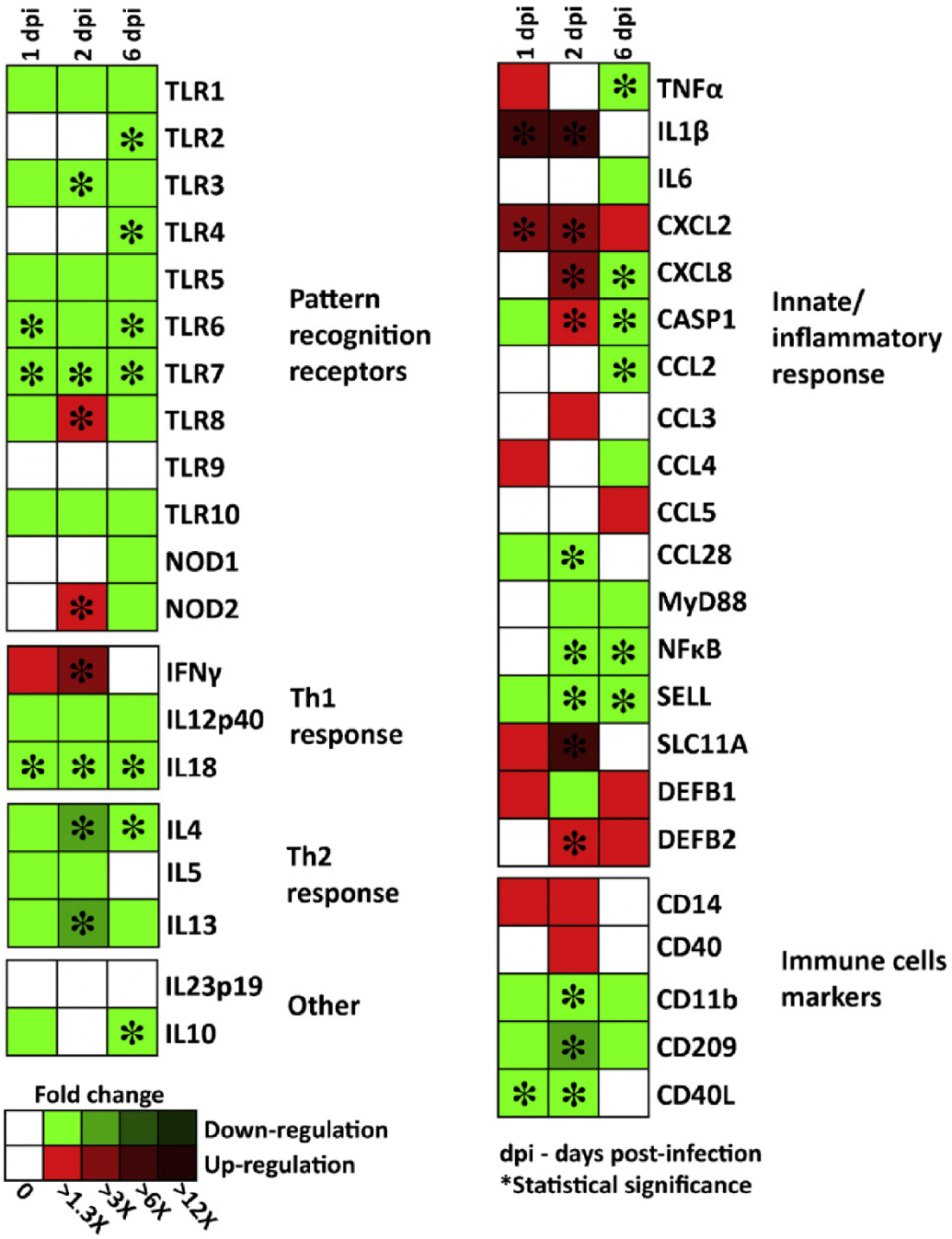

Fig. 3. Expression of immune-related genes in MLN of pigs experimentally infected with *S. typhimurium* by qPCR. Data are shown as the fold change in gene expression in infected pigs compared to controls. Values lower than 1 were calculated as 1/fold change.

by its influence on the speed and intensity of the host inflammatory response, facilitating the rapid activation of host defense [35]. In this work, we observed a strong up-regulation of SLC11A1 at 2 dpi and its expression was significantly correlated to the grade of tissue invasion by *Salmonella* and neutrophils infiltration. Consequently, this could indicate that regulation of SLC11A1 acts as a mechanism of orchestration of inflammatory response in MLN of *S. typhimurium* infected pigs, as has been previously reported in mice [33].

Herein, *Salmonella* infection resulted in down-regulation of CD11b and its mRNA level was negatively correlated with pathogen burden as well as macrophages and neutrophils count in MLN. Differently from human, swine CD11b is only expressed by a subpopulation of granulocytes and lacks expression by monocytes and macrophages [36]. In addition, among the four DC subpopulations found throughout the porcine intestinal immune system, DC from Peyer's patches (PP) have been described as $CD11b^{-}$, whereas DC in MLN are predominantly $CD11b^{+}$ [37]. Previous reports highlight *S. typhimurium* transport from intestine to the draining MLN *via* PP DC as the most predominant penetration route in infection models [9,35,38]. Therefore, down-regulation of CD11b could be attributed to an increase in MLN of cells that do not express this cell marker such as macrophages, and probably DC from PP.

Activated caspase 1 (CASP1) contribute to the control of *Salmonella* infection by processing and maturating the

Table 3
Statistical association between mRNA gene expression and *S. typhimurium* load and neutrophil and macrophage count.

	S. typhimurium	Neutrophils	Macrophages
S. typhimurium		0.844**	0.517*
Neutrophils	0.844**		0.594*
Macrophages	0.517*	0.594*	
CASP1	0.415	0.288	0.059
CCL2	0.452	0.226	−0.247
CCL3	0.645**	0.518*	0.252
CCL4	0.429	0.321	0.029
CCL5	−0.088	−0.129	0.112
CCL28	−0.311	−0.531	−0.392
CD11b	−0.712**	−0.571*	−0.710**
CD14	0.519*	0.550*	0.085
CD40	0.520*	0.338	0.091
CD40L	−0.731**	−0.759**	−0.616*
CD209	−0.473	−0.547*	−0.730**
CXCL2	0.630**	0.624**	0.181
CXCL8	0.605*	0.547*	0.203
DEFB1	0.006	−0.026	−0.110
DEFB2	0.541*	0.515*	0.423
IFNγ	0.668**	0.703**	0.202
IL1β	0.750**	0.650**	0.367
IL4	−0.622*	−0.720**	−0.706*
IL5	−0.595*	−0.432	−0.286
IL6	0.064	−0.100	−0.169
IL10	0.312	0.144	0.108
IL12p40	−0.515*	−0.297	−0.602*
IL13	−0.426	−0.397	−0.772**
IL18	−0.739**	−0.609*	−0.638**
IL23p19	0.035	−0.115	−0.286
MyD88	−0.155	−0.294	−0.392
NFκb	−0.225	−0.365	−0.511*
NOD1	0.290	0.053	0.066
NOD2	0.550*	0.391	0.230
SELL	−0.436	−0.591*	−0.549*
SLC11A1	0.727**	0.594*	0.424
TLR1	−0.201	−0.371	−0.418
TLR2	0.388	0.235	−0.236
TLR3	−0.771**	−0.624**	−0.521*
TLR4	0.033	0.029	−0.498*
TLR5	−0.163	−0.129	−0.395
TLR6	−0.304	−0.347	−0.355
TLR7	−0.415	−0.594*	−0.424
TLR8	0.429	0.365	0.186
TLR9	−0.040	−0.085	0.303
TLR10	−0.283	−0.521*	−0.408
TNFα	0.382	0.206	−0.222

Positive and negative values denote positive and negative association between variables, respectively. Zero means no association.
* $p < 0.05$.
** $p < 0.01$.

pro-inflammatory cytokines IL1β and IL18 [39]. In this study, CASP1 exhibited up-regulation at 2 dpi, followed by down-regulation at 6 dpi. However, its substrates showed a different expression pattern: IL1β was strongly up-regulated at 1 and 2 dpi, whereas IL18 was down-regulated all along infection. In murine MLN and spleen, IL18 is the predominant CASP1 substrate that mediates resistance to oral *S. typhimurium* infection [40]. IL18 acts synergistically with IL12 in the induction of IFNγ production by antigen stimulated T cells in human and mice [41]. Nevertheless, we uncovered an increase of IFNγ expression, in spite of the absence of significant changes in IL12p40 regulation along infection. The lack of significant associations between mRNA levels of IL12p40/IL18 and IFNγ (Supplementary data file 1) could confirm the independence of IFNγ expression respect IL12p40 or IL18 regulation. Moreover, up-regulation of IFNγ could be explained by the fact that NK cells are important producers of this cytokine in pigs [41]. Together, these results might indicate that in porcine infections by *S. typhimurium*, IL18 and IL12 do not play the same role as in human and mice salmonellosis. It could also be inferred that repression of this cytokines is a mechanism whereby *Salmonella* may limit the protective cell-mediated immune response early in infection, as has been previously proposed [42].

Our results also evidenced a decrease in mRNA levels of genes coding for cytokines and receptors related to DC-T-cell interaction. CD40L expression is induced shortly after T-cell activation and represents an early activation marker of T lymphocytes [43]. Activated T cells enhance IL-12 production by interaction of their receptor ligand CD40L with CD40 on DCs or macrophages [44]. Since CD40L was

down-regulated at 1 and 2 dpi, this could also be related to the expression profile uncovered for IL12p40. CD209 was also down-regulated at 2 dpi. This gene codes for a C-type lectin which mediates strong adhesion between DC to resting T cells and is essential in establishing the DC induced T cell proliferation [45]. Besides, it has been reported that CD209-driven interaction between activated neutrophils and DC induce maturation of the latter and enable these cells to trigger an intense T cells proliferation and Th 1 polarization [46].

Since MLN underwent substantial changes in cellularity after infection, neutrophil extravasation primarily, down-regulation CD40L and CD209 could be attributed to the infiltration of cells that do not express these molecules. However, the decrease in mRNA levels of IL12p40, which is produced by activated T cells, as well as reports asserting the prevention of T cells activation as a strategy used by *Salmonella* to evade immune response [8] lead as to infer that this machinery could be employed by the bacteria in swine MLN infection.

TLRs and NODs function as sentinels of infection *via* recognition of pathogen-associated molecular patterns (PAMPs) and induction of appropriate innate and adaptive immune responses to invaders [47]. In this work, we found that except TLR-8 and NOD2, which were up-regulated at 2 dpi, most of the PRR were significantly down-regulated after *Salmonella* challenge. Rydstrom and Wick [30] relate that the absence of signaling through TLR4, TLR5 or both TLR4/5 simultaneously did not compromise phagocytes recruitment to PP and MLN. These authors inferred that such deficiency is probably compensated by recognition of bacterial ligands by other PRR. The occurrence of the TLR signaling at the very first moments of the bacterial challenge should not be excluded. According with both assumptions, we also observed an increase of phagocytes in MLN, in spite of repression of TLR2, TLR3, TLR4 TLR6 and TLR7.

Together, our results suggest a possible synergy between TLR8 and NOD2 in the recognition of *S. typhimurium* in pig infections. TLR8 and NOD2 are expressed by monocytes, macrophages and DC [48–50]. Yrlid et al. [51] state that the application of the agonistic TLR7/8 ligand R848 triggered a massive migration of intestinal DC into MLN. Intriguingly, our results revealed a highly significant correlation ($p < 0.01$) between mRNA levels of TLR8 and NOD2 (Supplementary data file 1). Moreover, expression of none of these genes was correlated with macrophage or neutrophil count in MLN. Therefore, up-regulation of NOD2 and TLR8 at 2 dpi could be attributed to the migration of *Salmonella* infected DC from intestine to MLN. The higher tissue pathogen load observed at 2dpi, in addition to previous reports asserting DC-carriage as the most important mechanism of *Salmonella* dissemination from gut to MLN [9,35,38], cooperate with this hypothesis.

Different methods were employed in this work to assure the presence of *Salmonella* in the tissue and elucidate its influence in immune response. Results revealed that the *Salmonella* burden in the tissue fluctuated during infection depending on host immune response. A coincident up-regulation of pro-inflammatory mediators and infiltration of phagocytes at 2 dpi reduced substantially the pathogen burden in MLN at 6 dpi. In spite of this, isolation of *S. typhimurium* from samples of pigs belonging to 6 dpi group revealed that the pathogen maintained itself in MLN. These findings are in agreement with published observations demonstrating that, after oral infection, *S. typhimurium* persists in myeloid cells in the MLN, despite host immune response [52].

In summary, our results sustain MLN as a vital barrier preventing systemic dissemination of *S. typhimurium* and controlling infection in pigs. According with our previously published proteomic data [53], the presence of *Salmonella* in these organs triggered the induction of innate immune response, marked by a substantial infiltration of phagocytes and up-regulation of pro-inflammatory genes. Such response resulted in a relevant decrease in pathogen burden, but host mechanisms were not able to eliminate *S. typhimurium* from tissue completely. Although porcine salmonellosis by *S. typhimurium* result in milder disease compared to mice, our results also lead us to infer that, in swine infections, *S. typhimurium* might interferes with the DC-T-cells interaction. This strategy could be related to the maintenance of infected animals as bacterial carriers.

Acknowledgements

We thank Erena Ruiz-Mora and Reyes Alvarez for skillful technical assistance. This work was supported by EU funds provided by EADGENE and SABRE Projects, by the Excellence Project of the Junta de Andalucía Government P07-AGR-02672 and by two National R&D Program Grant of the Spanish Ministry of Education and Science (AGL2008-00400 and AGL2011-28904). RPM is a predoctoral researcher supported by the FPU Research Program of the Spanish Ministry of Education and Science.

Appendix A. Supplementary data

Supplementary data associated with this article can be found, in the online version, at http://dx.doi.org/10.1016/j.cimid.2012.11.003.

References

[1] EFSA. The European union summary report on trends and sources of zoonoses, zoonotic agents and food-borne outbreaks in 2009. EFSA Journal 2011;9(3):2090.
[2] Wild PH, McEwan DG, Wagner S, Rogov VV, Brady NR, Richter B, et al. Phosphorylation of the autophagy receptor optineurin restricts *Salmonella* growth. Science 2011, http://dx.doi.org/10.1126/science.1205405.
[3] Boyen F, Haesebrouck F, Maes D, Van Immerseel F, Ducatelle R, Pasmans F. Non-typhoidal *Salmonella* infections in pigs: a closer look at epidemiology, pathogenesis and control. Veterinary Microbiology 2008;130:1–19.
[4] Callaway TR, Edrington TR, Anderson RC, Byrd JA, Nisbet DJ. Gastrointestinal microbial ecology and the safety of our food supply as related to *Salmonella*. Journal of Animal Science 2008;86:E163–72.
[5] Fosse J, Seegers H, Magras C. Prevalence and risk factors for bacterial food-borne zoonotic hazards in slaughter pigs: a review. Zoonoses and Public Health 2009;56:429–54.
[6] Wick MJ. Living in the danger zone: innate immunity to *Salmonella*. Current Opinion in Microbiology 2004;7:51–7.
[7] Eckmann L, Kagnoff MF. Cytokines in host defense against *Salmonella*. Microbes and Infection 2001;3:1191–200.

[8] Bueno SM, González PA, Schwebach JR, Kalergis AM. T cell immunity evasion by virulent *Salmonella enterica*. Immunology Letters 2007;111:14–20.
[9] Voedisch S, Koenecke C, David S, Herbrand H, Förster R, Rhen M, et al. Mesenteric lymph nodes confine dendritic cell-mediated dissemination of *Salmonella enterica* serovar Typhimurium and limit systemic disease in mice. Infection and Immunity 2009;77:3170–80.
[10] Veldhuizen EJA, Koomen I, Ultee T, van Dijk A, Haagsman HP. *Salmonella* serovar specific upregulation of porcine defensins 1 and 2 in a jejunal epithelial cell line. Veterinary Microbiology 2009;136:69–75.
[11] Ge S, Danino V, He Q, Hinton JCD, Granfors K. Microarray analysis of response of *Salmonella* during infection of HLA-B27-transfected human macrophage-like U937 cells. BMC Genomics 2010;11:456–68.
[12] Ciraci C, Tuggle CK, Wannemuehler MJ, Nettleton D, Lamont SJ. Unique genome-wide transcriptome profiles of chicken macrophages exposed to *Salmonella*-derived endotoxin. BMC Genomics 2010;11:545–55.
[13] Niewold TA, Veldhuizen EJA, van der Meulen J, Haagsman HP, de Wit AAC, Smits MA, et al. The early transcriptional response of pig small intestinal mucosa to invasion by *Salmonella enterica* serovar *typhimurium* DT104. Molecular Immunology 2007;44:1316–22.
[14] Mastroeni P, Sheppard M. *Salmonella* infections in the mouse model: host resistance factors and in vivo dynamics of bacterial spread and distribution in the tissues. Microbes and Infection 2004;6(4):398–405.
[15] Liu X, Lu R, Xia Y, Sun J. Global analysis of the eukaryotic pathways and networks regulated by *Salmonella typhimurium* in mouse intestinal infection in vivo. BMC Genomics 2010;11:722–47.
[16] Bearson BL, Bearson SMD. Host specific differences alter the requirement for certain *Salmonella* genes during swine colonization. Veterinary Microbiology 2011, http://dx.doi.org/10.1016/j.vetmic.2010.12.026.
[17] Mittrücker HW, Kaufmann SHE. Immune response to infection with *Salmonella typhimurium* in mice. Journal of Leukocyte Biology 2000;67:457–63.
[18] Skjolaas KA, Burkey TE, Dritz S, Minton JE. Effects of *Salmonella enterica* serovar Typhimurium (ST) and Choleraesuis (SC) on chemokine and cytokine expression in swine ileum and jejuna epithelial cells. Veterinary Immunology and Immunopathology 2006;111:199–209.
[19] Collado-Romero M, Arce C, Ramirez-Boo M, Carvajal A, Garrido JJ. Quantitative analysis of the immune response upon *Salmonella typhimurium* infection along the porcine intestinal gut. Veterinary Research 2010;41:23.
[20] Wang Y, Couture OP, Qu L, Uthe JJ, Bearson SMD, Kuhar D, et al. Analysis of porcine transcriptional response to *Salmonella enterica* serovar Choleraesuis suggests novel targets of NFκB are activated in the mesenteric lymph node. BMC Genomics 2008;9:437.
[21] Yubero N, Jimenez-Marín A, Barbancho M, Garrido JJ. Two cDNAs coding for the porcine CD51 (αV) integrin subunit: cloning, expression analysis, adhesion assays and chromosomal localization. Gene 2011, http://dx.doi.org/10.1016/j.gene.2011.04.006.
[22] Bullido R, Gomez del Moral M, Alonso F, Ezquerra A, Zapata A, Sánchez C, et al. Monoclonal antibodies specific for porcine monocytes/macrophages: macrophage heterogeneity in the pig evidenced by the expression of surface antigens. Tissue Antigens 1997;49:403–13.
[23] Park HJ, Kim HJ, Park SH, Shin EG, Kim JH, Kim HY. Direct and quantitative analysis of *Salmonella enterica* serovar Typhimurium using real-time PCR from artificially contaminated chicken meat. Journal of Microbiology and Biotechnology 2008;18:1453–8.
[24] Livak KJ, Schmittgen TD. Analysis of relative gene expression data using real-time quantitative PCR and the $2^{-\Delta\Delta CT}$ method. Methods 2001;25:402–8.
[25] Willems E, Leyns L, Vandesompele J. Standardization of real-time PCR gene expression data from independent biological replicates. Analytical Biochemistry 2008;379:127–9.
[26] Kwa SF, Beverley P, Smith AL. Peyer's patches are required for the induction of rapid Th1 responses in the gut and mesenteric lymph nodes during an enteric infection. Journal of Immunology 2006;176:7533–41.
[27] Rydström A, Wick MJ. Monocyte recruitment, activation, and function in the gut-associated lymphoid tissue during oral *Salmonella* infection. Journal of Immunology 2007;178:5789–801.
[28] Piriou-Guzylack L, Salmon H. Membrane markers of the immune cells in swine: an update. Veterinary Research 2008;39:54.
[29] Burdon PCE, Martin C, Rankin SM. The CXC chemokine MIP-2 stimulates neutrophil mobilization from the rat bone marrow in a CD49d-dependent manner. Blood 2005;105:2543–8.
[30] Rydström A, Wick MJ. Monocyte and neutrophil recruitment during oral *Salmonella* infection is driven by MyD88-derived chemokines. European Journal of Immunology 2009;39:3019–30.
[31] Wang Y, Qu L, Uthe JJ, Bearson SMD, Kuhar D, Lunney JK, et al. Global transcriptional response of porcine mesenteric lymph nodes to *Salmonella enterica* serovar Typhimurium. Genomics 2007;90:72–84.
[32] Uthe JJ, Royaee A, Lunney JK, Stabel TJ, Zhao SH, Tuggle CK, et al. Porcine differential gene expression in response to *Salmonella enterica* serovars Choleraesuis and Typhimurium. Molecular Immunology 2007;44:2900–14.
[33] Valdez Y, Diehl GE, Vallance BA, Grassl GA, Guttman JA, Brown NF, et al. Nramp1 expression by dendritic cells modulates inflammatory responses during *Salmonella typhimurium* infection. Cellular Microbiology 2008;10:1646–61.
[34] Wu H, Cheng D, Wang L. Association of polymorphisms of Nramp1 gene with immune function and production performance of large white pig. Journal of Genetics and Genomics 2008;35:91–5.
[35] Halle S, Bumann D, Herbrand H, Willer Y, Dahne S, Forster R, et al. Solitary intestinal lymphoid tissue provides a productive port of entry for *Salmonella enterica* serovar Typhimurium. Infection and Immunity 2007;75:1577–85.
[36] Domínguez J, Alvarez B, Alonso F, Thacker E, Haverson K, McCullough K, et al. Workshop studies on monoclonal antibodies in the myeloid panel with CD11 specificity. Veterinary Immunology and Immunopathology 2001;80:111–9.
[37] Bimczok D, Sowa EN, Faber-Zuschratter H, Pabst R, Rothkötter H-J. Site-specific expression of CD11b and SIRPa (CD172a) on dendritic cells: implications for their migration patterns in the gut immune system. European Journal of Immunology 2005;35:1418–27.
[38] Tam MA, Rydström A, Sundquist M, Wick MJ. Early cellular responses to *Salmonella* infection: dendritic cells, monocytes, and more. Immunological Reviews 2008;225:140–62.
[39] Fantuzzi G, Dinarello CA. Interleukin-18 and interleukin-1 beta: two cytokine substrates for ICE (caspase-1). Journal of Clinical Immunology 1999;19:1–11.
[40] Raupach B, Peuschel SK, Monack DM, Zychlinsky A. Caspase-1-mediated activation of interleukin-1β (IL-1β) and IL-18 contributes to innate immune defenses against *Salmonella enterica* serovar Typhimurium infection. Infection and Immunity 2006;74:4922–6.
[41] Domeika K, Berg M, Eloranta ML, Alm GV. Porcine interleukin-12 fusion protein and interleukin-18 in combination induce interferon-γ production in porcine natural killer and T cells. Veterinary Immunology and Immunopathology 2002;86:11–21.
[42] Elhofy A, Marriott I, Bost KL. *Salmonella* infection does not increase expression and activity of the high affinity IL-12 receptor. Journal of Immunology 2000;165:3324–32.
[43] Daoussis D, Andonopoulos AP, Liossis SNC. Targeting CD40L: a promising therapeutic approach. Clinical and Diagnostic Laboratory Immunology 2004;11:635–41.
[44] Lyakh L, Trinchieri G, Provezza L, Carra G, Gerosa F. Regulation of interleukin-12/interleukin-23 production and the T-helper 17 response in humans. Immunological Reviews 2008;226:112–31.
[45] Geijtenbeek TBH, Torensma R, van Vliet SJ, van Duijnhoven GCF, Adema GJ, van Kooyk Y, et al. Identification of DC-SIGN, a novel cendritic cell–specific ICAM-3 receptor that supports primary immune responses. Cell 2000;100:575–85.
[46] Tsuda M, Inaba M, Sakaguchi Y, Fukui J, Ueda Y, Omae M, et al. Activation of granulocytes by direct interaction with dendritic cells. Clinical and Experimental Immunology 2007;150:322–31.
[47] Albiger B, Dahlberg S, Henriques-Normark B, Normark S. Role of the innate immune system in host defence against bacterial infections: focus on the Toll-like receptors. Journal of Internal Medicine 2007;261:511–28.
[48] Delbridge LM, O'Riordan MXD. Innate recognition of intracellular bacteria. Current Opinion in Immunology 2007;19:10–6.
[49] Gorden KB, Gorski KS, Gibson SJ, Kedl RM, Kieper WC, Qiu X, et al. agonists reveal functional differences between human TLR7 and TLR8. Journal of Immunology 2005;174:1259–68.
[50] Tohno M, Ueda W, Azuma Y, Shimazu T, Katoh S, Wang JM, et al. Molecular cloning and functional characterization of porcine nucleotide-binding oligomerization domain-2 (NOD2). Molecular Immunology 2008;45:194–203.
[51] Yrlid U, Milling SWF, Miller JL, Cartland S, Jenkins CD, MacPherson GG. Regulation of intestinal dendritic cell migration and activation by plasmacytoid dendritic cells, TNF-α and type 1 IFNs after feeding a TLR7/8 ligand. Journal of Immunology 2006;176:5205–12.

[52] Monack DM, Bouley DM, Falkow S. *Salmonella typhimurium* persists within macrophages in the mesenteric lymph nodes of chronically infected Nramp1$^{+/+}$ mice and can be reactivated by IFNγ neutralization. Journal of Experimental Medicine 2004;199:231–41.

[53] Martins RP, Collado-Romero M, Martínez-Gomáriz M, Carvajal A, Gil C, Lucena C, et al. Proteomic analysis of porcine mesenteric lymph-nodes after *Salmonella typhimurium* infection. Journal of Proteomics 2012;75:4457–70.

JOURNAL OF PROTEOMICS 75 (2012) 4457–4470

Available online at www.sciencedirect.com

SciVerse ScienceDirect

www.elsevier.com/locate/jprot

Proteomic analysis of porcine mesenteric lymph-nodes after *Salmonella typhimurium* infection☆

Rodrigo Prado Martins[a], Melania Collado-Romero[a], Montserrat Martínez-Gomáriz[b], Ana Carvajal[c], Concepción Gil[b], Concepción Lucena[a], Ángela Moreno[a], Juan J. Garrido[a,*]

[a]Grupo de Genómica y Mejora Animal, Departamento de Genética, Universidad de Córdoba, Campus de Rabanales, 14071 Córdoba, Spain
[b]Unidad de Proteómica, Universidad Complutense de Madrid—Parque Científico de Madrid, 28040 Madrid, Spain
[c]Departamento de Sanidad Animal, Facultad de Veterinaria, Universidad de León, 24071, León, Spain

ARTICLE INFO

Article history:
Received 29 December 2011
Accepted 22 March 2012
Available online 3 April 2012

Keywords:
Pig
Salmonella typhimurium
Mesenteric lymph nodes
DIGE
Pyroptosis
Cross-presentation

ABSTRACT

In this study we employed for the first time an *in vivo* approach coupled to DIGE-based proteomics to explore the response of porcine mesenteric lymph nodes (MLN) to *Salmonella typhimurium* infection. MLN samples were collected from four control and twelve infected pigs (at 1, 2 and 6 days post infection) for histological analysis, protein and RNA purification. Afterwards, expressed proteins were screened by differential in gel analysis and data were analyzed by bioinformatic tools to generate interaction networks, and identify enriched signaling pathways and biological annotations. *S. typhimurium* labeling in tissue and phagocyte infiltration were analyzed by immunohistochemistry and RNA was employed to determine the relative expression of immune-related genes by quantitative RNA analysis. The proteome response of porcine MLN to infection was associated to the induction of processes such as phagocyte infiltration, cytoskeleton remodeling and pyroptosis. Moreover, our results suggest that *S. typhimurium* antigens are cross-presented *via* MHC-I in a proteasome-dependent manner in porcine MLN. Since pathogen burden in tissue was noticeably reduced at the end of the time course, we infer that host innate and adaptive immunity act in association in MLN to control *S. typhimurium* dissemination in swine infections.
This article is part of a Special Issue entitled: Farm animal proteomics.

1. Introduction

European pig herd is acknowledged as the second largest in the world, taking charge of the production of the most consumed meat in Europe [1]. Among the wide range of hazards transmitted to humans by the consumption of pork or pork products, *Salmonella* is considered a major health threat worldwide [2,3]. According to the European Food Safety Authority (EFSA), *Salmonella* is the most frequently reported cause of food-borne outbreaks in the European Union (EU) [4]. Besides, it is supposed that approximately 30% of the human salmonellosis cases are caused by *Salmonella* enterica serovar *typhimurium* (herein, *S. typhimurium*) from pork or pork products [2]. In spite of extensive contributions exploring the murine salmonellosis, the pathogenesis of pig infections with broad host range serotypes of *Salmonella* was largely neglected until recently [5]. Pigs are typically asymptomatic carriers of *S. typhimurium* and this commensal-like state establishes a significant reservoir for *Salmonella* contamination of food during harvest and processing [6]. Although the persistence of *Salmonella* in gut-associated

☆ This article is part of a Special Issue entitled: Farm animal proteomics.

* *Corresponding author at:* Grupo de Genómica y Mejora Animal, Departamento de Genética, Facultad de Veterinaria, Universidad de Córdoba, Campus de Rabanales, Edif. C5 1ª planta, 14071 Córdoba, Spain. Tel.: +34 957 212692.
E-mail address: ge1gapaj@uco.es (J.J. Garrido).

1874-3919/$ – see front matter © 2012 Elsevier B.V. All rights reserved.
doi:10.1016/j.jprot.2012.03.045

lymph nodes of infected pigs has been previously reported, the extraintestinal part of a *S. typhimurium* infection in swine is not well-documented [5]. A recent report demonstrated that the prevalence of *Salmonella* in the lymph nodes of slaughter pigs ranged from 0% to 39.6% in EU, being infected pigs the dominant route of transmission in countries with high *Salmonella* prevalence [4]. Therefore, a thorough knowledge of how *S. typhimurium* interacts with the porcine lymphoid organs and consequently maintains itself in infected hosts consists in an essential step for the development of efficient control measures aiming to protect our food supply in the farm-fork process. Infection induces changes in mRNA and protein expression profiles of host cells. Basing on this, comparative proteome analyses are often used to generate more detailed understanding of molecular mechanisms behind diseases [7]. In fact, *in vivo* models combined with proteomic technological advances represent unprecedented means of characterizing host–pathogen interactions [8]. This approach enables a systematic identification and classification of host proteins involved in infection, providing new targets for disease prevention and treatment strategies [9]. For these reasons, in this study we employed a model of *in vivo* experimental infection followed by DIGE proteomics and bioinformatic data analysis to elucidate the molecular mechanisms undergone by swine porcine mesenteric lymph nodes (MLN) upon *S. typhimurium* infection.

2. Material and methods

2.1. *In vivo Salmonella infection and tissue sampling*

The experimental infection design was described elsewhere [10]. Briefly, sixteen weaned piglets of approximately four weeks of age and fecal-negative for *Salmonella* were randomly allocated to control (4 piglets) or infected groups (12 piglets). Control (0 day post-infection — dpi) pigs were necropsied 2 h before the experimental infection and those ones belonging to the infected groups were orally challenged with 10^8 cfu of *S. typhimurium* phagetype DT104. Afterwards, infected pigs were randomly sampled and necropsied at 1, 2 and 6 dpi (four animals at each time point). Finally, MLN from all experimental animals were collected after necropsies and immediately frozen in liquid nitrogen for protein isolation or fixed in 10% neutral buffered formalin for histological processing. All procedures involving animals were performed in accordance with the European regulations regarding the protection of animals used for experimental and other scientific purposes. Piglets were housed in experimental isolation facilities of the University of León (Spain). Animal care and procedures were in accordance with the guidelines of the Good Experimental Practices (GEP), under the supervision of the Ethical and Animal Welfare Committee of the University of León (Spain).

2.2. *Protein extraction and labeling*

Samples were homogenized on ice in a proportion of 1.5 mL of buffer per 100 mg of tissue using a glass tissue-lyser. Lysis buffer was composed of 7 M urea, 2 M thiourea, 4% w/v CHAPS, 0.5 mM PMSF and protease inhibitor cocktail (Roche, Basel, Switzerland). After sonication (3×20 s pulses on ice, with cooling intervals of 2 min in between) and centrifugation (14,000 *g* for 10 min, at 4 °C), supernatants were precipitated with 2D-Clean-Up Kit (GE Healthcare, Buckinghamshire, UK) and resuspended in 100 μL of DIGE buffer (10 mM Tris, 7 M urea, 2 M thiourea, 2% w/v CHAPS). Subsequently, protein concentration was determined using Bradford Protein Assay (Bio-Rad, Hercules, CA, USA). CyDye labeling was performed following the manufacturer's instructions (GE Healthcare). Briefly, 50 μg of protein per sample was minimally labeled with 400 pmol of Cy3 or Cy5 fluorochromes (dissolved in 99.8% DMF) for 30 min on ice in the dark. Then, reactions were quenched with lysine (10 mM/50 μg of protein). An internal standard, which was included in all DIGE gels, was prepared by pooling equal amounts of protein from each biological sample and labeling with Cy2 dye in the same conditions of separate samples.

2.3. *DIGE*

Sixteen individual samples were randomly distributed across eight DIGE gels. To produce unbiased results and minimize system variation, half of samples from each time point were labeled with Cy5 and the remaining ones with Cy3 (for details, see Supplementary data file 1). For each gel, the same amount of internal standard, Cy3 and Cy5 labeled samples (50 μg each) was pooled and diluted with an equivalent volume of rehydration buffer (7 M urea, 2 M thiourea, 4% w/v CHAPS, 100 mM DTT and 2% pharmalytes, pH 3–11). Afterwards, pools were loaded into 24 cm 3–11 non-linear pH range IPG strips (GE Healthcare) by cup loading. Strips were previously hydrated for 8 h with 7 M urea, 2 M thiourea, 4% w/v CHAPS, 2% pharmalytes 3–11, DeStreak 100 mM (GE Healthcare) and blue bromophenol traces. IEF was performed with an IPGphor II unit (GE Healthcare) at 20 °C. Before second dimension, strips were equilibrated first for 12 min in reducing solution (6 M urea, 100 mM Tris–HCl pH 8.0, 30% v/v glycerol, 2% w/v SDS and 2% w/v DTT) and secondly for 5 min in alkylating solution (6 M urea, 100 mM Tris–HCl pH 8.0, 30% v/v glycerol, 2% w/v SDS and 2.5% w/v iodoacetamide). IPG strips were subsequently loaded onto homogeneous 12% T, 2.6% C (piperazine diacrylamide) polyacrylamide gels and proteins were separated by electrophoresis at 20 °C, 15 W/gel, using Ettan-DALTsix electrophoresis unit (GE Healthcare).

2.4. *Image acquisition and DIGE analysis*

Proteins were visualized using a Typhoon 9400 scanner (GE Healthcare) with CyDye filters. For the Cy3, Cy5 and Cy2 image acquisition, the 532 nm/580 nm, 633 nm/670 nm and 488 nm/520 nm excitation/emission wavelengths were used, respectively, and 100 μm as pixel size. Image cropping and filtering were carried out with Image Quant v.5.1 software (GE Healthcare). Analyses for detection of different abundance between spots from different replicates were performed with the DIA (differential in gel analysis) module of the DeCyder 6.5 package (GE Healthcare). Inter-gel variability was corrected by matching and normalization of the internal standard spot maps using the Biological Variance Analysis (BVA) module. The internal standard image gel with the greatest number of spots was used as a master gel. BVA module was also employed for comparative cross-gel statistical analyses, basing on spot

normalized volume ratio (Cy3:Cy2 and Cy5:Cy2). Variation in abundance among all experimental conditions was accessed by One-way ANOVA. For paired comparisons, independent Student's t-test was carried out. Spots present in at least 85% of gels and exhibiting changes in abundance with a p-value less than 0.05 were considered as differentially abundant spots.

2.5. *Mass spectrometry and protein identification*

Differentially abundant spots were excised from gels for subsequent in-gel reduction, alkylation and digestion with trypsin [11]. Briefly, spots were washed twice with water, shrunk for 15 min with 100% acetonitrile and dried in a Savant SpeedVac for 30 min. Samples were then reduced with 10 mM DTT in 25 mM ammonium bicarbonate (56 °C, 30 min) and alkylated with 55 mM iodoacetamide in 25 mM ammonium bicarbonate for 15 min in the dark. Finally, samples were digested overnight with 12.5 ng/μL sequencing-grade trypsin (Roche) in 25 mM ammonium bicarbonate (pH 8.5) at 37 °C. After digestion, the supernatant was collected, and 1 μL was spotted onto a MALDI target plate and allowed to air-dry at room temperature. Matrix (0.4 μL of a 3 mg/mL) solution of α-cyano-4-hydroxy-cinnamic acid (CHCA; Sigma-Aldrich, St. Louis, USA) in 50% acetonitrile was added to the dried peptide digest spots and allowed again to air-dry at room temperature. MALDI-TOF MS analysis was performed in a 4800 Proteomics Analyzer MALDI-TOF/TOF mass spectrometer (Applied Biosystems, Framingham, MA, USA) operated in positive reflector mode, with an accelerating voltage of 20,000 V. All mass spectra were calibrated internally using peptides from the autodigestion of trypsin. MALDI-TOF MS analysis produced peptide mass fingerprints and the peptides observed were collected and represented as a list of monoisotopic molecular weights with an S/N greater than 15. The suitable precursors for MS/MS sequencing analyses were selected and fragmentation was carried out using the CID on (atmospheric gas was used) 1 KV ion reflector mode and precursor mass Windows ±5 Da. The plate model and default calibration were optimized for the MS/MS spectra processing. For protein identification, the UniProtKB/Swiss-Prot Data Base was searched in batch mode using GPS Explorer v3.6 software (Applied Biosystems) with a licensed version 2.1 of MASCOT. Search parameters were: carbamidomethyl cystein as fixed modification, methionine oxidation as variable modification, peptide mass tolerance 50–100 ppm, peptide charge state +1, one missed trypsin cleavage site and MS/MS fragments tolerance 0.3 Da. The parameters for the combined search (peptide mass fingerprint and MS/MS spectra) were the same described above. In all protein identification, the probability scores were greater than the score fixed by MASCOT as significant with a p-value less than 0.05.

2.6. *Systems biology analysis*

Protein data sets were uploaded into ArrayUnlock (AU, Integromics, Granada, Spain) and Ingenuity Pathway Analysis (IPA, Ingenuity Systems, www.ingenuity.com) for bioinformatic analysis. The AU "Biological Enrichment" tool was used to find biological annotations associated to the list of differently abundant proteins. To this end, AU applies a statistical test based on the hypergeometric distribution to compute p-values and the false discovery ratio (FDR) of Benjamini and Hochberg to correct them. GO terms and KEGG pathways were chosen as annotations to be evaluated in the analysis (refer to AU manual for detailed information: http://www.integromics.com). Protein interaction networks were automatically generated, ranked by score and depicted on IPA as follows: each node in the network diagram represented a protein and its relationship with other molecules was represented by a line (solid and dotted lines represent direct and indirect association respectively). Nodes with a colored background were input proteins detected in this study while non-colored nodes were proteins inserted by IPA based upon the Ingenuity Knowledge Base to produce a highly connected network. Fisher's exact test was used to calculate a p-value determining the probability that each biological function assigned to the data set was due to change alone. Score estimated the probability that a collection of proteins equal to or greater than the number in a network could be achieved by chance alone. Scores of 3 or higher were considered to have a 99.9% confidence of not being generated by random chance alone. IPA Knowledge Base was used as a reference set for statistical analysis of enriched functions/pathways.

2.7. *Western blot analysis*

Equivalent amounts of total protein (30 μg) from control and infected animals were electrophoretically fractionated in 12% (w/v) SDS-PAGE gels and transferred onto a PVDF membrane (Millipore, Bedford, MA, USA). After blockage with 5% skimmed milk in TBS-T (10 mM Tris pH 7.4, 150 mM NaCl, 0.05% Tween-20) for 1 h at room temperature, membrane was incubated overnight at 4 °C with some of the following antibodies: anti-vimentin, clone V9 monoclonal antibody (Chemicon/Millipore, Billerica, MA, USA); rabbit polyclonal to FKBP52 (ab97306, Abcam, Cambridge, UK); anti-14-3-3 β (K-19) rabbit polyclonal antibody (Santa Cruz Biotechnologies, Santa Cruz, CA, USA) and anti-L-plastin polyclonal antibody (kindly gifted by Dr. Francisco Rivero from University of Hull, UK). Secondary peroxidase-linked anti-rabbit or anti-mouse antibodies were used to generate immunocomplexes that were visualized with an enhanced chemiluminescence reagent (Chemiluminescent HRP substrate, Millipore). Membranes were scanned in a FLA-5100 imager (Fujifilm, Tokyo, Japan) and signal intensity was determined using Multigauge software (Fujifilm, Tokyo, Japan). Student's t test was conducted between control and infected groups using SPSS 15.0 for Windows (SPSS Inc, Chicago, IL, USA). A p-value below 0.05 was considered statistically significant. To confirm equal sample loading, all membranes were reblotted with anti-GAPDH monoclonal antibody (GenScript, Picastaway, NJ, USA).

2.8. *Histological analysis*

Paraffin sections (5 μm) of formalin fixed samples were routinely processed and stained with hematoxylin and eosin (H&E). For immunohistochemistry, heat-mediated antigen retrieval in 0.01 M citric acid and labeling were performed as described elsewhere [12], employing the anti-vimentin monoclonal antibody (Chemicon/Millipore), a monoclonal antibody specific for porcine macrophages (clone 4E9/11) [13] and a rabbit antiserum against the somatic antigen of *S. typhimurium*.

2.9. *Real-time quantitative PCR*

Real-time quantitative PCR (qPCR) technology was used to determine the relative expression of the genes coding for CASP1, IL1β, CXCL2, CXCL8 and IFNγ. RNA extractions, cDNA synthesis and qPCR assays were carried out according to Collado-Romero et al. [10]. Primer pairs used for amplifications can be found as supporting information (Supplementary data file 2). The relative gene expression was assessed by the $2^{-\Delta\Delta Cq}$ method [14] using cyclophilin-A and beta-actin as reference genes [15]. Afterwards, fold change values were standardized as proposed by Willems et al. [16]. Fold changes of 1 denoted no change in gene expression. Values lower than 1 and higher than 1 denoted down and up-regulation respectively. Standardized data were analyzed by Kruskal–Wallis and Mann–Whitney tests using the software SPSS 15.0 for Windows (SPSS Inc).

3. Results

3.1. *Experimental infection and histological analysis*

Clinical signs characterized as fever, lethargy, weight loss and diarrhea were observed in infected pigs. Although symptoms peaked at 2 dpi, a clinical improvement of disease was noticed along the time of infection, since animals showed normal feces and corporal temperature at 6 dpi. Lymphadenitis marked by a strong infiltration of neutrophils and macrophages was observed in infected animals (Fig. 1A, B). Besides, immunohistochemistry assays confirmed the presence of *S. typhimurium* in MLN after infection. In the same way of the clinical profile observed, *Salmonella* was more evident at 2 dpi and poorly detected at 6 dpi (Fig. 1C–F). Labeling of *S. typhimurium* antigens was observed

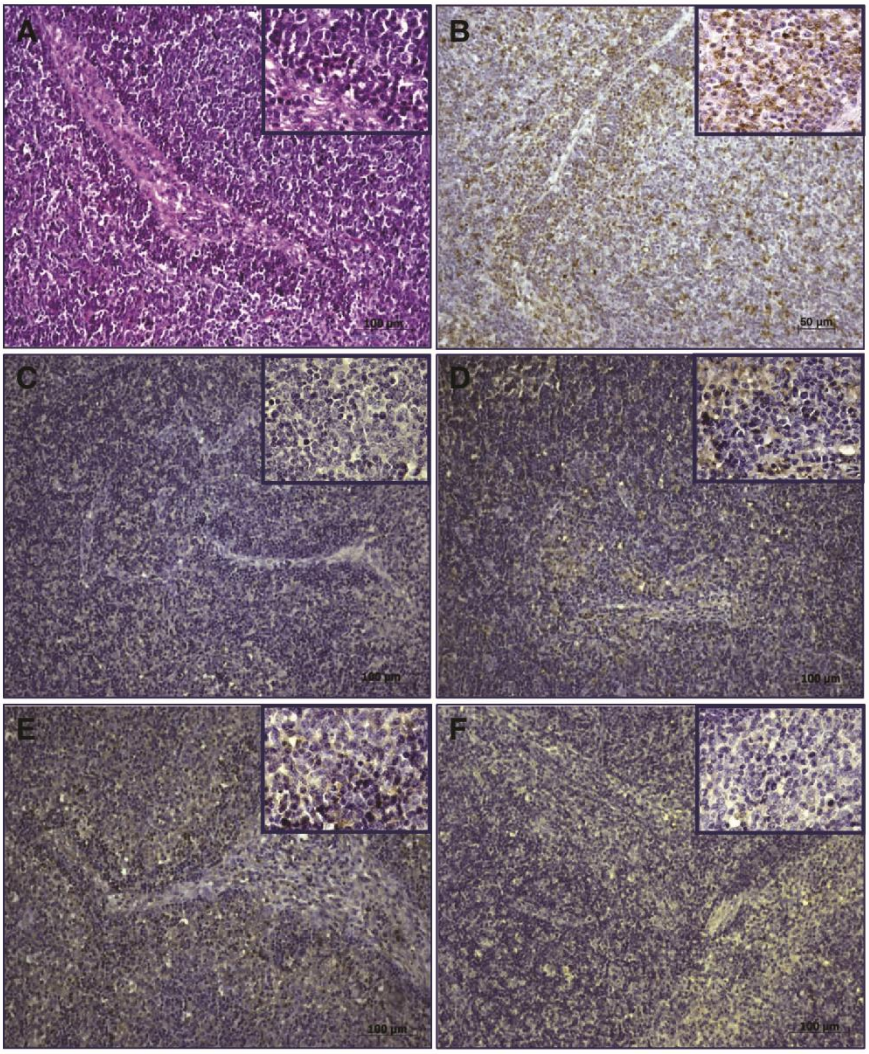

Fig. 1 – Histological analysis of porcine mesenteric lymph nodes (MLN) upon *Salmonella typhimurium* infection. (A) H&E staining demonstrates an evident phagocyte infiltration around trabeculae at 2 days post infection (dpi). (B) Infiltration of macrophages after infection was also observed by immunohistochemistry. (C–F) *S. typhimurium* labeling at 0 (C), 1(D), 2 (E) and 6 (F) dpi. Labeling was more observed at 2 dpi and poorly detected at 6 dpi.

in the cytoplasm of mononuclear cells and neutrophils located mainly in the diffuse lymphatic tissue around trabeculae.

3.2. *DIGE analysis and identification of differently abundant proteins*

DIGE approach was employed to detect changes in the proteome of porcine MLN after oral infection with *S. typhimurium*. Differential in gel analysis uncovered 54 spots exhibiting significant abundance changes as a consequence of the bacterial challenge (Fig. 2A). Paired analyses between infected and control groups detected 16, 43 and 16 differently changed spots at 1, 2 and 6 dpi, respectively. Furthermore, a predominance of spots that were significantly more abundant in relation to controls was observed in all infected groups (Fig. 2B). Among the screened spots, 48 could be identified and corresponded to 38 unique proteins (Table 1, see Additional information). In some cases multiple spots were identified as the same protein, thus indicating the occurrence of post-translational modifications or different isoforms. As shown in Fig. 2C, by comparing data from each of the infected groups, we detected only seven proteins exhibiting significant changes along the whole time course. These are actin (ACTB), growth factor receptor-bound protein 2 (GRB2), BTB/POZ domain-containing protein KCTD12 (KCTD12), protein-L-isoaspartate (D-aspartate) O-methyltransferase (PCMT1), PDZ and LIM domain protein 1 (PDLIM1), tubulin gamma 1 (TUBG1) and vimentin (VIM).

3.3. *Validation of selected proteins by Western blot and immunohistochemistry*

To validate DIGE results, we performed Western blot analysis for four proteins: VIM, plastin-2 (LCP1), 14-3-3 (YWHAZ) and peptidyl–prolyl cis–trans isomerase FKBP4 (FKBP4). All of them showed the same abundance trends revealed by differential in gel analysis (Fig. 3B–I). Additionally, we also checked changes in abundance of VIM by immunohistochemistry assays (Fig. 3A). Consistent with DIGE, immunohistochemistry demonstrated that VIM was less abundant in infected animals when compared to controls. Besides difference in abundance, distribution of VIM in tissue was markedly different before and after infection. At 0 dpi, VIM was diffusely labeled in lymph nodes whereas at 2 dpi, staining was restricted to germinal centers and large irregularly-shaped mononuclear cells located near trabeculae.

3.4. *Quantification of immune-related genes by qPCR*

In order to confirm the regulation of host immune response mechanisms upon infection with *S. typhimurium*, qPCR expression profiling was performed for some genes encoding innate/inflammatory and T cell response mediators. In general, screened genes showed a similar expression trend, which was marked by up-regulation at 2 dpi and decrease of mRNA levels or absence of significant changes at 6 dpi (Fig. 4).

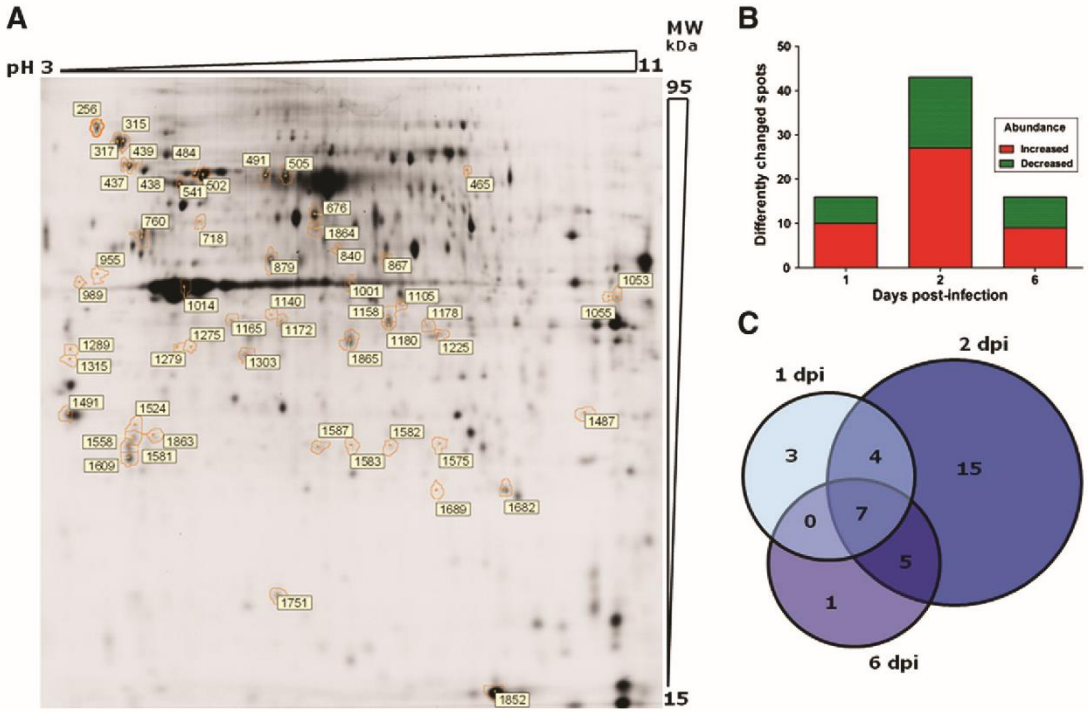

Fig. 2 – DIGE analysis of mesenteric lymph node proteins from controls and *Salmonella typhimurium* infected pigs. (A) Representative DIGE gel. Spots showing significant changes in abundance are indicated by numbers. (B) Bars demonstrate the number of spots exhibiting significant increase or decrease of abundance at 1, 2 and 6 days post-infection (dpi). (C) Venn diagram depicts the number of differently abundant proteins at each time point (1, 2 or 6 dpi) and commonly identified along the whole time course.

Table 1 – List of differently expressed protein in porcine MLN after oral infection with *S. typhimurium*.

Spot no.	Mass	pI	Score	Sequence coverage (%)	Protein ID	Name	Gene	1 *vs* 0		2 *vs* 0		6 *vs* 0		ANOVA
								p-value	Ratio	p-value	Ratio	p-value	Ratio	
1491	27899	4.73	447	53	P63104	14-3-3 protein zeta/delta	YWHAZ	0.16	−1.03	0.025	−1.18	0.01	−1.08	0.013
438	72402	5.07	278	11	P11021	78 kDa glucose-regulated protein	HSPA5	0.99	−1	0.046	1.3	0.91	1.01	0.049
439	72402	5.07	337	31	P11021	78 kDa glucose-regulated protein	HSPA5	0.77	1.02	0.058	1.22	0.56	−1.07	0.044
437	72402	5.07	367	14	P11021	78 kDa glucose-regulated protein	HSPA5	0.018	−1.25	0.32	−1.08	0.35	1.07	0.0033
1001	42052	5.29	410	26	Q6QAQ1	Actin, cytoplasmic 1	ACTB	0.32	−1.05	0.075	−1.08	0.023	−1.16	0.04
1014	42052	5.29	442	45	Q6QAQ1	Actin, cytoplasmic 1	ACTB	0.74	−1.01	0.0013	−1.13	0.1	−1.07	0.024
1165	42052	5.29	220	17	Q6QAQ1	Actin, cytoplasmic 1	ACTB	0.039	−1.3	0.046	−1.3	0.54	−1.08	0.021
879	47797	5.61	335	41	P61158	Actin-related protein 3	ACTR3	0.83	1.01	0.043	−1.08	0.81	−1.01	0.024
1864	57341	6.43	242	17	Q2XQV4	Aldehyde dehydrogenase, mitochondrial	ALDH2	0.24	1.09	0.0012	1.59	0.22	1.15	0.0016
1180	39020	6.43	224	23	P19619	Annexin A1	ANXA1	0.095	1.85	0.00016	2.86	0.59	1.15	0.0025
1158	39020	6.43	427	48	P19619	Annexin A1	ANXA1	0.058	2.08	5.40E-06	2.84	0.67	1.14	0.002
1581	30307	5.48	75	23	P18648	Apolipoprotein A–I	APOA1	0.74	1.04	0.012	−1.4	0.12	−1.21	0.0074
1689	22017	5.32	63	5	Q8HXK9	Apoptosis-associated speck-like protein containing a CARD	PYCARD	0.022	−1.35	0.71	−1.03	0.48	−1.06	0.034
1275	35964	5.51	101	23	Q96CX2	BTB/POZ domain-containing protein KCTD12	KCTD12	0.00092	−1.3	0.0016	−1.34	0.093	−1.28	0.031
1279	35964	5.51	51	4	Q96CX2	BTB/POZ domain-containing protein KCTD12	KCTD12	0.015	−1.24	0.014	−1.27	0.013	−1.4	0.0064
256	92698	4.75	98	10	Q29092	Endoplasmin	HSP90B1	1	1	0.0094	1.27	0.19	1.13	0.03
867	47096	6.30	303	46	A6M931	Eukaryotic initiation factor 4A-III	EIF4A3	0.96	−1	0.35	−1.03	0.065	−1.08	0.041
1487	25261	7.82	83	32	Q1JPH6	Eukaryotic translation initiation factor 4H	EIF4H	0.1	1.15	0.0063	1.39	0.14	1.13	0.0032
1053	39851	8.30	91	12	P04075	Fructose-bisphosphate aldolase A	ALDOA	0.13	−1.05	0.01	1.14	0.15	1.11	0.0072
1587	25304	5.89	390	39	P62993	Growth factor receptor-bound protein 2	GRB2	0.041	1.15	0.016	1.28	0.043	1.11	0.022
1575	24579	7.01	177	17	Q3T054	GTP-binding nuclear protein Ran	RAN	0.63	−1.08	0.023	1.65	0.39	1.26	0.039
1303	38151	5.60	298	25	P62871	Guanine nucleotide-binding protein G(I)/G(S)/G(T) subunit beta-1	GNB1	0.5	1.02	0.075	−1.09	0.82	−1.01	0.049
491	70340	5.60	175	11	Q6S4N2	Heat shock 70 kDa protein 1B	HSPA1B	0.96	1.01	0.012	1.61	0.4	−1.13	0.011
484	71082	5.37	548	45	P11142	Heat shock cognate 71 kDa protein	HSPA8	0.016	1.14	0.009	1.28	0.12	1.11	0.015
502	71082	5.37	471	40	P11142	Heat shock cognate 71 kDa protein	HSPA8	0.27	1.1	0.026	1.28	0.62	1.04	0.04
315	85121	4.93	230	20	O02705	Heat shock protein HSP 90-alpha	HSP90AA1	0.29	1.12	0.019	1.34	0.036	1.17	0.036
317	85121	4.93	375	31	O02705	Heat shock protein HSP 90-alpha	HSP90AA1	0.41	1.06	0.0078	1.41	0.33	1.12	0.015

Table 1 (*continued*)

Spot no.	Mass	pI	Score	Sequence coverage (%)	Protein ID	Name	Gene	1 *vs* 0		2 *vs* 0		6 *vs* 0		ANOVA
								p-value	Ratio	p-value	Ratio	p-value	Ratio	
1852	16212	7.10	405	66	P02067	Hemoglobin subunit beta	HBB	0.097	−1.46	0.0011	−2.02	0.033	−1.77	0.023
465	69788	8.68	379	21	O60506	Heterogeneous nuclear ribonucleoprotein Q	SYNCRIP	0.72	1.05	0.01	2.23	0.53	1.08	0.0038
1225	30097	6.61	97	12	Q14847	LIM and SH3 domain protein 1	LASP1	0.071	1.1	0.33	−1.06	0.022	1.2	0.0084
1865	36716	6.16	141	7	P11708	Malate dehydrogenase, cytoplasmic	MDH1	0.27	−1.05	0.021	−1.15	0.71	−1.02	0.013
1178	36314	6.76	112	14	Q5E9E1	PDZ and LIM domain protein 1	PDLIM1	0.022	1.34	0.00065	1.6	0.047	1.2	0.00089
1105	41137	6.77	57	2	Q08752	Peptidyl–prolyl cis–trans isomerase D	PPID	0.024	1.22	0.0034	1.41	0.058	1.12	0.0017
718	51839	5.31	147	17	Q9TRY0	Peptidyl–prolyl cis–trans isomerase FKBP4	FKBP4	0.21	1.15	0.03	1.32	0.068	1.23	0.019
541	70815	5.20	388	29	P13796	Plastin-2	LCP1	0.015	1.13	0.19	−1.08	0.34	1.08	0.043
1315	29092	4.57	185	30	P12004	Proliferating cell nuclear antigen	PCNA	0.16	1.1	0.0036	−1.29	0.61	−1.04	0.015
1682	11653	9.10	193	32	Q29576	Proteasome subunit beta type-8 (fragment)	PSMB8	0.91	1.02	0.00073	1.71	0.023	1.49	0.0014
676	57146	5.98	134	12	P30101	Protein disulfide-isomerase A3	PDIA3	0.048	1.22	0.0067	1.61	0.072	1.65	0.04
1583	24745	6.71	76	15	P80895	Protein-L-isoaspartate (D-aspartate) O-methyltransferase	PCMT1	0.0091	1.13	0.00015	1.4	0.01	1.29	0.00017
1524	23464	5.12	227	28	P19803	Rho GDP-dissociation inhibitor 1	ARHGDIA	0.6	1.03	0.032	−1.14	0.56	−1.03	0.03
1558	23464	5.12	184	36	P19803	Rho GDP-dissociation inhibitor 1	ARHGDIA	0.79	1.01	0.0023	−1.19	0.095	−1.12	0.0071
1609	22836	5.09	191	23	Q9TU03	Rho GDP-dissociation inhibitor 2	ARHGDIB	0.7	1.04	0.035	−1.27	0.44	−1.07	0.037
1751	17292	5.76	158	54	Q6DUB7	Stathmin	STMN1	0.016	1.23	0.19	−1.1	0.3	1.14	0.013
1172	37833	7.03	89	9	Q2TBL6	Transaldolase	TALDO1	0.096	1.13	0.0066	1.33	0.048	1.21	0.0075
760	50804	4.94	507	58	Q2XVP4	Tubulin alpha-1B chain	TUBA1B	0.11	1.07	0.086	−1.1	0.93	−1	0.013
840	51458	5.75	154	20	Q0VCD2	Tubulin gamma-1 chain	TUBG1	0.00032	1.24	0.01	1.28	0.0017	1.28	0.004
955	53757	5.06	136	20	P31000	Vimentin	VIM	0.028	−2.1	0.007	−2.54	0.0062	−2.15	0.0017
989	51874	4.94	68	13	P48670	Vimentin (fragment)	VIM	0.15	−1.39	0.048	−1.74	0.026	−1.67	0.025
505	N/A	N/A	N/A	N/A	N/A	N/A		0.25	−1.14	0.89	−1.02	0.036	−1.37	0.023
1055	N/A	N/A	N/A	N/A	N/A	N/A		0.81	−1.01	0.037	1.2	0.068	1.09	0.032
1140	N/A	N/A	N/A	N/A	N/A	N/A		0.041	1.23	0.023	1.34	0.065	1.3	0.033
1289	N/A	N/A	N/A	N/A	N/A	N/A		0.94	1	0.041	−1.25	0.097	−1.15	0.034
1582	N/A	N/A	N/A	N/A	N/A	N/A		0.59	1.06	0.01	1.56	0.32	1.16	0.012
1863	N/A	N/A	N/A	N/A	N/A	N/A		0.096	1.3	0.025	1.13	0.0038	1.41	0.031

N/A not analyzed.

3.5. *Biological data interpretation*

Bioinformatic tools were employed to biologically interpret protein list obtained from DIGE analysis, aiming to gain an insight into networks, biological processes, molecular functions and pathways associated with the proteome response of porcine MLN to *S. typhimurium*. Three interaction networks were generated by IPA data analysis (Table 2) and the nature of

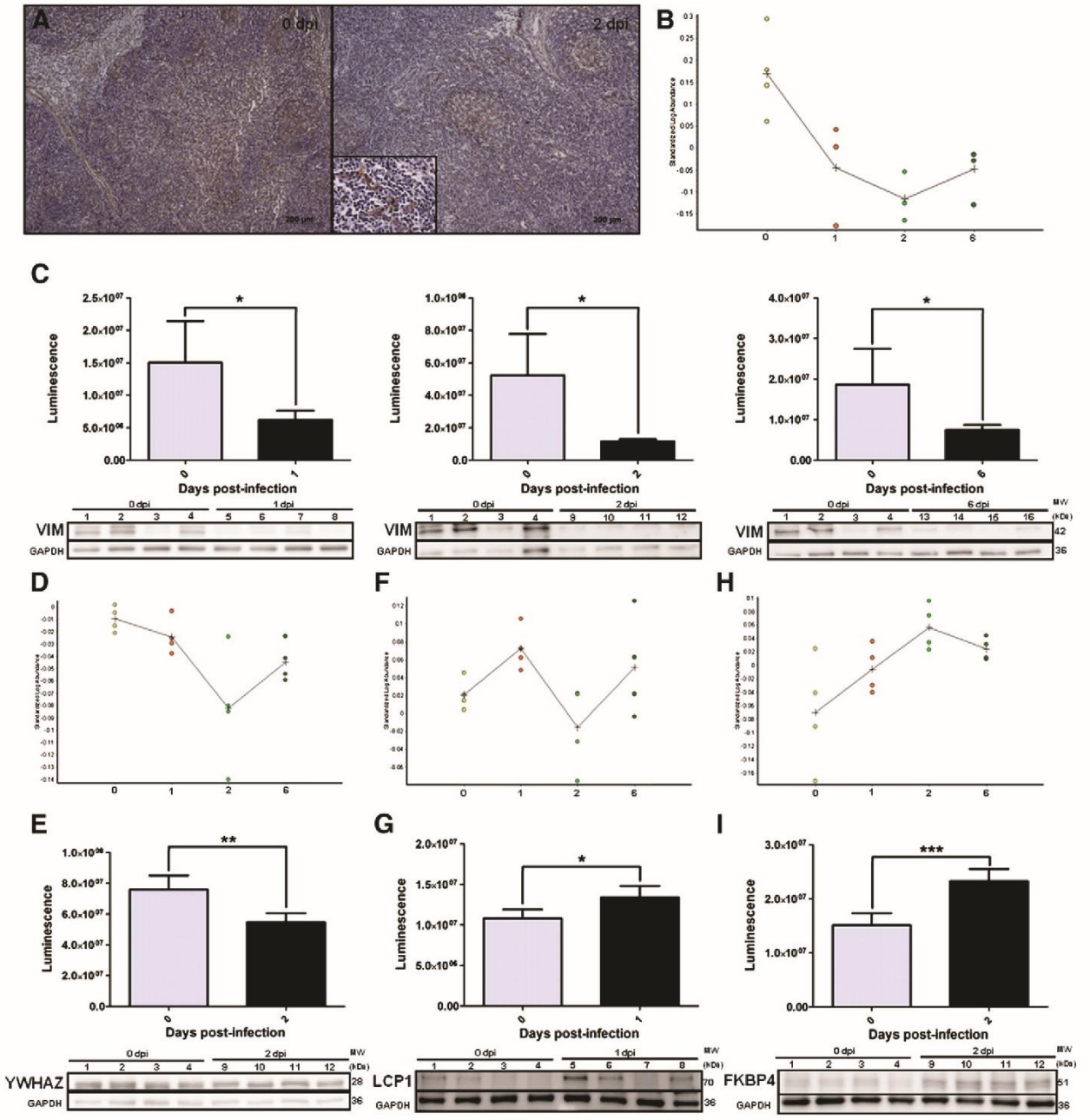

Fig. 3 – Data validation by Western blot and immunohistochemistry. (A) Immunohistochemistry shows a decrease of VIM abundance in MLN and labeling of large irregularly-shaped mononuclear cells located near trabeculae after infection. (B–I) Standard abundance by DIGE and Western blot analysis of validated proteins at 1, 2 and 6 dpi: (B, C) VIM, (D, E) YWHAZ, (F, G) LCP1, (H, I) FKBP4.

relationships displayed by the molecules integrated in each network was accessed based on the scientific information contained in the Ingenuity Knowledge Criteria. The major network depicted the existence of 83 direct and 39 indirect relationships which integrated 20 of the proteins differently altered after *S. typhimurium* infection (Fig. 5). Furthermore, "Post-translational modification", "Protein folding" and "Cellular assembly and organization" were identified as putative functions associated to the proteins included in this network. Network 1 also demonstrated the central role of the heat shock proteins in the proteome response of porcine MLN to *S. typhimurium* as well as the regulatory interactions of these proteins with NFκB and caspase. As other relevant results of network analysis, the following could be highlighted: the activation relationship of GRB2 and ALDH2 (aldehyde dehydrogenase) with p38 MAP kinase depicted in network 2 and the direct activation/inhibition relationship between IFNγ and PSMB8 (proteasome subunit beta type-8) shown in network 3

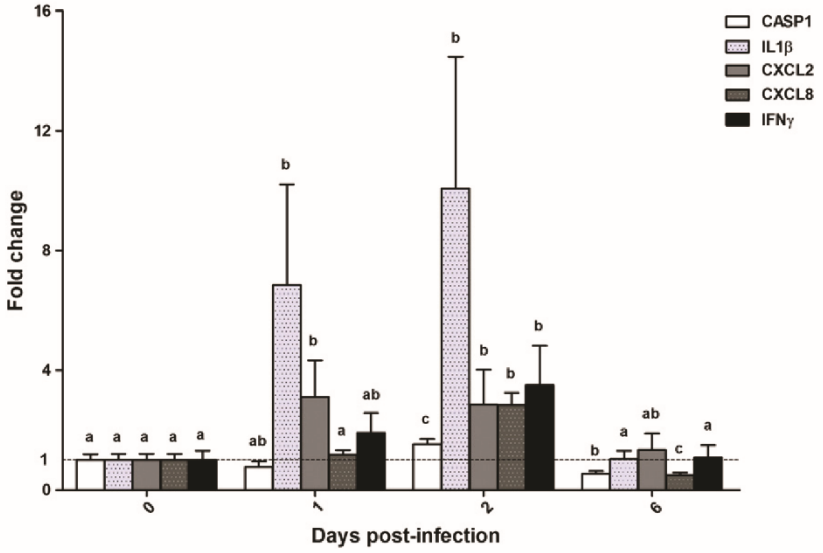

Fig. 4 – Expression profiling of immune-related genes in mesenteric lymph nodes of pigs experimentally infected with *Salmonella typhimurium* by qPCR. Data are shown as the fold change in gene expression in infected pigs compared to controls. Values lower than 1 and higher than 1 denote down and up-regulation respectively. The same letters above the bars indicate no significant differences ($p<0.05$).

(Supplementary data file 1). Gene ontology (GO) annotations associated to differently abundant proteins were found out by the AU "Biological Enrichment" tool. "Cell motility" and "Anti-apoptosis" were the top enriched biological processes identified (Supplementary data file 4). In addition, "Protein folding" and "Rho GDP-dissociation inhibitor activity" were uncovered as the molecular functions more related to the differently abundant proteins (Supplementary data file 5). Pathway analysis was based on the Ingenuity Canonical Pathways Libraries and KEGG database. The top canonical and KEGG pathways significantly altered after the bacterial challenge are described in Table 3. Corroborating data from network analysis, heat shock proteins were observed to take part in different molecular routes. We also detected a similar tendency in DIGE analysis for differently abundant proteins associated to the "Antigen processing and presentation pathway" (Fig. 6A). Interestingly, all of them exhibited an increase of abundance at 2 dpi (Fig. 6B).

4. Discussion

Proteome approaches are being increasingly used in many different systems to investigate host–microbe interactions. In this context, *in vivo* models are crucial to reflect the multiple events undergone by host upon pathogen infection. Although the systemic pathology induced by *S. typhimurium* has been extensively studied using the mouse model [6], the complex

Table 2 – Protein interaction networks associated to the response of porcine MLN to *S. typhimurium* infection.

ID	Score [a]	Focus molecule [b]	Molecules in the network [c]	Top functions
1	54	20	14-3-3, **ACTB**, actin, **ACTR3**, alpha tubulin, **ANXA1**, **ARHGDIA**, **ARHGDIB**, Arp2/3, caspase, Ck2, **EIF4A3**, F actin, **FKBP4**, **HBB**, Hsp70, Hsp90, HSP, **HSP90AA1**, **HSP90B1**, **HSPA5**, **HSPA8**, **HSPA1B**, **LASP1**, **LCP1**, MHC class I (complex), NFκB (complex), **PDIA3**, **PYCARD**, RNA polymerase II, **STMN1**, **TUBA1B**, **TUBG1**, tubulin, **YWHAZ**	Post-translational modification, Protein folding, Cellular assembly and organization
2	20	10	Akt, **ALDH2**, **ALDOA**, Ap1, **APOA1**, CaMKII, ERK1/2, FAM59A, FSH, **GNB1**, **GRB2**, histone h3, histone h4, IG9, insulin, Jnk, LDL, Lh, LOC81691, MAP2K1/2, Mapk, MIR155HG, Nfat (family), P38 MAPK, **PCMT1**, **PCNA**, PDGF BB, **PDLIM1**, PI3K (complex), Pkc(s), PLC gamma, Rac, **SYNCRIP**, trypsin, **VIM**	Cellular movement, cell cycle, lipid metabolism
3	14	7	BPNT1, CDC37L1, CEACAM3, CHI3L2, CLEC5A, DEFB104A/DEFB104B, DNAJB7, **EIF4H**, FKBP6, Gbp4, GBP6, H60a, HSP90AB1, IFNG, IKBKE, **KCTD12**, KMO, **MDH1**, MLEC, Myhs, NDRG4, PGRMC2, **PPID**, **PSMB8**, Raet1b, **RAN**, SLC28A1, SLC5A2, **TALDO1**, Taok2 (mouse), TGFB1, TNF, TRAF6, TREM3, TTC28	Cell death, cell-to-cell signaling and interaction, inflammatory response

[a] Calculated with right-tailed Fisher's test.
[b] Number of input molecules in the network.
[c] Input molecules are highlighted in bold.

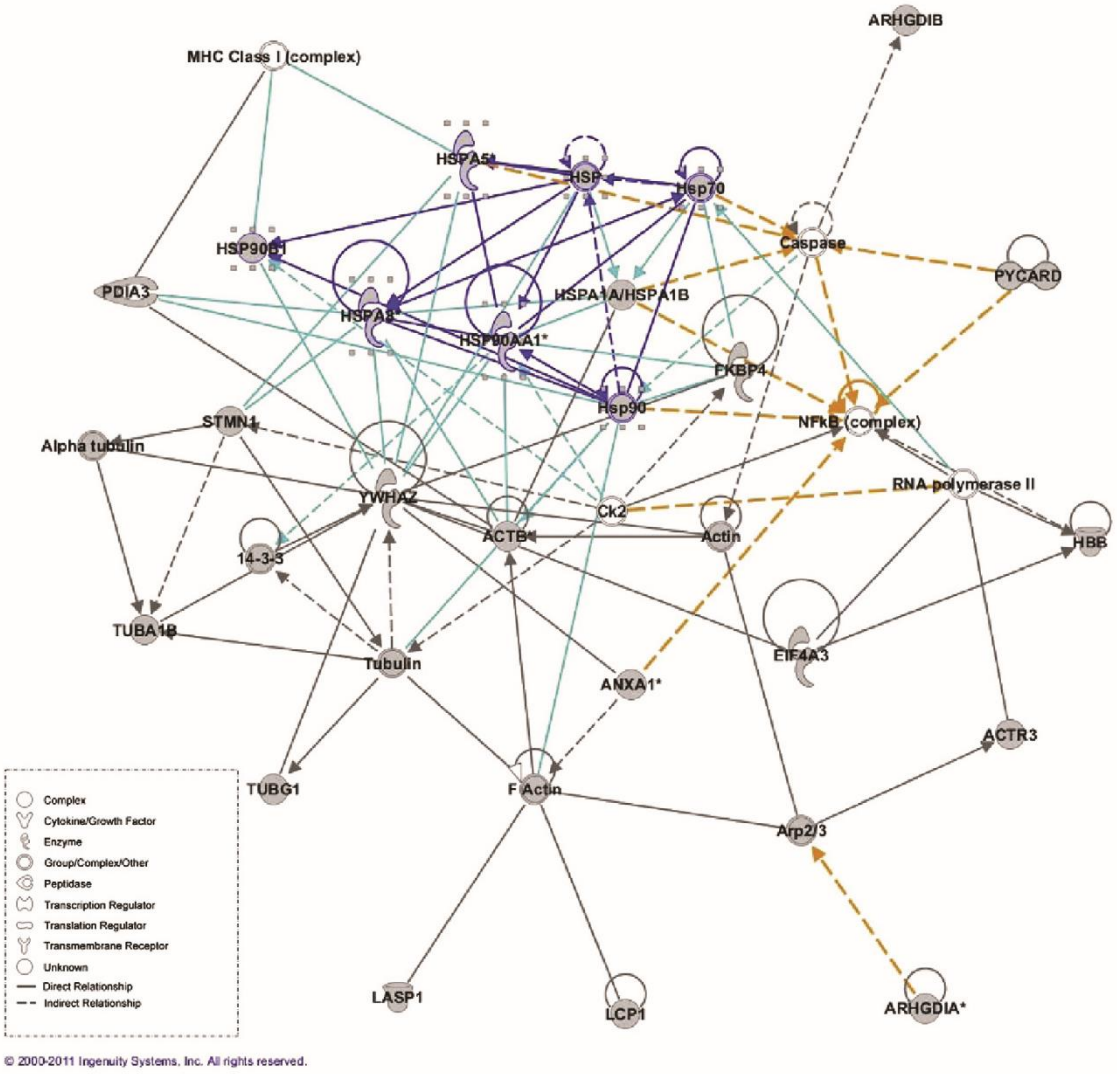

Fig. 5 – Gene network analysis of porcine MLN after *S. typhimurium* infection. "Post-translational modification, Protein folding, Cellular assembly and organization" gene networks. Activation relationships are highlighted in yellow. Blue lines represent interactions entailing heat shock proteins. Light blue lines represent interactions between heat shock proteins and other molecules.

molecular mechanisms underlying the intestinal infection caused by bacteria in food-producing animals are still not fully understood [17]. To address this issue, in this work we employed for the first time an *in vivo* approach coupled to DIGE-based proteomic analysis to detect changes in the porcine MLN proteome in response to *S. typhimurium* infection.

After bacteria challenge, the effectiveness of the experimental infection was confirmed by the observation of clinical signs of enteric disease in all infected animals. Distinct to mice, *S. typhimurium* generally causes little or no systemic involvement in pigs [17]. Nevertheless, in our *in vivo* model we observed in MLN the presence of the pathogen associated to the cytoplasm of infiltrated phagocytes, in concordance with previously reported evidences that, in mice, *S. typhimurium* is shuttled to MLN by infected phagocytes [18,19]. Since major protein changes were detected at 2 dpi, coinciding with a higher presence of *S. typhimurium* in infiltrated phagocytes, it could be inferred that proteome response of porcine MLN to the infection is strongly related to changes in tissue cellularity and pathogen burden. Consistent with this, we found that "Cell motility" was the most significantly enriched biological process after *S. typhimurium* infection (see Supplementary data file 4).

In general, our results indicated a modulation of diverse normal host functions upon *S. typhimurium* infection. This can be related with the complex interplay between *Salmonella* and its host that involves the coordinated stimulation and down-regulation of cell functions by type III secretion systems 1 and 2 (T3SS1 and T3SS2) effectors for benefits of bacteria [20]. Firstly, bacterial internalization involves manipulation of the Rho family GTPases resulting in actin cytoskeleton rearrangements [21,22]. In our study, we observed that regulators of Rho protein

Table 3 – Top four enriched canonical and Kegg pathways in porcine MLN after *S. typhimurium* infection.

Pathways	p-value [a]	Ratio [b]	Input molecules
Kegg pathways			
Antigen processing and presentation	1.4E-06	5.7E-02	PDIA3, HSP90AA1, HSPA8, HSPA5, HSPA1B
Pathogenic *Escherichia coli* infection	2.7E-04	6.1E-02	TUBA1B, ACTB, YWHAZ
MAPK signaling pathway	3.3E-04	1.8E-02	HSPA1B, HSPA5, HSPA8, GRB2, STMN1
Shigellosis	4E-04	6.1E-02	TUBA1B, ACTB, YWHAZ
Ingenuity canonical pathways			
Glucocorticoid Receptor signaling	5.9E-08	2.7E-02	HSPA8, HSP90B1, HSPA1B, GRB2, ANXA1, FKBP4, HSP90AA1, HSPA5
14-3-3-mediated signaling	1.4E-07	5E-02	GRB2, PDIA3, TUBG1, YWHAZ, VIM, TUBA1B
Aldosterone signaling in epithelial cells	9.8E-07	3.5E-02	HSPA8, HSP90B1, HSPA1B, PDIA3, HSP90AA1, HSPA5
Protein ubiquitination pathway	1.5E-05	2.2E-02	HSPA8, HSP90B1, HSPA1B, HSP90AA1, PSMB8, HSPA5

[a] Fisher's exact test.
[b] Ratio (number of input molecules in a given pathway, divided by total number of molecules that make up that pathway).

signaling such as GDP dissociation inhibitors (GDI) ARHGDIA (Rho GDI-1) and ARHGDIB (Rho GDI-2) were less abundant after *Salmonella* infection. Because GDI hinder the dissociation of guanosine diphosphate from Rho proteins, maintaining GTPases in an inactive form [23], our proteomic data suggest an increasing of GTPases activity in porcine infected MLN as a result of the repression of Rho GDI activity.

Although T3SS effectors modulate host Rho GTPases activity for the benefit of the bacteria, mechanisms of host immune response, such as phagocytosis and chemotaxis, are

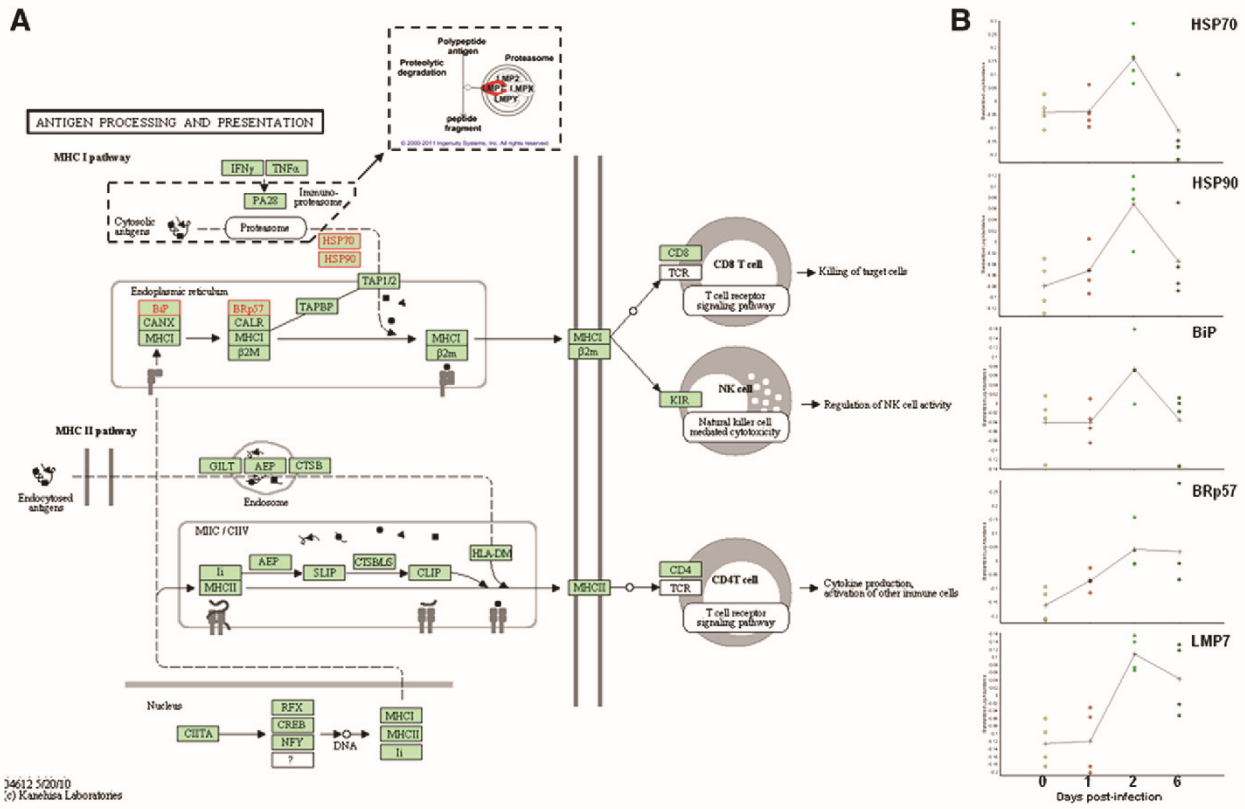

Fig. 6 – Antigen processing and presentation pathway. Differently abundant proteins associated to this pathway are highlighted in red (A) and their standard abundance after infection by DIGE is depicted in (B). Dotted line indicates a pathway detail from Ingenuity Pathway Analysis. The image was generated by Kegg pathways from the Kanehisa laboratories and is subject to their copyright conditions.

driven by extensive local reorganization of the actin cytoskeleton dependent on Rho GTPase activity. Therefore, cytoskeletal changes undergone by MLN in response to infection reflect a mix of outcomes induced by both *Salmonella* and host. Following actin polymerization by activation of the Rho GTPases, recovery of normal cellular architecture was observed once *S. enterica* has completely invaded target cells [24]. However, after bacterial uptake, *Salmonella* can initiate a second round of actin polymerization, resulting in formation of an F-actin coat around replicating intracellular bacteria [20]. In line with this, we observed changes in proteins involved in processes such as actin filament binding and bundle formation. Thus, PDLIM1, a kinase known for their critical role in regulating actin polymerization downstream of the Rho GTPase cascade [25], was more abundant at 1, 2 and 6 dpi. On the other hand, ACTB exhibited a decrease of abundance along the whole time course. According to Galan and Zhou [22] the *Salmonella* effector SipA binds to actin promoting a significant reduction in the concentration of its monomeric conformation. In addition, SipA increases the stability of actin bundles by modulating plastin actin-bundling activity [26]. Interestingly, we observed that L-plastin was more abundant in the beginning of infection and this result could consist in another evidence of SipA activity in MLN.

In the same way of ACTB, VIM, one of the constituents of cytoskeletal intermediate filaments (IF) network, exhibited a decrease of abundance after infection. Moreover, immunohistochemistry assays revealed that this protein was evidently accumulated in cells which morphology and localization in tissue were equivalent to *Salmonella* infected phagocytes. Protective IF cages similar to those composed by F-actin also coalesce around *Salmonella*-containing vacuoles [27]. Assembly of both proteins during *Salmonella* intracellular replication is reported to be interdependent and disruption of either leads to release of bacteria in the cytoplasm [28]. Moreover, annexin A1 (ANXA1), which was initially related to anti-inflammatory functions [29], appears to be involved in controlling association of F-actin with phagosomes thereby affecting phagosome formation. ANXA1 binds to, bundles and colocalizes with F-actin during phagocytic cup formation and on mature phagosomes [30]. Intriguingly, this protein exhibited the most prominent increase of abundance in the porcine MLN after infection. Thus, the uncovered reduction of monomeric forms of actin and vimentin as well as the augment of PDLIM1 and ANXA1 in MLN probably causes rearrangements in the cytoskeleton of infected cells that are necessary for phagosome formation and *Salmonella* replication. Triggering of GTPase activity in MLN was also disclosed by the abundance increase of GTP-binding nuclear protein Ran (RAN), found in this study. RAN is a major regulator of nucleocytoplasmic transport, controlling its rate and directionality by cycling between inactive (GDP-bound) and active (GTP-bound) conformations [31]. Recent studies assert that RAN is noticeably upregulated in fish after viral or bacterial infection [32] and its activity is associated to the enhancement of phagocytosis [31]. Evidences in mammals demonstrate that RAN is also involved in LPS endotoxin response [33] and nuclear import of STAT3 [34]. The increase of RAN abundance observed in this study could consist in a GTPase response carried out by the host against *S. typhimurium*. However, the role of this protein in *Salmonella* infections has not been elucidated so far.

In addition to cytoskeleton rearrangements, *S. typhimurium* infection induced cell death mechanisms, which in combination to the inflammatory cell infiltration observed in our study, could point toward the occurrence of pyroptosis in porcine MLN. Pyroptosis is a CASP1 dependent inflammatory form of cell death induced by *Salmonella* and other intracellular microorganisms that is characterized by the release of potent mediators of inflammation such as IL1b and IL18 [35]. Although our proteomic study did not allow for an observation of the changes in CASP1, we do see it at mRNA level at 2 dpi accompanied by a high increase of IL1b gene expression (Fig. 4). In agreement with that finding, functional analysis of the proteomic results disclosed an enrichment of the mitogen-activated protein kinase (MAPK) signaling pathway upon infection (Table 3), additionally verified by mRNA quantification of the downstream pro-inflammatory chemokines CXCL2 and CXCL8, which were both up-regulated at 2 dpi. These results represent a further indication of pyroptosis induction, since the production of pro-inflammatory cytokines is carried out *via* activation of MAPK and consequent regulation of the transcription factors NF-κB and AP1 [22,36].

Although pyroptosis represents an important innate immune effector mechanism against intracellular bacteria, *Salmonella* has developed strategies to overcome it [37,38]. Apparently, this pathogen voids pyroptosis effectiveness by delaying its onset and infecting new macrophages after escaping from lysed cells [35]. However, released bacteria should be able to survive to neutrophil uptake and killing by reactive oxygen species, in order to re-infect cells and maintain their replicative cycle in tissue [38]. Intriguingly, our results indicate that *Salmonella* burden in MLN was reduced along infection. This is probably related to the strong infiltration of phagocytic cells observed at 2 dpi that could be causing the substantial decrease of *S. typhimurium* labeling in tissue at 6 dpi. In addition, we observed an enrichment of the anti-apoptosis process after infection. Although the role of each protein associated to this mechanism is unknown for us, we speculate that apoptosis is avoided by swine, hampering cell-to-cell spread of bacteria through subsequent rounds of macrophage infection. Therefore, our results could demonstrate that in spite of manipulating host machinery, *S. typhimurium* is not able to effectively evade the porcine MLN response. Nevertheless, the presence of live *S. typhimurium* in tissue at 6 dpi (data not shown) reinforces the hypothesis that this pathogen develops some mechanism to maintain itself in MLN at low levels. Further research will be necessary to bring significant insight into how and how long *S. typhimurium* persists in porcine MLN after infection.

Changes in proteins related to the modulation of host second line of defense were also identified after infection. Thus, we uncovered an increase in abundance of proteins involved in different steps of the antigen processing and presenting pathway (Table 3). Strikingly, these proteins exhibited similar quantitative changes, being all of them more abundant at 2 dpi, when *S. typhimurium* and proteome changes were more evident. Additionally, activation of T-cells was also deduced by the increase in mRNA levels of IFNγ (see Fig. 4), a cytokine that promotes Th1 differentiation leading to cellular immunity. Therefore, our data suggest

that the process of antigen presentation properly functions in porcine MLN after *S. typhimurium* infection.

It is known that antigenic peptides presented by MHC-I are produced through cytosolic degradation of intracellular proteins by proteasome [39]. Otherwise, presentation of exogenous antigens has been classically attributed to MHC class II [40]. Additionally, the term *cross-presentation* was introduced as an alternative mechanism to define a process in which antigens acquired from the extracellular environment are present by antigen-presenting cells (APCs) to CD8+ T cells *via* their own MHC-I molecules [41]. Interestingly, this mechanism could explain the clear indications of adaptive immunity induction *via* MHC-I which is derived from the proteomic results obtained in our work. Since *Salmonella* is confined in host cell inside phagosomes, its antigens theoretically would be protected from cytosolic degradation by proteasome, unless the phagosome is a competent organelle for antigen cross-presentation as has been previously stated by Houde et al. [42]. In this alternative scenario, phagocytosed proteins reach cytosol by chaperone retrotranslocation mechanisms, subsequently degradated by proteasomes located in the cytoplasmic side of phagosomes and then, the generated peptides gain access to the phagosome lumen *via* TAP, bind MHC-I molecules and activate CD8+ T-cells [40,42]. Transcriptomic analysis carried out by us (Martins et al., unpublished data) highlighted the upregulation of TAP and MHC-I mRNA in MLN of *S. typhimurium* infected pigs. In the proteomic study present here, HSP90 and other three chaperones associated with degradation and retrotranslocation of proteins to cytosol (HSP70, BiP/HSPA5 and BRp57/PDIA) [43] were detected at higher levels in infected samples. Also, the proteasome subunit beta type-8 (PSMB8 or LMP7) was also found to be more abundant in MLN after infection. The hydrolyzing activities of proteasomes are conferred upon stimulation of cells with IFNγ [39]. This process results in the replacement of its 20S core subunits by LMP2 (iβ1), MECL1 (iβ2) and LMP7 (iβ5), constituting the so-called immunoproteasome [42]. In line with the direct activation/inhibition relationship between IFNγ and PSMB8 depicted in network 3 (see Supplementary data file 3) and the previously referred reports [39,41], we found out that the highest levels of PSMB8 in tissue is coinciding with the increase of IFNγ mRNA at 2 dpi. Since proteasomal activity is dependent on the ubiquitination of its targets [41], the significant enrichment of the "Protein ubiquitination pathway" uncovered by IPA analysis gives an additional evidence of the enhancement of protein degradation by immunoproteasome as a result of infection.

In conclusion, our results suggest that, in spite of modulating normal host functions and replicating intracellularly, *S. typhimurium* fails to effectively damper immune response elements during infections in pigs. The proteome response of porcine MLN to infection was associated to the induction of innate immunity processes such as phagocyte infiltration and pyroptosis. Moreover, we could infer that *S. typhimurium* antigens are cross-presented *via* MHC-I in a proteasome-dependent manner and this mechanism probably triggers an early cytotoxic response against bacteria. Although both innate and adaptive immune responses might control pathogen dissemination, further research will be necessary to elucidate the strategies exploited by *S. typhimurium* to establish the asymptomatic-carrier state in swine infections.

Supplementary material related to this article can be found online at doi:10.1016/j.jprot.2012.03.045.

Acknowledgments

We thank Erena Ruiz-Mora and Reyes Alvarez for skilful technical assistance. This research was supported by EU funds provided by EADGENE and SABRE Projects, by the Excellence Project of the Junta de Andalucía Government P07-AGR-02672 and by the National R&D Program of the Spanish Ministry of Science and Innovation (grants AGL2008-00400 and AGL2011-28904). Right to use AU and IPA bioinformatic tools was granted by the Andalusian Platform of Bioinformatics (University of Málaga, Spain). RPM is a predoctoral researcher supported by the FPU Research Program of the Spanish Ministry of Education.

Additional information

Additional MS/MS information is available in http://www.uco.es/servicios/scai/id_proteomics.html.

REFERENCES

[1] Fosse J, Seegers H, Magras C. Prevalence and risk factors for bacterial food-borne zoonotic hazards in slaughter pigs: a review. Zoonosis Public Health 2009;56:429–54.
[2] Methner U, Rammler N, Fehlhaber K, Rösler U. *Salmonella* status of pigs at slaughter — bacteriological and serological analysis. Int J Food Microbiol 2011;151:15–20.
[3] Foley SL, Lynne AM, Nayak R. *Salmonella* challenges: prevalence in swine and poultry and potential pathogenicity of such isolates. J Anim Sci 2008;86:E149–62.
[4] Anon. The European Union summary report on trends and sources of zoonoses, zoonotic agents and food-borne outbreaks in 2009. EFSA J 2011;9:1–378.
[5] Boyen F, Haesebrouck F, Maes D, Van Immerseel F, Ducatelle R, Pasmans F. Non-typhoidal *Salmonella* infections in pigs: a closer look at epidemiology, pathogenesis and control. Vet Microbiol 2008;130:1–19.
[6] Bearson BL, Bearson SMD. Host specific differences alter the requirement for certain *Salmonella* genes during swine colonization. Vet Microbiol 2011;150:215–9.
[7] Bendixen E, Danielsen M, Larsen K, Bendixen C. Advances in porcine genomics and proteomics — a toolbox for developing the pig as a model organism for molecular biomedical research. Brief Funct Genomics 2010;9:208–19.
[8] Zhang CG, Chromy BA, McCutchen-Maloney SL. Host–pathogen interactions: a proteomic view. Expert Rev Proteomics 2005;2:187–202.
[9] Hartlova A, Krocova Z, Cerveny L, Stulik J. A proteomic view of the host–pathogen interaction: the host perspective. Proteomics 2011;11:3212–20.
[10] Collado-Romero M, Arce C, Ramírez-Boo M, Carvajal A, Garrido JJ. Quantitative analysis of the immune response upon *Salmonella typhimurium* infection along the porcine intestinal gut. Vet Res 2010;41:23.
[11] Sechi S, Chait BT. Modification of cysteine residues by alkylation. A tool in peptide mapping and protein identification. Anal Chem 1998;70:5150–8.
[12] Yubero N, Jiménez-Marín A, Barbancho M, Garrido JJ. Two cDNAs coding for the porcine CD51 (α_V integrin subunit: cloning, expression analysis, adhesion assays and chromosomal localization. Gene 2011;481:29–40.

[13] Bullido R, Gomez del Moral M, Alonso F, Ezquerra A, Zapata A, Sánchez C, et al. Monoclonal antibodies specific for porcine monocytes/macrophages: macrophage heterogeneity in the pig evidenced by the expression of surface antigens. Tissue Antigens 1997;49:403–13.
[14] Livak KJ, Schmittgen TD. Analysis of relative gene expression data using real-time quantitative PCR and the $2^{-\Delta\Delta CT}$ method. Methods 2001;25:402–8.
[15] Vandesompele J, De Preter K, Pattyn F, Poppe B, Van Roy N, De Paepe A, et al. Accurate normalization of real-time quantitative RT-PCR data by geometric averaging of multiple internal control genes. Genome Biol 2002;3:1–12.
[16] Willems E, Leyns L, Vandesompele J. Standardization of real-time PCR gene expression data from independent biological replicates. Anal Biochem 2008;379:127–9.
[17] Paulin SM, Jagannathan A, Campbell J, Wallis TS, Stevens MP. Net replication of *Salmonella* enterica serovars Typhimurium and Choleraesuis in porcine intestinal mucosa and nodes is associated with their differential virulence. Infect Immun 2007;75:3950–60.
[18] Bueno SM, Wozniak A, Leiva ED, Riquelme SA, Carreño LJ, Hardt W-D, et al. *Salmonella* pathogenicity island 1 differentially modulates bacterial entry to dendritic and non-phagocytic cells. Immunology 2010;130:273–87.
[19] Haimovich B, Venkatesan MM. *Shigella* and *Salmonella*: death as a means of survival. Microbes Infect 2006;8: 568–77.
[20] Pizarro-Cerda J, Cossart P. Bacterial adhesion and entry into host cells. Cell 2006;124:715–27.
[21] Malik-Kale P, Jolly CE, Lathrop S, Winfree S, Luterbach C, Steele-Mortimer O. *Salmonella* — at home in the host cell. Front Microbiol 2011;2:125.
[22] Galán JE, Zhou D. Striking a balance: modulation of the actin cytoskeleton by *Salmonella*. Proc Natl Acad Sci USA 2000;97: 8754–61.
[23] DerMardirossian C, Bokoch GM. GDIs: central regulatory molecules in Rho GTPase activation. Trends Cell Biol 2005;15: 356–63.
[24] Holden DW. Trafficking of the *Salmonella* vacuole in macrophages. Traffic 2002;3:161–9.
[25] te Velthuis AJW, Isogai T, Gerrits L, Bagowski CP. Insights into the molecular evolution of the PDZ/LIM family and identification of a novel conserved protein motif. PLoS One 2007;2:e189.
[26] Silva CV, Cruz L, Araújo NS, Angeloni MB, Fonseca BB, Gomes AO, et al. A glance at *Listeria* and *Salmonella* cell invasion: different strategies to promote host actin polymerization. Int J Med Microbiol 2012;302:19–32.
[27] Guignot J, Servin AL. Maintenance of the *Salmonella*-containing vacuole in the juxtanuclear area: a role for intermediate filaments. Microb Pathog 2008;45:415–22.
[28] Haglund CM, Welch MD. Pathogens and polymers: microbe–host interactions illuminate the cytoskeleton. J Cell Biol 2011;195:7–17.
[29] Parente L, Solito E. Annexin 1: more than an anti-phospholipase protein. Inflamm Res 2004;53:125–32.
[30] Patel DM, Ahmad SF, Weiss DG, Gerke V, Kuznetsov SA. Annexin A1 is a new functional linker between actin filaments and phagosomes during phagocytosis. J Cell Sci 2011;124:578–88.
[31] Zhao Z, Jiang C, Zhang X. Effects of immunostimulants targeting Ran GTPase on phagocytosis against virus infection in shrimp. Fish Shellfish Immunol 2011;31:1013–8.
[32] Han F, Wang XQ, Yao CL, Wang ZY. Molecular characterization of Ran gene up-regulated in large yellow croaker (*Pseudosciaena crocea*) immunity. Fish Shellfish Immunol 2010;29:327–33.
[33] Kang AD, Wong PM, Chen H, Castagna R, Chung SW, Sultzer BM. Restoration of lipopolysaccharide-mediated B-cell response after expression of a cDNA encoding a GTP-binding protein. Infect Immun 1996;64:4612–7.
[34] Cimica V, Chen HC, Iyer JK, Reich NC. Dynamics of the STAT3 transcription factor: nuclear import dependent on Ran and importin-β1. PLoS One 2011;6:e20188.
[35] Miao EA, Rajan JV. *Salmonella* and caspase-1: a complex interplay of detection and evasion. Front Microbiol 2011;2:85.
[36] Broz P, Monack DM. Molecular mechanisms of inflammasome activation during microbial infections. Immunol Rev 2011;243:174–90.
[37] Guiney DG, Fierer J. The role of the spv genes in *Salmonella* pathogenesis. Front Microbiol 2011;2:129.
[38] Miao EA, Leaf IA, Treuting PM, Mao DP, Dors M, Sarkar A, et al. Caspase-1-induced pyroptosis is an innate immune effector mechanism against intracellular bacteria. Nat Immunol 2010;11:1136–42.
[39] Kloetzel PM, Ossendorp F. Proteasome and peptidase function in MHC-class-I-mediated antigen presentation. Curr Opin Immunol 2004;16:76–81.
[40] Cresswell P, Ackerman AL, Giodini A, Peaper DR, Wearsch PA. Mechanisms of MHC class I-restricted antigen processing and cross-presentation. Immunol Rev 2005;207:145–57.
[41] Lattanzi L, Rozera C, Marescotti D, D'Agostino G, Santodonato L, Cellini S, et al. IFNγ boosts epitope cross-presentation by dendritic cells via modulation of proteasome activity. Immunobiology 2011;216:537–47.
[42] Houde M, Bertholet S, Gagnon E, Brunet S, Goyette G, Laplante A, et al. Phagosomes are competent organelles for antigen cross-presentation. Nature 2003;425:402–6.
[43] Imai T, Kato Y, Kajiwara C, Mizukami S, Ishige I, Ichiyanagi T, et al. Heat shock protein 90 (HSP90) contributes to cytosolic translocation of extracellular antigen for cross-presentation by dendritic cells. Proc Natl Acad Sci USA 2011;108:16363–8.

Martins et al. Veterinary Research 2013, 44:120
http://www.veterinaryresearch.org/content/44/1/120

VETERINARY RESEARCH

RESEARCH Open Access

Pyroptosis and adaptive immunity mechanisms are promptly engendered in mesenteric lymph-nodes during pig infections with *Salmonella enterica* serovar Typhimurium

Rodrigo Prado Martins[1], Carmen Aguilar[1], James E Graham[2], Ana Carvajal[3], Rocío Bautista[4], M Gonzalo Claros[4] and Juan J Garrido[1*]

Abstract

In this study, we explored the transcriptional response and the morphological changes occurring in porcine mesenteric lymph-nodes (MLN) along a time course of 1, 2 and 6 days post infection (dpi) with *Salmonella* Typhimurium. Additionally, we analysed the expression of some *Salmonella* effectors in tissue to complete our view of the processes triggered in these organs upon infection. The results indicate that besides dampening apoptosis, swine take advantage of the flagellin and prgJ expression by *Salmonella* Typhimuriun to induce pyroptosis in MLN, preventing bacterial dissemination. Furthermore, cross-presentation of *Salmonella* antigens was inferred as a mechanism that results in a rapid clearance of pathogen by cytotoxic T cells. In summary, although the *Salmonella* Typhimurium strain employed in this study was able to express some of its major virulence effectors in porcine MLN, a combination of early innate and adaptive immunity mechanisms might overcome virulence strategies employed by the pathogen, enabling the host to protect itself against bacterial spread beyond gut-associated lymph-nodes. Interestingly, we deduced that clathrin-mediated endocytosis could contribute to mechanisms of pathogen virulence and/or host defence in MLN of *Salmonella* infected swine. Taken together, our results are useful for a better understanding of the critical protective mechanisms against *Salmonella* that occur in porcine MLN to prevent the spread of infection beyond the intestine.

Introduction

Infections by *Salmonella* are a major health problem in the developing and developed world. In the European Union, despite the current decreasing trend of human cases, *Salmonella* persists as the main cause of food-borne outbreaks [1]. Pork is considered to be a significant source of *Salmonella* to humans next to eggs and poultry meat [2]. Indeed, according to the European food safety authority (EFSA), *Salmonella enterica* serovar Typhimurium (herein *Salmonella* Typhimurium) is the second serovar most frequently reported in human salmonellosis and infection by this pathogen is mostly associated with the consumption of contaminated pork [1].

Since the food industry and direct contact with infected animals represent the main sources of non-typhoid *Salmonella* [3], prevention of human salmonellosis depends significantly on decreasing the prevalence of infection in livestock hosts [4]. *Salmonella* Typhimurium infected pigs generally carry this serotype asymptomatically in the tonsils, intestines and gut-associated lymphoid tissue, posing an important threat to animal and human health [5]. Epidemiological studies assert that *Salmonella* prevalence in slaughter swine lymph nodes varies widely at the country level, ranging from0 to 29% [2]. Although salmonellosis in pigs has been the subject of intensive research [5], a thorough knowledge of the pathogenesis of porcine infections with broadhost range *Salmonella* serotypes is still necessary. A combination of

* Correspondence: ge1gapaj@uco.es
[1]Grupo de Genómica y Mejora Animal, Departamento de Genética, Facultad de Veterinaria, Universidad de Córdoba, Campus de Rabanales, Edificio Gregor Mendel C5, 14071, Córdoba, Spain
Full list of author information is available at the end of the article

system-wide approaches and in vivo infection models is expected to generate precise and novel data to analyze the response to *Salmonella* infections in pigs [6]. Thus, whole-genome expression analysis has been used to explore gene expression changes during infection of pigs by *Salmonella*, contributing to identify molecules and pathways associated with the host response to infection [7,8]. More recently, proteomic techniques have also been employed as a step towards a detailed understanding of the disease mechanisms [9,10]. However, despite this, there is a need to deepen understanding of the biological processes that control host-pathogen interaction and *Salmonella* persistence in porcine lymphatic tissue, which could provide new targets for treatment and control of salmonellosis in this species. Therefore, the objective of the current study was to explore the early transcriptional response of porcine mesenteric lymph-nodes (MLN) to *Salmonella* Typhimurim using a time-course analysis of an in vivo infection. In addition, the expression of some pathogen virulence effectors, as well as the morphological alterations associated with the presence of the bacteria in the tissue were also evaluated.

Materials and methods

Experimental infection and tissue sampling

Sixteen crossbred weaned piglets of approximately four weeks of age, serologically and fecal-negative for *Salmonella* were used in an experimental infection described elsewhere [11]. Briefly, twelve piglets were orally infected with 10^8 cfu of a *Salmonella* Typhimurium phagetype DT104 strain isolated from a naturally infected pig [11], whereas the control group (4 animals) received sterile medium. Non-infected control pigs were necropsied prior to the experimental infection (0 day post-infection – dpi) and four randomly chosen infected piglets were necropsied at 1, 2 or 6 dpi. Samples of MLN were collected from all experimental animals and immediately frozen in liquid nitrogen for RNA and protein isolation or fixed in 10% neutral buffered formalin for histological processing. All procedures involving animals were performed in accordance with the European regulations regarding the protection of animals used for experimental and other scientific purposes. Piglets were housed in experimental isolation facilities of the University of Leon (Spain). Animal care and procedures were in accordance with the guidelines of the Good Experimental Practices (GEP), under the supervision of the Ethical and Animal Welfare Committee of the University of Leon (Spain).

RNA purification

After treatment with RNAlater-ICE (Ambion, Inc, Austin, TX, USA), MLN samples were soaked in RLT buffer (Qiagen, Valencia, CA, USA) and disrupted in a rotor-stator homogenizer. RNA was isolated using the AllPrep DNA/RNA/Protein Mini Kit (Qiagen), digested with the RNase-Free DNase Set (Qiagen) according to the manufacturer's instructions and routinely precipitated with ethanol. RNA integrity was evaluated using the Experion RNA automated electrophoresis system (Bio-Rad, Hercules, CA, USA) before being quantified using a ND-1000 spectrophotometer (Nanodrop Technologies, Wilminton, USA).

Microarray analysis

Gene expression analysis was carried out using the GeneChip Porcine Genome Array of the Affymetrix platform (Affymetrix Inc., Santa Clara, CA, USA) at the Genomics Unit of CABIMER (Andalusian Center for Molecular Biology and Regenerative Medicine, Seville, Spain). This chip contains 23 937 probe sets to interrogate 23 256 transcripts in the pig, which represents 20 201 genes. The One-Cycle Eukaryotic Target Labeling Assay was used to obtain biotinylated cRNA to be used in the subsequent chip hybridization according to the manufacturer's instructions (Expression Analysis Technical Manual, Affymetrix). The biotinylated cRNA targets were then cleaned up, fragmented, and hybridized with the GeneChip Porcine Genome Array following Affymetrix recommended protocols. Chips were washed, stained with a GeneChip Fluidics Station 450 (Affymetrix) using the standard fluidics protocol and scanned with an Affymetrix GeneChip Scanner 3000 (Affymetrix). Probe signal intensities were captured and processed with the GeneChip Operating Software 1.4.0.036 (Affymetrix) and the resulting CEL files were reprocessed using robust multi-array average normalization (RMA) [12]. Because the aim of analysis was to detect changes in gene expression along a time-course of infection, differentially expressed (DE) genes were accessed by the BATS (Bayesian Analysis of Time Series) software package [13], using default settings. A Bayes Factor (BF) value of 0.05 was used as cutoff to rank significantly regulated transcripts. Since the Affymetrix Porcine GeneChip is not fully annotated in all the features, it was re-annotated with Blast2GO [14] with a minimum E-value of 10^{-10} and a minimum similarity of 50%.

Systems biology analysis

The list of genes that showed significant changes in expression was uploaded into Ingenuity Pathway Analysis (IPA, Ingenuity Systems Inc, Redwood City, CA, USA) [15] for bioinformatics analysis. Additionally, the DAVID Bioinformatic Database [16] was used applying the default settings to refine some data from IPA analysis. Gene interaction networks were automatically generated, ranked by score and depicted on IPA as follows: each

node in the network diagram represented a gene and its relationship with other molecules was represented by a line (solid and dotted lines represent direct and indirect association respectively). Nodes with a red background were input genes detected in this study while grey nodes were molecules inserted by IPA based upon the Ingenuity Knowledge Base to produce a highly connected network. The score estimated the probability that a collection of genes equal to or greater than the number in a network could be achieved by chance alone. Scores of 3 or higher were considered to have a 99.9% confidence of not being generated by random chance alone. For statistical analysis of enriched functions/pathways, an IPA Knowledge Base was used as a reference set and the Fisher's exact test was employed to estimate the significance of association. *P*-values below 0.05 were considered statistically significant. For graphical representation of the canonical pathways, the ratio indicates the percentage of genes taking part in a pathway that could be found in an uploaded data set and –log(*p*-value) means the level of confidence of association. The threshold line represented a *p*-value of 0.05.

Relative gene expression analysis by qPCR

Real-time quantitative PCR (qPCR) assays were performed as previously described [11]. Fold change values were calculated by the $2^{-\Delta\Delta Cq}$ method [17] using beta-actin as the reference gene. Afterwards, data were standardized as proposed by Willems et al. [18] and analyzed by Kruskal–Wallis and Mann–Whitney tests using the software SPSS 15.0 for Windows (SPSS Inc, Chicago, IL, USA). Fold changes of 1 denoted no change in gene expression. Values lower and higher than 1 denoted down and up-regulation respectively. To be represented in Table 1, a fold change of down-regulated genes was calculated as $-1/2^{-\Delta\Delta Cq}$. Primer pairs used for amplifications can be found as supporting information (see Additional file 1).

Western blot analysis

For protein extractions, MLN samples from all experimental animals were separately homogenized on ice with lysis buffer (7 M urea, 2 M thiourea, 4% w/v CHAPS, 0.5 mM PMSF) using a glass tissue-lyser and protein lysate concentration was determined using a Bradford Protein Assay (Bio-Rad). Subsequently, protein from individual replicates belonging to the same group was pooled (30 ug total), electrophoretically fractionated in 12% (w/v) SDS-PAGE gels and transferred onto a PVDF membrane (Millipore, Bedford, MA, USA). Western blot assays were carried out as described by Martins et al. [10] employing the following primary antibodies: 4B7/8 for swine histocompatibility class I antigen (SLAI) detection [19], 1 F12 for swine histocompatibility class II antigen (SLAII) detection [19], anti-CTLA4 (Epitomics, Burlingame, CA, USA) and anti-Clathrin light chain (ab24579, Abcam, Cambridge, UK). To confirm equal sample loading, membranes were reblotted with anti-GAPDH monoclonal antibody (GenScript, Picastaway, NJ, USA) and no statistical differences for GAPDH abundance were observed between groups in all assays. Membranes were scanned in an FLA-5100 imager

Table 1 Microarray data validation by qPCR.

Gene	MICROARRAY				qPCR			
	Fold change			BF	Fold change			*p*-value
	1 dpi	2 dpi	6 dpi		1 dpi	2 dpi	6 dpi	
CD180	1.7	2.6	1.5	0.0000429	1.1	1.8	1.2	0.010
CD1A	1.1	−1.4	1.2	0.00047793	−1.4	−2.5	1.2	0.013
DAB2	−1.2	−2.6	−1.2	6.62E-13	−3.1	−6.5	−2.6	0.001
EIF4H	−1.1	−1.1	−1.1	0.0000101	−1.5	−1.4	−1.8	0.021
ENPP6	1.3	2.0	−1.2	0.0000448	1.2	1.8	−1.7	0.000
F13A1	1.4	2.2	−1.1	0.00000227	1	1.7	−2.2	0.012
HLA-B[b]	1.0	−1.1	−1.2	0.00023747	−1.4	−1.4	−1.9	0.047
HLA-DRB5[b]	1.0	−1.1	1.0	0.0000311	−1.4	−1.6	−2	0.036
HSPA1B[a]	3.3	1.4	−1.1	0.0001166	2.5	1.4	−1.3	0.025
HSPH1	2.3	1.7	−1.0	0.00000424	1.5	1.1	−2	0.003
IL16	−1.0	−1.2	−1.1	8.12E-07	1	−1.1	−1.5	0.035
LPCAT2	1.2	2.3	1.0	0.0000146	1.4	2	−1.3	0.010
PSMC2	−1.0	−1.0	−1.1	0.00105861	−1.1	−1.4	−1.8	0.036
TRAC	−1.0	−1.1	−1.1	0.00000951	−1.5	−1.8	−1.8	0.010

[a]Data from microarray analysis are mean values from two different probes. [b]Amplified with SLA-B and SLA-DRB5 primers.

(Fujifilm, Tokyo, Japan) and signal intensity was determined using Multigauge software (Fujifilm, Tokyo, Japan) as previously described [10].

Histopathology, immunohistochemistry and confocal microscopy analysis

Paraffin sections (5 μm) of formalin fixed samples were routinely processed and stained with hematoxylin and eosin (H&E) to evaluate tissue morphology. For immunohistochemistry assays, a standard avidin-biotin peroxidase method was performed as described elsewhere [20] employing 1 F12 monoclonal antibody and a biotinylated anti-mouse Ig (Dako, Barcelona, Spain) as a secondary antibody. Immunofluorescence using confocal microscopy was performed employing the anti-SLAII 1 F12 monoclonal antibody, a rabbit polyclonal antibody against the *Salmonella* somatic (O4, 5, 12) antigen [10] and a rabbit polyclonal antibody anti-*Salmonella* Typhimurium flagellin [21]. Fluorescein isothiocyanate (FITC)-conjugated goat anti-rabbit IgG (Sigma-Aldrich, St. Louis, MO, USA) and Alexa Fluor 594 anti-mouse IgG (Life Technologies, Carlsbad, CA, USA) were used as secondary antibodies. Immunostaining was performed as described by Robertson et al. [22]. Briefly, deparaffinized sections of formalin fixed MLN were blocked for 30 min with 1% bovine serum albumin and 2% foetal calf serum in PBS. Then, sections were incubated overnight at 4 °C with primary antibodies, washed three times with PBS for 5 min and incubated for 1 h at 37 °C with fluorescent secondary antibodies. For negative controls, primary antibody was omitted. Finally, sections were washed three times for 5 min in PBS containing 1.43 μM 4′,6-diamidino-2-phenylindole (DAPI, Life Technologies). Samples were subsequently evaluated and imaged using an LSM 5 Exciter confocal microscope (Carl Zeiss, Jena, Germany).

Cell death analysis

Formalin fixed MLN samples were evaluated for cell death by terminal deoxynucleotidyl transferase dUTP nick end labeling (TUNEL), employing the TUNEL Apoptosis Detection Kit for Paraffin-embedded Tissue Sections (GenScript, Picastaway, NJ, USA) according to the manufacturer's instructions. Briefly, proteinase K treated samples were permeabilized with 0.1% Triton X-100 and 0.1% sodium citrate for 10 min and incubated with Blocking Solution II (GenScript) for 30 min. Subsequently, tissues were covered with 50 μL of TUNEL Reaction Mixture (GenScript), incubated at 37 °C for 1 h in a dark humidified chamber and washed in PBS. Sections were examined in an LSM 5 Exciter confocal microscope (Carl Zeiss MicroImaging GmbH, Jena, Germany) using excitation wave 450–500 nm and emission wave 515–565 nm (green). Fluorescence intensity was quantified with the ImageJ software 1.46r [23] and data were analyzed by ANOVA (p-value cutoff of 0.05) using SPSS 15.0 for Windows (SPSS Inc).

Selective capture of transcribed sequences (SCOTS)

Selective capture of *Salmonella* transcripts from MLN of pigs at 2 dpi was performed by the SCOTS method [24], following the procedure described by Sheikh et al. [25]. Briefly, 5 μg of total RNA from infected MLN samples was converted into first strand cDNA by using random priming and Superscript III reverse transcription (Life Technologies). Subsequently second strand cDNA was produced employing DNA polymerase I (Klenow fragment, Life Technologies). To create a corresponding in vitro *Salmonella* Typhimurium cDNA sample for comparison, the same bacterial isolate employed in the experimental infection was grown to early-log growth phase (OD_{600} = 0.3) and late-log growth phase (OD_{600} = 0.8) in Luria Bertani (LB) broth. Afterwards, *Salmonella* Typhimurium transcripts were selectively captured from in vivo and in vitro double stranded cDNA by hybridization to sonicated biotinylated genomic *Salmonella* DNA, which was previously blocked with *Salmonella* ribosomal DNA fragments. Microbial cDNA-genomic DNA hybrids were then captured by binding to streptavidin-coated beads (Dynabeads M-280 streptavidin, Invitrogen) and bacterial transcripts were eluted by alkaline denaturation. Eluted bacterial cDNA was then PCR-amplified with conserved primers and finally purified using Qiagen PCR column purification kit (Qiagen). After that, one round captured and purified cDNA from both in vitro and in vivo conditions were quantified by spectrophotometry and used as template (10 ng) for qPCR assays as described above. Primer pairs used for amplifications can be found as supporting information (see Additional file 2). Gene expression levels were estimated employing *gyrA* as the reference gene. Since tissue from uninfected pigs was negative for *Salmonella*, those samples could not be used as reference for fold change calculations of pathogen gene expresion. In addition, most screened genes showed Cq values inferior to those observed for *gyrA* in infected MLN. For these reasons, gene expression levels were alternatively estimated as follows: *gyrA* Cq – target gene Cq. Higher values meant higher expression levels and vice-versa.

Results

Transcriptional changes in porcine MLN upon *salmonella* Typhimurium infection and data validation

Microarray technology coupled to a Bayesian analysis was employed to explore the transcriptional response of porcine MLN to *Salmonella* Typhimurium along a time course of 1, 2 and 6 dpi. BATS, a method specifically designed for the analysis of time series microarray data

[10], revealed significant changes in expression (BF < 0.05) for 290 transcripts, representing 285 unique genes, as a result of the bacterial challenge (see Additional file 3). Then, to validate data, qPCR assays were performed on a panel of fourteen genes identified by BATS analysis. As expected, all of them were confirmed to be significantly regulated ($p < 0.05$) after infection (Table 1). Furthermore, an identical expression trend was observed for most screened genes by qPCR and microarray analysis.

Biological interpretation of microarray data

To translate microarray data into functional biological information, bioinformatics tools were employed to gain an insight into networks, functions and pathways associated with the transcriptomic response of porcine MLN to *Salmonella* Typhimurium (see Additional file 4). IPA analysis generated 17 gene interaction networks integrated by molecules associated with mechanisms such as cell-mediated immune response, cell-to-cell signaling and interaction, tissue morphology, cell movement and cell death. Networks 1 and 4 (Figure 1) revealed direct relationships between molecules taking part in five of the ten top enriched canonical pathways after infection (Figure 2). Moreover, network 4 demonstrated a central role for heat shock proteins and MHC encoding genes in the establishment of different mechanisms carried out in MLN in response to *Salmonella* Typhimurium. IPA also ascertained the enrichment of biological functions other than those identified by network analysis (Table 2). Thus, "Inflammatory disease" was the Ingenuity biofunction more significantly related to the differentially expressed genes, followed by "Protein synthesis" and "Antigen presentation".

Modulation of immune response mechanisms

Wide transcriptomic data analysis by bioinformatics tools revealed an enrichment of distinct mechanisms leading to immune response activation in porcine MLN upon *Salmonella* Typhimurium infection and depicted connections between them. As illustrated in Figure 3A, the association between "CTLA-4 signaling in cytotoxic T lymphocytes" and "Clathrin-mediated endocytosis signaling" pathways was established by the regulation of shared genes. Then, we checked the abundance level of cytotoxic T-lymphocyte-associated protein 4 (CTLA-4) and clathrin light chain A (CLTA) by Western blot, noting that CLTA was more abundant in infected animals whereas CTLA4 showed reduced levels after infection (Figure 3B). Since changes in *CTLA4* expression could not be detected by microarray analysis, we verified *CTLA4* mRNA levels by qPCR (Figure 3C). In accordance with Western blot assays, *CTLA4* was observed to be significantly down-regulated in infected animals at 1 and 6 dpi. Concerning *CLTA*, a similar trend towards up-regulation was observed at mRNA (Figure 3D) and protein levels.

System biology analysis also revealed the involvement of MHC encoding genes in many processes triggered in MLN in response to *Salmonella* Typhimurium. Thus, changes undergone by these molecules were evaluated employing different approaches. Firstly, Western blot analysis demonstrated that major histocompatibility antigens class I (MHCI) and class II (MHCII) were more abundant in tissue at 1 dpi (Figure 4A). Similarly, immunohistochemistry revealed higher MHCII expression at initial stages of infection, with increased levels of this molecule mainly detected in large irregularly-shaped mononuclear cells (Figure 4B-E). Then, confocal microscopy analysis uncovered the presence of *Salmonella* Typhimurium antigens in cells showing high levels of MHCII (Figure 4H-K), suggesting a connection between the increase of this receptor at the protein level and the presence of pathogen in tissue. Curiously, *MHCI* and *MHCII* (annotated in data sets as HLA-B and HLA-DRB, respectively) were found to be down-regulated by microarray analysis. Since these results were confirmed by qPCR (Figure 4F-G), a divergence between transcriptomic and proteomic changes could be highlighted for these molecules in infected MLN.

Tissue morphology and cell death

"Cell death" was one of the most significantly altered biological functions after infection and integrated the highest number of differentially expressed genes ($n = 78$). In order to find GO subcategories associated to genes implicated in this function, a data set arranged into "Cell death" by IPA was loaded into the DAVID Bioinformatic Database. As expected, enriched terms were related to cell proliferation, differentiation and death (see Additional file 5). Among them, processes such as "Negative regulation of apoptosis" and "Antiapoptosis" were found to be enriched all along the infection, suggesting an inhibition of apoptosis. To deepen and sharpen these results, TUNEL analysis followed by confocal microscopy was performed to elucidate the cell death mechanisms induced in MLN after *Salmonella* Typhimurium infection. As shown in Figure 5A-D and 5I, DNA damage detected by TUNEL staining peaked at 1 dpi and decreased at 2 and 6 dpi compared to controls. Afterwards, expression levels of *CASP1* and *CASP3*, the main pyroptosis and apoptosis inducers respectively, were quantified by qPCR. *CASP1* mRNA was significantly up-regulated at 2 dpi and down-regulated at 6 dpi (Figure 5J), whereas no significant changes were observed for *CASP3* (Figure 5K). Finally, lymph-node sections were H&E-stained to analyse the structural changes undergone by tissue as a consequence of infection (Figure 5E-H). Besides the loss of the typical lymph-node micro-architecture,

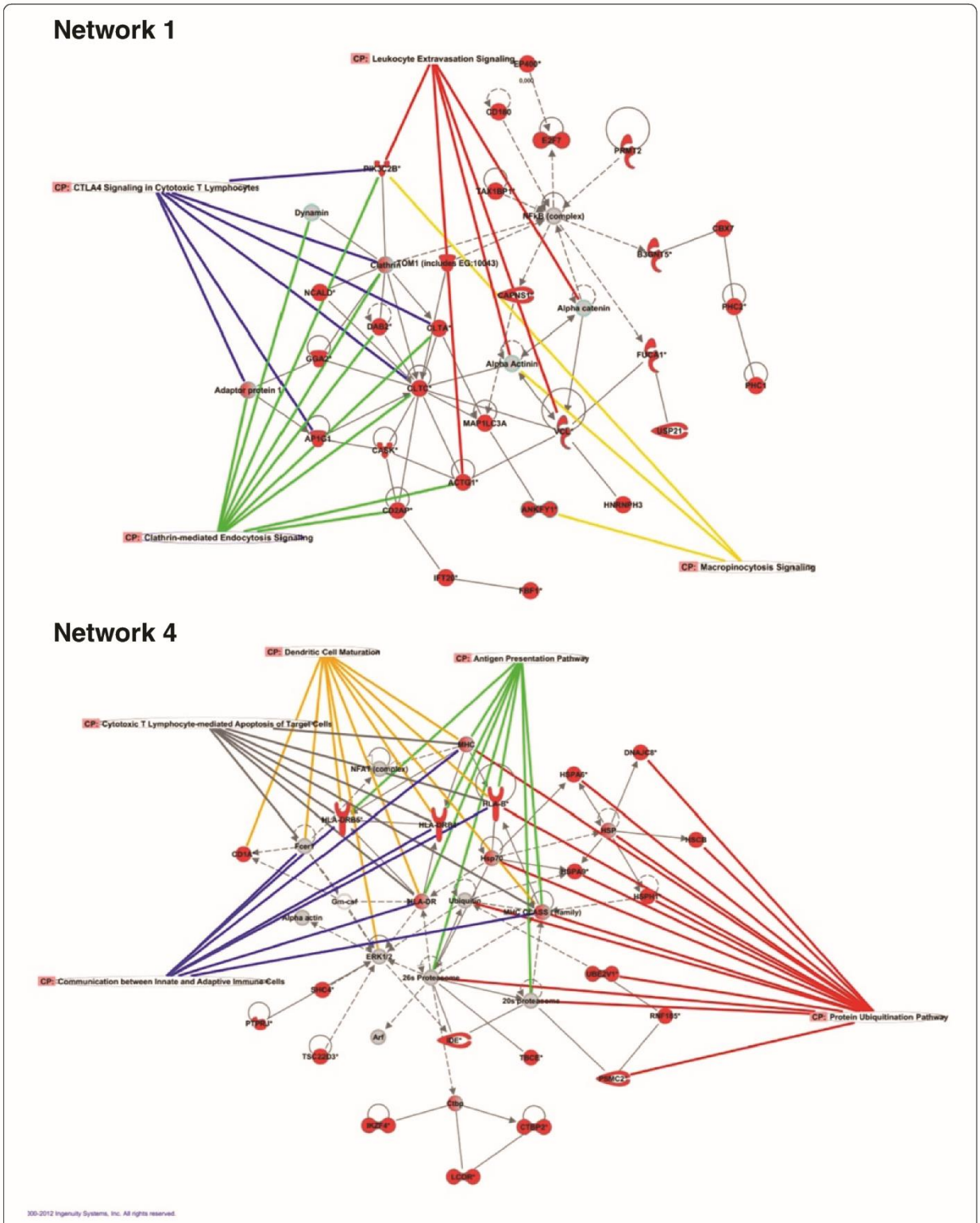

Figure 1 Gene network analysis by Ingenuity Pathway Analysis (IPA). Visual representation of networks 1 and 4. Red and grey nodes are input and IPA-inserted molecules respectively. Colored lines highlight genes that take part in an enriched Canonical Pathway.

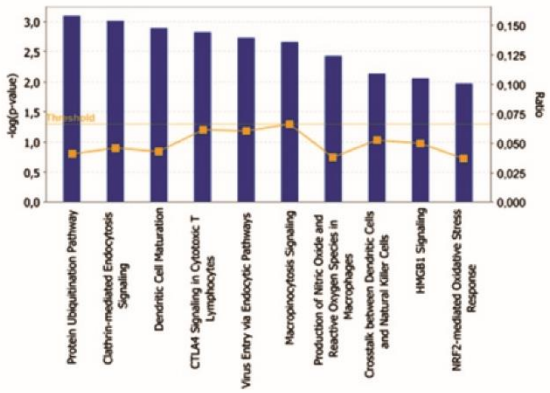

Figure 2 Top 10 enriched canonical pathways. Blue bars and yellow squares denote –log(*p*-value) and ratio respectively. Threshold line represents a *p*-value of 0.05.

phagocyte infiltration was the main alteration detected after infection, being observed mainly at 1 and 2 dpi.

Salmonella Typhimurium localization and gene expression in vivo

Salmonella Typhimurium was detected in MLN along the whole studied time course, with higher *Salmonella* levels being observed at 2 dpi (data not shown). Confocal microscopy analysis revealed two distinct bacterial populations according to location and labeling. As shown in Figure 4H-K and Figure 6A, some bacteria were labeled as spherical structures located in the perinuclear zone of mononuclear cells. In addition, regular bacilli shaped structures showing a different distribution were also detected (Figure 6B). Although Z-stack confocal images indicate that, most likely, this second population was found in an extracellular environment (see Additional file 6), further experiments will be necessary to clarify whether the pathogen is in the cytosol or outside the cell. Ultimately, expression of some *Salmonella* genes in vivo was also studied by the SCOTS approach and compared to in vitro conditions. Type III secretion systems (TTSS) encoded genes (*sopB, avrA, sifA, sseL and prgJ*) and *spvB* were found to be expressed by *Salmonella* Typhimurium in porcine MLN. Notably, lower expression of these genes was detected in vitro when compared to in vivo. The results regarding genes coding for flagella components and regulators show higher expression levels in vitro for *fliA, fliC* whereas *fljA* mRNA was observed to be more expressed in vivo (Figure 6C).

Table 2 Top five biological functions enriched in MLN of pigs infected with *Salmonella* Typhimurium.

Annotations	*p*-Value[a]	Input genes (n)
Inflammatory disease	4.64E-05 – 2.65E-02	13
Protein synthesis	6.52E-05 – 1.86E-02	32
Antigen presentation	1.8E-04 – 1.68E-02	5
Cell death	1.8E-04 – 2.67E-02	78
Cell-to-cell signaling and interaction	1.8E-04 – 2.67E-02	27

[a]*p*-values were calculated with the right-tailed Fisher's Test.

Discussion

Gut-associated lymphoid tissues have been proved to be an important niche for *Salmonella* during pig infections. Previous reports stated that *Salmonella* Typhimurium can be found in MLN of infected pigs from 2 h [5] up to 6 weeks after oral inoculation [26] and sustain these organs as immune inductive sites during pig salmonellosis [6,7,10,26,27]. For this reason, in this work we aimed at dissecting host response mechanisms occurring in porcine MLN upon interaction with *Salmonella* Typhimurium. Additionally, expression of some *Salmonella* virulence effectors was also analyzed in infected tissues attempting to integrate information from both the host and pathogen.

The systems biology analysis reported in this study demonstrates the involvement of MHC molecules in several mechanisms triggered in swine MLN after bacterial challenge. Intriguingly, both MHCI and MHCII encoding genes were found to be down-regulated all along the studied time course, in spite of the increased levels observed for these receptors at 1 dpi by Western blot and microscopic analysis. We envisage that initially, antigen presenting cells bearing high levels of MHC migrate to MLN leading to an increase of these receptors in tissue, as suggested by the detection of *Salmonella* antigens in cells showing high levels of MHCII. Subsequently, processes carried out in MLN might reduce MHC mRNA and protein expression levels at later times of infection. Previous studies demonstrate that *Salmonella* interferes with antigen presentation by reducing MHCII surface expression via a mechanism dependent on the *Salmonella* pathogenicity island (SPI)-2 encoded effector SifA [28-30]. It is noteworthy that in this study we show that *sifA* is expressed by *Salmonella* Typhimurium in porcine MLN. Besides, it has been previously observed by us [21] and others [27] that pig infections with *Salmonella* Typhimurium do not produce an up-regulation of cytokines involved in T helper 1 (Th1) response in MLN, on the contrary to previous reports in mice [31]. These findings could be related to the ability of pathogens to limit antigen presentation to CD4 restricted T cells by reducing MHCII levels in infected cells. *Salmonella* removes mature MHCII complexes from the cell surface by enhancing their ubiquitination in a clathrin and AP2-dependent way [29]. Curiously, we identified the "Protein ubiquitination pathway" and "Clathrin-mediated

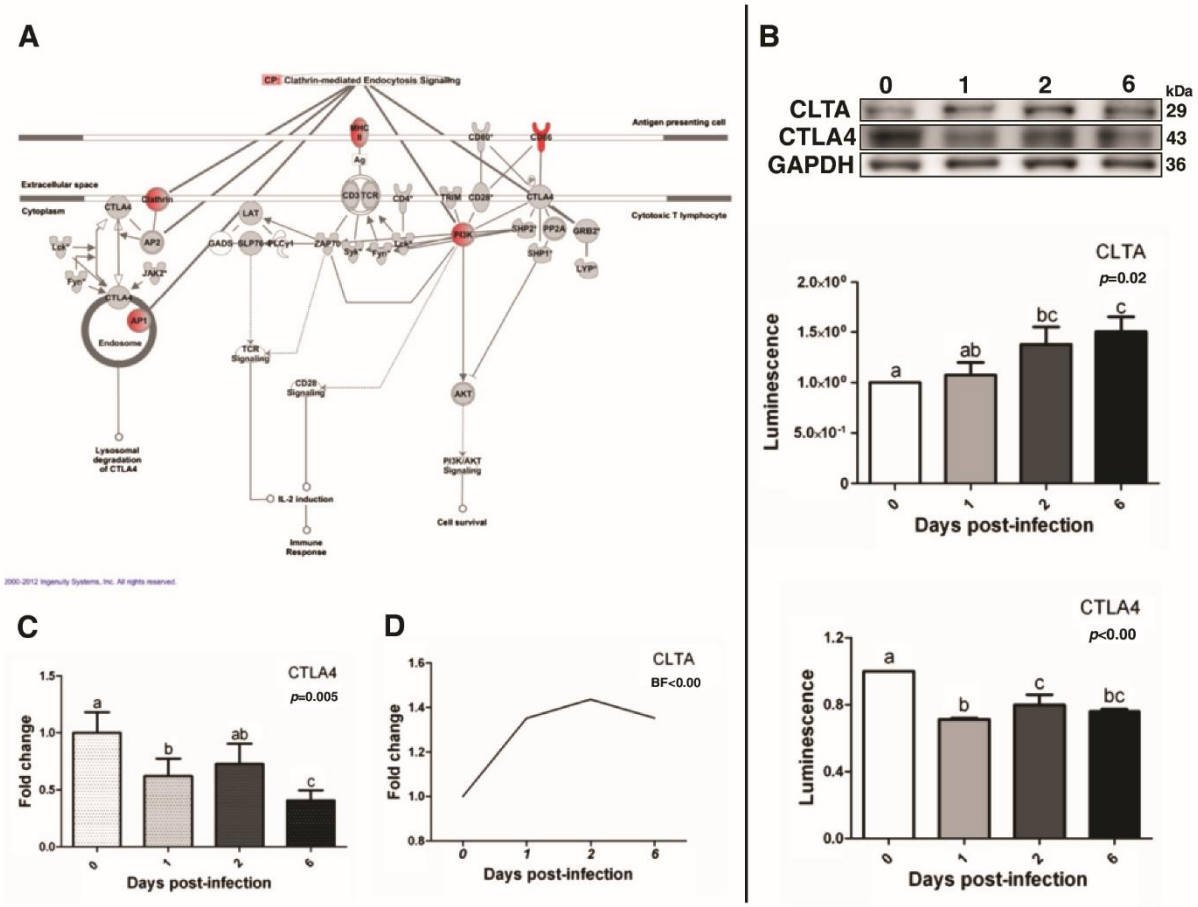

Figure 3 Interaction between CTLA-4 signaling in cytotoxic T lymphocytes and Clathrin-mediated endocytosis signaling pathways. A: visual representation of CTLA-4 signaling in cytotoxic T lymphocyte pathway stressing the regulation of molecules taking part in Clathrin-mediated endocytosis signaling. Red and grey nodes are input and IPA-inserted molecules respectively. **B**: Western blot analysis of CTLA4 and CLTA in MLN at 1, 2 and 6 dpi. **C**: mRNA quantification of *CTLA4* by qPCR. **D**: expression pattern of *CLTA* mRNA by microarray analysis.

endocytosis signaling" as the most significantly affected canonical pathways upon infection. In spite of the reported use of clathrin-mediated endocytosis in bacterial-induced internalization, *Salmonella* is not able to employ this machinery to invade [32]. So, instead of promoting direct entry of the pathogen to host cells, enrichment of clathrin-mediated endocytosis could be related to the modulation of MHCII expression by *Salmonella* found in tissue. Therefore, this evidence as a whole could suggest a hampering of processes mediated by MHCII in swine MLN following *Salmonella* infection.

On the contrary, network analysis also associated "Clathrin-mediated endocytosis signaling" to "CTLA4 signaling in cytotoxic T lymphocytes' pathway", bringing to light a possible role of the former process in adaptive immunity triggering. CTLA4, an important negative regulator of the T cell immune response [33], is endocytosed via a clathrin and dynamin-dependent route in activated T-cells [34]. According to Johanns et al. [35], up-regulation of *CTLA4* in regulatory T cells restrains effector T cell activation at early infection time points and allows the increase of bacterial burden during murine salmonellosis. Similarly, Inoue et al. [33] state that CTLA4-mediated Treg immunosuppression is critical in preventing the host from eliminating invasive pathogens. Given that, CTLA4 down-regulation, concurrent with clathrin up-regulation after the bacterial challenge, could indicate the repression of a mechanism of T cell inhibition in porcine MLN upon *Salmonella* Typhimurium infection. However, since clathrin could be involved in the establishment of both host immunity mechanisms and virulence strategies evolved by the pathogen, a deeper investigation of processes mediated by this molecule during infection is necessary and could

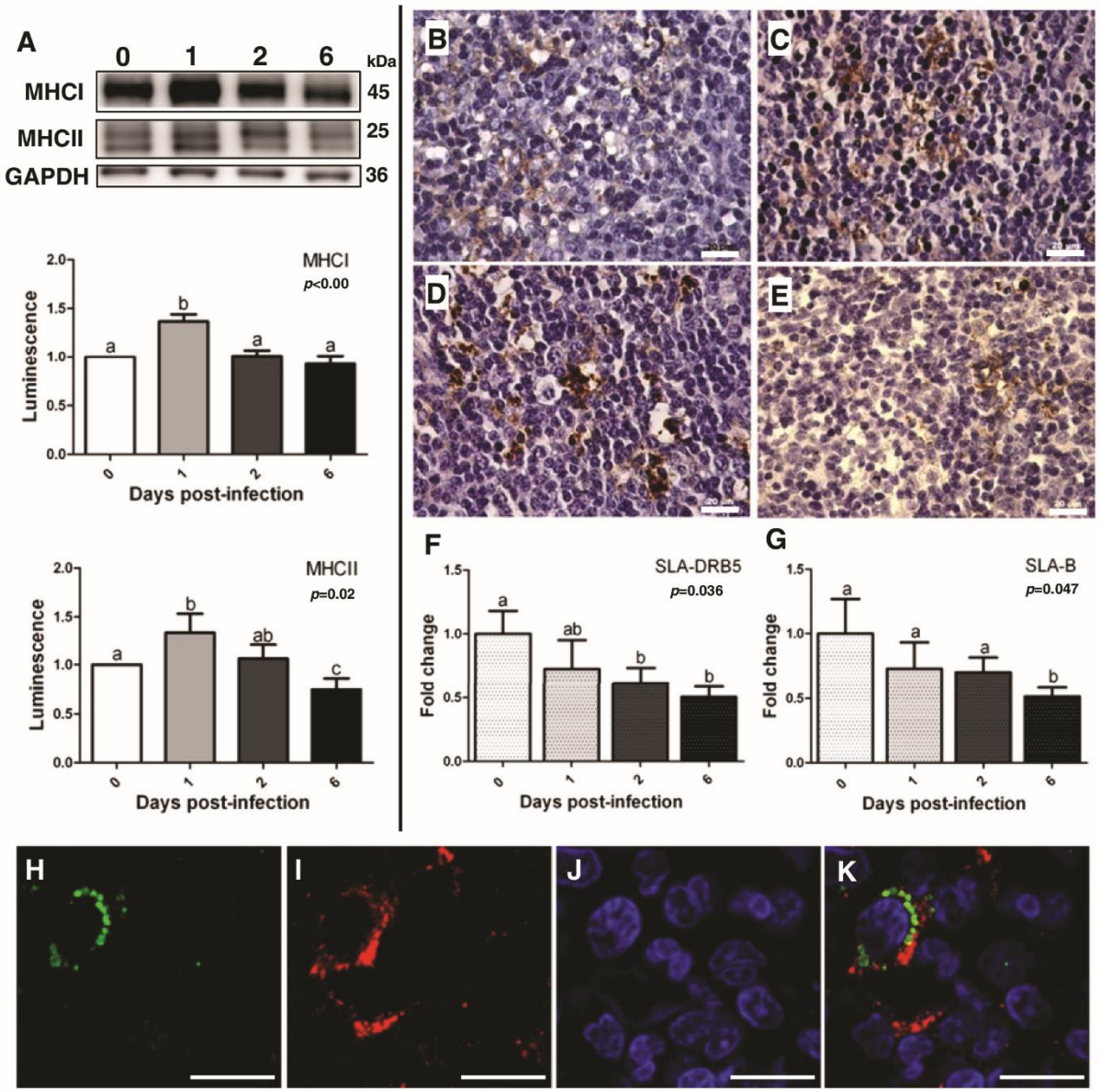

Figure 4 Analysis of MHC molecules in porcine MLN after *Salmonella* Typhimurium infection. A: Western blot analysis of MHC class I and II at 1, 2 and 6 dpi. **B-E**: MHCII labeling in tissue at 0 **(B)**, 1**(C)**, 2 **(D)** and 6 **(E)** dpi by immunohistochemistry. Scale bar = 20 μm. **F-G**: mRNA quantification of SLA-DRB5 (MHCII) **(F)** and SLA-B (MHCI) **(G)** by qPCR. **H-K**: confocal analysis of *Salmonella* Typhimurium infected MLN demonstrate the presence of the pathogen in MHCII positive cells. *Salmonella* Typhimurium-FITC **(H)**, MHCII-Alexa Fluor® 594 **(I)**, DAPI **(J)** and merge **(K)**.

provide relevant knowledge on the pathogenesis of porcine salmonellosis.

Current results also pointed to the generation of adaptive immunity mechanisms in infected tissue at a short time after infection. High MHCI levels observed by Western blot at 1 dpi reinforce our previous evidence that *Salmonella* antigens are cross-presented in swine MLN at initial stages of infection [10]. Cross-presentation is a mechanism that enables antigen presenting cells to prime CD8+ T cells via their own MHCI molecules [36]. Interestingly, it has been reported that differently from MHCII, *Salmonella* is not able to reduce MHCI surface expression of infected cells and consequently avoid early host cytotoxic response [28-30]. Therefore, cross-presentation might lead to an early *Salmonella* Typhimurium clearance by cytotoxic T cells during porcine infections, in agreement with the stimulation of *Salmonella*-specific CD8 T cells readily observed after

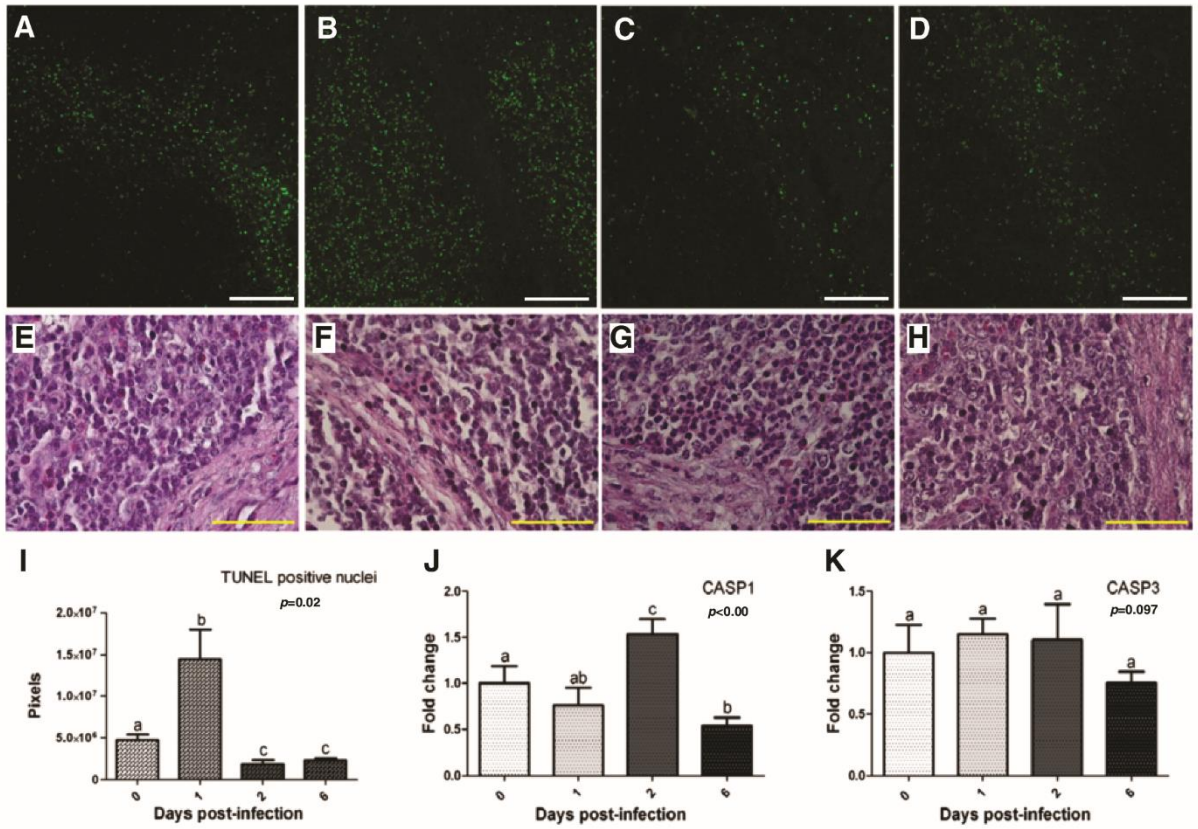

Figure 5 Cell death and histopathologic analysis of MLN from *Salmonella* Typhimurium infected pigs. A-D: Terminal deoxynucleotidyl transferase dUTP nick end labeling (TUNEL) analysis at 0 **(A)**, 1**(B)**, 2 **(C)** and 6 **(D)** dpi. Scale bar = 100 μm. **E-H**: H&E staining of at 0 **(E)**, 1**(F)**, 2 **(G)** and 6 **(H)** dpi. Scale bar = 50 μm. **I**: Quantification of TUNEL fluorescent labeling shows an increase of positive nuclei at 1 dpi and a decrease to levels inferior than the controls at 2 and 6 dpi. **J-K**: mRNA quantification of *CASP1* **(J)** and *CASP3* **(K)** by qPCR.

mice and human infections [37]. Additionally, *CD180*, an inducer of B cell proliferation, activation and differentiation [38], was uncovered to be up-regulated all along infection. Taken together, our results indicate that both cellular and humoral immunity mechanisms are effectively engendered in porcine MLN at a short time after infection with *Salmonella* Typhimurium. Thus, the dynamics of this protective response could be decisive in the course of infection by this pathogen in pigs.

Evidence of pyroptosis induction and apoptosis dampening in infected MLN were disclosed in the current study, supporting our previous reports [10]. Thus, microarray data mining detected an enrichment of processes such as "Negative regulation of apoptosis" and "Antiapoptosis" after the bacterial challenge, in addition to up-regulation of genes encoding for an inhibitor of apoptosis proteins (IAP) like XIAP and PDCL3. Induction of apoptosis has been asserted as a strategy that facilitates *Salmonella* cell-to-cell spread during systemic infection [39]. Nevertheless, it has also been reported that AvrA, a *Salmonella* effector protein, prevents the apoptotic elimination of host cell niche as a pathogen evasion mechanism [40]. Intriguingly, we observed in vivo expression of *spvB* and *sseL*, both major *Salmonella* Typhimurium apoptosis inducers, and the apoptosis inhibitor *avrA*, indicating that *Salmonella* appeared to execute virulence mechanisms to modulate apoptosis in porcine MLN in its favor.

As in apoptosis, pyroptotic cells show DNA fragmentation, nuclear condensation and positive TUNEL staining [41,42]. However, pyroptosis inherently results in inflammation due to caspase-1-mediated maturation of pro-IL-1β and pro-IL-18 and release of the cytoplasmic content, whereas the apoptotic cell is considered to be immunologically silent [43]. In the current study, increase of TUNEL positive labeling was observed in the tissue at 1 dpi, as well as infiltration of inflammatory cells and IL1β up-regulation. Therefore, we propose that once apoptosis is dampened, the infected cell undergoes pyroptosis in swine MLN, producing pathogen discharge to the extracellular milieu and clearance of bacteria by innate mechanisms. In support of this, we previously

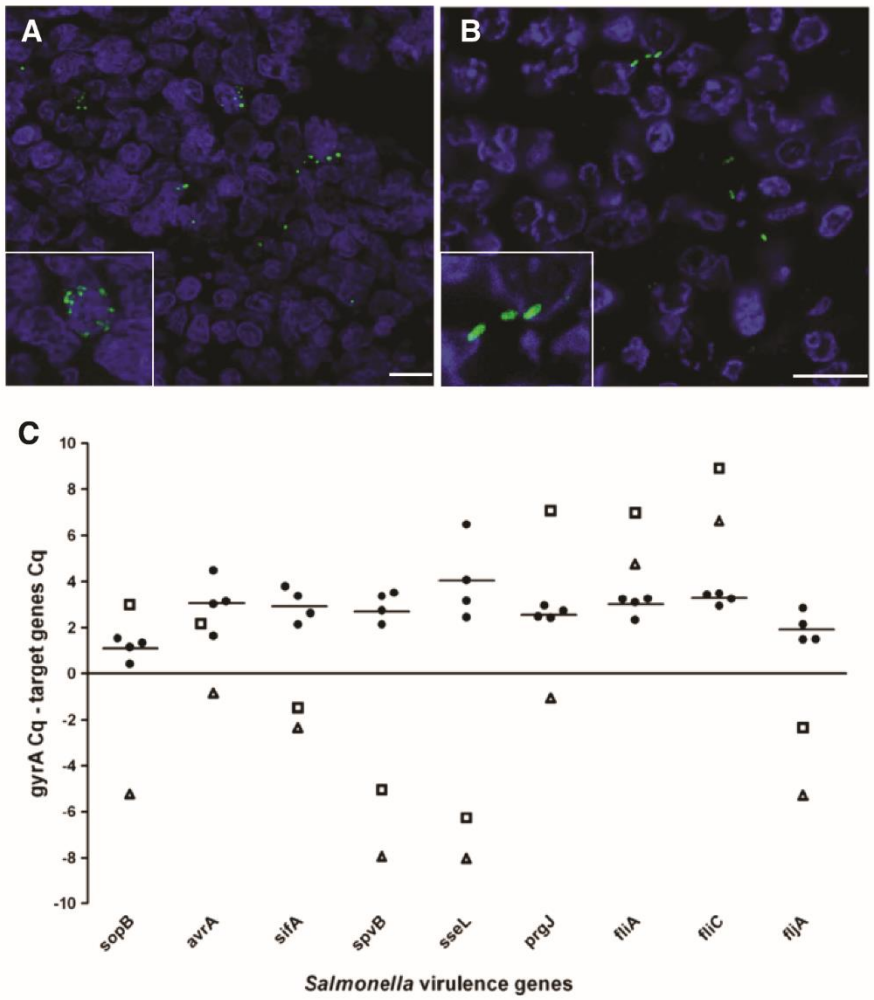

Figure 6 *Salmonella* Typhimurium labeling and gene expression in porcine MLN. A-B: Different labeling profiles found for *Salmonella* Typhimurium in porcine MLN. Scale bar = 10 μm. **(A)** Pathogen detection as spherical structures in the perinuclear zone of mononuclear cells. **(B)** Staining of bacilli shaped structures. **C**: Analysis of *Salmonella* Typhimurium gene expression by SCOTS in vivo and in vitro. Black dots and bars respectively represent individual and mean expression values from analysis of cDNA from pig infected MLN. Triangles (early logarithmic phase) and squares (late logarithmic phase) denote gene expression data from *Salmonella* Typhimurium cultures. Higher values mean higher expression levels and vice-versa.

reported an increase of phagocyte counts and mRNA levels of pro-inflammatory genes upon infection with *Salmonella* Typhimurium and a significant reduction of the pathogen burden at 6 dpi [21].

In line with this, an elegant study by Miao et al. [44] stated that *Salmonella* Typhimurium is able to damper pyroptosis for its own advantage by avoiding flagellin expression during infection of mice. Interestingly, we found expression of *Salmonella* Typhimurium flagella component (FliC) and regulators (FliA and FljA) in infected MLN. Additionally, flagella expression by infecting bacteria found in tissue was also corroborated by labeling using a specific polyclonal antibody. *Salmonella enterica* alternately expresses two different flagellar filament proteins, FljB and FliC, in a process known as flagellar phase variation. In spite of the high homology level found between these proteins, their middle surface exposed sequences of amino acids are divergent, resulting in distinct antigenicities [45]. It is noteworthy that our results demonstrate higher expression levels for *fliC* and its regulator *fliA* in vitro than in vivo. On the contrary, *fljA*, which is cotranscribed with *fljB,* was more expressed in *Salmonella* Typhimurium found in vivo. Moreover, this gene was notably less expressed than *fliA* and *fliC* in both early and late logarithmic phase cultures. Based on this, we deduced a skewing toward FliC flagellin expression by bacteria in vitro. Besides, we drew the inference that a more heterogeneous flagellin

expression is found in *Salmonella* Typhimurium replicating in vivo and that induction of flagellar phase variation could be a strategy adopted by this pathogen to hinder pig immune response. Expression of prg*J* was also uncovered in swine MLN. Curiously, repression of this effector has been reported as a mechanism of pyroptosis inhibition in vivo [46]. Thus, it could be inferred that expression of flagellin and *prgJ* by *Salmonella* Typhimurium found in tissue might enable pigs to use pyroptosis to clear bacteria in gut associated lymph-nodes, protecting itself from pathogen dissemination. Nevertheless, an issue that should be addressed by our assumption is why pathogen burden in tissue peaks after pyroptosis triggering. Miao and Rajan [46] stated that in a single cell, pyroptosis only takes place at late times of infection, following bacteria replication. So, we inferred that increase of pathogen load at 2 dpi may be due to the release of replicated *Salmonella* from cells dead by pyroptosis.

Notably, the presence of TUNEL positive cells in MLN was significantly reduced at 2 and 6 dpi, suggesting a decrease of cell death by apoptosis or pyroptosis. As with any physiological process, excessive pyroptosis is detrimental to the host [41]. So, modulation of this pathway by the host aiming to restore tissue integrity should be expected. Actually, we observed up-regulation of *MAP3K7* and *TRAF7*, both involved in NF-kB and survival pathway activation, at 2 and 6 dpi. However, evidence indicates that inhibition of caspase-dependent apoptosis primes cells towards programmed necrosis [47]. Since the mechanisms that dictate the cellular decision to survive by activating NF-kB or to die through apoptosis or necroptosis are still unclear [48] further research is necessary to clarify these results.

In conclusion, the results provided led us to infer that although the *Salmonella* Typhimurium strain employed in this study was able to express some of its major virulence effectors in porcine MLN, a combination of early host triggered innate and adaptive immunity mechanisms might overcome virulence strategies employed by pathogens. Besides preventing apoptosis, swine appear to take advantage of flagellin and prgJ expression by pathogens to induce pyroptosis in MLN. In this context, pyroptosis might consist in a host protective mechanism that prevents pathogen spread beyond gut-associated lymph-nodes. Furthermore, cross-presentation of *Salmonella* antigens in MLN might result in a rapid clearance of pathogens by cytotoxic T cells. Functional relevance was also shown by clathrin-mediated endocytosis that could contribute to mechanisms of pathogen virulence and/or host defence in MLN of *Salmonella* infected swine. Further analysis of examined mechanisms may support the discovery of novel strategies of host defense against *Salmonella* at the intestinal level.

Additional files

Additional file 1: Primer pairs employed in host differential expression analysis by real-time quantitative PCR. Table showing sequences and accession numbers of primers used for differential expression analysis in porcine mesenteric lymph-nodes.

Additional file 2: Primer pairs employed in the analysis of *Salmonella* Typhimurium virulence genes expressed in vivo. Table showing sequences and accession number of primers used for quantification of *Salmonella* Typhimurium transcripts expressed in porcine mesenteric lymph-nodes.

Additional file 3: Differentially expressed transcripts. Table showing chip ID, gene name, fold change and Bayes Factor value of transcripts differentially expressed in swine mesenteric lymph-nodes.

Additional file 4: Ingenuity Pathway Analysis annotations. Excel spreadsheet describing networks, biofunctions and canonical pathways found to be enriched in swine mesenteric lymph-nodes after *Salmonella* Typhimurium infection.

Additional file 5: DAVID Bioinformatic Database analysis of genes involved in Cell Death. Excel spreadsheet describing Gene Ontology terms associated to gene data set involved in Cell Death.

Additional file 6: Detection of *Salmonella* Typhimurium in mesenteric lymph-nodes of infected swine. Video showing confocal analysis (Z-stack tool) of *Salmonella* Typhimurium labeled in mesenteric lymph nodes of infected swine.

Competing interests
The authors declare that they have no competing interests.

Authors' contributions
RPM was responsible for the whole study, including lab work, data analysis and interpretation, as well as the writing of the manuscript. CA participated in the confocal analysis. JEG collaborated with SCOTS analysis. AC performed the experimental infection and collected the tissue samples. RB and MGC performed microarray data processing. JJG conceived and designed the project and participated in the interpretation and discussion of the results, as well as in the writing of the manuscript. All authors read and approved the final manuscript.

Acknowledgements
We thank Erena Ruiz Mora, Juana Molina and Reyes Alvarez for skillful technical assistance, Esther Peralbo for technical support in confocal microscopy analysis (IMIBIC) and Eloisa Andújar and Mónica Pérez from the Genomic Unit of CABIMER for their excellent array technical assistance. This work was supported by the Junta de Andalucía (P07-AGR-02672), the Spanish Ministry of Science and Innovation (AGL2008-00400 and AGL2011-28904) and EU funds through the SABRE project and EADGENE network. RPM and CA are predoctoral researchers supported by the FPU Research Program of the Spanish Ministry of Education and Science.

Author details
[1]Grupo de Genómica y Mejora Animal, Departamento de Genética, Facultad de Veterinaria, Universidad de Córdoba, Campus de Rabanales, Edificio Gregor Mendel C5, 14071, Córdoba, Spain. [2]Department of Microbiology and Immunology, University of Louisville, School of Medicine, 40202, Louisville, KY, USA. [3]Departamento de Sanidad Animal, Facultad de Veterinaria, Universidad de León, 24071, León, Spain. [4]Plataforma Andaluza de Bioinformática, Universidad de Málaga, Parque Tecnológico de Andalucía, 29590, Málaga, Spain.

Received: 30 January 2013 Accepted: 25 November 2013
Published: 5 December 2013

References
1. EFSA: **The European Union summary report on trends and sources of zoonoses, zoonotic agents and food-borne outbreaks in 2009.** *EFSA J* 2011, **9**:2090.

2. Baptista FM, Halasa T, Alban L, Nielsen LR: **Modelling food safety and economic consequences of surveillance and control strategies for Salmonella in pigs and pork.** *Epidemiol Infect* 2011, **139:**754–764.
3. Sánchez-Vargas FM, Abu-El-Haija MA, Gómez-Duarte OG: **Salmonella infections: an update on epidemiology, management, and prevention.** *Travel Med Infect Dis* 2011, **9:**263–277.
4. Gopinath S, Carden S, Monack D: **Shedding light on salmonella carriers.** *Trends Microbiol* 2012, **20:**320–327.
5. Boyen F, Haesebrouck F, Maes D, Van Immerseel F, Ducatelle R, Pasmans F: **Non-typhoidal salmonella infections in pigs: a closer look at epidemiology, pathogenesis and control.** *Vet Microbiol* 2008, **130:**1–19.
6. Tuggle CK, Bearson SM, Uthe JJ, Huang TH, Couture OP, Wang YF, Kuhar D, Lunney JK, Honavar V: **Methods for transcriptomic analyses of the porcine host immune response: application to salmonella infection using microarrays.** *Vet Immunol Immunopathol* 2010, **138:**280–291.
7. Wang Y, Couture OP, Qu L, Uthe JJ, Bearson SM, Kuhar D, Lunney J, Nettleton D, Dekkers JC, Tuggle CK: **Analysis of porcine transcriptional response to salmonella enterica serovar choleraesuis suggests novel targets of NFkappaB are activated in the mesenteric lymph node.** *BMC Genomics* 2008, **9:**437.
8. Huang TH, Uthe JJ, Bearson SM, Demirkale CY, Nettleton D, Knetter S, Christian C, Ramer-Tait AE, Wannemuehler MJ, Tuggle CK: **Distinct peripheral blood RNA responses to salmonella in pigs differing in salmonella shedding levels: intersection of IFNG, TLR and miRNA pathways.** *PLoS One* 2011, **6:**e28768.
9. Collado-Romero M, Martins RP, Arce C, Moreno Á, Lucena C, Carvajal A, Garrido JJ: **An in vivo proteomic study of the interaction between salmonella typhimurium and porcine ileum mucosa.** *J Proteomics* 2012, **75:**2015–2026.
10. Martins RP, Collado-Romero M, Martínez-Gomáriz M, Carvajal A, Gil C, Lucena C, Moreno A, Garrido JJ: **Proteomic analysis of porcine mesenteric lymph-nodes alter salmonella typhimurium infection.** *J Proteomics* 2012, **75:**4457–4470.
11. Collado-Romero M, Arce C, Ramirez-Boo M, Carvajal A, Garrido JJ: **Quantitative analysis of the immune response upon salmonella typhimurium infection along the porcine intestinal gut.** *Vet Res* 2010, **41:**23.
12. Irizarry RA, Hobbs B, Collin F, Beazer-Barclay YD, Antonellis KJ, Scherf U, Speed TP: **Exploration, normalization, and summaries of high density oligonucleotide array probe level data.** *Biostatistics* 2003, **4:**249–264.
13. Angelini C, Cutillo L, De Canditiis D, Mutarelli M, Pensky M: **BATS: a Bayesian user-friendly software for analyzing time series microarray experiments.** *BMC Bioinformatics* 2008, **9:**415.
14. Conesa A, Götz S, García-Gómez JM, Terol J, Talón M, Robles M: **Blast2GO: a universal tool for annotation, visualization and analysis in functional genomics research.** *Bioinformatics* 2005, **21:**3674–3676.
15. **Ingenuity Systems: Home** [www.ingenuity.com]
16. da Huang W, Sherman BT, Lempicki RA: **Systematic and integrative analysis of large gene lists using DAVID bioinformatics resources.** *Nat Protoc* 2009, **4:**44–57.
17. Livak KJ, Schmittgen TD: **Analysis of relative gene expression data using real-time quantitative PCR and the $2^{-\Delta\Delta CT}$ method.** *Methods* 2001, **25:**402–408.
18. Willems E, Leyns L, Vandesompele J: **Standardization of real-time PCR gene expression data from independent biological replicates.** *Anal Biochem* 2008, **379:**127–129.
19. Bullido R, Gomez del Moral M, Alonso F, Ezquerra A, Zapata A, Sánchez C, Ortuño E, Alvarez B, Domínguez JJ: **Monoclonal antibodies specific for porcine monocytes/macrophages: macrophage heterogeneity in the pig evidenced by the expression of surface antigens.** *Tissue Antigens* 1997, **49:**403–413.
20. Yubero N, Jiménez-Marín A, Barbancho M, Garrido JJ: **Two cDNAs coding for the porcine CD51 (α_V integrin subunit: cloning, expression analysis, adhesion assays and chromosomal localization.** *Gene* 2011, **481:**29–40.
21. Martins RP, Collado-Romero M, Arce C, Lucena C, Carvajal A, Garrido JJ: **Exploring the immune response of porcine mesenteric lymph nodes to salmonella enterica serovar typhimurium: an analysis of transcriptional changes, morphological alterations and pathogen burden.** *Comp Immunol Microbiol Infect Dis* 2013, **36:**149–160.
22. Robertson D, Savage K, Reis-Filho JS, Isacke CM: **Multiple immunofluorescence labelling of formalin-fixed paraffin-embedded (FFPE) tissue.** *BMC Cell Biol* 2008, **9:**13–22.
23. Schneider CA, Rasband WS, Eliceiri KW: **NIH Image to ImageJ: 25 years of image analysis.** *Nat Methods* 2012, **9:**671–675.
24. Graham JE, Clark-Curtiss JE: **Identification of mycobacterium tuberculosis RNAs synthesized in response to phagocytosis by human macrophages by selective capture of transcribed sequences (SCOTS).** *Proc Natl Acad Sci USA* 1999, **96:**11554–11559.
25. Sheikh A, Charles RC, Sharmeen N, Rollins SM, Harris JB, Bhuiyan MS, Arifuzzaman M, Khanam F, Bukka A, Kalsy A, Porwollik S, Leung DT, Brooks WA, LaRocque RC, Hohmann EL, Cravioto A, Logvinenko T, Calderwood SB, McClelland M, Graham JE, Qadri F, Ryan ET: **In vivo expression of salmonella enterica serotype typhi genes in the blood of patients with typhoid fever in Bangladesh.** *PLoS Negl Trop Dis* 2011, **5:**e1419.
26. Rostagno MH, Eicher SD, Lay DC Jr: **Immunological, physiological, and behavioral effects of salmonella enterica carriage and shedding in experimentally infected finishing pigs.** *Foodborne Pathog Dis* 2011, **8:**623–630.
27. Uthe JJ, Royaee A, Lunney JK, Stabel TJ, Zhao SH, Tuggle CK, Bearson SM: **Porcine differential gene expression in response to salmonella enterica serovars choleraesuis and typhimurium.** *Mol Immunol* 2007, **44:**2900–2914.
28. Van Parys A, Boyen F, Verbrugghe E, Leyman B, Bram F, Haesebrouck F, Pasmans F: **Salmonella typhimurium induces SPI-1 and SPI-2 regulated and strain dependent downregulation of MHC II expression on porcine alveolar macrophages.** *Vet Res* 2012, **43:**52.
29. Lapaque N, Hutchinson JL, Jones DC, Méresse S, Holden DW, Trowsdale J, Kelly AP: **Salmonella regulates polyubiquitination and surface expression of MHC class II antigens.** *Proc Natl Acad Sci USA* 2009, **106:**14052–14057.
30. Mitchell EK, Mastroeni P, Kelly AP, Trowsdale J: **Inhibition of cell surface MHC class II expression by salmonella.** *Eur J Immunol* 2004, **34:**2559–2567.
31. Eckmann L, Kagnoff MF: **Cytokines in host defense against salmonella.** *Microbes Infect* 2001, **3:**1191–1200.
32. Veiga E, Cossart P: **The role of clathrin-dependent endocytosis in bacterial internalization.** *Trends Cell Biol* 2006, **16:**499–504.
33. Inoue S, Bo L, Bian J, Unsinger J, Chang K, Hotchkiss RS: **Dose-dependent effect of anti-CTLA-4 on survival in sepsis.** *Shock* 2011, **36:**38–44.
34. Qureshi OS, Kaur S, Hou TZ, Jeffery LE, Poulter NS, Briggs Z, Kenefeck R, Willox AK, Royle SJ, Rappoport JZ, Sansom DM: **Constitutive clathrin-mediated endocytosis of CTLA-4 persists during T cell activation.** *J Biol Chem* 2012, **287:**9429–9440.
35. Johanns TM, Ertelt JM, Rowe JH, Way SS: **Regulatory T cell suppressive potency dictates the balance between bacterial proliferation and clearance during persistent salmonella infection.** *PLoS Pathog* 2010, **6:**e1001043.
36. Houde M, Bertholet S, Gagnon E, Brunet S, Goyette G, Laplante A, Princiotta MF, Thibault P, Sacks D, Desjardins M: **Phagosomes are competent organelles for antigen cross-presentation.** *Nature* 2003, **425:**402–406.
37. Lee SJ, Dunmire S, McSorley SJ: **MHC class-I-restricted CD8 T cells play a protective role during primary salmonella infection.** *Immunol Lett* 2012, **148:**138–143.
38. Chaplin JW, Kasahara S, Clark EA, Ledbetter JA: **Anti-CD180 (RP105) activates B cells to rapidly produce polyclonal Ig via a T cell and MyD88-independent pathway.** *J Immunol* 2011, **187:**4199–4209.
39. Haimovich B, Venkatesan MM: **Shigella and salmonella: death as a means of survival.** *Microbes Infect* 2006, **8:**568–577.
40. Wu H, Jones RM, Neish AS: **The salmonella effector AvrA mediates bacterial intracellular survival during infection in vivo.** *Cell Microbiol* 2012, **14:**28–39.
41. Labbé K, Saleh M: **Pyroptosis: A Caspase-1-dependent programmed cell death and a barrier to infection.** In *Progress in Inflammation Research: The Inflammasomes.* Edited by Couillin I, Pétrilli V, Martinon F. Basel: Springer Basel AG; 2011:17–36.
42. Duprez L, Wirawan E, Vanden Berghe T, Vandenabeele P: **Major cell death pathways at a glance.** *Microbes Infect* 2009, **11:**1050–1062.
43. Fink SL, Cookson BT: **Apoptosis, pyroptosis, and necrosis: mechanistic description of dead and dying eukaryotic cells.** *Infect Immun* 2005, **73:**1907–1916.
44. Miao EA, Leaf IA, Treuting PM, Mao DP, Dors M, Sarkar A, Warren SE, Wewers MD, Aderem A: **Caspase-1-induced pyroptosis is an innate immune effector mechanism against intracellular bacteria.** *Nat Immunol* 2010, **11:**1136–1142.
45. Bonifield HR, Hughes KT: **Flagellar phase variation in Salmonella enterica is mediated by a posttranscriptional control mechanism.** *J Bacteriol* 2003, **185:**3567–3574.

46. Miao EA, Rajan JV: **Salmonella and caspase-1: a complex interplay of detection and evasion.** *Front Microbiol* 2011, **2**:85.
47. Moquin D, Chan FK: **The molecular regulation of programmed necrotic cell injury.** *Trends Biochem Sci* 2010, **35**:434–441.
48. Christofferson DE, Yuan J: **Necroptosis as an alternative form of programmed cell death.** *Curr Opin Cell Biol* 2010, **22**:263–268.

doi:10.1186/1297-9716-44-120
Cite this article as: Martins *et al.*: Pyroptosis and adaptive immunity mechanisms are promptly engendered in mesenteric lymph-nodes during pig infections with *Salmonella enterica* serovar Typhimurium. *Veterinary Research* 2013 **44**:120.

Developmental and Comparative Immunology 41 (2013) 100–104

Contents lists available at SciVerse ScienceDirect

Developmental and Comparative Immunology

journal homepage: www.elsevier.com/locate/dci

Short communication

Innate and adaptive immune mechanisms are effectively induced in ileal Peyer's patches of *Salmonella typhimurium* infected pigs

Rodrigo Prado Martins [a], Valentina Lorenzi [a], Cristina Arce [a], Concepción Lucena [a], Ana Carvajal [b], Juan José Garrido [a,*]

[a] Grupo de Genómica y Mejora Animal, Departamento de Genética, Facultad de Veterinaria, Universidad de Córdoba, Campus de Rabanales, Edificio Gregor Mendel C5, 14071 Córdoba, Spain
[b] Departamento de Sanidad Animal, Facultad de Veterinaria, Universidad de León, 24071 León, Spain

ARTICLE INFO

Article history:
Received 20 February 2013
Revised 23 April 2013
Accepted 24 April 2013
Available online 3 May 2013

Keywords:
Peyer's patches
Salmonella typhimurium
Laser-capture microdissection
Immune response

ABSTRACT

In this report we employed laser-capture microdissection (LCM) coupled to qPCR technology and bioinformatic analysis to characterize, for the first time, the response of Peyer's patches (PP) from orally infected animals to *Salmonella typhimurium*, in a model of non-typhoidal salmonellosis. Pathogen was highly found in the cytoplasm of phagocytes in PP and differential gene expression analysis indicated an up-regulation of proinflammatory molecules, establishment of a Th1 driven response and triggering of DC and T-cell activity. Furthermore, predictions by bioinformatic analysis pointed to an activation of processes regarding stimulation and maturation of DC, influx of leukocytes in tissue and T lymphocytes priming and differentiation. In short, the approach used in this study proved to be a promising strategy to explore infectious processes. Indeed, it revealed an effective induction of innate and adaptive immune mechanisms in swine PP which appear to be distinct from those observed in mesenteric lymph nodes and closely related to response of gut mucosa.

1. Introduction

Despite the current improvement in sanitation and hygiene, *Salmonella* persists as a significant cause of disease worldwide. Data from the Centers for Disease Control (CDC) assert that *Salmonella* alone causes approximately 1 million foodborne infections annually in the United States (CDC, 2011). Similarly, *Salmonella* is reported as the main cause of food-borne outbreaks in the European Union, being *Salmonella enterica* serovar *Typhimurium* (herein *Salmonella typhimurium*) the second most frequently isolated serovar from human infections (EFSA, 2012).

Advances in mammalian models of *Salmonella* infection are expected to result in new understanding of salmonellosis pathogenesis, contributing to the control and cure of human cases (Gopinath et al., 2012). In this context, pigs can be stressed as an ideal model for investigating human non-typhoidal salmonellosis, since upon infection with *S. typhimurium* swine undergo a self-limiting enterocolitis similar to the clinical manifestation observed in man.

Studies on the murine model of typhoid fever state that to cause infection, ingested *S. typhimurium* primarily invade M cells in the small intestine and then accesses Peyer's patches (PP), resulting in a massive inflammatory response in these organs (Broz et al., 2012). Therefore, besides their role in the immune surveillance of the intestinal lumen, PP are relevant mediators of infections by *S. typhimurium*. Although previous studies have employed gut loops models to extrapolate the response of PP to *S. typhimurium* (Meurens et al., 2009; Nunes et al., 2010), the function of these organs in the context of oral non-typhoidal infections has never been explored to date. To address this issue, we employed for the first time laser-capture microdissection (LCM) coupled to qPCR technology and bioinformatic analysis to provide an accurate view of the immune mechanisms modulated in PP of pigs orally infected with *S. typhimurium*.

2. Material and methods

2.1. Experimental infection

Eight crossbred piglets of approximately four weeks of age, confirmed to be fecal-negative for *Salmonella*, were randomly allocated to control or infected groups (four animals each), being control (0 day post-infection – dpi) pigs necropsied 2 h before the experimental infection. Pigs belonging to the infected group were orally challenged with 10^8 cfu of *S. typhimurium* phagetype DT104 and euthanized at 2 dpi. Ileum samples were collected from all piglets and immediately frozen in liquid nitrogen for RNA isolation or fixed in 10% neutral buffered formalin for immunohistochemistry

* Corresponding author. Tel.: +34 957218730; fax: +34 957212072.
E-mail address: ge1gapaj@uco.es (J.J. Garrido).

0145-305X/$ - see front matter © 2013 Elsevier Ltd. All rights reserved.
http://dx.doi.org/10.1016/j.dci.2013.04.020

assays. All procedures involving animals were performed under the supervision of the Ethical and Animal Welfare Committee of the University of León (Spain), in accordance with the European regulations regarding the protection of animals used for experimental and other scientific purposes.

2.2. Laser-capture microdissection and RNA preparations

Frozen gut samples from all experimental animals were embedded in optimal cutting temperature compound (Sakura Finetek USA, Torrance, CA, USA) and cut into serial 20 μm sections. Before microdissection, eight cryostat sections from each pig were mounted on glass slides and treated with RNAlater-ICE (Ambion) according to manufacturer instructions. Subsequently, PP follicles were laser-microdissected and captured from terminal ileum sections avoiding contamination by adjacent cells with a PALM MicroBeam device (Carl Zeiss MicroImaging GmbH, Jena, Germany), by Auto-Laser Pressure Catapulting (LPC) mode (Fig. 1A–C). Catapulted tissue was soaked in 15 μl of RLT buffer (Qiagen, Valencia, CA, USA) poured in 200 μl microtubes caps and RNA purifications were carried out employing the RNeasy Mini Kit (Qiagen). Eluted RNA was digested with RNase-Free DNase Set (Qiagen) and RNA quality was checked by Experion RNA analysis (Bio-Rad, Hercules, CA, USA). Finally, RNA was amplified using the SuperScript™ RNA Amplification System (Invitrogen, Carlsbad, CA, USA), as indicated by manufacturer.

2.3. Real-time quantitative PCR (qPCR)

Amplified RNA from infected and control animals was reverse transcribed to cDNA using the qScript cDNA Synthesis kit (Quanta BioSciences, Gaithersburg, MD, USA) and qPCR assays were performed according to Martins et al. (2013) to determine the relative expression of 30 genes coding for molecules taking part in distinct immune response processes such as inflammation, DC-T cell interaction and T helper cell response. Primers used for amplifications can be found as supporting information (see Supplementary File 1). Afterwards, relative gene expression was assessed by the $2^{-\Delta\Delta Cq}$ method (Livak and Schmittgen, 2001). In this analysis, qPCR data were presented as the fold change in gene expression normalized to an endogenous reference gene and relative to the uninfected controls. Fold change values higher than 1 meant up-regulation. Values inferior to 1 were calculated as −1/fold change and denoted down-regulation. Data were analyzed by Student's *t*-test using the software SPSS 15.0 for Windows® (SPSS, Inc). A *p*-value bellow 0.05 was considered statistically significant.

2.4. Bioinformatic data analysis

Ingenuity Pathway Analysis (IPA, Ingenuity Systems, www.ingenuity.com) Downstream Effects tool was used to identify functions that are expected to be activated in tissue, given the observed gene expression patterns. Predictions were made by *z*-score algorithm and values higher and lower than 2 meant that activation state was statistically increased and decreased respectively. IPA Path Designer was also employed to illustrate some mechanisms modulated by genes evaluated in this study.

2.5. Immunohistochemistry

To verify the presence of *S. typhimurium* in PP, paraffin sections (5 μm) of formalin fixed samples were routinely processed and immunostained as described elsewhere (Martins et al., 2013), employing a specific anti-*Salmonella* rabbit antiserum.

3. Results and discussion

Ileal loops models have provided valuable information regarding the response of gut mucosa to *Salmonella*. Nevertheless, accumulating evidences indicate that ingested *Salmonella* undergo phenotypical changes during its passage along host gastrointestinal tract that influence the infectious process (Alvarez-Ordóñez et al., 2011). Thus, it could be speculated that infection conditions employed by this approach is substantially different from those found in natural infections. Basing on this, in this report we describe for the first time the regulation of immune response mechanisms in the PP of orally infected animals, in the context of non-typhoidal salmonellosis. Besides, LCM was used to isolate and analyze cell exclusively from PP follicles. Microdissection has been successfully employed in cancer research to provide precise knowledge on tumor biology (Cheng et al., 2013). Here, LCM coupled to qPCR technology enabled us to characterize changes in infected PP with reduced interference from non-target cells, generating more accurate data than previously reported.

Immunohistochemistry assays demonstrated that *S. typhimurium* was notably found in PP (Fig. 1D and E), agreeing with preceding reports that highlight these organs as the main portal of pathogen entry to host mucosa (Broz et al., 2012; Schauser et al., 2004). Moreover, differential expression analysis revealed significant regulation of 21 out 30 genes encoding pattern-recognition receptors (PRR), chemokines, DC and T-cell activation markers, Th response mediators and other immune-related molecules (Table 1). Proinflammatory genes such as IL1β, CXCL2 and TNFα were found to be up-regulated as a consequence of infection. This response could be associated to recognition of invading *Salmonella* via PRR by macrophages and dendritic cells in PP, resulting in pathogen phagocytosis, secretion of chemokines and recruitment of additional inflammatory cells into the site of invasion (Broz et al., 2012). In line with this, a strong up-regulation was uncovered for all screened PRR (TLR2, 4, 5, 8 and NOD2) and pathogen labeling was mainly observed in the cytoplasm of large irregular-shaped mononuclear cells and some polymorphonuclear cells (Fig. 1F). Inflammation induced by IL1 has been considered a key mechanism in *Salmonella* pathogenesis at mucosa level (Raupach et al., 2006). However, a previous report employing porcine gut loops did not detect up-regulation of IL1β and chemokines encoding genes in PP upon *S. typhimurium* infection (Meurens et al., 2009). Although we believe that this discrepancy could be attributed to differences between approaches, PP areas not analyzed by us, such as dome and interfollicular zones, might affect the response of these organs to infection. Thus, this fact could also justify the observed differences between current study and others on the whole PP.

In general, results indicated that similarly to the murine typhoid model (Tam et al., 2008), mechanisms of innate immune response are effectively induced in PP during swine oral infections by *S. typhimurium*. Apart from contributing to bacterial clearance in tissue, as suggested by our previous observations (Martins et al., 2013), this response could be related to triggering of host second line of defense. Genes coding for molecules involved in DC activation (CD80, CD83, CD40, IL12p40, IL23p19 and CCR7) were found to be up-regulated in infected PP (Supplementary File 2). The same was observed for molecules required for T-cell mediated processes (IFNγ, CD40L, CD28, CCL19 and IL21). Of note, high mRNA levels were observed for IFNγ and IL12p40, despite the absence of IL18 up-regulation. Although this interleukin act synergistically with IL12 in the induction of IFNγ production and cell-mediated immunity, a previous study demonstrated that IL-18 is relevant for resistance to the systemic infection but not during the intestinal phase of salmonellosis (Raupach et al., 2006). Concurrently, down-regulation or absence of expression was uncovered for Th2 (IL4 and IL13)

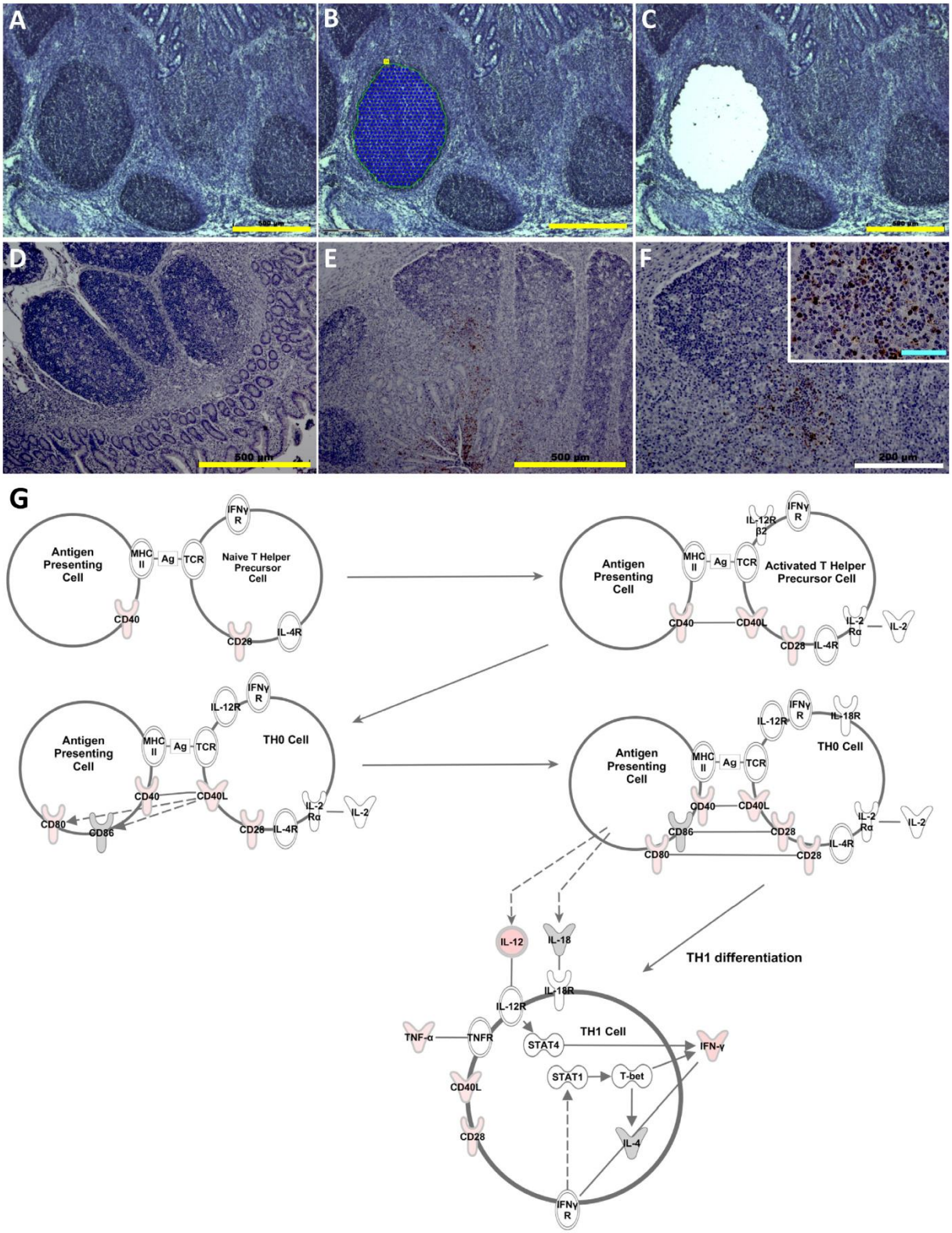

Fig. 1. Laser-capture microdissection, pathogen detection and gene expression analysis in Peyer's patches of *S. typhimurium* infected pigs. (A–C) LCM: After their identification in tissue (A), PP follicles were selected (B) and collected by Auto-Laser Pressure Catapulting mode (C). (D–F) Immunohistochemistry: *S. typhimurium* was immunolabeled in control (D) and infected tissue (E–F). Yellow, white and blue bars correspond to 500, 200 and 50 µm respectively. (G) Visual representation of T-helper cell differentiation pathway by Ingenuity Pathways Analysis: Colored nodes represent screened genes. Red and grey mean up-regulation and non-significant change in expression respectively. (For interpretation of the references to colour in this figure legend, the reader is referred to the web version of this article.)

Table 1
Relative gene expression in Peyer's Patches of pigs experimentally infected with *S. typhimurium*, at 2 dpi.

Gene	0 dpi		2 dpi		*p*-value[b]
	FC[a]	SD	FC	SD	
CASP1	1	1.26	2.66	3.51	0.266
CCL19	1	0.12	3.47	0.81	<0.001
CCL21	1	0.72	2.98	3.09	0.292
CCR7	1	0.57	5.98	2.16	0.002
CD11b	1	0.32	6.53	1.51	<0.001
CD28	1	1.01	6.96	3.38	0.028
CD40	1	0.29	3.66	0.89	0.001
CD40L	1	0.27	2.02	0.56	0.020
CD80	1	0.62	9.69	6.34	0.006
CD83	1	0.20	2.07	0.41	0.012
CD86	1	0.34	1.19	0.50	0.710
CTLA4	1	0.69	3.96	2.91	0.142
CXCL2	1	0.33	5.78	2.85	0.002
IL1β	1	1.29	79.22	43.06	0.004
IL4	1	1.02	1.38	1.05	0.868
IL12p40	1	0.97	20.22	19.15	0.007
IL13	n.a.	n.a.	n.a.	n.a.	n.a.
IL16	1	0.73	1.43	1.41	0.902
IL17A	n.a.	n.a.	n.a.	n.a.	n.a.
IL18	1	0.42	1.07	0.52	0.940
IL21	1	0.32	3.93	2.97	0.032
IL23	1	0.16	2.58	0.25	0.000
IFNγ	1	0.96	17.66	9.94	0.005
NOD2	1	0.72	16.48	20.82	0.042
SELL	1	0.13	-2.5	0.026	<0.001
TLR2	1	0.82	17.14	8.37	0.013
TLR4	1	0.11	2.23	0.92	0.015
TLR5	1	0.38	14.05	7.45	0.001
TLR8	1	0.56	4.67	2.17	0.005
TNFα	1	0.24	2.41	0.51	0.002

[a] Fold change mean values ($n = 4$ per group). Values higher than 1 meant up-regulation. Those inferior to 1 were calculated as −1/fold change and denoted down-regulation.
[b] *p*-values bellow 0.05 were considered statistically significant. n.a.: not amplified.

and Th17 (IL17A) inducers, suggesting a trend to Th1 orientation in *S. typhimurium* infected PP (Fig. 1G). In accordance with these observations, Collado-Romero et al. (2012) detected a general trend toward down-regulation of Th2 and Th17 responses in ileum mucosa of *S. typhimurium* infected pigs, validating the importance of processes carried out by PP in the development of immune response at mucosal level during non-typhoidal salmonellosis. To further confirm results from differential expression analysis, a bioinformatic algorithm was used to predict the modulation of some immunity mechanisms after infection, by combining results disclosed for the screened genes and relating them with the available literature. Processes such leukocytes recruitment, stimulation of DC and macrophages, DC maturation and influx of neutrophils were predicted to be activated as a consequence of infection. The same was detected for mechanisms of T lymphocytes proliferation, priming and differentiation (see Supplementary File 3).

Intriguingly, up-regulation of Th1 response was not observed by us in mesenteric lymph nodes (MLN) of *S. typhimurium* infected pigs. Furthermore, contrary to the clear induction of DC and T-cell activity uncovered by current results, DC-T-cells interaction was inferred to be compromised in these organs after infection (Martins et al., 2013). Therefore, it is tempting to speculate that, in spite of their similar functions as components of gut associated lymphoid tissue, PP trigger mechanisms distinct from those occurring in MLN upon oral infection with *S. typhimurium*. Besides, it could be deduced that inhibition of T-cell activation by DCs, largely reported as an evasion mechanism evolved by *S. typhimurium* (Bueno et al., 2012), might not be induced in swine PP or is effectively counteracted by host response.

In short, combination of an *in vivo* infection model with LCM and gene expression analysis proved to be a promising strategy to clarify the role of specific cell populations during infectious processes. This approach enabled us to gain an insight into the immunity mechanisms carried out in PP during non-typhoidal salmonellosis. Results pointed to an effective induction of innate and adaptive immune responses in this organs, inferred to be different from those observed in MLN and closely related to the processes carried out at intestinal mucosa after infection. Data provided here could represent useful information for the establishment of control and therapeutic strategies focused on the enhancement of immunity against *Salmonella* at gut level.

Acknowledgements

We thank Erena Ruiz-Mora and Reyes Alvarez for skillful technical assistance. This work was supported by EU funds provided by EADGENE and SABRE Projects, by the Excellence Project of the Junta de Andalucía Government P07-AGR-02672 and by two National R&D Program Grant of the Spanish Ministry of Education and Science (AGL2008-00400 and AGL2011-28904). RPM is a predoctoral researcher supported by the FPU Research Program of the Spanish Ministry of Education and Science.

Appendix A. Supplementary data

Supplementary data associated with this article can be found, in the online version, at http://dx.doi.org/10.1016/j.dci.2013.04.020.

References

Alvarez-Ordóñez, A., Begley, M., Prieto, M., Messens, W., López, M., Bernardo, A., Hill, C., 2011. *Salmonella* spp. survival strategies within the host gastrointestinal tract. Microbiology 157, 3268–3281.
Broz, P., Ohlson, M.B., Monack, D.M., 2012. Innate immune response to *Salmonella typhimurium*, a model enteric pathogen. Gut Microbes 3, 62–70.
Bueno, S.M., Riquelme, S., Riedel, C.A., Kalergis, A.M., 2012. Mechanisms used by virulent *Salmonella* to impair dendritic cell function and evade adaptive immunity. Immunology 137, 28–36.
Centers for Disease Control and Prevention (CDC), 2011. Vital signs: incidence and trends of infection with pathogens transmitted commonly through food – foodborne diseases active surveillance network, 10 U.S. sites, 1996–2010. MMWR Morb. Mortal. Wkly Rep. 60, 749–755.
Cheng, L., Zhang, S., MacLennan, G.T., Williamson, S.R., Davidson, D.D., Wang, M., Jones, T.D., Lopez-Beltran, A., Montironi, R., 2013. Laser-assisted microdissection in translational research: theory, technical considerations, and future applications. Appl. Immunohistochem. Mol. Morphol. 21, 31–47.
Collado-Romero, M., Martins, R.P., Arce, C., Moreno, Á., Lucena, C., Carvajal, A., Garrido, J.J., 2012. An *in vivo* proteomic study of the interaction between *Salmonella typhimurium* and porcine ileum mucosa. J. Proteomics 75, 2015–2026.
European Food Safety Authority (EFSA), 2012. The European Union summary report on trends and sources of zoonoses, zoonotic agents and food-borne outbreaks in 2010. EFSA J. 9, 2597.
Gopinath, S., Carden, S., Monack, D., 2012. Shedding light on *Salmonella* carriers. Trends Microbiol. 20, 320–327.
Livak, K.J., Schmittgen, T.D., 2001. Analysis of relative gene expression data using real-time quantitative PCR and the $2^{-\Delta\Delta CT}$ method. Methods 25, 402–408.
Martins, R.P., Collado-Romero, M., Arce, C., Lucena, C., Carvajal, A., Garrido, J.J., 2013. Exploring the immune response of porcine mesenteric lymph nodes to Salmonella enterica serovar typhimurium: an analysis of transcriptional changes, morphological alterations and pathogen burden. Comp. Immunol. Microbiol. Infect. Dis. 36, 149–160.
Meurens, F., Berri, M., Auray, G., Melo, S., Levast, B., Virlogeux-Payant, I., Chevaleyre, C., Gerdts, V., Salmon, H., 2009. Early immune response following *Salmonella enterica* subspecies *enterica* serovar *typhimurium* infection in porcine jejunal gut loops. Vet. Res. 40, 5.
Nunes, J.S., Lawhon, S.D., Rossetti, C.A., Khare, S., Figueiredo, J.F., Gull, T., Burghardt, R.C., Bäumler, A.J., Tsolis, R.M., Andrews-Polymenis, H.L., Adams, L.G., 2010. Morphologic and cytokine profile characterization of *Salmonella enterica* serovar *typhimurium* infection in calves with bovine leukocyte adhesion deficiency. Vet. Pathol. 47, 322–333.
Raupach, B., Peuschel, S.K., Monack, D.M., Zychlinsky, A., 2006. Caspase-1-mediated activation of interleukin-1beta (IL-1beta) and IL-18 contributes to innate immune defenses against *Salmonella enterica* serovar *typhimurium* infection. Infect. Immun. 74, 4922–4926.

Schauser, K., Olsen, J.E., Larsson, L.I., 2004. Immunocytochemical studies of *Salmonella typhimurium* invasion of porcine jejunal epithelial cells. J. Med. Microbiol. 53, 691–695.

Tam, M.A., Rydström, A., Sundquist, M., Wick, M.J., 2008. Early cellular responses to *Salmonella* infection: dendritic cells, monocytes, and more. Immunol. Rev. 225, 140–162.

Salmonella Typhimurium elicits specific humoral and cell-mediated immune responses in porcine Peyer's patches.

Running title: Response of porcine Peyer's patches to *Salmonella*

Rodrigo P. Martins[1], Carmen Aguilar[1], Valentina Lorenzi[1], Ángeles Jiménez-Marín[1], Sara Zaldívar-López[1], Héctor Argüello[1], Juber Herrera-Uribe[1], Ana Carvajal[2], Rocío Bautista[3], M. Gonzalo Claros[3], Juan J. Garrido[1]*

[1] Grupo de Genómica y Mejora Animal, Departamento de Genética, Facultad de Veterinaria, Universidad de Córdoba, Campus de Rabanales, Edificio Gregor Mendel C5, 14071 Córdoba, Spain.
[2] Departamento de Sanidad Animal, Facultad de Veterinaria, Universidad de León, 24071 León, Spain.
[3] Plataforma Andaluza de Bioinformática, Universidad de Málaga, Parque Tecnológico de Andalucía, 29590 Málaga, Spain

***Corresponding author:** Juan J. Garrido, ge1gapaj@uco.es

Keywords: Pig, *Salmonella enterica* serovar Typhimurium, Peyer's patches follicles, laser capture microdissection, cross-presentation, neutrophils.

Number of words: 6,088

The authors declare no conflict of interest

ABSTRACT

Salmonella enterica serovar Typhimurium (*S*. Typhimurium) is a broad-host-range pathogen that causes self-limiting gastroenteritis in farm animals and human. We coupled a swine model of non-typhoid salmonellosis to laser capture microdissection and microarray analysis to gain new insights into the immune mechanisms underlying response to *Salmonella* in the follicles of Peyer's patches, the main portal of bacterial entry. Our analysis pointed out the overexpression of genes involved in the formation of germinal centers, confirming that infection leads to humoral responses by assembling mediators of B-cell-T-cell interactions and by inducing the expression of cytokines involved in B-cell mediated immunity. Moreover, the notable infiltration of cells carrying *Salmonella* upon infection, together with the increased expression of genes coding for molecules involved in antigen transport, immunoproteasome activation and MHCI pathway suggested the cross-presentation of bacterial antigens at 2 days after infection. These findings revealed the essential role of Peyer's patches in the humoral and cell-mediated immune response of pigs against *Salmonella*.

INTRODUCTION

Salmonella species are a leading bacterial cause of disease, exerting considerable impact on global human health. It is estimated that 93.8 million cases of gastroenteritis due *Salmonella* occur worldwide leading to 155,000 deaths each year (1). Pathogenesis of infections by *Salmonella enterica* serovar Typhimurium (herein *S.* Typhimurium) has been extensively studied using the murine typhoid model. However, one limitation of this approach is the fact that *S.* Typhimurium typically causes a self-limiting gastroenteritis rather than typhoid fever in humans. For this reason, pathogenesis of gastroenteritis by non-typhoid *Salmonella* (NTS) remained largely unexplored until recently, when alternative animal models of infection became more widely used (2). Of note, pigs undergo a self-limiting enterocolitis after *S.* Typhimurium infection (3, 4) that parallels the clinical manifestation observed in people (5). In light of this, swine could be considered an ideal model for investigating the pathogenesis of human non-typhoidal salmonellosis.

Following stomach passage, *Salmonella* must adhere to gut cells and subsequently cross the intestinal epithelium to establish infection. In fact, accumulating evidences demonstrate that Peyer's patches (PP) are the main portal of *S.* Typhimurium entry into host mucosa (6-8). These organs are clusters of organized lymphoid tissue located in the small intestine, which act as sites of antigen sampling and induction of mucosal immune responses (9). Upon enteric infections, PP follicles undergo substantial changes leading to the formation of germinal centers, structures intimately associated to fundamental aspects of adaptive immunity such as production of B cell-mediated responses and generation of immunological memory (10).

In a previous work, laser capture microdissection (LCM) was successfully used to provide a preliminary view of the immune response elicited in porcine PP follicles in an infection with NTS (11). Results manifested that induction of T cell mediated processes, together with the prompted mechanisms of innate immune response, could be contributing to bacterial clearance in this tissue. In the current study, transcriptome profiling was applied to gain further insights into the adaptive immune responses induced in PP during swine infections by *S.* Typhimurium.

MATERIALS AND METHODS

Experimental infection and tissue sampling

Eight crossbred commercial (landrace x large white) weaned female piglets of approximately four weeks of age and confirmed to be fecal-negative for *Salmonella* were randomly allocated to control or infected groups (four animals each). After 7 days of adaptation, control (0 day post-infection - dpi) pigs were necropsied 2 h before the experimental infection, whereas infected group was orally challenged with 10^8 cfu/ml of a *Salmonella* Typhimurium phagetype

DT104 and subsequently necropsied at 2 dpi. The strain used was a field isolate obtained from a naturally infected pig (12). Ileum samples were collected from all experimental animals and immediately frozen in liquid nitrogen for RNA and protein isolation or fixed in 10% neutral buffered formalin for histological processing. Piglets were housed in experimental isolation facilities of the University of León (Spain). All procedures involving animals were performed in accordance with the European regulations regarding the protection of animals used for experimental and other scientific purposes and its protocol approved by the Ethical and Animal Welfare Committee of the University of León (Approval number: #3-2005).

LCM and RNA preparations

Frozen gut samples were embedded in optimal cutting temperature compound (Sakura Finetek USA, Torrance, CA, USA) and cut into serial 20 µm sections. Before microdissection, eight cryostat sections from each pig were mounted on glass slides and treated with RNAlater-ICE (Ambion) according to manufacturer instructions. Afterwards, cells from PP follicles were laser-microdissected and captured from terminal ileum sections (15 cm from the ileocaecal junction) by Auto-Laser Pressure Catapulting mode (Figure 1A and B) with a PALM MicroBeam device (Carl Zeiss MicroImaging GmbH, Jena, Germany). Catapulted tissue was soaked in 15 µl of RLT buffer (Qiagen, Valencia, CA, USA) poured in 200 µl microtubes caps and RNA purifications were carried out employing the RNeasy Mini Kit (Qiagen). Eluted RNA was digested with RNase-Free DNase Set (Qiagen) and RNA quality was checked by Experion RNA analysis (Bio-Rad, Hercules, CA, USA).

Microarray analysis

Gene expression analysis was carried out using the GeneChip Porcine Genome Array by Affymetrix platform (Affymetrix Inc., Santa Clara, CA, USA) at the Genomics Unit of CABIMER (Andalusian Center for Molecular Biology and Regenerative Medicine, Seville, Spain) as previously described (3). Probe signal intensities were captured and processed with the GeneChip Operating Software 1.4.0.036 (Affymetrix) and the resulting CEL files were reprocessed using robust multi-array average normalization (RMA). Then, differentially expressed (DE) genes were accessed by the Rank Products (RP) method (13) using default settings. A FDR adjusted p-value of 0.05 was used as cutoff to rank significantly regulated transcripts. After initial quality control one infected sample was discarded. Since the Affymetrix Porcine GeneChip is not fully annotated in all the features, it was re-annotated with Blast2GO (14). Gene expression datasets were validated by real-time quantitative PCR. For data visualization, a heatmap was created using the gplots (version 3.0.1) R package (15). Microarray data files have been deposited in NCBI's Gene Expression Omnibus repository (16) and are accessible through GEO Series accession number GSE101442.

Systems biology analysis

For biological functions analysis of microarray data, the list of significantly regulated genes was uploaded into Ingenuity Pathway Analysis (IPA, Ingenuity Systems). Gene interaction networks were automatically generated, ranked by score and depicted on IPA. Score estimated the probability that a collection of genes equal to or greater than the number in a network could be achieved by chance alone and values of 3 or higher were considered to have a 99.9% confidence of not being generated by random chance alone. For statistical analysis of enriched functions/pathways, IPA Knowledge Base was used as reference set and Fisher's exact test was employed to estimate the significance of association. P-values below 0.05 were considered statistically significant. The activation z-score was employed to predict the activation state of enriched functions and upstream regulators. Predictions with z-score values higher or lower than 2 and a p-value ≤0.05 denoted a statistically increased or decreased activation state respectively. In pathway and network diagrams, nodes represented a gene, and its relationship with other molecules was represented by a line (solid and dashed lines represented direct and indirect associations, respectively). Nodes with a red or green background were input genes (from microarray results) found to be up or down-regulated, respectively. Grey and white nodes were molecules added by IPA based on predictions of the Ingenuity Knowledge Base to produce diagrams.

Real-time quantitative PCR (qPCR)

RNA from infected and control samples was reverse transcribed to cDNA using the qScript cDNA Synthesis kit (Quanta BioSciences, Gaithersburg, MD, USA) and real-time quantitative PCR (qPCR) assays were performed to access gene relative expression by the $2^{-\Delta\Delta Cq}$ method (17) as previously described (3). Beta-actin was used as reference gene and fold change values higher or lower than 1 meant up-regulation or down-regulation respectively. Subsequently, data were compared by Student's t-test using the software SPSS 15.0 for Windows® (SPSS, Inc) and a p-value below 0.05 was considered statistically significant. Primer pairs used for amplifications can be found as supporting information (see Table S1).

Western blot analysis

For protein extractions, catapulted tissue was homogenized with lysis buffer (150 mM sodium chloride, 1.0% NP-40, 50 mM Tris pH 8.00 and 5 mM PMSF) and incubated at room temperature for 30 min. Subsequently, samples were disrupted by vortexing for 30 sec and lysate concentration was determined using Bradford Protein Assay (Bio-Rad). Protein from individual replicates belonging to the same group was pooled (2.5 ug per sample), electrophoretically fractionated in 12% (w/v) SDS-PAGE gels and transferred onto a PVDF membrane (Millipore, Bedford, MA, USA). Western blot assays were carried out as previously

described (18) using the following primary antibodies: mouse anti-swine histocompatibility class I (SLA-I) 4B7/8 (19), rabbit anti-NLRC5 antibody (ab105411, Abcam, Cambridge, UK) and mouse anti-porcine CD5 1H6/8 (20). To confirm equal sample loading, membranes were reblotted with anti-GAPDH monoclonal antibody (GenScript, Picastaway, NJ, USA). Membranes were scanned in a FLA-5100 imager (Fujifilm, Tokyo, Japan) and signal intensity was determined using Multigauge software (Fujifilm, Tokyo,Japan).

Histological analysis

Immunohistochemistry was conducted with 5-µm sections of paraffin-embedded samples as described elsewhere . (21). In brief, mouse anti-porcine macrophage 4E9/11 (19), anti-swine histocompatibility class I (SLA-I) 4B7/8 and anti-porcine TLR2 1H11 (22) as well as rabbit anti-NLRC5 (ab105411, Abcam) and anti-Apolipoprotein AI (ab75922, Abcam) were used as primary antibodies. Biotinylated anti-mouse and anti-rabbit Ig (Dako, Barcelona, Spain) were used to detect immune complexes. Immunofluorescence using confocal microscopy was performed using the anti-porcine macrophage 4E9/11 mouse antibody, anti-NLRC5 polyclonal antibody (ab105411, Abcam) and a rabbit antiserum against *Salmonella* Typhimurium flagellin (3). Fluorescein isothiocyanate (FITC)-conjugated goat anti-rabbit IgG (Sigma-Aldrich, St. Louis, MO, USA) and Alexa Fluor 594 anti-mouse IgG (Life Technologies, Carlsbad, CA, USA) were used as secondary antibodies. Immunostaining was performed as previously described (23). Subsequently, samples were evaluated and imaged using a LSM 5 Exciter confocal microscope (Carl Zeiss, Jena, Germany).

RESULTS

Processes related to cell movement and activation are primarily induced in *Salmonella* infected follicles

A total of 164 transcripts, corresponding to 152 unique genes, were found to be differently expressed in PP follicles at 2 dpi with *S.* Typhimurium (Table S2). Then, bioinformatic tools were used to translate microarray data into biological information. It was revealed that infection mainly resulted in an enrichment of genes involved in cellular movement, followed by other host functions such as immune cell trafficking, inflammatory response and cell-to-cell signalling and interaction (Table S3, worksheets 1, 2 and 3). Obtained IPA z-score was employed to predict the effect of the uncovered gene expression changes on distinct biological processes. We found more up- than down-regulated genes in infected samples (Figure 2). Among those results, we found that mechanisms related to migration and activation of leukocytes were the most significantly activated in *S.* Typhimurium infected PP follicles (Table S2). Activation of lymphocytes, and especially T-lymphocytes, showed the highest activation z-score values (see

Table S3, worksheet 4). To confirm results from bioinformatic predictions, we carried out a series of assays. Firstly, hematoxylin-eosin staining disclosed the presence of phagocytes, mainly neutrophils, in PP upon infection (Figure 1C and D), and the absence in PP from control pigs. This finding could be further related to the presence of pathogen in tissue, since *S.* Typhimurium antigens were co-localized in follicles areas of neutrophils accumulation, being mostly observed in the cytoplasm of polymorphonuclear cells (Figure 1E). Lastly, we quantified the abundance of CD5 in tissue by western blot to estimate the induction of lymphocytes activation in follicles, uncovering higher levels of this molecule in infected samples (Figure 1F).

Adaptive immune responses are properly induced in Peyer's patches follicles during infections by NTS

Genes involved in immune response were found up-regulated in PP of infected animals. Subsequent network analysis depicted direct and indirect relationships between genes taking part in distinct processes of this biological function (Table S3, worksheet 1). The major network generated by the prediction tool integrated genes involved in the communication between innate and adaptive immune cells, as well as in dendritic cell maturation (Figure 3A). Interestingly, all genes involved in these processes were found to be up-regulated, and were directly or indirectly related with type I and II interferon (*IFN*) genes. In light of the role of PP follicles in the establishment of adaptive immune responses, we additionally verified the differential expression of genes involved in the formation of germinal centers. This analysis confirmed an up-regulation of the main mediators of B-cell-T-cell interactions and cytokines involved in the triggering of B-cell mediated immunity (Figure 3B).

IFNγ is the main upstream regulator of the transcriptional response carried out in PP during non-typhoidal salmonellosis

IPA-generated z-score results were used to identify and predict the activation state of upstream regulators, aiming to explain gene expression changes observed in tissue after infection. In this analysis, IFNγ was found to be the main regulator of transcriptional changes observed in PP follicles in response to *S*. Typhimurium (Table 1), modulating the expression of 53 out of 152 (35%) of the differently regulated molecules in the dataset (see Table S3, worksheet 5). Genes *STAT1* and *STAT3*, both transcriptional factors involved in interferon signalling, as well as IFNα were detected among the upstream regulators most significantly implicated in tissue response to infection (Table 1). Additionally, network analysis displayed that IFNγ up-regulation mostly led to the activation of related genes (Figure 4A). Although significant changes in *IFNγ* mRNA levels were not detected by microarray analysis, we observed by qPCR that this gene was more expressed in infected than control samples. Moreover, results

of bioinformatic data mining were confirmed by a selected qPCR expression profile of IFNγ-target genes (Figure 4B) and also by immunohistochemical assays (Figure 4C).

NLRC5 resulted up-regulated in PP follicles of *S.* Typhimurium infected swine

Antigen processing and major histocompatibility complex class I (MHCI) presentation was found presumably activated via *HLA-A*, *PSMB9*, *B2M*, and *TAP1* upregulation. Network analysis complemented with the IPA molecule activity predictor tool revealed that *NLRC5* up-regulation can induce the activation of genes coding for molecules involved in different stages of the antigen presentation via MHCI pathway, being all of them up-regulated after infection (Figure 5A and 5B). In order to functionally validate these results, we initially checked changes in the abundance of NLRC5 and MHCI in tissue by western blot. In accordance with transcriptomic data, the bacterial challenge resulted in an increase of both molecules in tissue at protein level (Figure 6A). Additionally, immunohistochemistry assays uncovered higher levels of NLRC5 in follicles at 2 dpi (Figure 6B and 6C). Further analysis using immunofluorescence followed by confocal analysis detected the presence of NLRC5 in polymorphonuclear cells (Figure 6D) and strikingly, double labelling of NLRC5 and macrophages in infected tissue revealed that these cells did not express NLRC5 (Figure 6E). Higher levels of MHCI were also detected in infected PP follicles, being this receptor mainly localized in the cytoplasm of mononuclear phagocytes (Figure 6F and 6G).

DISCUSSION

Until recently, the pathogenesis of infections by NTS was largely overlooked due to the dominance of the murine model of typhoid fever and the lack of alternative models for the study of salmonellosis (2). Considering the anatomical and physiological similarities of swine and human PP (9) as well as the correspondence between disease caused by *S.* Typhimurium in pig and man (4, 5), in the current study we combined a swine model of non-typhoid salmonellosis with LCM and microarrays analysis to dissect the mechanisms carried out in PP follicles upon infection with *S.* Typhimurium.

The follicles of secondary lymphoid organs consist in a microenvironment that favours the interaction of B and T cells with each other as well as with antigen presenting DCs and antigen exposing follicular dendritic cells (FDCs) (24). Upon gut infections, protein antigens trigger the germinal center reaction in PP follicles, giving rise to specialized structures that play a key role in the generation of long-lived plasma cells and memory B-cells (25). The GC response has a well characterized dependence on T-follicular helper cells (Tfh), which are CD4+ mature cells that provide essential help to B-cells during this process via cytokines such as IL21, IL4, and IL10 (24, 26). Interestingly, *IL21* and *IL10* genes were found in this study to be up-regulated in

infected follicles and the same was observed for genes coding for IL-21 regulators (*STAT3* and *STAT1*), IL4 regulator (*STAT6*), IFNγ, IL6, IL12 and TGF-β. In line with this, Coquerelle and Moser (27) report that FDC stimulates Tfh differentiation by producing IL6 upon type I interferon signalling and collaborate with B-cell activation by releasing large amounts of active TGF-β. Apart from the cytokine environment, the ligation of B cells CD40 and CD80 with CD40L and CD28 on activated Th cells is crucial for formation of GC (28, 29). Strikingly, these mediators were also uncovered by us to be up-regulated. Taken together our results indicate GC formation and establishment of humoral immunity mechanisms in ileum PP follicles shortly (2 days) after NTS infection. This is the first report about GC formation in NTS *Salmonella* infection and results differ from previous studies in other areas of research in PP response which mention that GC arises 4 to 5 days after immunization(28).

The microscopic analysis of tissue revealed that PP follicles underwent a notable infiltration of neutrophils upon infection, being *S.* Typhimurium predominantly detected in the cytoplasm of polymorphonuclear cells (PMN). During mice infections, the infiltration of neutrophils is usually observed in the PP subepithelial dome and interfollicular area (7). Therefore, the remarkable infiltration of neutrophils observed by us in PP follicles led us to speculate that apart from killing of bacteria, these cells could carry *Salmonella* to follicles and take part in further immunity mechanisms. In fact, it has been reported that neutrophils may influence adaptive responses by acting either directly on T cells or indirectly through DC modulation (30). Physical interactions involving neutrophils, DC and T cells have been shown to result in T cell activation following DC acquisition of antigens delivered by polymorphonuclear cells (PMN) (31, 32). In our previous work (11), we suggest the existence of a Th1 response to *Salmonella*, based on the ability of DC to present *Salmonella* antigens by MHC class II molecules. Here, several evidences of cross-presentation induction were found, probably linked to the uptake of viable neutrophils by DC as has been previously observed (33). Cross-presentation defines the process by which professional APC present peptides from extracellular antigens via their own MHCI molecules to CD8+ T cells (34). In this work, bioinformatic mining of microarray data disclosed an up-regulation of genes encoding molecules involved in different steps of the antigen presentation pathway via MHCI. Gene coding for BATF3, a transcription factor required for development of DC subsets capable of priming CD8+ T-cell responses (35, 36) was found to be up-regulated in this study. In addition, IFNγ, followed by IFNα and their signal transducers STAT1 and STAT3 were identified as the most relevant upstream regulators of the transcriptional response carried out in follicles upon *S*. Typhimurium infection. A number of studies have reported the ability of type I and type II IFNs to promote CD8+ T cell cross-priming against exogenous antigens, playing an essential role in controlling infections. In particular, IFNα induces the differentiation of monocytes into DC, known as IFN-DC, which are highly efficient in mediating antigen cross-presentation (37). Both type I and II IFN boost cross-

presentation of antigens by DC via the modulation of immunoproteasome activity (38, 39). In this context, up-regulation of genes coding for molecules involved in antigen transport and MHCI presentation (*TAP1*, *PSMB9*, *B2M*) together with a high expression of *IRF1* (Interferon Regulatory Factor 1) and *UBD* (Ubiquitin D) was observed in porcine PP after *S*. Typhimurium infection. IRF1 and UBD are essential for the expression of the immunoproteasome subunits and for the subsequent presentation of antigens to CD8+ T cells (40, 41). These findings, supported by previous evidences (34, 42, 43), suggest that DCs cross-present *Salmonella* antigens in porcine PP after engulfment of infected neutrophils, in line with our previous observations in *S*. Typhimurium infected mesenteric lymph nodes (3).

In addition to the indirect modulation of the cross-presentation by transferring *Salmonella* antigens to DC, neutrophils could play a more active role in the CD8+ T cell response to infection. Some studies have reported that both human and murine neutrophils can acquire a phenotype consistent with a possible APC function, including their potential to cross-present antigens to CD8+T-cells in response to a broad range of microbial pathogens (30, 44). Interestingly, in this work we observed that PMN cells other than macrophages showed high levels of NLRC5, a NOD-like receptor newly identified as a key regulator of the MHCI antigen presentation pathway in infected tissues (45). Immunohistochemistry and western blot assays demonstrated that NLRC5 was increased at protein level in infected tissue and analysis of microarray data also related the up-regulation of this gene with the activation of molecules involved in the Ag presentation via MHCI. From our results, it can be inferred that infected neutrophils could directly cross-present *S.* Typhimurium antigens to CD8+ T-cells in porcine PP. However, despite that NLRC5 has been recently characterized as one of the main transcriptional regulators of MHCI molecules in immune cells (46), direct antigen presentation by neutrophils has thus far not been demonstrated in pigs, especially with respect to an induction of antigen-specific CD8+T-cells response upon cross-presentation of microbial proteins.

In summary, this study disclosed a prominent role for PP follicles in the establishment of immune responses against *S.* Typhimurium. Results indicated evidence of GC formation and the establishment of humoral immunity responses in tissue at 2 dpi. Interestingly, several evidences of cross-presentation triggering were found. These results reveal novel aspects of gut immune response to non-typhoid *Salmonella* infections that could contribute to the establishment of therapies and vaccine approaches against salmonellosis.

AUTHORS CONTRIBUTIONS

RPM was responsible for the whole study, including lab work and LCM, and contributed to writing of the manuscript. VM and CA collected the tissue samples by LCM and participated in

the histological analysis. AC, HA and AJM carried out the experimental infections. MGC and RB performed bioinformatics analysis. SZL and JHU significantly contributed to the biological interpretation of data. JJG conceived and designed the project and participated in the interpretation and discussion of the results, as well as in the writing of the manuscript. All authors read and approved the final manuscript.

CONFLICT OF INTEREST STATEMENT

The authors declare that the research was conducted in the absence of any commercial or financial relationships that could be construed as a potential conflict of interest.

ACKNOWLEDGEMENTS

We thank Reyes Alvarez for skilful technical assistance, Esther Peralbo for technical support in confocal microscopy analysis and Eloísa Andújar and Mónica Pérez for their excellent array technical assistance. We thank the Andalusian Platform of Bioinformatics (PAB) from the University of Málaga for granting the right to use IPA bioinformatic tool. This work was based on part of a PhD Thesis (47) from University of Córdoba (Spain)

FUNDING

This work was supported by the Spanish Ministry of Science and Innovation (AGL2014-54089-R). RPM was a predoctoral researcher supported by the FPU Research Program of the Spanish Ministry of Education and Science. SZL is a postdoctoral researcher supported by the Postdoctoral Trainee Program of the Spanish Ministry of Economy and Competitiveness (FPDI-2013-15619). HA is a postdoctoral researcher supported by the Juan de la Cierva Postdoctoral Trainee Program of the Spanish Ministry of Economy and Competitiveness (FJCI-2014-22877).

REFERENCES

1. Majowicz SE, Musto J, Scallan E, Angulo FJ, Kirk M, O'Brien SJ, et al. The global burden of nontyphoidal Salmonella gastroenteritis. *Clin Infect Dis* (2010) 50(6):882-9. doi: 10.1086/650733.

2. Tsolis RM, Xavier MN, Santos RL, Baumler AJ. How to become a top model: impact of animal experimentation on human Salmonella disease research. *Infect Immun* (2011) 79(5):1806-14. doi: 10.1128/IAI.01369-10.

3. Martins RP, Aguilar C, Graham JE, Carvajal A, Bautista R, Claros MG, et al. Pyroptosis and adaptive immunity mechanisms are promptly engendered in mesenteric lymph-nodes during pig infections with Salmonella enterica serovar Typhimurium. *Vet Res* (2013) 44:120. doi: 10.1186/1297-9716-44-120.

4. Boyen F, Haesebrouck F, Maes D, Van Immerseel F, Ducatelle R, Pasmans F. Non-typhoidal Salmonella infections in pigs: a closer look at epidemiology, pathogenesis and control. *Vet Microbiol* (2008) 130(1-2):1-19. doi: 10.1016/j.vetmic.2007.12.017.

5. Sanchez-Vargas FM, Abu-El-Haija MA, Gomez-Duarte OG. Salmonella infections: an update on epidemiology, management, and prevention. *Travel Med Infect Dis* (2011) 9(6):263-77. doi: 10.1016/j.tmaid.2011.11.001.

6. Broz P, Ohlson MB, Monack DM. Innate immune response to Salmonella typhimurium, a model enteric pathogen. *Gut Microbes* (2012) 3(2):62-70. doi: 10.4161/gmic.19141.

7. Tam MA, Rydstrom A, Sundquist M, Wick MJ. Early cellular responses to Salmonella infection: dendritic cells, monocytes, and more. *Immunol Rev* (2008) 225:140-62. doi: 10.1111/j.1600-065X.2008.00679.x.

8. Martinoli C, Chiavelli A, Rescigno M. Entry route of Salmonella typhimurium directs the type of induced immune response. *Immunity* (2007) 27(6):975-84. doi: 10.1016/j.immuni.2007.10.011.

9. Makala LH, Suzuki N, Nagasawa H. Peyer's patches: organized lymphoid structures for the induction of mucosal immune responses in the intestine. *Pathobiology* (2002) 70(2):55-68. doi: 67305.

10. El Shikh ME, Pitzalis C. Follicular dendritic cells in health and disease. *Front Immunol* (2012) 3:292. doi: 10.3389/fimmu.2012.00292.

11. Martins RP, Lorenzi V, Arce C, Lucena C, Carvajal A, Garrido JJ. Innate and adaptive immune mechanisms are effectively induced in ileal Peyer's patches of Salmonella typhimurium infected pigs. *Dev Comp Immunol* (2013) 41(1):100-4. doi: 10.1016/j.dci.2013.04.020.

12. Arguello H, Carvajal A, Naharro G, Rubio P. Evaluation of protection conferred by a Salmonella Typhimurium inactivated vaccine in Salmonella-infected finishing pig farms. *Comp Immunol Microbiol Infect Dis* (2013) 36(5):489-98. doi: 10.1016/j.cimid.2013.05.002.

13. Breitling R, Armengaud P, Amtmann A, Herzyk P. Rank products: a simple, yet powerful, new method to detect differentially regulated genes in replicated microarray experiments. *FEBS Lett* (2004) 573(1-3):83-92. doi: 10.1016/j.febslet.2004.07.055.

14. Conesa A, Gotz S, Garcia-Gomez JM, Terol J, Talon M, Robles M. Blast2GO: a universal tool for annotation, visualization and analysis in functional genomics research. *Bioinformatics* (2005) 21(18):3674-6. doi: 10.1093/bioinformatics/bti610.

15. Warnes GR, Bolker B, Bonebakker L, Gentleman R, Huber W, Liaw A, et al. gplots: Various R programming tools for plotting data. *R package version* (2009) 2(4):1.

16. Barrett T, Wilhite SE, Ledoux P, Evangelista C, Kim IF, Tomashevsky M, et al. NCBI GEO: archive for functional genomics data sets--update. *Nucleic Acids Res* (2013) 41(Database issue):D991-5. doi: 10.1093/nar/gks1193.

17. Livak KJ, Schmittgen TD. Analysis of relative gene expression data using real-time quantitative PCR and the 2(-Delta Delta C(T)) Method. *Methods* (2001) 25(4):402-8. doi: 10.1006/meth.2001.1262.

18. Martins RP, Collado-Romero M, Martinez-Gomariz M, Carvajal A, Gil C, Lucena C, et al. Proteomic analysis of porcine mesenteric lymph-nodes after Salmonella typhimurium infection. *J Proteomics* (2012) 75(14):4457-70. doi: 10.1016/j.jprot.2012.03.045.

19. Bullido R, Gomez del Moral M, Alonso F, Ezquerra A, Zapata A, Sanchez C, et al. Monoclonal antibodies specific for porcine monocytes/macrophages: macrophage heterogeneity in the pig evidenced by the expression of surface antigens. *Tissue Antigens* (1997) 49(4):403-13.

20. Pescovitz MD, Book BK, Aasted B, Dominguez J, Bullido R, Trebichavsky I, et al. Analyses of monoclonal antibodies reacting with porcine CD5: results from the Second International Swine CD Workshop. *Vet Immunol Immunopathol* (1998) 60(3-4):269-73.

21. Yubero N, Jimenez-Marin A, Barbancho M, Garrido JJ. Two cDNAs coding for the porcine CD51 (alphav) integrin subunit: cloning, expression analysis, adhesion assays and chromosomal localization. *Gene* (2011) 481(1):29-40. doi: 10.1016/j.gene.2011.04.006.

22. Alvarez B, Revilla C, Domenech N, Perez C, Martinez P, Alonso F, et al. Expression of toll-like receptor 2 (TLR2) in porcine leukocyte subsets and tissues. *Vet Res* (2008) 39(2):13. doi: 10.1051/vetres:2007051.

23. Robertson D, Savage K, Reis-Filho JS, Isacke CM. Multiple immunofluorescence labelling of formalin-fixed paraffin-embedded (FFPE) tissue. *BMC Cell Biol* (2008) 9:13. doi: 10.1186/1471-2121-9-13.

24. Cerutti A, Puga I, Cols M. New helping friends for B cells. *Eur J Immunol* (2012) 42(8):1956-68. doi: 10.1002/eji.201242594.

25. Acheson DW, Luccioli S. Microbial-gut interactions in health and disease. Mucosal immune responses. *Best Pract Res Clin Gastroenterol* (2004) 18(2):387-404. doi: 10.1016/j.bpg.2003.11.002.

26. Allen CD, Okada T, Cyster JG. Germinal-center organization and cellular dynamics. *Immunity* (2007) 27(2):190-202. doi: 10.1016/j.immuni.2007.07.009.

27. Coquerelle C, Moser M. DC subsets in positive and negative regulation of immunity. *Immunol Rev* (2010) 234(1):317-34. doi: 10.1111/j.0105-2896.2009.00887.x.

28. Gatto D, Brink R. The germinal center reaction. *J Allergy Clin Immunol* (2010) 126(5):898-907; quiz 8-9. doi: 10.1016/j.jaci.2010.09.007.

29. Zotos D, Tarlinton DM. Determining germinal centre B cell fate. *Trends Immunol* (2012) 33(6):281-8. doi: 10.1016/j.it.2012.04.003.

30. Beauvillain C, Delneste Y, Scotet M, Peres A, Gascan H, Guermonprez P, et al. Neutrophils efficiently cross-prime naive T cells in vivo. *Blood* (2007) 110(8):2965-73. doi: 10.1182/blood-2006-12-063826.

31. Megiovanni AM, Sanchez F, Robledo-Sarmiento M, Morel C, Gluckman JC, Boudaly S. Polymorphonuclear neutrophils deliver activation signals and antigenic molecules to dendritic cells: a new link between leukocytes upstream of T lymphocytes. *J Leukoc Biol* (2006) 79(5):977-88. doi: 10.1189/jlb.0905526.

32. Morel C, Badell E, Abadie V, Robledo M, Setterblad N, Gluckman JC, et al. Mycobacterium bovis BCG-infected neutrophils and dendritic cells cooperate to induce specific T cell responses in humans and mice. *Eur J Immunol* (2008) 38(2):437-47. doi: 10.1002/eji.200737905.

33. Alfaro C, Suarez N, Onate C, Perez-Gracia JL, Martinez-Forero I, Hervas-Stubbs S, et al. Dendritic cells take up and present antigens from viable and apoptotic polymorphonuclear leukocytes. *PLoS One* (2011) 6(12):e29300. doi: 10.1371/journal.pone.0029300.

34. Houde M, Bertholet S, Gagnon E, Brunet S, Goyette G, Laplante A, et al. Phagosomes are competent organelles for antigen cross-presentation. *Nature* (2003) 425(6956):402-6. doi: 10.1038/nature01912.

35. Tussiwand R, Lee WL, Murphy TL, Mashayekhi M, Kc W, Albring JC, et al. Compensatory dendritic cell development mediated by BATF-IRF interactions. *Nature* (2012) 490(7421):502-7. doi: 10.1038/nature11531.

36. Patel R, Sad S. Transcription factor Batf3 is important for development of CD8+ T-cell response against a phagosomal bacterium regardless of the location of antigen. *Immunol Cell Biol* (2016) 94(4):378-87. doi: 10.1038/icb.2015.98.

37. Spadaro F, Lapenta C, Donati S, Abalsamo L, Barnaba V, Belardelli F, et al. IFN-alpha enhances cross-presentation in human dendritic cells by modulating antigen survival, endocytic routing, and processing. *Blood* (2012) 119(6):1407-17. doi: 10.1182/blood-2011-06-363564.

38. Arellano-Garcia ME, Misuno K, Tran SD, Hu S. Interferon-gamma induces immunoproteasomes and the presentation of MHC I-associated peptides on human salivary gland cells. *PLoS One* (2014) 9(8):e102878. doi: 10.1371/journal.pone.0102878.

39. Gessani S, Conti L, Del Corno M, Belardelli F. Type I interferons as regulators of human antigen presenting cell functions. *Toxins (Basel)* (2014) 6(6):1696-723. doi: 10.3390/toxins6061696.

40. Namiki S, Nakamura T, Oshima S, Yamazaki M, Sekine Y, Tsuchiya K, et al. IRF-1 mediates upregulation of LMP7 by IFN-gamma and concerted expression of immunosubunits of the proteasome. *FEBS Lett* (2005) 579(13):2781-7. doi: 10.1016/j.febslet.2005.04.012.
41. Lukasiak S, Schiller C, Oehlschlaeger P, Schmidtke G, Krause P, Legler DF, et al. Proinflammatory cytokines cause FAT10 upregulation in cancers of liver and colon. *Oncogene* (2008) 27(46):6068-74. doi: 10.1038/onc.2008.201.
42. Salerno-Goncalves R, Sztein MB. Priming of Salmonella enterica serovar typhi-specific CD8(+) T cells by suicide dendritic cell cross-presentation in humans. *PLoS One* (2009) 4(6):e5879. doi: 10.1371/journal.pone.0005879.
43. Lopez-Medina M, Perez-Lopez A, Alpuche-Aranda C, Ortiz-Navarrete V. Salmonella modulates B cell biology to evade CD8(+) T cell-mediated immune responses. *Front Immunol* (2014) 5:586. doi: 10.3389/fimmu.2014.00586.
44. Davey MS, Morgan MP, Liuzzi AR, Tyler CJ, Khan MWA, Szakmany T, et al. Microbe-specific unconventional T cells induce human neutrophil differentiation into antigen cross-presenting cells. *J Immunol* (2014) 193(7):3704-16. doi: 10.4049/jimmunol.1401018.
45. Yao Y, Qian Y. Expression regulation and function of NLRC5. *Protein Cell* (2013) 4(3):168-75. doi: 10.1007/s13238-012-2109-3.
46. Staehli F, Ludigs K, Heinz LX, Seguin-Estevez Q, Ferrero I, Braun M, et al. NLRC5 deficiency selectively impairs MHC class I- dependent lymphocyte killing by cytotoxic T cells. *J Immunol* (2012) 188(8):3820-8. doi: 10.4049/jimmunol.1102671.
47. Martins RP. Swine immune response to Salmonella enterica serovar Typhimurium. A functional genomics approach: University of Cordoba (Spain) (2013).

FIGURE LEGENDS

Figure 1. Laser capture microdissection, histological analysis and CD5 quantification in PP follicles upon infection with *S.* Typhimurium. A-B: After their identification (A), PP follicles were microdissected by Auto-Laser Pressure Catapulting. C-D: H/E staining of ileum sections demonstrating PP follicles before (C) and after (D) the bacterial challenge. A highlighted in (D), infection resulted in a relevant infiltration of neutrophils. E: fluorescent labelling of *S.* Typhimurium in tissue. Pathogen was mainly detected in the perinuclear zone of polymorphonuclear cells. Scale bar = 20 μm F: western blot assays uncovered increased levels of CD5 in infected tissue. Statistical significance was calculated using Student's t test. ** denotes a p-value inferior to 0.01.

Figure 2. Heatmap analysis of microarray data in *S.* Typhimurium infected PP follicles. Hierarchical clustering of statistically significant microarray gene expression from infected and control pigs. Red color reflects higher level of expression, whereas green tonalities are associated to a decreased expression level.

Figure 3. Network analysis of microarray data and qPCR assays in *S.* Typhimurium infected PP follicles. A: major generated network depicted a common up-regulation of genes taking part in communication between innate and adaptive immune cells and dendritic cell maturation pathways. B: differential gene expression analysis by qPCR revealed an up-regulation of molecules involved in the formation of geminal centers in infected PP follicles. Statistical significance was calculated using Student's t test.

Figure 4. IFNγ is the main regulator of transcriptional response of PP follicles to non-typhoid *Salmonella*. A: network analysis disclosed that IFNγ up-regulation resulted in the activation or inhibition (orange and blue lines respectively) of 53 genes differently expressed after infection. Data were inconsistent for genes linked with yellow lines and effect could not be predicted for those linked with grey lines. B: differential expression analysis by qPCR for a sort of IFNγ-target genes confirmed the predicted effect of IFNγ in the expression of downstream molecules. Statistical significance was calculated using Student's t test. One, two or three asterisk denotes a p-value inferior to 0.05, 0.01 and 0.001 respectively. C: immunohistochemistry assays further corroborated the effect of IFNγ up-regulation in target molecules at protein level. White and yellow bars denote 200 and 100 μm respectively.

Figure 5. NLRC5 activates the antigen presentation via MHCI pathway after infection with non-typhoid *Salmonella*. Network analysis (A) disclosed direct relationships between NLCR5 and distinct molecules involved in the antigen presentation via MHCI (B).

Figure 6. *S.* Typhimurium infected PP follicles showed increased levels of NLRC5 and MHCI at protein level. A: western blot assays demonstrated an increase of NLRC5 and MHCI in infected follicles. Statistical significance was calculated using Student's t test. One or two asterisks denote a p-value inferior to 0.05 and 0.01 respectively. B-C: Immunohistochemistry assays uncovered increased levels of NLRC5 in infected PP follicles. D: Confocal microscopy analysis detected NLRC5 in polymorphonuclear cells (merge image: NLRC5-FITC and DAPI; white and yellow bars denote 10 and 50 μm respectively). E: NLRC5 was not detected in macrophages (merge image: NLRC5-FITC, 4E9/11 anti-macrophage-Alexa Fluor® 594 and DAPI; white bar denotes 10 μm). F-G: Higher levels of MHCI were observed in follicles after infection, being labelling mainly observed in the cytoplasm of mononuclear phagocytes.

SUPPLEMENTARY MATERIAL

Table S1. Primer pairs used in host differential expression analysis by real-time quantitative PCR.

Table S2. Differentially expressed transcripts in infected Peyer's Patches follicles.

Table S3. Ingenuity Pathway Analysis (IPA) annotations.

TABLES

Table 1. Predicted activation state of biological functions and upstream regulators

Category	Predicted Activation State	Activation z-score	*p*-value*
Downstream effect			
Migration of phagocytes	Increased	2,930	6,33E-13
Cell movement of phagocytes	Increased	2,928	4,09E-11
Cell movement of leukocytes	Increased	2,342	4,54E-10
Cell movement of myeloid cells	Increased	3,012	9,53E-10
Leukocyte migration	Increased	2,498	3,35E-09
Activation of leukocytes	Increased	3,213	4,77E-09
Activation of blood cells	Increased	3,514	4,96E-09
Activation of cells	Increased	3,378	1,80E-08
Quantity of leukocytes	Increased	2,564	1,92E-08
Homing of leukocytes	Increased	2,604	2,64E-08
Upstream regulator			
IFNG	Activated	4,211	1,04E-26
lipopolysaccharide	Activated	4,918	6,03E-23
poly rI:rC-RNA	Activated	4,291	4,60E-22
Interferon alpha	Activated	2,541	5,35E-21
TNF	Activated	4,107	1,46E-18
IL1B	Activated	4,096	1,05E-17
STAT3	Activated	3,039	1,43E-17
STAT1	Activated	3,110	2,58E-17
IL6	Activated	2,861	4,18E-17
NFkB (complex)	Activated	4,092	6,77E-16

*Calculated with Fisher's exact test. *P*-values bellow 0.05 were considered statistically significant.

Figure 1

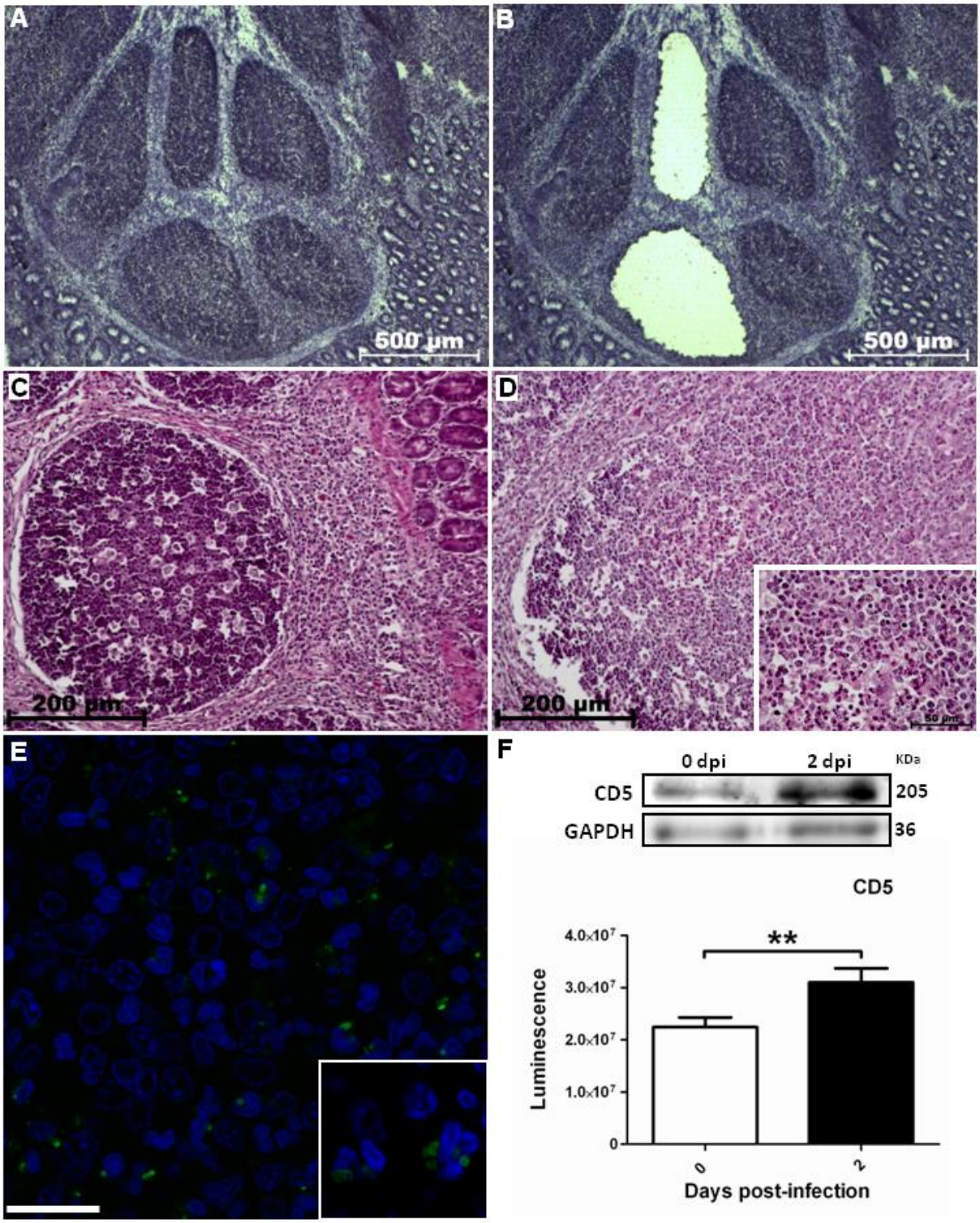
A
500 µm
B
500 µm
C
200 µm
D
200 µm
50 µm
E
F
0 dpi
2 dpi
KDa
CD5
205
GAPDH
36
CD5
**
Luminescence
4.0x10^7
3.0x10^7
2.0x10^7
1.0x10^7
0
0
2
Days post-infection

Figure 2

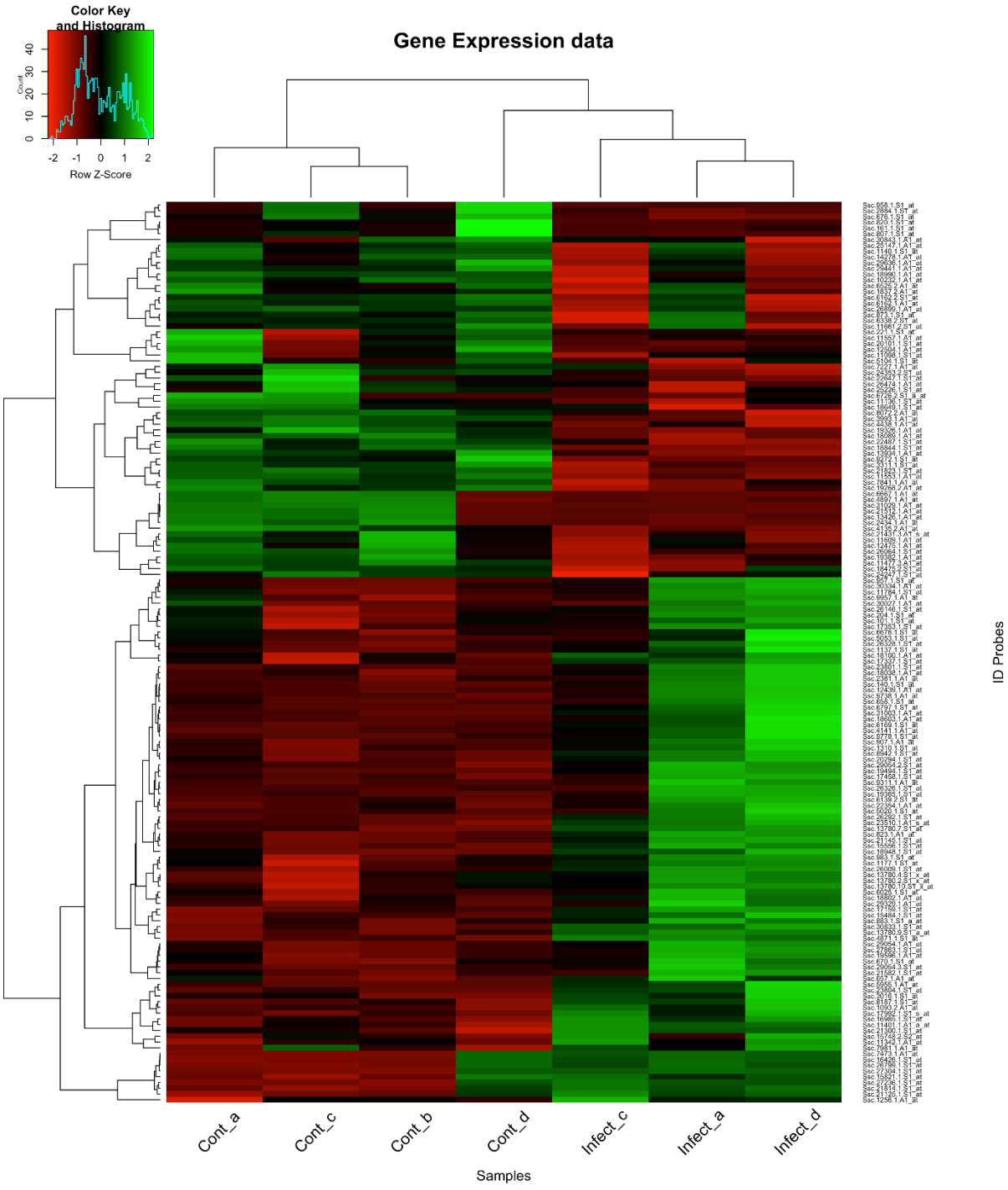
Color Key
and Histogram
Count
0
10
20
30
40
-2
-1
0
1
2
Row Z-Score
Gene Expression data
ID Probes
Cont_a
Cont_c
Cont_b
Cont_d
Infect_c
Infect_a
Infect_d
Samples

Figure 3

A

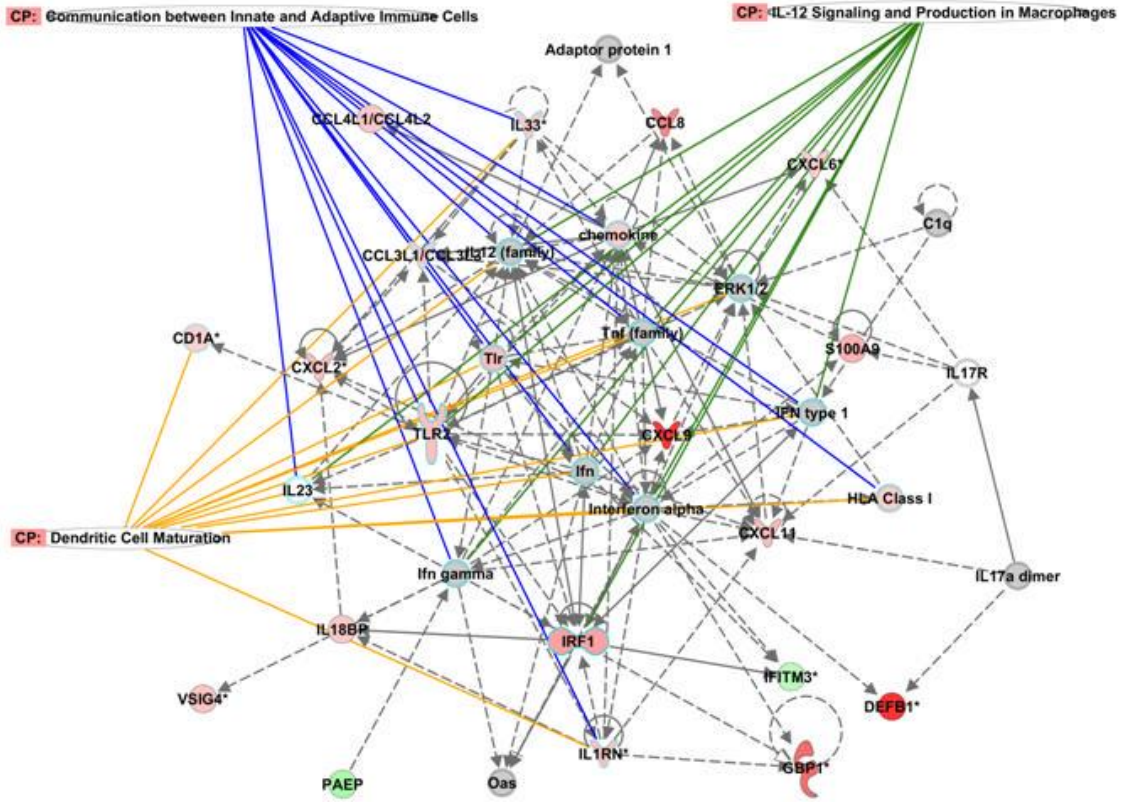
CP: Communication between Innate and Adaptive Immune Cells
CP: IL-12 Signaling and Production in Macrophages
CP: Dendritic Cell Maturation
Adaptor protein 1
CCL4L1/CCL4L2
IL33*
CCL8
CXCL6*
C1q
chemokine
CCL3L1/CCL3L2
IL12 (family)
ERK1/2
CD1A*
Tnf (family)
S100A9
CXCL2*
Tlr
IL17R
IFN type 1
TLR2
CXCL9
Ifn
IL23
HLA Class I
Interferon alpha
CXCL11
Ifn gamma
IL17a dimer
IL18BP
IRF1
IFITM3*
VSIG4*
DEFB1*
IL1RN*
GBP1*
PAEP
Oas

B

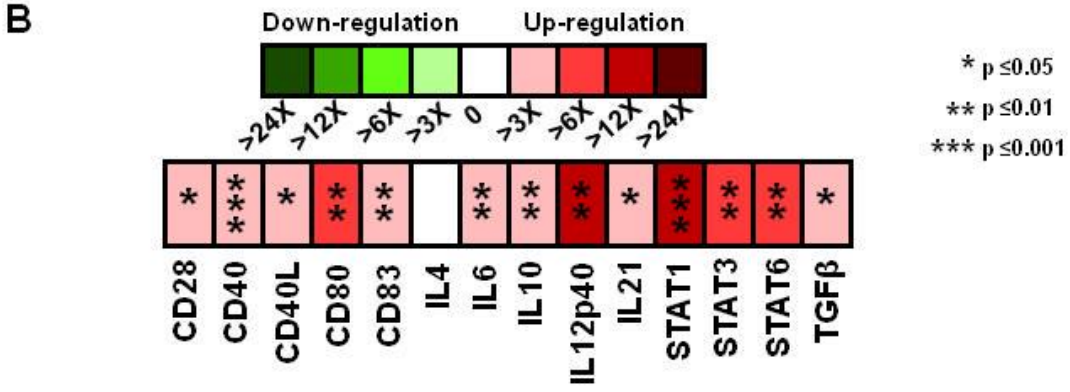
Down-regulation
Up-regulation
>24X
>12X
>6X
>3X
0
>3X
>6X
>12X
>24X
* p ≤0.05
** p ≤0.01
*** p ≤0.001
CD28
CD40
CD40L
CD80
CD83
IL4
IL6
IL10
IL12p40
IL21
STAT1
STAT3
STAT6
TGFβ

Figure 4

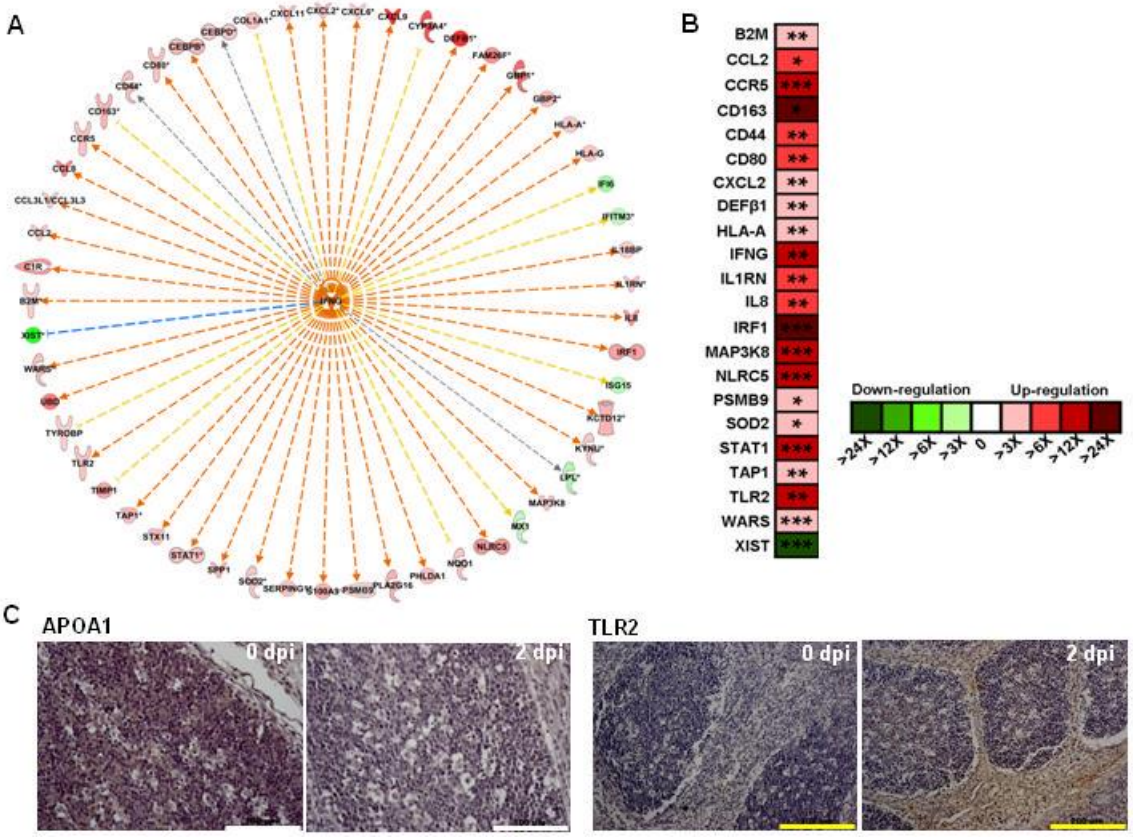
A
B
B2M **
CCL2 *
CCR5 ***
CD163 *
CD44 **
CD80 **
CXCL2 **
DEFβ1 **
HLA-A **
IFNG **
IL1RN **
IL8 **
IRF1 ***
MAP3K8 ***
NLRC5 ***
PSMB9 *
SOD2 *
STAT1 ***
TAP1 **
TLR2 **
WARS ***
XIST ***
Down-regulation
Up-regulation
>24X
>12X
>6X
>3X
0
>3X
>6X
>12X
>24X
C
APOA1
0 dpi
2 dpi
TLR2
0 dpi
2 dpi

Figure 5

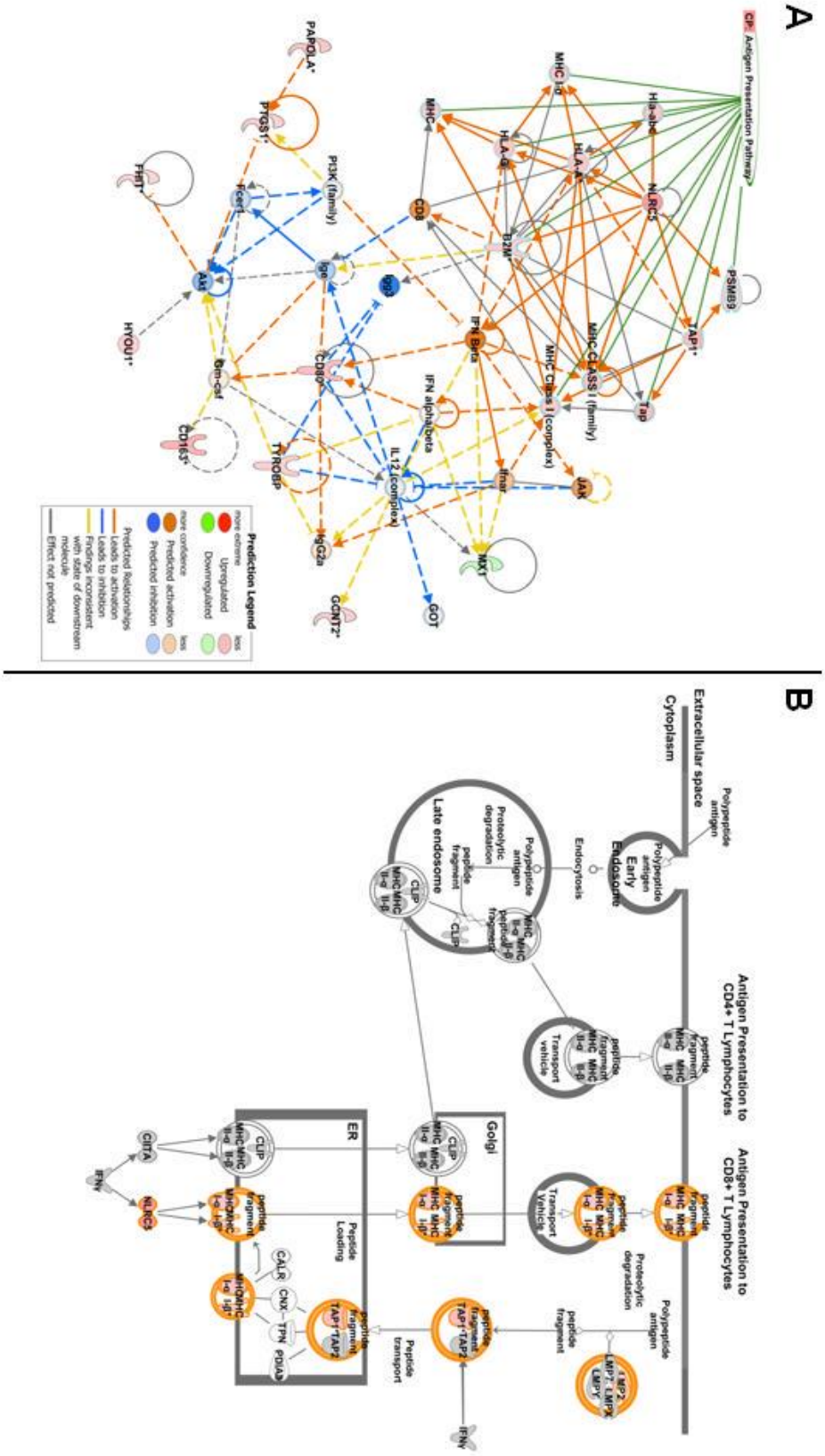
A
CP: Antigen Presentation Pathway
PAPOLA*
PTGS1*
PI3K (family)
Fcer1
FHIT*
HYOU1*
Akt
Src
Stat3
CD8
MHC I-a
MHC-I
HLA-G
HLA-A
Hla-abc
NLRC5
B2M*
PSMB9
TAP1*
IFN Beta
MHC Class I (complex)
Tap
IFN alpha/beta
IL12 (complex)
Ifnar
JAK
Mx1
GOT
GCNT2*
IgG2a
TYROBP
CD163*
Gm-csf
CD80*
Prediction Legend
more extreme
Upregulated
Downregulated
less
more confidence
Predicted activation
Predicted inhibition
less
Predicted Relationships
Leads to activation
Leads to inhibition
Findings inconsistent with state of downstream molecule
Effect not predicted
B
Extracellular space
Cytoplasm
Polypeptide antigen
Early Endosome
Endocytosis
Late endosome
Proteolytic degradation
peptide fragment
MHC II-α MHC II-β
CLIP
Transport vehicle
Antigen Presentation to CD4+ T Lymphocytes
Antigen Presentation to CD8+ T Lymphocytes
Golgi
ER
Peptide Loading
Peptide transport
CIITA
IFNγ
NLRC5
CALR
CNX
TPN
PDIA3
TAP1 TAP2
LMP2 LMP7 LMP10
Proteolytic degradation
Polypeptide antigen
peptide fragment

Figure 6

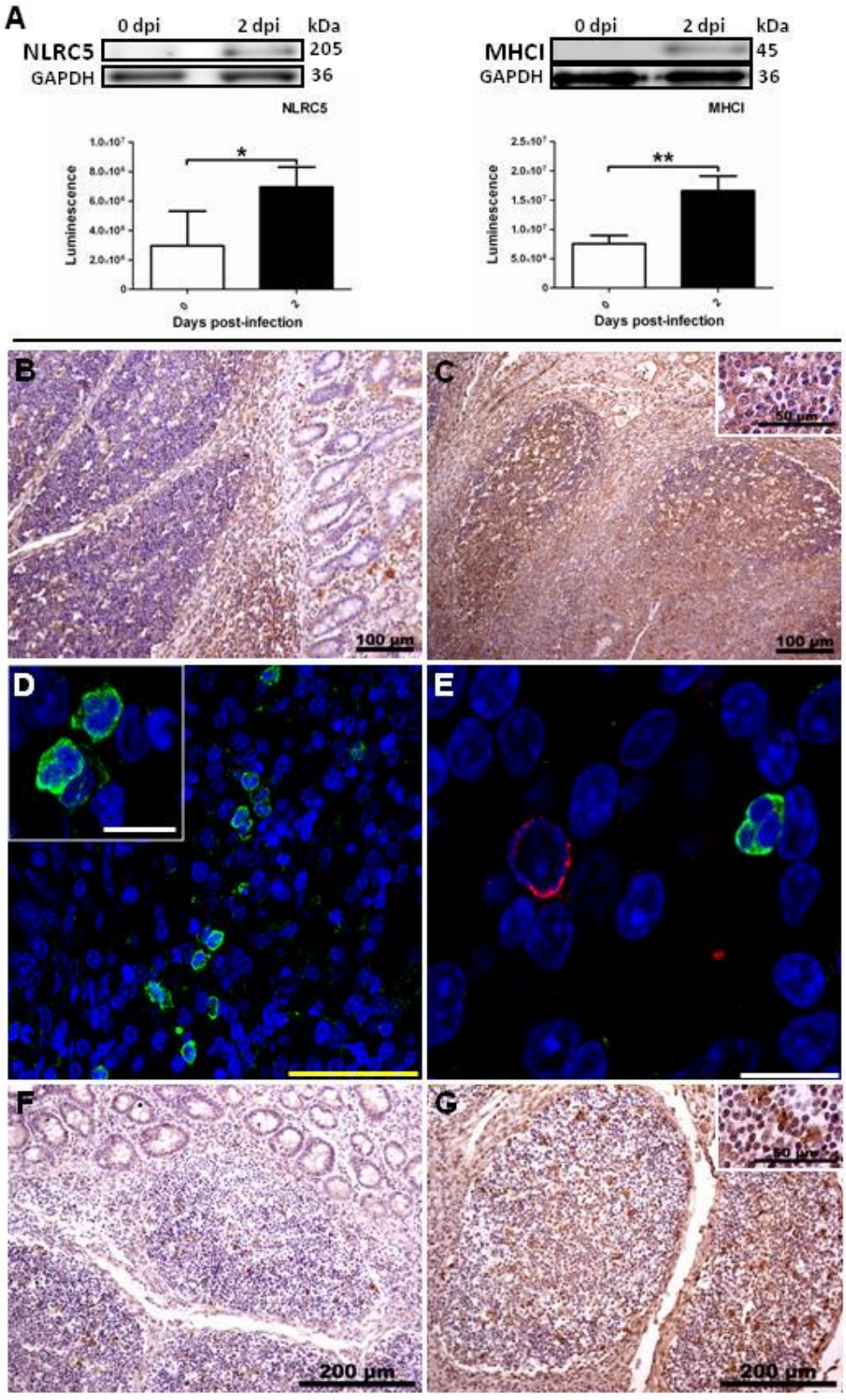
A
0 dpi
2 dpi
kDa
NLRC5
205
GAPDH
36
NLRC5
Luminescence
*
Days post-infection
MHCI
45
36
MHCI
**
B
C
50 µm
100 µm
D
E
F
G
200 µm

3.3 Post-doctorat

Après mon doctorat, j'ai voulu mettre à profit les compétences scientifiques acquises dans la recherche appliquée pour m'orienter vers un domaine de recherche plus fondamentale. Pendant mon activité postdoctorale au sein de l'équipe de Robin Fahraeus (UMR 1162 - Inserm, Université Paris Descartes-Paris Diderot-Paris 13), je me suis intéressé aux bases moléculaires de la présentation d'antigènes par le CMH-I et aux stratégies développées par les pathogènes pour entraver ce processus.

Pendant longtemps, les peptides antigéniques présentés par le CMH-I ont été attribués exclusivement à la digestion par le protéasome de protéines endogènes [28] (**Figure 13A**). Néanmoins, l'équipe Fahraeus a démontré que d'autres peptides, issus d'un processus indépendant de la dégradation de protéines, représentent une source majeure d'antigènes pour la voie du CMH-I [29-31]. Plus concrètement, ses travaux ont dévoilé que des peptides antigéniques de classe I sont produits pendant une étape précoce de la traduction, appelée en anglais *pioneer round of translation*. Ce processus consiste à une lecture des ARN pré-messagers, ayant pour but de contrôler leur qualité avant leur interaction avec les facteurs d'initiation de la traduction canonique. Les cellules sont donc capables d'utiliser les « sous-produits » de cette lecture, nommés *pioneer translation products* (PTPs), pour induire la réponse cytotoxique via le CMH-I (**Figure 13B**).

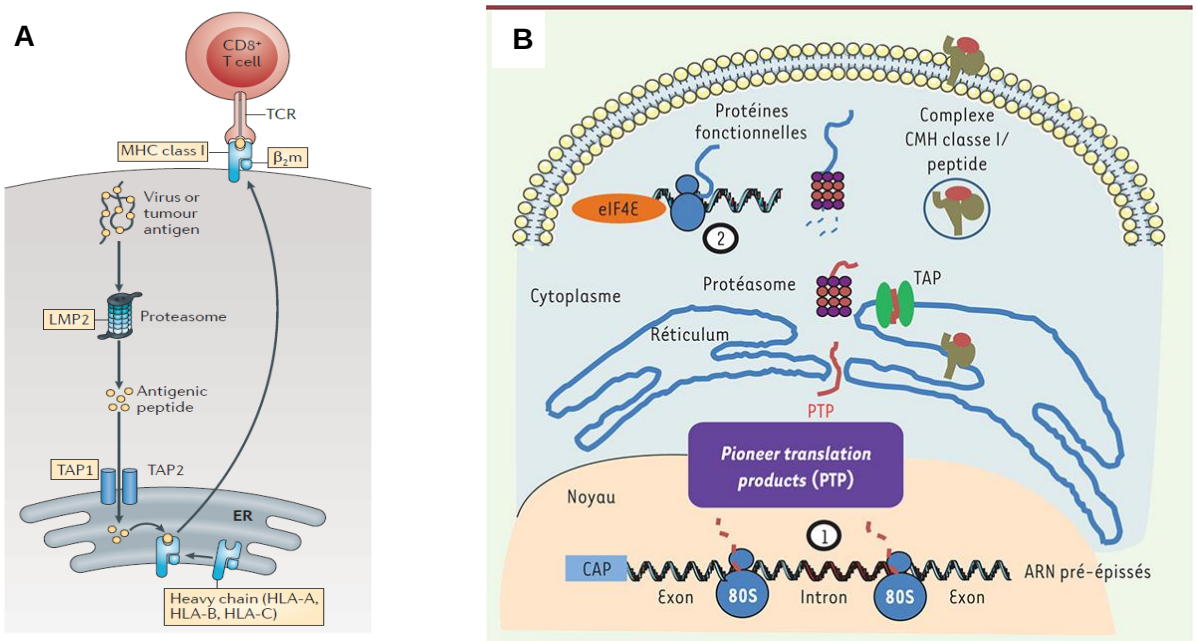

Figure 13 – Sources de peptides antigéniques pour la voie du CMH-I. A : Des protéines fonctionnelles sont dégradés par le protéasome pour donner origine aux peptides présentés par le CMH-I. D'après Kobayashi and van den Elsen [28]. **B : 1-** La lecture des ARN pré-messagers par des ribosomes nucléaires pendant la *pioneer round of translation* produit des polypeptides provenant de séquences exoniques et introniques appelés *pioneer translation products* (PTPs). Les PTPs sont dégradés par le protéasome et ensuite incorporés à la voie du CMH-I. **2 -** La dégradation de protéines fonctionnelles jouerait qu'un rôle mineur dans la production de peptides antigéniques de classe I. D'après Duvallet et al. [31].

Dans le cadre de mes travaux, j'ai d'abord collaboré à l'identification d'un facteur de l'hôte détourné par le virus d'Epstein-Barr (EBV) pour entraver la production de peptides antigéniques et par conséquent, échapper à la réponse immunitaire. Nous avons aussi développé un système de criblage de molécules d'intérêt pour le traitement des tumeurs associés à l'EBV. Les observations ainsi que les outils issus de cette collaboration m'ont permis de réaliser une étude avec pour objectif de décrypter l'influence de la maturation des ARNm sur la traduction canonique et la production de peptides antigéniques alternatifs (PTPs) pour la voie du CMH-I.

3.3.1 Détournement de la présentation d'antigènes par le virus d'Epstein-Barr

L'oncovirus d'Epstein-Barr est capable d'échapper au système immunitaire mais possède un talon d'Achille : EBNA1. Cette protéine est à la fois requise pour la réplication et la maintenance du génome viral, mais est également fortement antigénique. Concrètement, des lymphocytes T dirigés contre EBNA1 sont présents chez toutes les personnes infectées. Pour cette raison, le virus d'Epstein-Barr a développé une stratégie dans laquelle la séquence de l'ARNm d'EBNA1 codant pour une répétition de glycine et alanine (GAr, *glycine-alanine repeat*) présente dans la région N-terminale d'EBNA1, limite sa propre traduction. Ainsi, la traduction d'EBNA1 est restreinte à un niveau minimal pour assurer le maintien du virus, tout en minimisant sa reconnaissance par le système immunitaire [32].

Des travaux menés en collaboration avec l'équipe de Marc Blondel (Université de Bretagne Occidentale) a identifié la nucléoline (NCL) comme le premier facteur de la cellule hôte nécessaire à la limitation GAr-dépendante de la traduction d'EBNA1, et donc à la furtivité du virus d'Epstein-Barr ([33], ci-joint). Plus précisément, un système rapporteur développé chez la levure nous a permis d'observer que la surexpression de NSR1, le gène codant pour la NCL chez *Saccharomyces cerevisiae,* augmente l'effet inhibiteur *in cis* de GAr sur la traduction (**Figure 14**). Chez des cellules humaines, nous avons confirmé que la surexpression de NCL augmente l'inhibition GAr-dépendante de l'expression d'EBNA1, tandis que son inhibition limite la suppression de la traduction d'EBNA1 et de la présentation de peptides antigéniques dérivés d'EBNA1 (**Figure 15A-D**). De plus, nous avons montré que NCL interagit de façon directe avec les G-quadruplexes (G4s) formés par la séquence codant le domaine GAr dans l'ARNm d'EBNA1 et que le PhenDC3, un ligand connu des G4s, empêche cette interaction (**Figure 15E**) et bloque l'effet inhibiteur de GAr sur l'immunodétection d'EBNA1. Par conséquent, cette étude a mis en lumière une cible thérapeutique nouvelle et pertinente pour induire la reconnaissance par le système immunitaire des tumeurs liés au virus d'Epstein-Barr (**Figure 16**).

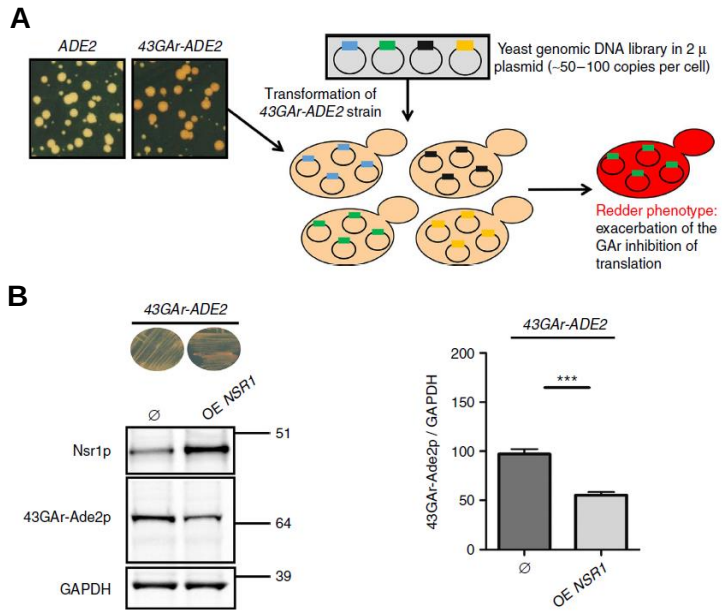

Figure 14 – *Screening* chez la levure de molécules contribuant à l'effet de GAr sur la traduction. A: L'expression à un niveau suffisant du gène rapporteur ADE2 chez *Saccharomyces cereviseae* confère la production de colonies blanches. La séquence d'ADN codant pour le motif GAr a été cloné en phase avec ADE2 (43GAr-ADE2) et incorporé à une souche de *S. cereviseae* qui a ainsi acquis le phénotype rose. Cette souche a été transformée avec une librairie d'ADN génomique de levure et les souches rouges (*redder phenotype*, expression réduite d'ADE2) ont été analysées pour la recherche de molécules contribuant à l'effet de GAr sur la traduction. Cette approche a identifié NSR1 (nucléoline chez les mammifères). **B:** Une analyse par WB a confirmé que la surexpression de NSR1 réduit l'expression de GAr-Ade2. Modifié de Lista et al. (2017) Nat Comm [33]

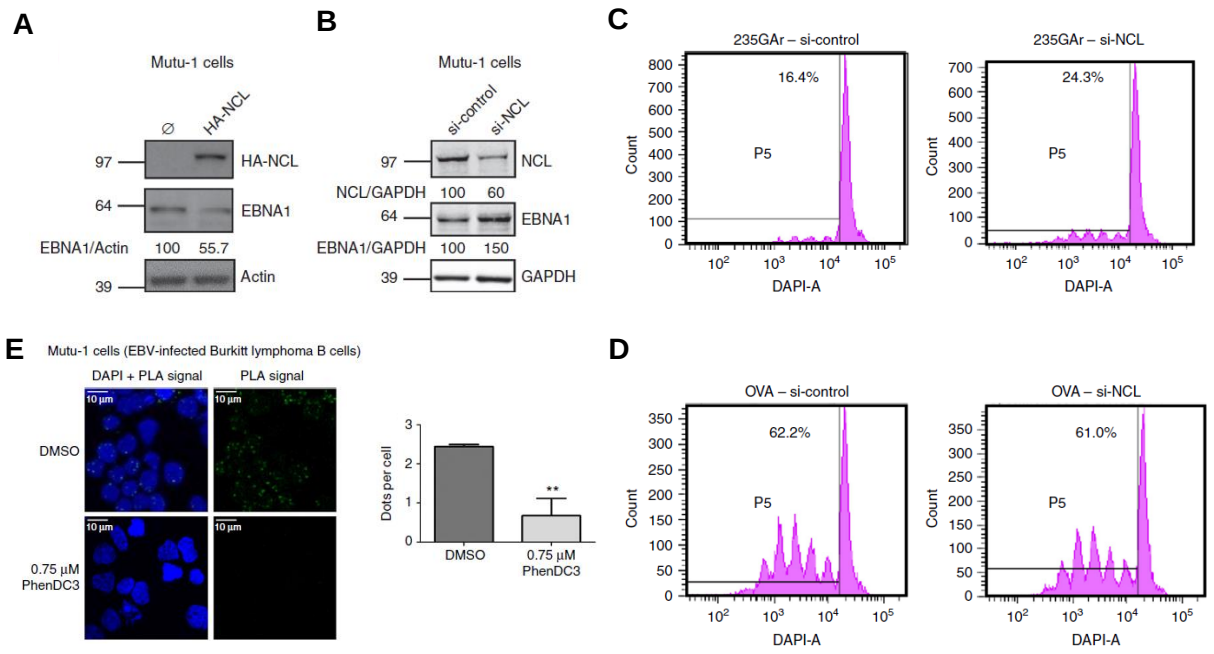

Figure 15 – La nucléoline contribue à la limitation GAr-dépendante de la traduction d'EBNA1 et de la présentation d'antigènes par la voie du CMH-I. A-B: *Western blot.* **A:** La surexpression de la nucléoline (NCL) chez la lignée cellulaire Mutu-1 (cellules B humaines infectées par l'EBV) réduit la traduction d'EBNA1. **B:** L'inhibition de l'expression de NCL par *silencing RNA* (siRNA) entraine une augmentation des niveaux d'EBNA1. **C-D:** Effet de l'inhibition de l'expression de la NCL sur la présentation d'antigènes. Des cellules de la lignée H1299 ont été transfectées avec le CMH-I murin (Kb) et une construction codant pour la protéine OVA avec ou sans le motif GAr. Les cellules ont été traitées avec des siRNA contrôles ou ciblant la NCL et cultivées avec des lymphocytes T $CD8^+$ spécifiques de l'OVA marqués avec le réactif Cell Trace Violet. Après 3 jours de co-culture, les niveaux de présentation antigénique ont été estimés par cytométrie selon les pourcentages de prolifération lymphocytaire. L'inhibition de la NCL augmente la présentation d'antigènes provenant de GAr-OVA (**C**) mais pas de l'OVA (**D**). E: Analyse de l'interaction entre la NCL et l'ARN d'EBNA1 par *Proximity Ligation Assay* (PLA), détaillée dans la section 3.3.2. Chaque interaction est visualisée comme un point (vert) dans les noyaux (bleu) des cellules. Le ligand de G-quadruplexes PhenDC3 empêche ces interactions. Modifié de Lista et al. (2017) Nat Comm [33]

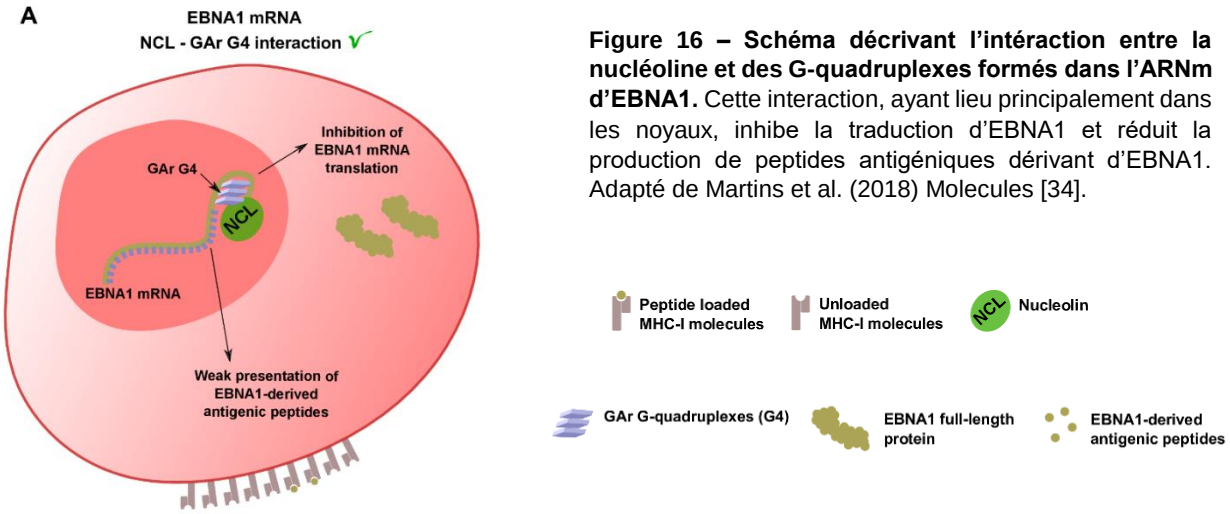

Figure 16 – Schéma décrivant l'intéraction entre la nucléoline et des G-quadruplexes formés dans l'ARNm d'EBNA1. Cette interaction, ayant lieu principalement dans les noyaux, inhibe la traduction d'EBNA1 et réduit la production de peptides antigéniques dérivant d'EBNA1. Adapté de Martins et al. (2018) Molecules [34].

3.3.2 Criblage de ligands de G-quadruplexes comme traitement de tumeurs associées au virus d'Epstein-Barr

Le rôle crucial joué par les interactions protéine-ARN dans le contrôle de multiples processus cellulaires physiologiques et pathologiques les a désignées comme cibles pour le développement de nouvelles thérapies. Cependant, le criblage de molécules interférant avec ces interactions demeure limité, principalement due à la complexité et spécificité des structures de l'ARN qui servent comme plateformes pour les protéines. Le repliement de ces structures dépend de divers médiateurs cellulaires qui, dans la plupart des cas, restent méconnus. De plus, des différences notables ont été observées dans la structure des ARNm synthétisées *in vitro* et *in cellulo.* Pour cette raison, la mise en place de méthodes *in cellulo* pour le criblage de molécules d'intérêt représente un enjeu majeur dans le cadre des interactions protéine-ARN.

L'utilisation de la technique *Proximity Ligation Assay* (PLA) pour démontrer l'interaction de la NCL avec des G4s présents dans l'ARN de EBNA1, ainsi que l'intérêt de cette interaction comme cible thérapeutique, nous a incité à utiliser le PLA pour le criblage d'autre ligands de G4 dans le but d'identifier des molécules candidates pour le traitement des tumeurs associés à EBV (**Figure 17**). Dans un premier temps, nous avons utilisé cette approche pour montrer que les ligands de G4 interfèrent différemment avec l'interaction entre la NCL et l'ARNm d'EBNA1. Des différences entre deux molécules avec une forte affinité pour l'ARN d'EBNA1 *in vitro* ont pu être dévoilées par le PLA *in cellulo* (**Figure 18**). Nous avons ainsi proposé une stratégie qui permettrait de surmonter les limitations des approches *in vitro* pour l'étude des interactions protéine-ARN [34]. Cette approche a été utilisée pour un criblage incluant des nouveaux ligands de G4 et a fait l'objet d'autres articles originales, d'un brevet et d'un chapitre de livre.

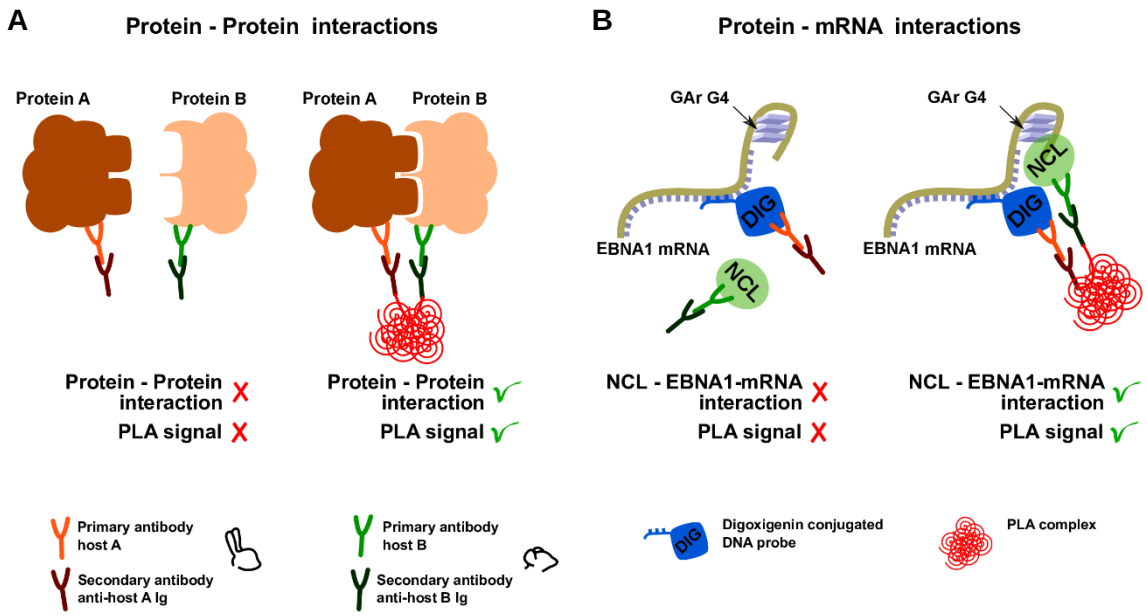

Figure 17 – Schéma décrivant le principe du *Proximity Ligation Assay* (PLA). A: Cette méthode a été originalement conçue pour étudier les interactions protéine-protéine. D'abord, une paire d'anticorps primaires produits chez deux espèces différentes est utilisée pour marquer deux protéines d'intérêt. Des anticorps secondaires conjugués à des amorces et ensuite deux réactions enzymatiques sont utilisés pour générer un produit complexe fluorescent *in situ* en cas de proximité entre les deux protéines cibles. **B:** Cette méthode a été adaptée pour l'étude des interactions protéine-ARN. Pour cela, l'ARN cible est marqué avec une sonde conjuguée à la digoxigénine. Ensuite, la technique est mise en place en utilisant un anticorps primaire anti-digoxigénine et un autre anticorps secondaire reconnaissant la protéine d'intérêt. Adapté de Martins et al. (2018) Molecules [34].

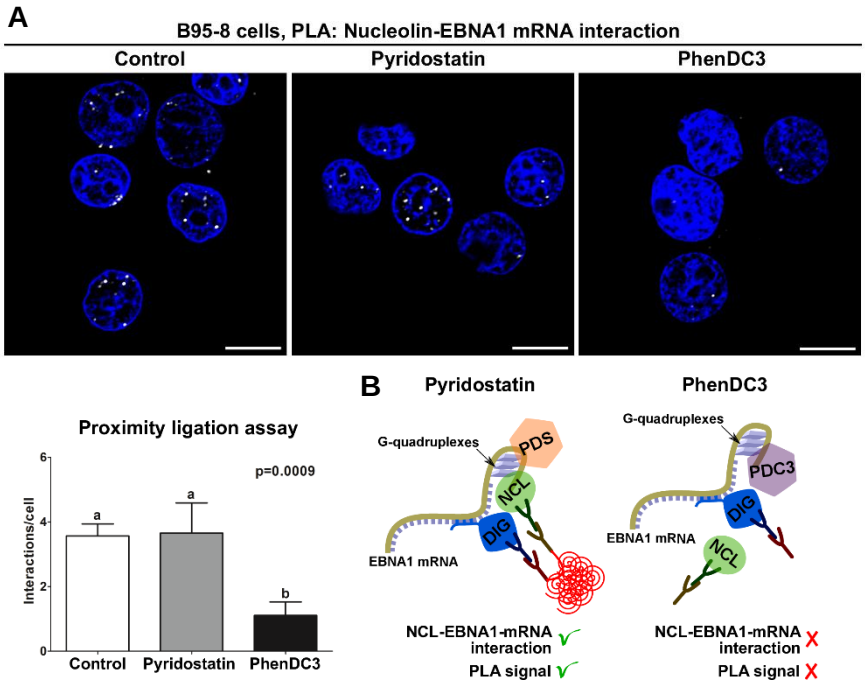

Figure 18 – Utilisation du *Proximity ligation assay* (PLA) pour le criblage de molécules intervenant sur les interactions protéine-ARN. A: La lignée cellulaire B95-8, transformée par l'EBV, a été traitée avec les ligands de G4 pyridostatin et PhenDC3. L'analyse par PLA a montré que PhenDC3 (PDC3), contrairement à la pyridostatin (PDS), empêche l'interaction de la nucleoine (NLC) avec les G-quadruplexes (G4) présents dans l'ARN messsager d'EBNA1. **B:** Schéma décrivant les résultats obtenus. Adapté de Martins et al. (2018) Molecules [34].

3.3.3 Mécanismes fondamentaux de la production de peptides antigéniques

Les peptides présentés par le CMH-I représentent un élément clé de la reconnaissance des cellules infectées et des tumeurs par le système immunitaire. Comme discuté précédemment, des études récentes ont dévoilé que les produits de traduction non-canonique sont une source importante de ces peptides. En effet, la lecture des ARN pré-messagers pendant le *pioneer round of translation* génère des peptides antigéniques provenant de séquences exoniques, introniques, aussi bien que des ARNm non-sens [29, 30].

Dans le cadre de mes travaux, j'ai utilisé différentes stratégies pour vérifier si le processus de maturation des ARNm influence la production de peptides pour la voie du CMH-I [35]. Nous avons d'abord exploité les particularités du motif GAr d'EBNA1 comme un outil pour manipuler les processus de traduction et présentation antigénique. Il a été montré que la fusion de la séquence de GAr à n'importe quelle séquence codante sans introns inhibe la traduction *in cis* et la production de peptides antigéniques de classe I [32]. Cependant, nous avons observé que cet effet inhibiteur est supprimé quand GAr est fusionné à des séquences portant des introns (**Figure 19**).

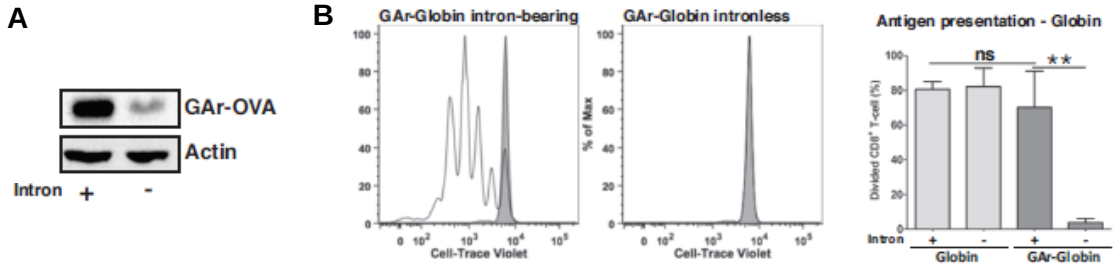

Figure 19 – La présence d'introns bloque l'effet de GAr sur la traduction et la présentation d'antigènes. **A :** Analyse par *Western blot*. **B :** Analyse de la présentation d'antigènes par la voie du CMH-I. Des lymphocytes spécifiques de l'épitope SIINFEKL provenant de la lignée de souris transgénique OT-1 ont été marqué avec Cell Trace Violet et mis en contact avec des cellules humaines (lignée H1299) transfectées avec le CMH-I murin (Kb) et des plasmides codant pour GAr-Globin avec (*intron-bearing*) ou sans introns (*intronless*). Les plasmides utilisés portaient également la séquence codante du peptide SIINFEKL. La prolifération lymphocytaire a été vérifiée par cytométrie en flux et le taux de cellules prolifératives (représentées par les pics blancs) a été calculée par apport à un contrôle non stimulé (pic gris). Les niveaux de présentation antigénique provenant de trois expériences indépendantes sont montrés dans le graphique à droite. Des constructions de globine (*globin*) sans GAr ont été utilisées comme contrôle. Modifié de Martins et al. (2019) Nucleic Acids Res.

Contrairement à la plupart des ARNm eucaryotes, l'ARNm de n'importe quelle séquence fusionnée au motif GAr reste confiné dans le noyau. Curieusement, nous avons observé que la présence d'introns modifie la localisation des ARNm portant le GAr, lesquels s'accumulent dans le cytoplasme (**Figure 20A**). De plus, la présence d'introns empêche l'interaction de l'ARN de GAr avec la nucléoline dans le noyau (**Figure 20B,** *proximity ligation assay – PLA,* décrit dans la section antérieure). Pour mieux comprendre ces observations, nous avons aussi analysé l'interaction GAr ARN-nucléoline par co-immunoprécipitation. Dans un premier temps, les lysats de cellules transfectées avec nos constructions d'ADN reportrices

ont été incubés avec un anticorps anti-nucléoline et les ARN co-précipités ont été analysés par PCR quantitative (co-immunoprécipitation *in vivo*). Parallèlement, ces lysats ont été mis en contact avec de la nucléoline recombinante et ensuite analysés par la même approche (co-immunoprécipitation *in vitro*). En accord avec nos observations par PLA, la co-immunoprécipitation *in vivo* a confirmé que la présence d'introns bloque l'interaction de la NCL avec l'ARNm de GAr (**Figure 20C**). Néanmoins, nous avons observé que cette interaction a lieu *in vitro* indépendamment de la présence d'introns dans l'ARN de GAr (**Figure 20D**). Ainsi, les G4 qui agissent comme plateformes pour la NCL sont aussi bien présents dans les ARN portant des introns que dans ses homologues sans introns. Cependant, l'épissage et d'autres processus ayant lieu sur l'ARN portant des introns empêchent cette interaction et modifient pourtant la composition de la particule ribonucléaire.

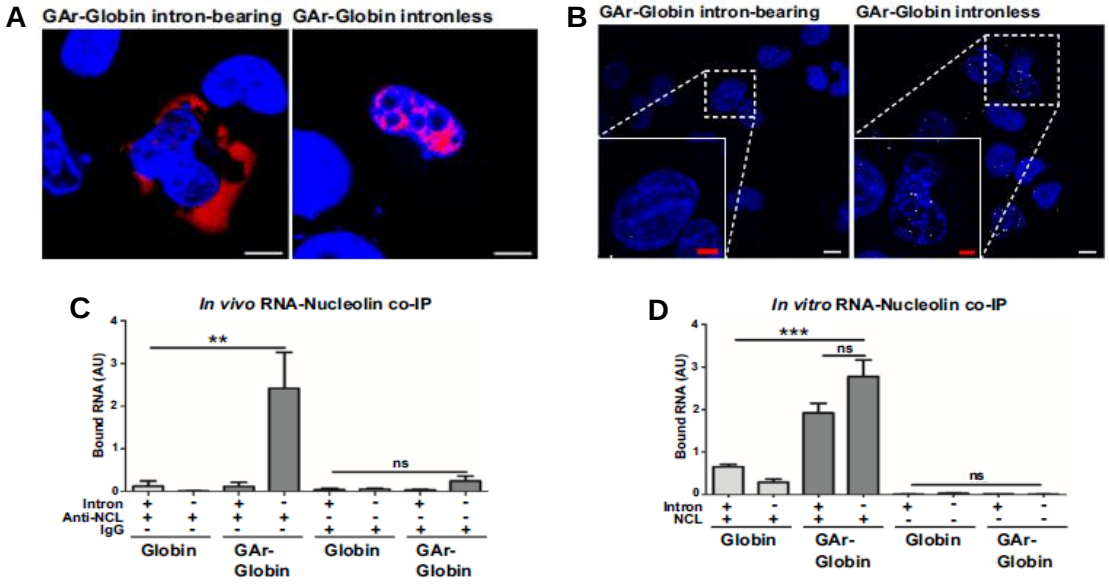

Figure 20 – Interaction de la nucléoline avec l'ARNm de GAr. A : Une analyse par *RNA-FISH* a montré que la présence d'introns modifie la localisation de l'ARNm de GAr. **B :** Le *proximity ligation assay (PLA, décrit dans la section antérieure)* a mis en évidence que la présence d'introns empêche l'interaction de la NCL avec l'ARNm de GAr. **C :** Co-immunoprécipitation *in vivo*. **D :** Co-immunoprécipitation *in vitro.* Contrairement aux observations *in vivo,* la NCL intéragit *in vitro* avec l'ARN de GAr indépendamment de la présence d'introns. Des constructions de globine (*globin*) sans GAr ont été utilisées comme contrôle. Modifié de Martins et al. (2019) Nucleic Acids Res. [35]

Ces résultats ont mis en évidence que les ARNm avec ou sans introns subissent des processus de maturation qui sont différents. De plus, d'autres analyses présentées dans l'article original [35], ont indiqué que les ARNm transcrits d'une séquence d'ADN portant des introns sont plus abondants mais, au même temps, traduits moins efficacement. Cependant, cette tendance est inversée quand ces mêmes séquences reportrices sont fusionnées à GAr, confirmant que son effet inhibiteur est bloqué dans le cadre des ARN destinés au processus d'épissage. Ce mécanisme et l'interaction entre la NCL et l'ARN de GAr ont été utilisés pour

montrer que l'épissage et le transport des ARN, ainsi que les protéines qui composent les ribonucléoprotéines peuvent modifier la production de peptides antigéniques pour la voie du CMH-I. Nous avons ensuite mis en place une stratégie expérimentale pour vérifier si ces observations étaient une conséquence de modifications sur le niveau de protéine ou si les peptides antigéniques de classe I sont en effet issus d'un mécanisme "protéine-indépendant". Des cellules transfectées avec la construction GAr-globin avec introns (*GAr-globin intron-bearing*) ont été traitées avec l'Isoginkgetin, une molécule inhibitrice de l'épissage. Ce traitement a entrainé l'accumulation de l'ARN pré-messager de GAr-globin dans le noyau (**Figure 21A-B**) et la réduction de sa traduction (**Figure 21C**). Néanmoins, il est important de souligner que, malgré cela, une augmentation de la présentation de peptides antigéniques provenant de GAr-globin a été constaté (**Figure 21D**).

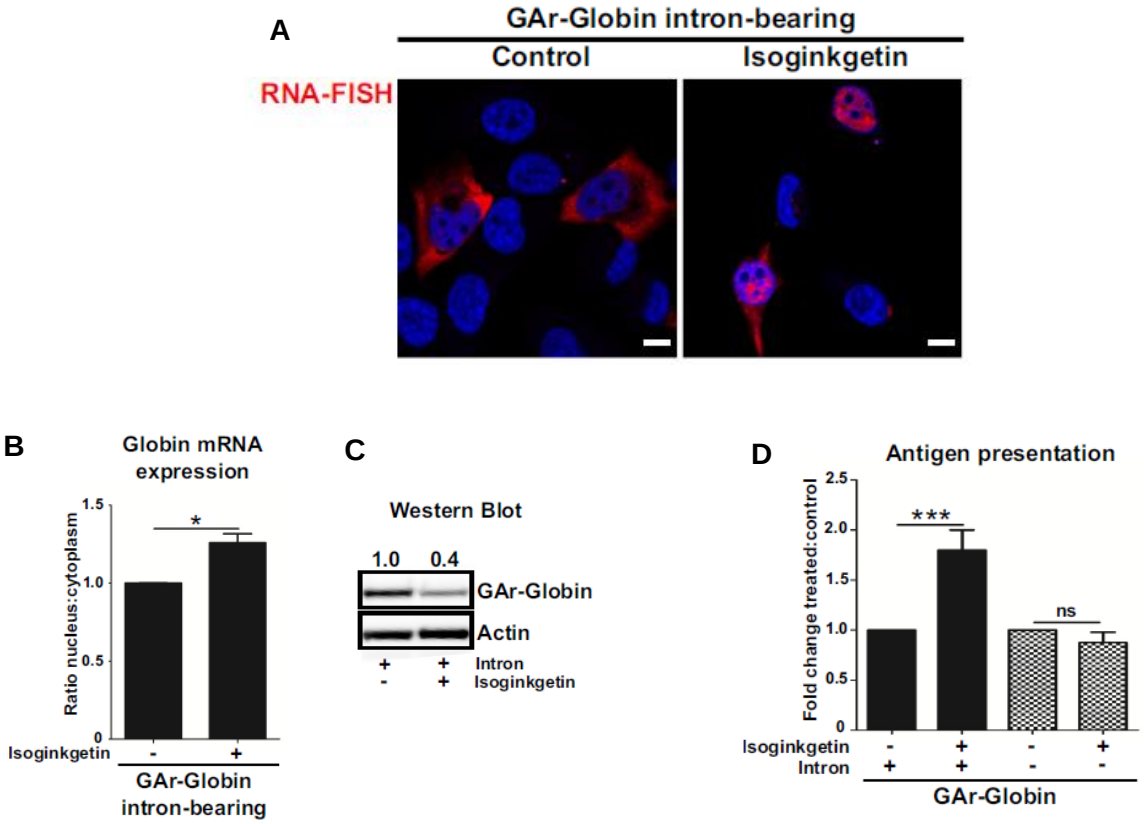

Figure 22 – Effet de l'inhibition de l'épissage sur la traduction et la présentation d'antigènes. A : Le traitement avec l'Isoginkgetin a induit l'accumulation de l'ARN de GAr-Globin dans le noyau (en rouge). Bleu = DAPI. Barre d'échelle = 10 µm. **B :** PCR quantitative, l'Isoginkgetin a augmenté la présence du pré-ARNm de GAr-globin dans le noyau. **C :** Le traitement a également réduit les niveaux protéiques de GAr-globin. **D :** Les taux de présentation des antigènes provenant de GAr-globin par le CMH-I a été estimé selon la procédure décrite dans la **Figure 19B.** L'inhibition de l'épissage a entrainé une augmentation de la présentation d'antigènes, malgré la réduction de la quantité de protéine. Modifié de Martins et al. (2019) Nucleic Acids Res. [35].

Nous avons également ajouté la séquence codante de l'*Internal ribosome entry site* (IRES) du virus de l'hépatite C humain (HCV) au niveau 5' UTR d'une construction de GAr fusionné à l'ovalbumine (HCV IRES-GAr OVA-intronless). L'IRES du HCV forme une boucle

qui empêche la traduction des ARNm par le mécanisme dépendent de la coiffe. Sa présence a ainsi augmenté l'inhibition de la traduction de l'ARN de GAr et, en même temps, a empêché son accumulation dans le noyau en induisant son transport vers le cytoplasme (**Figure 23A-B**). Il est à remarquer que, en utilisant cette stratégie, nous avons encore observé une augmentation de la présentation d'antigènes (**Figure 23C**) malgré la réduction du niveau de protéines. Nous avons ainsi démontré que le manque de corrélation entre la traduction et la production de peptides antigéniques de classe I n'est pas restreint aux ARNm présentant une localisation nucléaire.

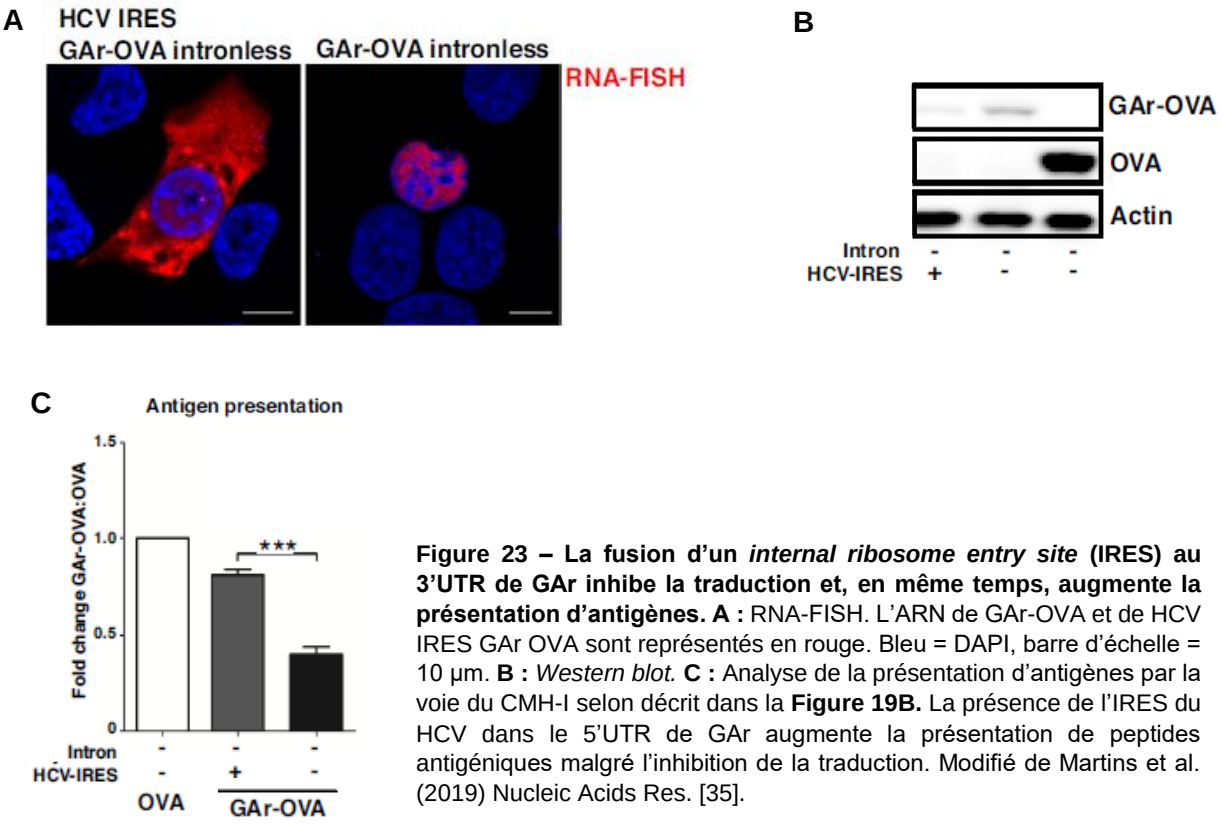

Figure 23 – La fusion d'un *internal ribosome entry site* (IRES) au 3'UTR de GAr inhibe la traduction et, en même temps, augmente la présentation d'antigènes. A : RNA-FISH. L'ARN de GAr-OVA et de HCV IRES GAr OVA sont représentés en rouge. Bleu = DAPI, barre d'échelle = 10 µm. **B :** *Western blot.* **C :** Analyse de la présentation d'antigènes par la voie du CMH-I selon décrit dans la **Figure 19B.** La présence de l'IRES du HCV dans le 5'UTR de GAr augmente la présentation de peptides antigéniques malgré l'inhibition de la traduction. Modifié de Martins et al. (2019) Nucleic Acids Res. [35].

L'effet inhibiteur de GAr sur la traduction est dépendant de l'interaction de son ARNm avec la NCL dans le noyau [33]. Pour confirmer les résultats indiquant que les protéines et les peptides antigéniques de classe I sont produits par des mécanismes indépendants, nous avons modifié cette interaction. D'abord, nous avons produit une construction d'ADN codant pour une variante de la NCL déplétée de son NLS (NCLΔNLS), présentant donc une localisation cytoplasmique. Des cellules ont été co-transfectées avec NCLΔNLS et une construction de GAr portant des introns (GAr-globin intron-bearing). Comme nous l'avons précédemment montré, l'insertion d'introns dans l'ARN de GAr le dirige vers la voie de maturation utilisée pour la plupart des transcrits des eucaryotes supérieurs, comprenant le

processus d'épissage et translocation vers le cytoplasme. L'interaction de la NCL avec GAr dans le cytoplasme (**Figure 24A**) a inhibé la traduction de GAr-globin (**Figure 24B**) sans affecter la production de peptides antigéniques (**Figure 24C**).

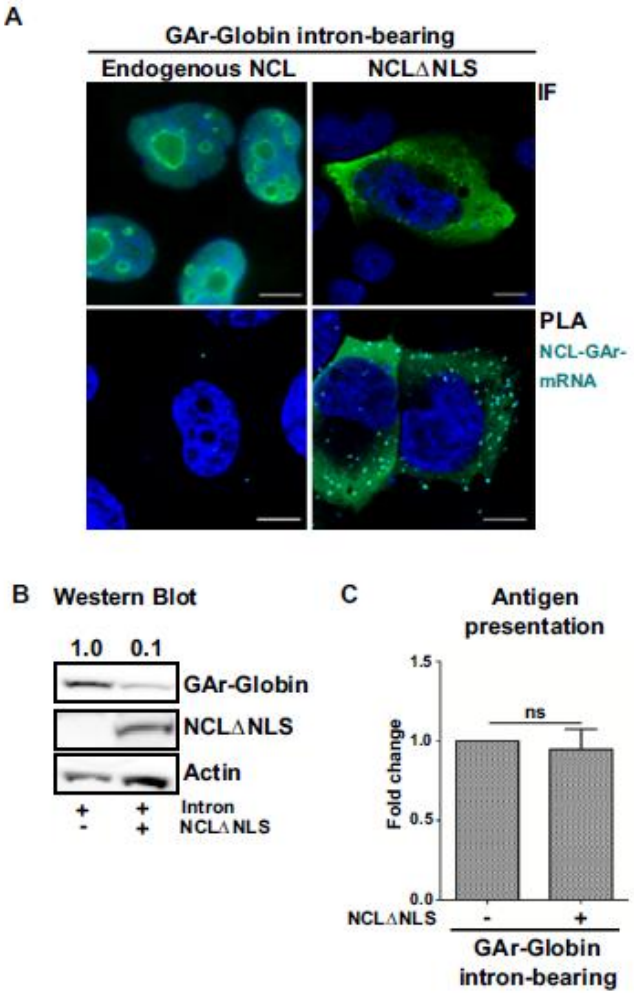

Figure 24 – Utilisation de l'interaction de la nucléoline avec l'ARN de GAr pour l'étude de la traduction et de la présentation d'antigènes. **A:** Des cellules ont été co-transfectées avec une construction codant pour la nucléoline déplétée de son NLS (NCLΔNLS) et la construction GAr-globin avec introns (GAr-globin intron-bearing). L'interaction GAr-NCLΔNLS a été observée dans le cytoplasme des cellules transfectées par PLA (*proximity ligation assay,* décrit dans la section antérieure). IF, immunofluorescence. La NCL est marquée en vert. Bleu = DAPI. Barre d'échelle = 10 µm. **B :** Quantification des protéines d'intérêt par *Western blot*. **C :** Analyse de la présentation d'antigènes par la voie du CMH-I selon décrit dans la **Figure 19B.** Cette stratégie a mis en évidence que les peptides antigéniques de classe I peuvent être produits sans influence du processus de traduction. Modifié de Martins et al. (2019) Nucleic Acids Res. [35].

Dans l'ensemble, ces observations ont confirmé la production de peptides antigéniques à partir d'un mécanisme de traduction non-canonique mis en place avant l'épissage de l'ARNm. La traduction des ARNm pour la production de protéines et pour la production de peptides antigéniques pour la voie du CMH-I relèvent de mécanismes indépendants, mettant en évidence le rôle majeur de sources autres que la dégradation des protéines par le protéasome dans le déclanchement de la réponse cytotoxique par la voie endogène. Ces résultats offrent de nouvelles perspectives pour le développement d'immunothérapies et de vaccins.

Ces travaux font l'objet de deux articles originaux, deux articles de revue et sont en lien avec un sujet de M2 et deux projets de thèse que j'ai eu l'opportunité de co-encadrer.

3.3.4 Encadrement

La supervision et l'encadrement d'étudiants a été une des missions principales de mon post-doctorat, principalement pendant les deux dernières années. En effet, j'ai contribué significativement à l'encadrement de trois thésardes et j'ai été le responsable de stage d'une étudiante en M2, d'une étudiante du Programme Erasmus, d'un étudiant de Médicine et d'une doctorante étrangère. J'ai aussi supervisé le travail d'une IE de mon ancienne équipe et de trois agents d'autres équipes en mission dans notre laboratoire. Les détails de mes activités d'encadrement les plus pertinentes sont données ci-dessous :

1. **Ewa SROKA**, doctorante, 10/2017 – 12/2018

Dans le cadre de son projet de thèse, Ewa a pour but de donner suite à des travaux explorant un modèle murin de présentation d'antigène par la voie du CMH-I que j'ai initié au sein de l'équipe Fahraeus. Ces travaux s'inscrivent dans une collaboration entre l'actuelle UMR1131 (INSERM, Université de Paris) et l'*International Centre for Cancer Vaccine Science* (University of Gdansk, Pologne).

Plus précisément, j'ai développé la lignée de souris transgénique Hbb-btstm1 en collaboration avec le service d'expérimentation animale de l'Institut Universitaire d'Hématologie – Université Paris Diderot. Nous avons introduit la séquence codante du peptide SIINFEKL de l'OVA dans le deuxième intron du gène *HBB* de souris C57/BL6, afin de générer un modèle animal qui permettrait d'étudier la production de peptides antigéniques provenant de la traduction des ARNm non-épissés. À l'aide de ce modèle, j'ai démontré que les produits de la traduction non-canonique des séquences introniques peuvent activer la réponse des lymphocytes T $CD8^+$ *in vivo* (**Figure 25**). Actuellement, Ewa utilise ce modèle pour mieux comprendre la production de substrats pour la voie du CMH-I *in vivo* et pour explorer le lien entre ce mécanisme et la réponse immunitaire contre les tumeurs. Je continue à contribuer au déroulement de son projet de thèse par des échanges téléphoniques et discussions en présentiel au laboratoire de l'équipe Fahraeus à Paris.

2. **Maria Camila TOVAR**, étudiante en M2, 01 – 06/2018

Le projet de Maria portait sur le rôle de l'autophagie dans la présentation d'antigènes. En utilisant les modèles *in vitro* que j'ai mis en place dans le cadre de mes travaux et sous ma supervision, Maria a produit des résultats qui suggèrent que l'autophagie participe à la production de peptides antigéniques pour la voie du CMH-I provenant de protéines qui tendent à former des agrégats dans le cytoplasme. Maria a obtenu une bourse pour poursuivre son

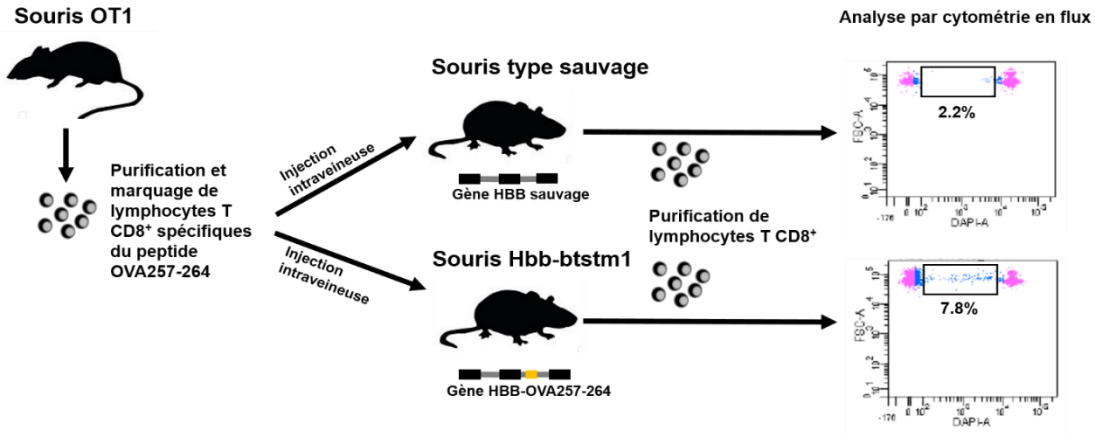

Figure 25 – Approche *in vivo* employée pour démontrer la présentation par le CMH-I de peptides antigéniques produits à partir de séquences introniques. Des lymphocytes T CD8$^+$ spécifiques du peptide SIINFEKL ont été purifiés à partir de ganglions lymphatiques de souris OT1 et marqués par le *Cell Trace Violet.* Ensuite, ces cellules ont été transférées dans des souris sauvages et dans les souris Hbb-btstm1, développées par notre équipe. Les rectangles noir et gris illustrent respectivement les exons et les introns du gène Hbb. Le rectangle jaune représente la séquence codante du peptide SIINFEKL, insérée dans le deuxième intron du gène Hbb des souris Hbb-btstm1. Suite à la purification de la population globale de cellules CD8$^+$ à partir des ganglions lymphatiques et de la rate des souris testées, la prolifération *in vivo* des lymphocytes T CD8$^+$ provenant des souris donneuses a été analysée par cytométrie en flux. Le pourcentage de cellules qui ont proliféré est montré dans les graphiques. Cette analyse démontre l'activation *in vivo* de lymphocytes T CD8$^+$ par la présentation d'antigènes produits à partir de la traduction d'une séquence intronique. *Sroka* and *Martins et al. Manuscrit en préparation.*

doctorat au sein de l'équipe Fahraeus et je contribue à sa thèse en tant que membre de son comité de suivi individuel, ainsi que par des échanges téléphoniques et discussions en présentiel au laboratoire de son équipe d'accueil.

3. **Petter BROHAGEN**, Étudiant de Médecine, Linkoping University- Suède, 09 – 12/2018 et **Aikaterini THERMOU**, Programme Erasmus, University of Patras-Grèce, 12/2017 – 05/2018

Dans le cadre de leurs stages, Petter et Aikaterini ont mis en place des analyses pour étudier la protéine LANA-1 de l'herpèsvirus humain type 8, responsable des sarcomes de Kaposi. LANA-1 est homologue de la protéine EBNA-1 de l'EBV et possède des domaines centraux similaires au motif GAr. Ces domaines sont caractérisés par la répétition de certains acides aminés, étant prédisposés à la formation de G4. Pour cette raison, Aikaterini et Petter ont travaillé sous ma supervision pour étudier l'effet des molécules ligands de G4 sur la traduction et la présentation d'antigènes provenant de cette protéine.

Pendant son stage, Aikaterini a produit des constructions d'ADN codant pour des variantes de LANA-1 déplétées de ces domaines centraux dans le but d'étudier leur impact sur la traduction. Ensuite, ces constructions ont été utilisées dans les travaux de Petter pour évaluer l'effet de ligands de G4. Nous avons démontré que la déplétion de ces trois domaines centraux réduit la traduction de LANA-1, mais augmente la présentation de peptides dérivés de cette protéine (**Figure 26A-B**). Nous avons aussi mis en évidence que les ligands de G4

testés interfèrent différemment sur la traduction et présentation d'antigènes de LANA-1 (**Figure 26C-E**). Ces observations sont probablement associées à la différence d'affinité des molécules testées par l'ARNm de LANA-1. Ces résultats font l'objet d'une publication en préparation que je signerais en tant que co dernier auteur. Suite à son stage, Petter a poursuivi ses études de Médecine et Aikaterini a intégré l'équipe Fahraeus pour son Master 2, où elle réalise à présent son doctorat.

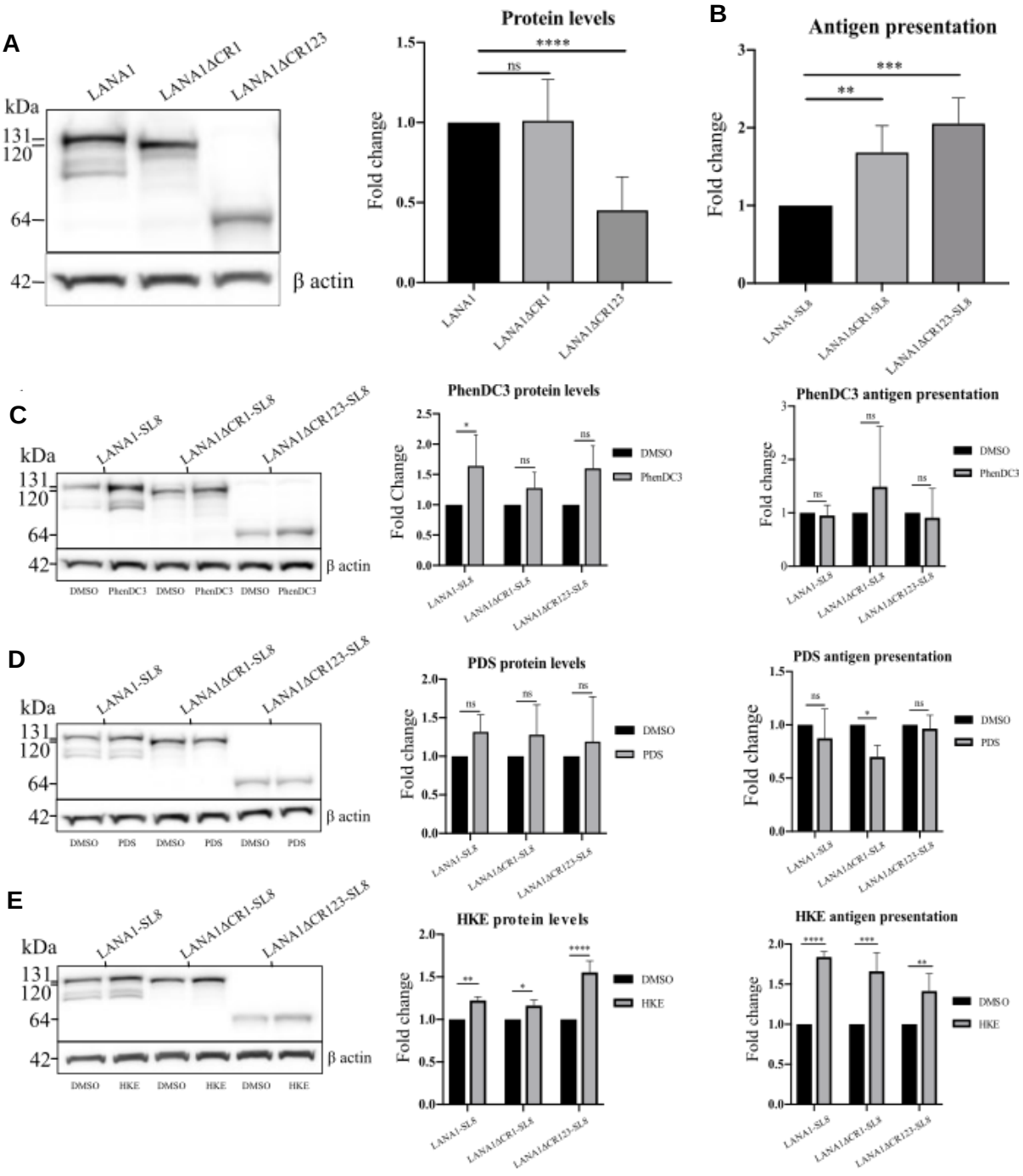

Figure 26 – Etudes sur la protéine LANA-1 de l'herpèsvirus humain de type 8. Des cellules transfectées avec des constructions de LANA-1 portant le peptide SIINFEKL ont été analysées par *Western blot* (**A**) et par le test de présentation antigénique présenté dans la Figure 19B (**B**). Les mêmes analyses ont été réalisées avec des cellules traitées avec les ligands de G4 PhenDC3 (**C**), PDS (**D**) et HKE (**E**). Modifié de Thermou et Brohagen et al. Manuscrit en préparation.

4 - **Natividad BELLIDO**, Doctorante, Université de Cordoue-Espagne, 11/2018

Natividad a été reçue au sein de l'équipe Fahraeus, dans le cadre d'une collaboration avec l'équipe *Génomica y mejora animale* de l'Université de Cordoue, où j'ai réalisé ma thèse de doctorat. J'ai formé Natividad aux techniques de présentation d'antigènes, dans le but de produire des données pour sa thèse de doctorat et compléter le dernier manuscrit de ma thèse. A son retour en Espagne, Natividad a mis à profit les compétences acquises pendant cette mission pour démontrer que les macrophages porcins sont capables de présenter des antigènes provenant de *Salmonella* Typhimurium par le CMH-I. Ces résultats seront utilisés dans une nouvelle version du manuscrit présenté dans la section 3.2.3 de ce mémoire (Martins et al. *under preparation*).

3.3.5 Articles en pièce jointe

[33] Lista, M. J., Martins, R. P., Billant, O., Contesse, M.-A., Findakly S., Pochard,P., Daskalogianni, C., Beauvineau, C., Guetta, C., Jamin, C., Teulade-Fichou, M.-P., Fåhraeus, R., Voisset, C., Blondel, M. (2017). Nucleolin directly mediates Epstein-Barr virus immune evasion through binding to G-quadruplexes of EBNA1 mRNA. Nature Communications, 8, 1-13.

[34] Martins, R. P., Findakly, S., Daskalogianni, C., Teulade-Fichou, M.-P., Blondel, M., Fåhraeus, R. (2018). In cellulo protein-mRNA interaction assay to determine the action of G-quadruplex-binding molecules. Molecules, 23 (12), 1-11.

[35] Martins, R. P., Malbert-Colas, L., Lista, M. J., Daskalogianni, C., Apcher, S., Pla, M., Findakly, S., Blondel, M., Fåhraeus, R. (2019). Nuclear processing of nascent transcripts determines synthesis of full-length proteins and antigenic peptides. Nucleic Acids Research, 47 (6), 3086-3100.

nature COMMUNICATIONS

ARTICLE

Received 7 Oct 2016 | Accepted 22 May 2017 | Published 7 Jul 2017

DOI: 10.1038/ncomms16043 OPEN

Nucleolin directly mediates Epstein-Barr virus immune evasion through binding to G-quadruplexes of EBNA1 mRNA

María José Lista[1], Rodrigo Prado Martins[2], Olivier Billant[1], Marie-Astrid Contesse[1], Sarah Findakly[2], Pierre Pochard[3], Chrysoula Daskalogianni[2], Claire Beauvineau[4], Corinne Guetta[4], Christophe Jamin[3], Marie-Paule Teulade-Fichou[4], Robin Fåhraeus[2], Cécile Voisset[1,*] & Marc Blondel[1,*]

The oncogenic Epstein-Barr virus (EBV) evades the immune system but has an Achilles heel: its genome maintenance protein EBNA1, which is essential for viral genome maintenance but highly antigenic. EBV has seemingly evolved a system in which the mRNA sequence encoding the glycine-alanine repeats (GAr) of the EBNA1 protein limits its expression to the minimal level necessary for function while minimizing immune recognition. Here, we identify nucleolin (NCL) as a host factor required for this process via a direct interaction with G-quadruplexes formed in GAr-encoding mRNA sequence. Overexpression of NCL enhances GAr-based inhibition of EBNA1 protein expression, whereas its downregulation relieves the suppression of both expression and antigen presentation. Moreover, the G-quadruplex ligand PhenDC3 prevents NCL binding to EBNA1 mRNA and reverses GAr-mediated repression of EBNA1 expression and antigen presentation. Hence the NCL-EBNA1 mRNA interaction is a relevant therapeutic target to trigger an immune response against EBV-carrying cancers.

[1] Institut National de la Santé et de la Recherche Médicale UMR1078; Université de Bretagne Occidentale, Faculté de Médecine et des Sciences de la Santé; Etablissement Français du Sang (EFS) Bretagne; CHRU Brest, Hôpital Morvan, Laboratoire de Génétique Moléculaire, 22 avenue Camille Desmoulins, Brest F-29200, France. [2] Cibles Thérapeutiques, Institut National de la Santé et de la Recherche Médicale UMR1162, Institut de Génétique Moléculaire, Université Paris 7, Hôpital St Louis, 27 rue Juliette Dodu, Paris F-75010, France. [3] Inserm UMR 1227, Lymphocytes B et Autoimmunité; Université de Bretagne Occidentale; CHRU Brest, Hôpital Morvan, Laboratoire d'Immunologie, Brest F-29200, France. [4] Chemistry, Modelling and Imaging for Biology, CNRS UMR9187 - Inserm U1196, Institut Curie, Université Paris-Sud, Campus universitaire, Bat. 110, Orsay F-91405, France. * These authors contributed equally to this work. Correspondence and requests for materials should be addressed to M.B. (email: marc.blondel@univ-brest.fr).

The Epstein-Barr virus (EBV) was the first oncogenic virus discovered in human[1–3] and has been linked to various cancers that include Burkitt and Hodgkin lymphomas and 10% of gastric cancers. Another example is the nasopharyngeal carcinoma, which is particularly frequent among men in China and Tunisia. Like all the gammaherpesviruses, EBV evades the host immune system but has an Achilles heel: its genome maintenance protein (GMP) EBNA1 (refs 4,5). Indeed, EBNA1 is essential for EBV genome replication and maintenance and as such expressed in all dividing EBV-infected cells. EBNA1 is also highly antigenic and $CD8^+$ T cells directed towards EBNA1 epitopes exist in all infected individuals. Hence, EBV has evolved a mechanism to limit EBNA1 production to the minimal level required for viral genome replication while keeping to a minimum the production of EBNA1-derived antigenic peptides presented to the cytotoxic T cells through the MHC class I pathway[4,6]. The central glycine-alanine repeat (GAr) of EBNA1 plays a critical role in this mechanism of immune evasion as it suppresses the translation of its own mRNA *in cis*[7,8]. The high level of EBNA1 protein and the efficient T cell response following the infection by an EBV strain encoding a truncated version of EBNA1 in which GAr has been deleted (EBNA1ΔGAr) demonstrates the critical role of GAr in EBNA1 immune evasion[7–10]. In line, a polymorphism in the length of GAr exists and, importantly, the effect of GAr is length-dependent as a longer domain displays a stronger inhibitory effect on both mRNA translation and antigen presentation[11].

The GAr-encoding mRNA sequence is GC rich and forms predicted G-quadruplex (G4) structures that have been implicated in the regulation of EBNA1 synthesis *in vitro*[12]. G4 are particular secondary structures of nucleic acid formed by the stacking of G-quartets which correspond to a planar arrangement of four guanines connected by Hoogsteen hydrogen bonds. G4 structures within G-rich DNA or RNA sequences have been implicated in gene regulation where they can affect transcription, alternative splicing and translation[13–17]. G4 modes of action are not completely understood, but cellular factors that can interact with these structures are emerging[18–20].

Nucleolin (NCL) is a multifunctional DNA/RNA-binding protein widely conserved among eukaryotes. It is involved in RNA metabolism, in particular in rRNA maturation[21]. NCL binds to G-rich sequences in coding and non-coding regions of various mRNA, many of which encode cancer-related proteins, and enhance their translation[22]. In addition, NCL binds to G4 structures within DNAs and RNAs. For example, NCL binds to and stabilizes G4 structures formed within the LTR promoter of HIV, thereby silencing the provirus transcription[23]. NCL also affects the transcription of c-MYC by binding to and stabilizing a G4 structure present in the promoter of this oncogene[17,24].

GAr-based EBNA1 immune evasion has been considered a relevant therapeutic target against EBV-related cancers as most tumour cells from EBV-related cancers are infected by EBV and thus express EBNA1 at a minimal level. Importantly, the latent infection by EBV is primarily restricted to a specific small pool of memory B cells. Hence, overcoming GAr-based self-inhibition of EBNA1 translation should unveil EBV-carrying tumour cells to cytotoxic T cells without having a significant effect on the vast majority of non-tumour host cells. As neither the mechanisms of GAr-mediated mRNA translation suppression in *cis* nor the cellular factors involved are known, we developed a yeast-based (*Saccharomyces cerevisiae*) assay that recapitulates the key aspects of the GAr-based inhibition of translation, including length dependency[25,26]. This assay was previously used to identify small molecular weight compounds that can stimulate EBNA1 expression both in yeast and mammalian cells and that relieve GAr-based limitation of antigen presentation[26].

Here, using this assay, we have isolated the yeast *NSR1* gene, which encodes the orthologue of human NCL, and show that NCL is a host factor required for GAr-based suppression of translation and to minimize antigen presentation. We also show that NCL directly interacts with G4 formed in the GAr-encoding sequence of EBNA1 mRNA. Finally, we show that this interaction is druggable, as the G4 ligand PhenDC3 prevents NCL from binding to G4 formed in the GAr mRNA sequence and stimulates EBNA1 expression and antigen presentation.

Hence, NCL is a host cell factor critically involved in EBNA1 immune evasion and the NCL-EBNA1 mRNA interaction appears to be a relevant therapeutic target to treat EBV-related cancers.

Results

***NSR1* mediates GAr effect on protein expression in yeast**. The yeast assay used in this genetic screen[26] is based on a fusion between the yeast Ade2p reporter protein and a GAr domain of 43 amino acid (43GAr). Because GAr is able to self-inhibit the translation of its own mRNA in yeast, this leads to a reduction in Ade2p level. This can easily be monitored in yeast as cells which express Ade2p at a functional level form white colonies, whereas cells that do not express Ade2p readily form red colonies and any intermediate level of Ade2p leads to the formation of pink colonies whose intensity of coloration is inversely proportional to the level of Ade2p expressed. Hence, a yeast strain expressing the *43GAr-ADE2* construct from the constitutive *ADH* promoter forms pink colonies, whereas a control strain expressing *ADE2* from the same promoter forms white colonies (Fig. 1a). We used the *43GAr-ADE2* strain to identify yeast genes whose overexpression leads to a redder phenotype meaning that they potentially exacerbate GAr-based inhibition of translation. For this purpose we transformed the *43GAr-ADE2* yeast strain by a yeast genomic DNA library consisting of small genomic fragments (~4 kb) cloned into a yeast 2 μ multicopy plasmid, which is present at ~50–100 copies per yeast cell, hence potentially allowing to assess the effect of overexpressing the vast majority of yeast gene on GAr-based inhibition of translation (indeed, the few yeast genes larger than 4 kb may not be fully overexpressed using this library). This way, we isolated two independent clones bearing overlapping genomic fragments that, among a few other genes, contained the yeast *NSR1* gene. We then subcloned *NSR1* gene alone under the control of the strong constitutive *GPD* promoter in a low copy number vector (CEN) and confirmed its ability, when overexpressed, to both confer a redder phenotype and exacerbate the ability of GAr to decrease 43GAr-Ade2p protein expression (Fig. 1b), whereas having no significant effect on Ade2p protein in the control strain (Supplementary Fig. 1a) or on *43GAr-ADE2* or *ADE2* mRNA levels (Supplementary Fig. 1b).

We then determined the effect of *NSR1* downregulation on GAr-based inhibition of protein expression. As *NSR1* is not essential in yeast, we deleted this gene in both *43GAr-ADE2* and *ADE2* strains and observed that its absence abolished the GAr inhibitory effect on 43GAr-Ade2p expression (first two lanes of the western blot in Fig. 1c). This effect was GAr-dependent as *NSR1* deletion had no effect on Ade2p protein level in the control strain (last two lanes of the western blot in Fig. 1c). As controls, we checked that *NSR1* deletion had no significant effect on *43GAr-ADE2* and *ADE2* mRNA levels (Supplementary Fig. 1c).

Human NCL can functionally replace Nsr1p in yeast. Next, we assessed the potential ability of NCL, the gene encoding the human NCL, to functionally complement the deletion of *NSR1* in yeast and found that the expression of NCL led to a decrease in

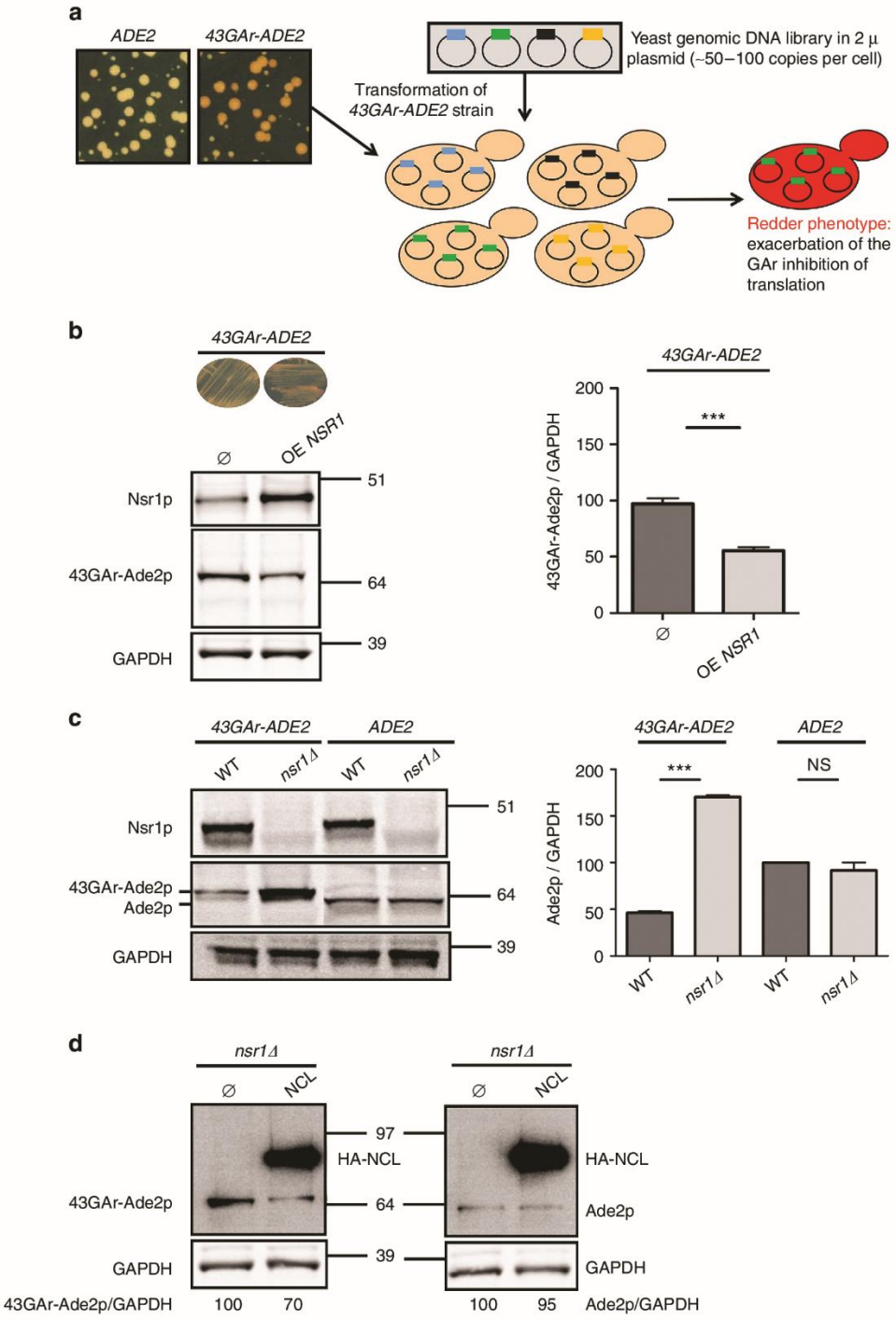

Figure 1 | Identification and confirmation of the critical role of nucleolin in GAr-based translation inhibition in yeast. (**a**) Rationale of the yeast-based genetic screen. Contrary to yeast cells expressing *ADE2* gene (left panel) that form white colonies on rich medium (YPD), those expressing the *43GAr-ADE2* fusion (right panel) form pink colonies due to the ability of GAr to self-limit the translation of its own mRNA in yeast as in human cells. On the basis of this model, we looked for yeast genes whose overexpression from high copy number plasmids leads to a redder phenotype, suggesting an exacerbation of the GAr-based translation inhibition. (**b**) Effect of *NSR1* overexpression on 43GAr-Ade2p protein level. The overexpression of *NSR1* gene, which encodes the yeast nucleolin, led to a redder phenotype associated to a decrease in 43GAr-Ade2p level as evidenced by SDS-PAGE and western blot analysis (left panel). GAPDH was used as a loading control. The mean 43GAr-Ade2p/GAPDH ratio from three independent experiments is shown in the right panel and the results compared using the Student's *t*-test. ***$P<0.001$. (**c**) Effect of *NSR1* gene deletion on 43GAr-Ade2p and Ade2p protein level. SDS-PAGE and western blot analysis showing that deletion of *NSR1* (*nsr1Δ*) had no effect on Ade2p level, whereas it strongly increased the level of 43GAr-Ade2p. GAPDH was used as a loading control. The mean 43GAr-Ade2p/GAPDH or Ade2p/GAPDH ratios from three independent experiments are shown in the right panel and the results compared using the Student's *t*-test (***$P<0.001$; NS: not significant). (**d**) Human nucleolin (NCL) is able to complement *NSR1* deletion. SDS-PAGE and western blot analysis of the yeast *nsr1Δ* strain expressing 43GAr-Ade2p (left) or Ade2p (right) and overexpressing (right lanes), or not (left lanes), HA-tagged human nucleolin (HA-NCL). GAPDH was used as a loading control. The 43GAr-Ade2p/GAPDH or Ade2p/GAPDH ratio is indicated below the gels. Blots represent $n \geq 3$.

43GAr-Ade2p level, while having no effect on Ade2p level (Fig. 1d). Of note, the human NCL was as efficient as the yeast Nsr1p (Supplementary Fig. 1d).

Taken together, these results show that Nsr1p, the yeast orthologue of NCL, is required for the GAr-based inhibition of protein expression in yeast. As NCL, the human nucleolin, is able to fully complement the deletion of the yeast *NSR1* gene, this suggests that NCL represents a host cell factor important for the GAr-mediated self-limitation of EBNA1 expression in EBV-infected human cells.

NCL also controls EBNA1 expression in EBV-infected cells. We next assessed the role of human NCL on GAr-based self-inhibition of translation in human cells. For this purpose, we first overexpressed HA-tagged NCL (HA-NCL) in three EBV-infected B cell lines: Mutu-1, B95.8 and Raji. As shown in Fig. 2a for Mutu-1 and in Supplementary Fig. 2a for B95.8 and Raji, overexpression of HA-NCL led to a significant decrease in EBNA1 endogenous level in these three cell lines, as compared to actin. Similar to yeast, this effect is GAr-dependent as overexpression of HA-NCL also decreased the level of transfected 235GAr-OVA (ovalbumin), the fusion protein that is used to assess the effect of GAr on MHC class I-restricted antigen presentation (see below), whereas having no significant effect on OVA alone, the control protein (Supplementary Fig. 2b). The relative levels of endogenous EBNA1 and NCL were also determined in B95.8, Mutu-1 and Raji cells (Supplementary Fig. 2c).

We then determined the effect of downregulating endogenous NCL on endogenous EBNA1 level in EBV-infected Burkitt lymphoma Mutu-1 cells using siRNA. As observed by others[27], we were not able to knockdown more than ~40–50% the expression of NCL, probably because it is an essential gene in mammalian cells. However, this partial downregulation led to a significant increase (~50%) in EBNA1 level (Fig. 2b) demonstrating that endogenous NCL expression restricts endogenous EBNA1 expression in EBV-infected cells.

To determine whether the impact of NCL level on EBNA1 expression is GAr-dependent, we then determined the effect of downregulating endogenous NCL on GAr-dependent suppression of protein expression in H1299 cells. Again, we were not able to knockdown more than ~40–50% the expression of NCL. However, this partial downregulation led to a significant increase in both EBNA1 (Fig. 2c) and 235GAr-OVA (Fig. 2d) protein levels to about the same extent (~80% and ~50%, respectively) than the increase of endogenous EBNA1 in Mutu-1 cells, whereas having no effect on EBNA1ΔGAr or on OVA alone. Quantifications of three independent experiments are shown in Supplementary Fig. 2d,e.

Next, we performed a metabolic ^{35}S methionine pulse-labelling experiment and we observed an increase in newly synthesized 235GAr-OVA following NCL downregulation (Fig. 2e, upper panel). In contrast, no increase in newly synthesized OVA was observed (Fig. 2e, lower panel). We did not observe any significant effect on the levels of GAr-carrying mRNAs (Supplementary Fig. 2f,g). Altogether, these results demonstrate that NCL downregulation does interfere with GAr-based suppression of translation.

These findings confirmed that, as in yeast, NCL represents a host cell factor critically involved in the GAr-dependent suppression of EBNA1 synthesis, a mechanism at the basis of EBV immune evasion in latently infected cells.

NCL knockdown overrides GAr-restricted antigen presentation. We next determined if downregulating NCL has an effect on GAr-restricted MHC class I antigen presentation. Indeed, as NCL downregulation led to a GAr-dependent increase in protein expression, it was also expected to stimulate antigen presentation. For this purpose, we determined the effect of siRNA-mediated NCL knockdown on the GAr-restricted presentation of the ovalbumin-derived SIINFEKL antigenic peptide ($OVA_{257-264}$) complexed with the murine k^b MHC class I receptor using a specific monoclonal antibody. FACS analysis revealed that NCL knockdown significantly increased ($+42.1\% \pm 1.37$, $P=0.0005$) the formation of this complex in 235GAr-OVA-expressing cells (Fig. 3a). In contrast, NCL knockdown only had a modest effect on OVA-expressing cells ($+19.7\% \pm 6.11$, $P=0.043$; Fig. 3b). In both cases, the efficiency of siRNA-mediated NCL downregulation and its effect on 235GAr-OVA or OVA expression were determined (Supplementary Fig. 3a).

We then tested whether the observed increase in antigen presentation following NCL downregulation does have an effect on T-cell activation. For this purpose, we determined the proliferation of naive $CD8^+$ T cells (OT1 cells) recognizing specifically the $OVA_{257-264}$ SIINFEKL epitope on the murine k^b MHC class I molecule. The OT1 cells were isolated from peripheral and mesenteric lymph-nodes of 12-week-old mice and stained with the CellTrace Violet fluorescent dye. Then, OT1 cells were mixed with H1299 cells expressing 235GAr-OVA and the k^b molecule. As a control, H1299 cells expressing OVA and the k^b molecule were used. As expected and due to the GAr inhibitory effect on both expression and antigen presentation, 235GAr-OVA-expressing H1299 cells led to a much weaker activation of OT1 cells (Fig. 3c, left panel) as compared to OVA-expressing H1299 cells (Fig. 3d, left panel), as determined by evaluating the number of dividing OT1 cells by FACS analysis. However, siRNA-mediated NCL knockdown in 235GAr-OVA-expressing H1299 cells significantly increased proliferation of OT1 cells (Fig. 3c, right panels), whereas it had no effect in OVA-expressing H1299 cells (Fig. 3d, right panels). The efficiency of siRNA-mediated NCL downregulation and its effect on 235GAr-OVA or OVA expression are shown in Supplementary Fig. 3b.

NCL directly interacts with G4 of GAr-encoding mRNA. NCL has been reported to bind to some G4 formed in both DNA[24] and RNA sequences[28]. G4 are composed and stabilized by the stacking of guanine tetrads which are assembled in a planar arrangement by Hoogsteen hydrogen bonding (Fig. 4a) and have been involved in the regulation of gene expression, DNA replication and telomere maintenance [20]. The G-rich sequence of GAr-encoding mRNA contains a cluster of 13 predicted G4 (ref. 29). Hence, we determined the ability of NCL to bind to these structures. For this purpose, we adapted a pulldown assay recently developed to identify RNA G4 binding proteins[28] to an 18 nt-long oligonucleotide containing the most probable G4 that can form in the GAr-encoding mRNA sequence. Briefly, this oligonucleotide (GQ) was linked to biotin and pulldown experiments using streptavidin-conjugated sepharose beads were performed. As a negative control, we used an oligonucleotide (GM) with a similar sequence except that the four guanines forming the G4 were replaced by adenines or uridines to completely abolish the G4 structure, as predicted using the QGRS-H predictor software[30]. As a positive control, we used ARPC2 30 nt-long oligonucleotide which corresponds to a G4 found in the *ARPC2* mRNA and that has been shown to bind NCL[28]. As shown in Fig. 4b, NCL was precipitated from H1299 cell extracts when using GQ or ARPC2 oligonucleotides, but not when using GM or empty beads showing that NCL binds to G4 formed in the GAr mRNA sequence.

Next, we performed the same pulldown experiment using recombinant NCL instead of cell lysate. Similar results were

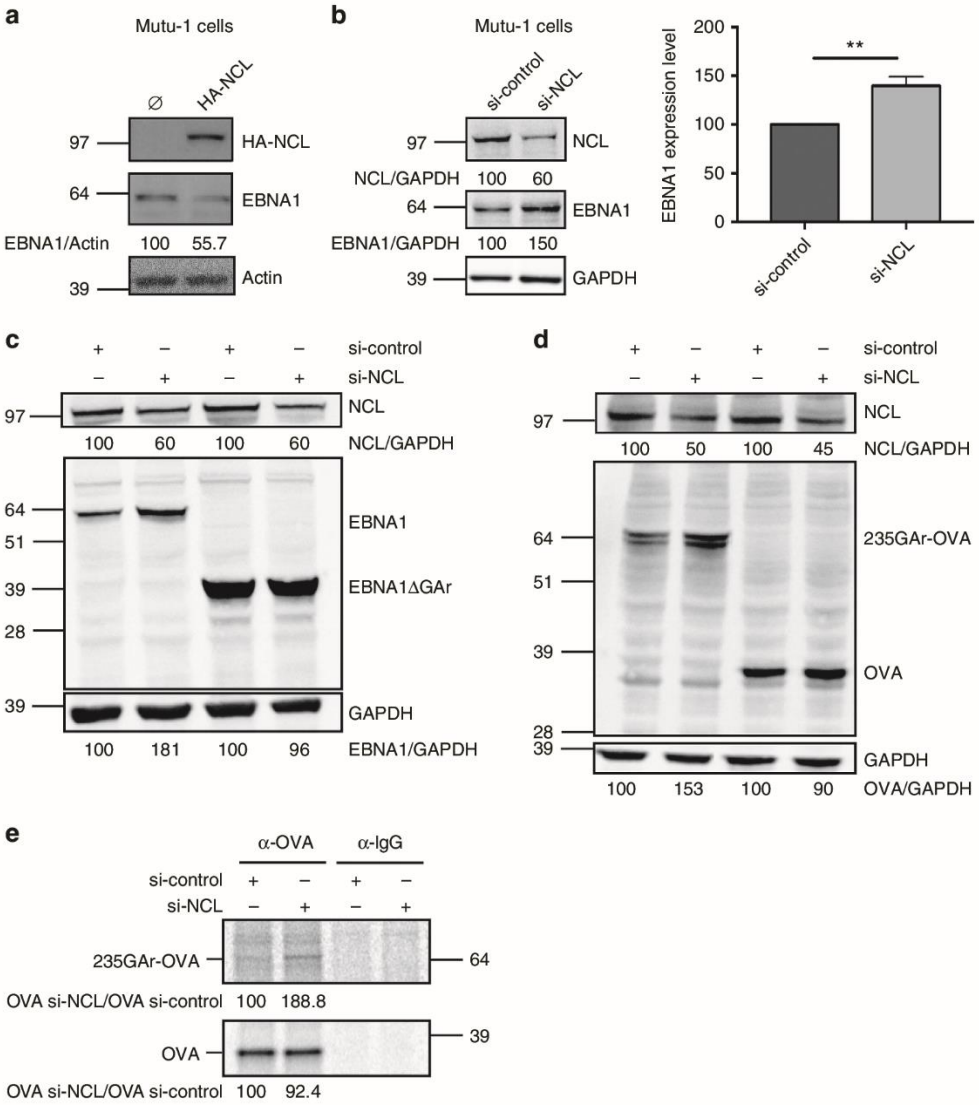

Figure 2 | NCL also mediates GAr-based translation inhibition in human cells. (**a**) SDS-PAGE and western blot analysis of the level of endogenous EBNA1 in the EBV-infected B cell line Mutu-1 overexpressing (right lane), or not (left lane), HA-tagged nucleolin (HA-NCL). Actin was used as a loading control. EBNA1/actin ratios are indicated below the gels. Blot represents $n \geq 3$. (**b**) SDS-PAGE and western blot analysis of the level of endogenous EBNA1 in the Mutu-1 cells in response to NCL knockdown. Mutu-1 cells were transfected with control siRNA or siRNA targeting NCL, as indicated. GAPDH was used as a loading control. EBNA1/GAPDH ratios are indicated below the gels. The efficiency of NCL downregulation was estimated by determining the NCL/GAPDH ratio in cells treated by siRNA targeting NCL versus cells treated by control siRNA. The mean EBNA1/GAPDH ratio from three independent experiments is shown in the right panel and the results obtained with siRNA targeting NCL compared with control siRNA using the Student's *t*-test (**$P < 0.01$). (**c**) SDS-PAGE and western blot analysis of the level of EBNA1 or EBNA1ΔGAr in response to NCL knockdown. H1299 cells were transfected with EBNA1 or EBNA1ΔGAr expressing vectors and with control siRNA or siRNA targeting NCL, as indicated. GAPDH was used as a loading control. EBNA1/GAPDH or EBNA1ΔGAr/GAPDH ratios are indicated below the gels. The efficiency of NCL downregulation was estimated by determining the level of remaining NCL in cells treated by siRNA targeting NCL versus cells treated by control siRNA. Blot represents $n \geq 3$ and a representative result is shown. (**d**) Same experiment as in **c** except that H1299 cells were transfected with chicken ovalbumin (OVA) or 235GAr-OVA. Blot represents $n \geq 3$ and a representative result is shown. (**e**) Autoradiographs showing relative mRNA translation efficiencies of 235GAr-OVA versus OVA in response to NCL knockdown. H1299 cells transfected with 235GAr-OVA (upper panel) or OVA (lower panel) constructs and with control siRNA or siRNA targeting NCL, as indicated, were pulse-labelled with [^{35}S] methionine, and lysates were subjected to immunoprecipitation with antibodies raised against OVA or IgG as a control, as indicated, and subjected to SDS-PAGE and autoradiography. Quantification of 235GAr-OVA or OVA signals are indicated.

obtained (Fig. 4c) showing that NCL directly binds GAr most probable G4.

Finally, we wanted to verify if, and where, the NCL-GAr G4 interaction occurs *in cellulo*. Hence, we performed a proximity ligation assay (PLA) to assess if endogenous NCL associates with endogenous EBNA1 mRNA in EBV-infected Mutu-1 cells. We observed PLA dots mostly in the nucleus or close to it (Fig. 5a) indicating that endogenous NCL does interact with endogenous EBNA1 mRNA and that this interaction mostly takes place in the nucleus and in the cytoplasm close to the nucleus. In contrast, no PLA dots were observed in the various controls (without the probe specific for EBNA1 mRNA or without antibodies). To assess whether this interaction is GAr-dependent, we repeated this PLA in H1299 cells expressing EBNA1 or EBNA1ΔGAr. Again, we

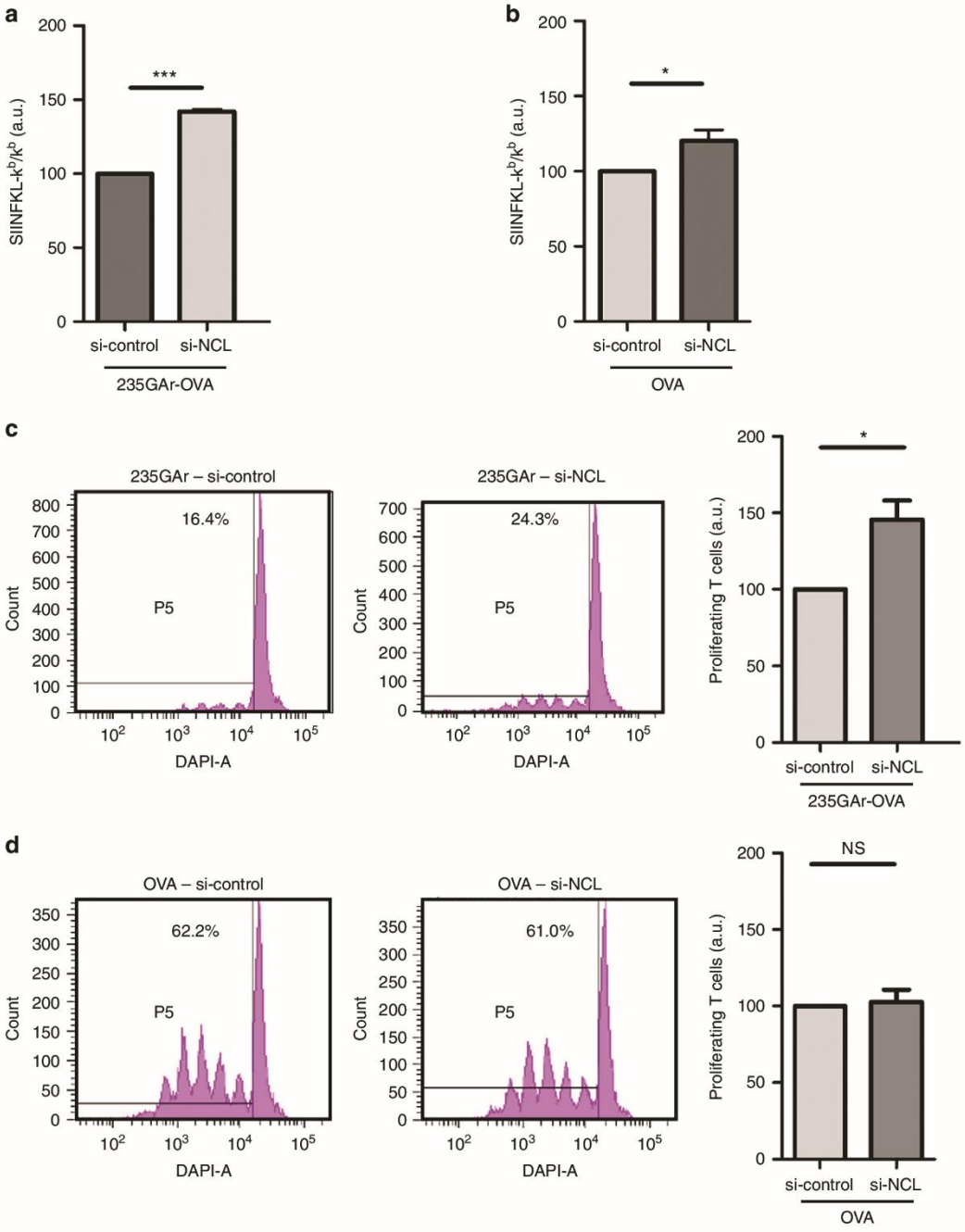

Figure 3 | NCL downregulation activates GAr-limited antigen presentation and recognition by specific T lymphocytes. (**a**) Effect of NCL knockdown on antigen presentation. H1299 were transfected with 235GAr-OVA and murine MHC class I K^b plasmids and with control siRNA or siRNA targeting NCL, as indicated, and the levels of Kb/OVA-derived antigenic peptide complexes determined using FACS analysis (a.u.: arbitrary units). These experiments were performed three times and the mean quantification of the complex level obtained in cells treated by si-NCL or by si-control are shown and compared using the Student's *t*-test (***$P<0.001$). (**b**) Same experiment as in **a** except that H1299 cells were transfected with OVA plasmid (*$P<0.05$). (**c**) Effect of NCL knockdown on T-cell proliferation. H1299 cells were transfected with mouse K^b and 235GAr-OVA plasmids and control siRNA (left) or siRNA targeting NCL (right). Afterwards cells were mixed with mouse naive $OVA_{257-264}$ (SIINFEKL) specific $CD8^+$ T-cells isolated from peripheral and mesenteric lymph-nodes and stained with CellTrace Violet. The proliferation of these SIINFEKL-specific T cells was determined by FACS analysis. Quantification of proliferating T lymphocytes when incubated in presence of cells treated by siRNA targeting NCL (si-NCL) or with control siRNA-treated cells (si-control) are shown on the right. The results were compared using the Student's *t*-test (*$P<0.05$). (**d**) Same experiment as in **c** except that H1299 were transfected with OVA plasmid (NS: not significant).

observed PLA dots in cells expressing the full-length EBNA1 mRNA (Fig. 5d,e). In contrast, almost no dots were detected in cells expressing EBNA1ΔGAr (Fig. 5d,e) indicating that the ability of NCL to interact with EBNA1 mRNA is GAr-dependent.

Taken together, these results indicate that NCL directly interacts with the GAr's G4 of the EBNA1 mRNA and that this interaction mostly takes place in the nucleus or in the cytoplasm in the vicinity of the nucleus.

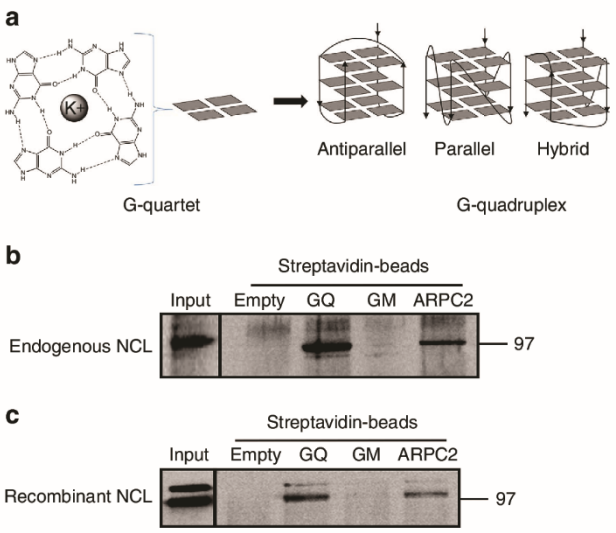

Figure 4 | NCL directly interacts with G4 formed in the GAr-encoding mRNA. (**a**) Schematic representation of a G-quadruplexe (G4) structure. (Left) self-assembly of four guanines held together by Hoogsteen hydrogen bonds (dashed lines) giving a G-quartet in presence of K^+ and schematic representation depicted by grey rectangles. Several G-quartets stack to form G4. (Right) the three main topologies adopted by G4 classified as function of strand orientation (indicated by arrows) and differing by loop arrangements. G4 RNA mostly adopt the parallel topology. (**b**) RNA pulldown using G4 forming RNA oligonucleotides covalently linked to biotin and streptavidin-coupled sepharose beads. Lysate from H1299 cells was applied to the following matrices: streptavidin-coupled beads either alone (Empty), or together with GQ (containing the most probable G4 of GAr mRNA), GM (same sequence except that G critical for G4 formation were replaced by adenines or uridines) or ARPC2 (containing a G4 present in *ARPC2* mRNA and that has been shown to bind NCL) RNA oligonucleotides. The sequence of these oligonucleotides is given in the Methods section. The proteins still bound to the beads after an 800 mM KCl wash were eluted and analysed by SDS-PAGE and western blot. (**c**) Same experiment as in **b** except that recombinant NCL was used instead of H1299 cell lysate.

PhenDC3 prevents GAr-based inhibition of protein expression. Next, we tested the effect of various G4 ligands on GAr-based inhibition of protein expression. Among the reported G4 ligands, pyridostatin (PDS, molecular structure depicted in Fig. 6a) and PhenDC3 (molecular structure depicted in Fig. 6b) (refs 31–33) are the best benchmark probes compatible with cellular assays. Indeed, PDS and PhenDC3 at micromolar concentrations have been shown to efficiently target various G4 in cell-based experiments[34]. As, at the same range of concentrations (1–5 μM), PDS has been shown to exacerbate GAr-based inhibition of protein expression in an *in vitro* coupled transcription-translation assay[29], we first tested the effect of this molecule on the level of 235GAr-OVA or OVA in H1299 cells. However, at the same concentration (5 μM), no clear effect on 235GAr-OVA or OVA expression was observed (Fig. 6a) suggesting that PDS may not be able to interfere with GAr-mediated inhibition of EBNA1 expression in a cellular context. We then tested PhenDC3 at the same concentration (5 μM) and found that it led to a significant increase in the steady-state level of 235GAr-OVA in H1299 cells (Fig. 6b, left panel). This effect is GAr-dependent since PhenDC3 had no significant effect on OVA expression (Fig. 6b, right panel) and is not due to an effect on the level of the corresponding RNA (Fig. 6c). Hence, one possibility is that PhenDC3 prevents the binding of NCL on EBNA1 mRNA G4.

PhenDC3 prevents NCL-EBNA1 mRNA interaction. To test this hypothesis, we performed the same G4 oligonucleotide pulldown assay as in Fig. 4c in the presence or absence of 10 μM PhenDC3 and we observed that PhenDC3 does prevent the binding of NCL on GAr G4 (Fig. 6d), readily explaining its effect on 235GAr-OVA expression. Of note, PhenDC3 also prevents the binding of NCL on ARPC2 G4 (Fig. 6d). In contrast, PDS had no effect on the binding of NCL on both types of G4 (Supplementary Fig. 4a). We also checked that PDS and PhenDC3 are both able to bind to the most probable G4 that can form in the GAr-encoding mRNA sequence by determining the ability of these two compounds to displace the thiazole orange (TO) fluorescent probe from the GAr's G4 oligonucleotide used in the pulldown experiments[35]. As shown in Supplementary Fig. 4b, both PhenDC3 and PDS bind the GAr's G4 but the affinity of PhenDC3 (DC_{50} ~0.26 μM) is higher than that of PDS (DC_{50} ~0.47 μM). Taken together these results suggest that PhenDC3, but not PDS, is also able to prevent the binding of NCL on these G4 structures by a competitive mechanism. This difference, which may be due, at least in part, to the lower affinity of PDS for GAr's G4, is consistent with the fact that PhenDC3 does interfere with the GAr self-inhibitory effect on protein expression whereas PDS is inactive.

To confirm that PhenDC3 prevents the binding of NCL on EBNA1 mRNA in more physiological settings, we tested the effect of PhenDC3 in the PLA experiment on EBV-infected Mutu-1 cells. As shown in Fig. 5b,c, the number of nuclear PLA dots per cell was significantly reduced (~threefold) when Mutu-1 cells were treated with 0.75 μM PhenDC3 confirming the ability of PhenDC3 to interfere with this interaction in a cellular context. The same result was obtained when using H1299 cells expressing transfected EBNA1 (Fig. 5d,e).

PhenDC3 increases EBNA1 expression in EBV-infected cells. Next, we tested PhenDC3 effect on endogenous EBNA1 expression in EBV-infected cells and found that it also increased the endogenous EBNA1 level in Mutu-1 (EBV-infected B-cells; Fig. 6e left panel) and NPC-6661 (EBV-infected cells derived from a nasopharyngeal carcinoma[36]; Fig. 6e right panel) cells. Importantly, PhenDC3 had no effect on EBNA1 mRNA level in Mutu-1 cells (Supplementary Fig. 4c). We also checked that PhenDC3 is not significantly toxic on Mutu-1 cells when used at a concentration range (0.5–1 μM) in which it increases the expression of EBNA1 (Supplementary Fig. 4d). Finally, we found that PDS had no effect on endogenous EBNA1 level in Mutu-1 cells (Supplementary Fig. 4e) confirming that, contrary to PhenDC3, PDS is not able to interfere with the GAr-based self-inhibition of protein expression.

To conclude, the PhenDC3 G4 ligand prevents the binding of NCL on GAr's G4 and, at the same time, leads to an increase in EBNA1 and 235GAr-OVA expression, thereby supporting the crucial role of NCL in GAr-based self-inhibition of translation by binding to G4 formed in the EBNA1 mRNA. Importantly, these results also indicate that NCL-EBNA1 mRNA interaction is druggable.

PhenDC3 activates GAr-limited antigen presentation. Finally, to assess the ability of PhenDC3 to interfere with GAr-based immune evasion, we performed the same OT1 T-cell proliferation assay as in Fig. 3c,d in the presence or absence of 5 μM PhenDC3. As shown in Fig. 7a, PhenDC3 significantly increased (twofold change) the proliferation of OT1 T cells added to 235GAr-OVA-expressing H1299 cells, whereas it had no effect on OT1 cells incubated with OVA-expressing cells. A western blot analysis

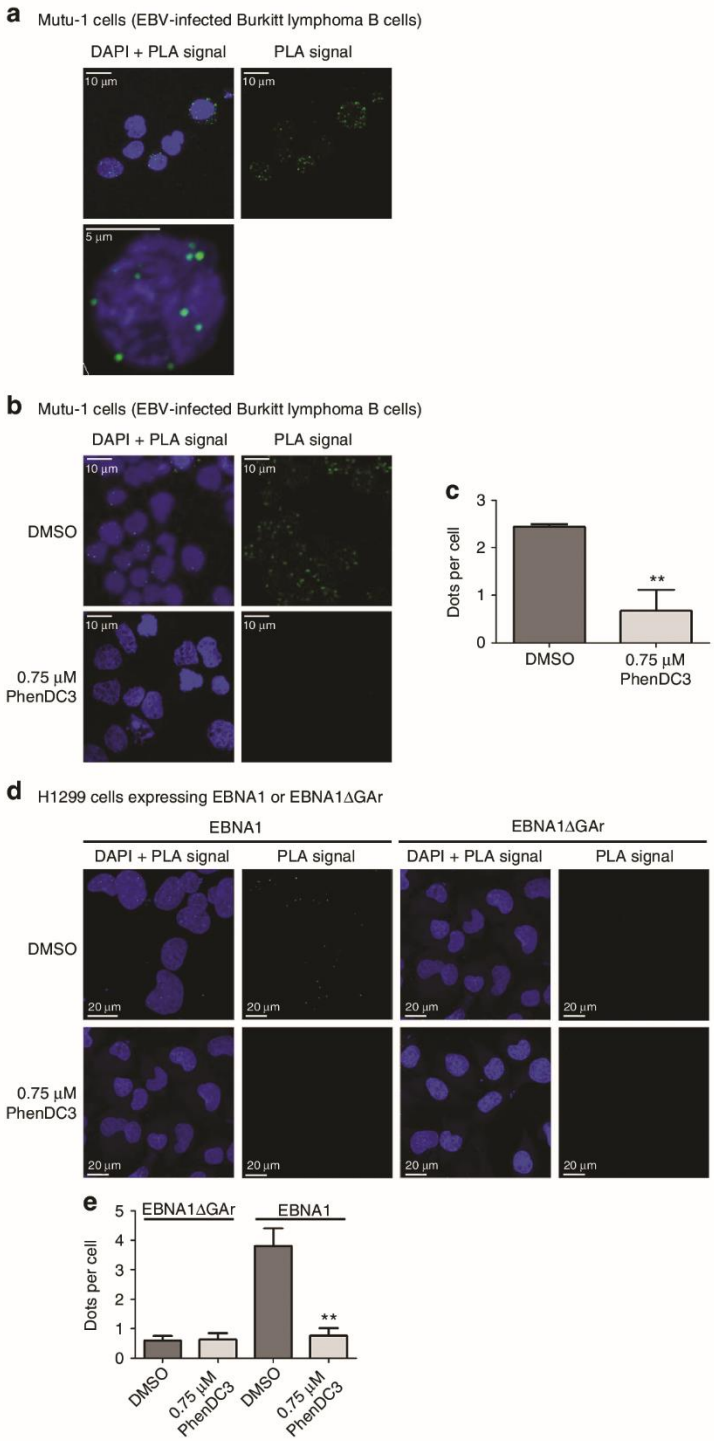

Figure 5 | NCL-EBNA1 mRNA interaction takes place in the nucleus. (**a**) Endogenous NCL interacts *in cellulo* with endogenous EBNA1 mRNA in the nucleus. Proximity ligation assay (PLA) experiment to determine if NCL interacts with EBNA1 mRNA *in cellulo* was performed in the EBV-infected Burkitt lymphoma cells Mutu-1. The green dots (PLA signal) indicate an interaction. PLA signals were shown together with DAPI staining (top left) and alone (top right). A zoom on the nucleus of a Mutu-1 cell is shown. (**b**) *In cellulo* nuclear interaction between NCL and EBNA1 mRNA is reduced upon treatment by 0.75 µM PhenDC3. Same experiment than in **a** except that Mutu-1 cells were treated by DMSO (top) or PhenDC3 (bottom). (**c**) The mean number of PLA dots per cell in DMSO- (vehicle) or 0.75 µM PhenDC3-treated Mutu-1 treated cells shown in **b** are indicated and compared using the Student's *t*-test (**$P<0.01$). (**d**) *In cellulo* nuclear interaction between NCL and EBNA1 mRNA is GAr-dependent. PLA experiments were performed in H1299 cells transfected with EBNA1 or EBNA1ΔGAr plasmids and treated or not with 0.75 µM PhenDC3. The green dots indicate an interaction. PLA signals were shown together with DAPI staining and alone. (**e**) The number of PLA dots per cells obtained in (**d**) treated by DMSO (vehicle) or 0.75 µM PhenDC3 are indicated and compared using the Student's *t*-test (**$P<0.01$).

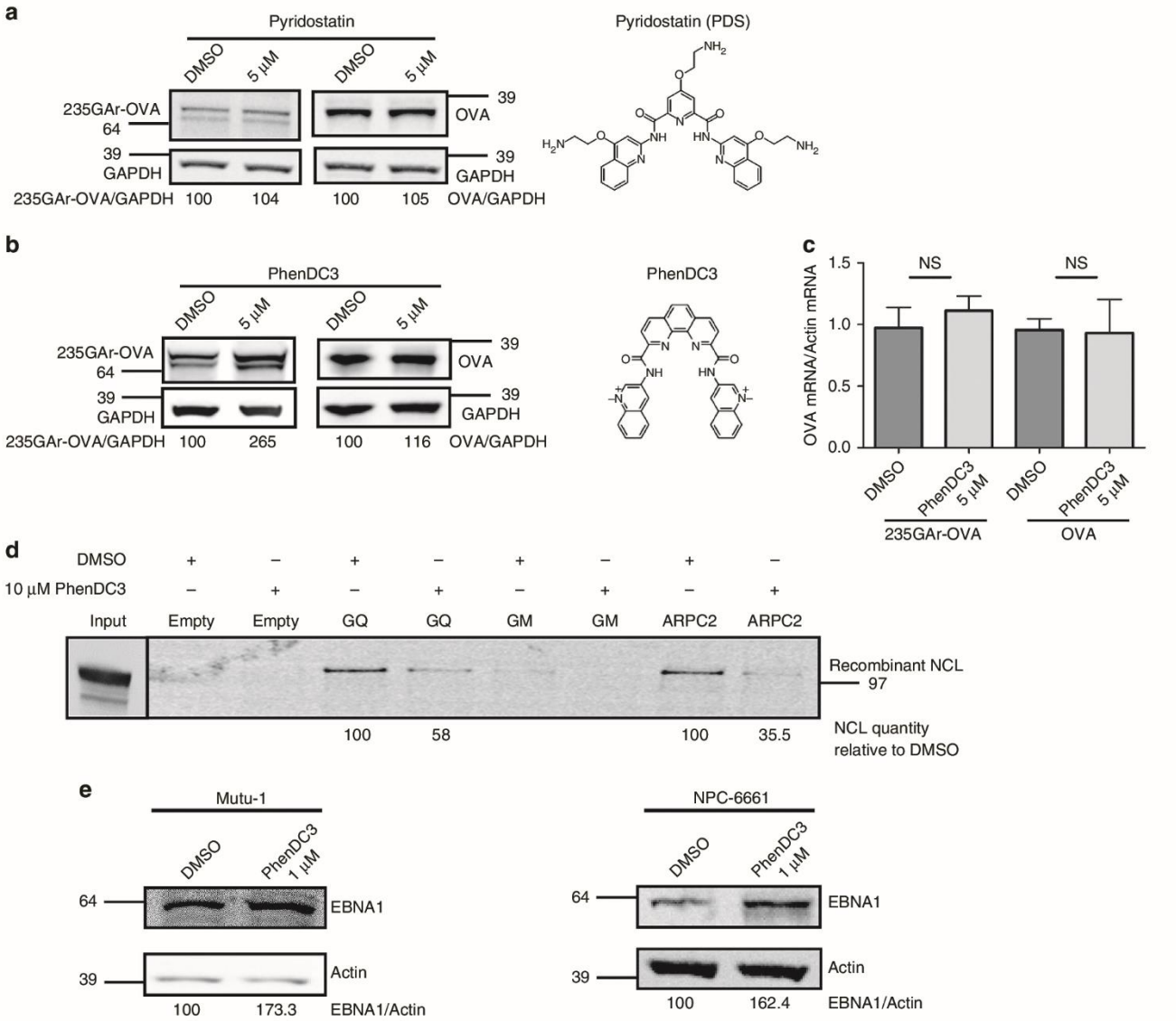

Figure 6 | PhenDC3 prevents GAr inhibition of protein expression and NCL binding to GAr's G4. (**a**) SDS-PAGE and western blot analysis of the level of 235GAr-OVA or OVA in response to pyridostatin (PDS) treatment. H1299 cells transfected with 235GAr-OVA (left) or OVA (right) plasmids were treated with 5 μM PDS (right lanes) or, as a control, with DMSO (left lanes). GAPDH was used as a loading control and 235GAr-OVA/GAPDH and OVA/GAPDH ratios are indicated below the gels. The chemical structure of PDS is depicted on the right. Blot represents $n \geq 3$. (**b**) SDS-PAGE and western blot analysis of the level of 235GAr-OVA or OVA in response to PhenDC3 treatment. Same experiments as in **a** except that cells were treated with 5 μM PhenDC3 which chemical structure is depicted on the right. Blot represents $n \geq 3$. (**c**) The effect of 5 μM PhenDC3 treatment on 235GAr-OVA or OVA mRNA level was determined by qRT-PCR. The results were compared using the Student's *t*-test (NS: not significant). (**d**) PhenDC3 competes for the binding of NCL on GAr and *ARPC2* G4. Same experiment than in Fig. 4c in the presence of 10 μM PhenDC3 or DMSO (vehicle) as indicated. (**e**) PhenDC3 increases endogenous EBNA1 expression in EBV-infected cells. The level of endogenous EBNA1 in Mutu-1 (EBV-infected B cells, left panel) and NPC-6661 (EBV-infected cells from nasopharyngeal carcinoma, right panel) cells in response to 1 μM PhenDC3 was determined by SDS-PAGE followed by western blot. Actin was used as a loading control and EBNA1/Actin ratio are indicated below the gels. Blots represent $n \geq 3$.

confirmed that PhenDC3 increases the level of 235GAr-OVA, whereas it has no effect on OVA (Fig. 7b).

Discussion

In this study, we have identified NCL as a host cell factor critically involved in GAr-based EBNA1 immune evasion by its ability to bind G4 formed in the GAr-encoding sequence of the EBNA1 mRNA. In line with this model, we showed that the G4 ligand PhenDC3 both prevents the binding of NCL on G4 of the EBNA1 mRNA, and increases EBNA1 expression and GAr-dependent antigen presentation. This indicates that the interaction between NCL and G4 of the EBNA1 mRNA is a relevant and druggable therapeutic target to treat EBV-related cancers. Interestingly, the G4 ligand PDS had no effect on EBNA1 expression *in cellulo* indicating that only some G4 ligands are able to interfere with NCL-EBNA1 mRNA interaction, which can be attributed to off-target binding and/or differences in pharmacological properties (cell penetration, intracellular distribution and so on). Of note, *in vitro*, PDS affinity for GAr's G4 appears significantly weaker than that of PhenDC3 which may contribute, at least in part, to the differential activity of these two G4 ligands on GAr. This also points out two different possible mechanisms of action for G4 ligands whose binding on G4 may either stabilize them or prevent

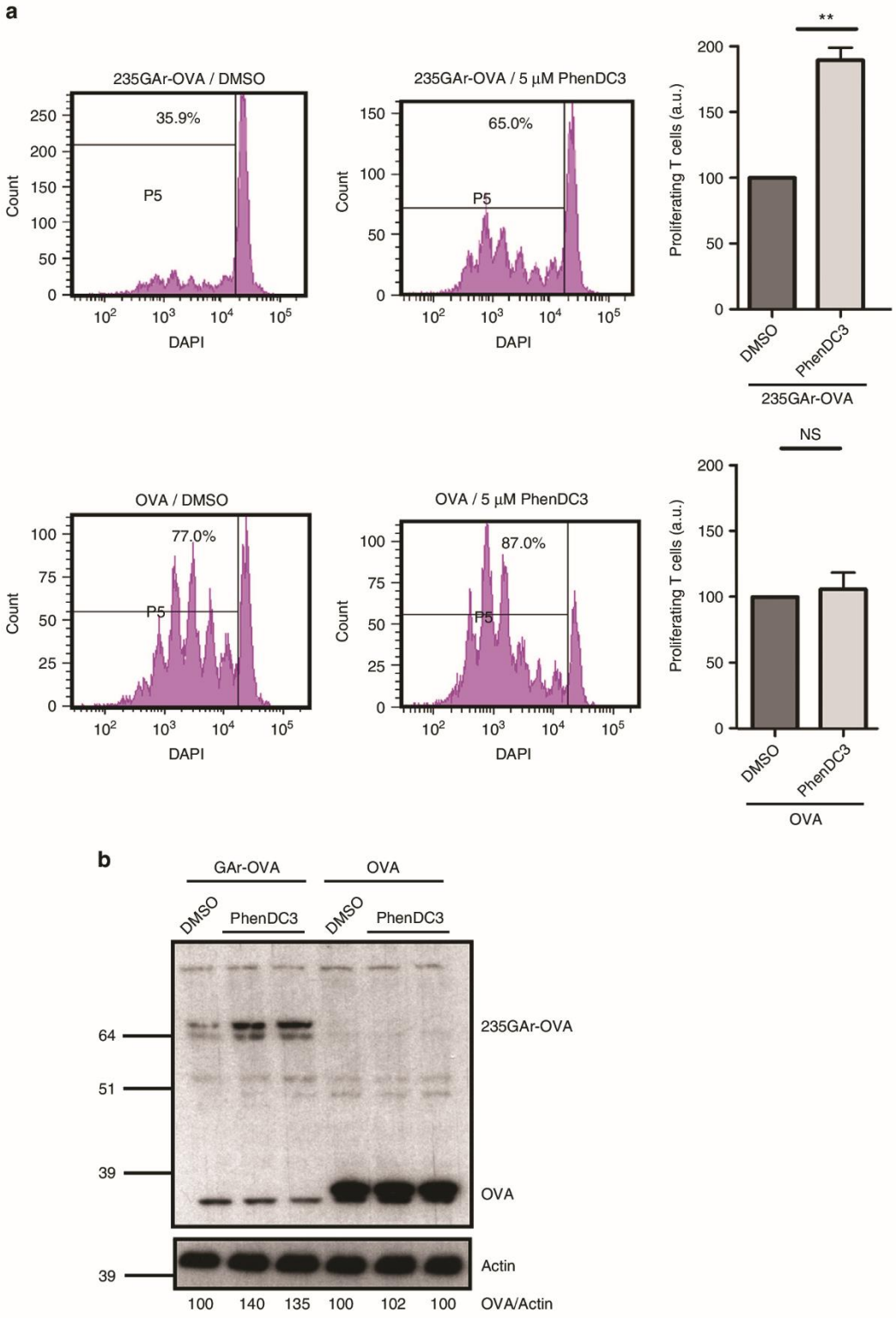

Figure 7 | PhenDC3 activates GAr-limited antigen presentation. (**a**) PhenDC3 increases T-cell proliferation. Same experiment as in Fig. 3c,d except that 235GAr-OVA (upper panels) and OVA (lower panels) expressing H1299 cells were treated with 5 µM PhenDC3 or, as control, with DMSO as indicated. Quantifications of proliferating T lymphocytes following PhenDC3 treatment as compared to DMSO-treated cells are shown in the graphs on the right. The results were compared using the Student's *t*-test (**$P<0.01$; NS: not significant). (**b**) SDS-PAGE and western blot analysis of cells used in **a**.

the binding of cellular partners by direct competition or by modifying G4 structure. In line with these hypotheses, we tested several PhenDC3 close chemical derivatives and observed that some, but not all, were active on EBNA1 expression (data not shown). Of note, PDS has been found to suppress EBNA1 expression in an *in vitro* coupled transcription-translation assay[29]

but it is not known, in this experiment, if this effect is related to a change in EBNA1 mRNA level or to G4 stabilization that may exacerbate the GAr-dependent translation inhibition.

This brings out an intriguing point regarding the role of NCL in GAr-based self-limitation of EBNA1 expression and antigenic presentation. Indeed, NCL has been also positively involved in EBV episome maintenance and transcription[27]. Hence, NCL appears to positively control both EBV episome maintenance and transcription on the one hand and the self-limitation of the EBV GMP expression on the other. As for EBV, one can consider it makes sense to have the same host cell protein regulating these two key aspects of EBV's latency. Indeed, if NCL level is low, then the maintenance and transcription of EBV episome should be compromised but, as a result of NCL role in GAr-based limitation of EBNA1 expression, EBNA1 mRNA should be more efficiently translated, which may compensate for its reduced level and favour the maintenance of EBV genome. On the contrary, if NCL level is high, then EBV episome will be efficiently maintained and transcribed, hence leading to a high level of EBNA1 mRNA, but then the increased NCL could further downregulate its translation, thereby limiting the level of EBNA1 protein and therefore its detection by the immune system. Importantly, the role of NCL in EBNA1 immune evasion involves its ability to interact with G4 structures present in EBNA1 mRNA, whereas its role in episome maintenance and transcription involves its ability to interact with EBNA1's N-terminal 100 amino acids (hence upstream of the GAr domain of EBNA1 protein). Therefore, targeting the NCL-EBNA1 mRNA interaction should specifically affect EBNA1 immune evasion.

What could be NCL mechanism of action in GAr-based self-inhibition of translation and antigen presentation? EBNA1 G4 may constitute a recognition signal for NCL that is, itself, directly or indirectly, responsible for translation inhibition by interfering with either translation initiation and/or elongation machinery. Alternatively, NCL could stabilize G4 that, themselves, may inhibit the ribosome progression. In either case, it is unlikely that the virus has developed a novel mechanism to exploit NCL for controlling gene expression. Rather, it is likely that this reflects a more general evolutionary conserved cellular pathway. The fact that NCL effect on GAr-based limitation of protein expression is also operant in yeast strengthens this hypothesis as yeast has no common evolutionary history with EBV. Hence, PhenDC3 and more generally G4 ligands represent chemical probes that will greatly help to characterize this pathway and to identify its physiological mRNA targets. To finish, as other oncogenic gamma herpesviruses like the Kaposi sarcoma-associated herpesvirus have evolved similar strategy of G4 clustering in the central coding regions of their GMP to evade the immune system, the results presented here may have applications for other gamma-herpesviruses-related diseases[29,37].

Methods

Yeast strains and culture media. All the yeast strains used in this study are derived from the W303 WT strain[38]: *MATa, leu2-3,112 trp1-1 can1-100 ura3-1 ade2-1 his3-11,15*. The *ade2Δ* strain genotype is: *MATa, leu2-3,112 trp1-1 can1-100 ura3-1 ade2-1:his5 S. pombe*. Yeast cells were grown and used as previously described[39]. The media used for yeast growth were: YPD (1% (w/v) yeast extract, 2% (w/v) peptone, 2% (w/v) glucose), 1/3 YPD (0.33% (w/v) yeast extract, 2% (w/v) peptone, 2% (w/v) glucose). Yeast minimal media w/o uracil (6.7% (w/v) yeast nitrogen base, 0.77% (w/v) amino acids without uracil, 2% (w/v) glucose). Yeast minimal media w/o uracil and tryptophan (6.7% (w/v) yeast nitrogen base, 0.72% (w/v) amino acids without uracil, 2% (w/v) glucose). Solid media contained 2% (w/v) agar.

Yeast-based genetic screen that allowed isolation of *NSR1*. A yeast genomic DNA library (a kind gift by F. Lacroute) constructed by inserting ~4 kb genomic DNA fragments (obtained by *Sau3A* partial digestion) at the unique BamHI site in the replicative 2 µ multicopy pFL44L vector containing *URA3*-marker, was transformed into 43GAr-Ade2p pink yeast strain using standard lithium acetate procedures[40]. This multicopy plasmid is present at ~50–100 copies per yeast cell. Transformants were selected on uracil-free minimal solid medium and a positive selection was carried out based on the redder colour phenotype. Out of ~20,000 transformants growing on uracil-free medium, 39 gave a redder phenotype. Plasmids originated from the pFL44-based library were extracted from these 39 redder transformants, purified and amplified in *Escherichia coli* and then retransformed into 43GAr-Ade2p yeast strain for confirmation of the redder phenotype. The extremities of the confirmed clones were sequenced using the following primers: F- 5′ GTGCTGCAAGGCGATTAAGT 3′ and R- 5′TGTGGAATTGTGAGCGGATA 3′. Two confirmed clones contained overlapping genomic fragments bearing the yeast *NSR1* gene.

Plasmid constructions. All vectors were constructed using standard cloning procedures. T4 DNA ligase and restriction enzymes were purchased from New England Biolabs. Plasmid maintenance was carried out in TOP10 *E. coli* strain. The p416 (*GPD*) containing *NSR1* gene was constructed as follows: *NSR1* coding sequence was amplified from genomic DNA of the *S. cerevisiae* W303 WT strain using the following primers: NSR1-F 5′ CGCGGATCCATGGCTAAGACTACTAAAGTAAAAGGTA AC 3′ and NSR1-R 5′ CCGCTCGAGCGGTTAATCAAATGTTTTCTTTGAACCAG 3′. The corresponding PCR fragment was cloned into *BamHI* and *XhoI* cloning sites of p416 (*GPD*) centromeric vector. To introduce a HA tag in frame with human *NCL*, its coding sequence was PCR-amplified from cDNA extracted from HEK293T cells using HA-NCL F- 5′ CGCGGATCCATGTACCCATACGATGTTCCAGATTACG CTGTGAAGCTCGCGAAGGCAG 3′ and NCL R- 5′ CCGCTCGAGCGGCTAT TCAAACTTCGTCTTCTTTCC 3′ primers and cloned into pCDNA3 vector (invitrogen) using *BamHI* and *XhoI* cloning sites. HA-NCL was then subcloned into the *S. cerevisiae* vector p414 (*GPD*). All generated constructs were amplified in the TOP10 *E. coli* strain, and sequenced by the Sanger method.

Generation of *nsr1Δ* yeast strains. *NSR1* gene deletion was carried out by replacement with kanMX6 cassette amplified from PFA6a-kanMX6 vector[41], using the following primers: F-5′ ACCAATTTCGGATCACTCAACCCAGGCAG GATAAAATAAGCGGATCCCCGGGTTAATTAA 3′ and R-5′ AAGAGAAAA AATTGAAATTGAAATTCATTTCATTTTCTCAGAATCCGAGCTCGTTTA AAC 3′. Then the PCR fragment was transformed into W303 *ade2Δ*, *43GAr-ADE2* and W303 *ade2Δ*, *ADE2* yeast strains using standard lithium acetate procedures[40]. The transformed cells were spread on YPD + 100 µg ml^{-1} kanamycin plates which were then incubated 5 days at 29 °C, after which the plates were replicated on fresh YPD + 100 µg ml^{-1} kanamycin plates, and the deletion of *NSR1* gene in kanamycin-resistant colonies was checked by PCR, using the following primers: *nsr1Δ* Fbis-5′ GTACTTAAGTGTAGCTGTTGC 3′ and *nsr1Δ* Rbis-5′ TAGAGATGGTGAATGAAAGG 3′.

Yeast protein extracts. Five millilitres of 0.8–1.0 $OD_{600\ nm}$ exponentially growing cells was collected and cell pellets were resuspended into 300 µl of lysis buffer (25 mM Tris-HCl pH 6.8; 10% glycerol; 5% β-mercaptoethanol; 5% SDS; 8 M Urea; 0.02% bromophenol blue).

Mammalian cells protein extracts. Whole cells were collected 48 h post transfection and lysed in 20 mM Tris-HCl, pH 7.5, 150 mM NaCl, 1% Igepal containing protease inhibitors (Roche, Germany). Samples were centrifuged at 16,000*g* for 20 min at 4 °C and protein concentrations were measured using a Bradford assay.

Western blotting. Equal protein quantities and volumes of all samples were loaded onto 10% NuPAGE Bis-Tris gels (invitrogen), and transferred onto 0.45 µm nitrocellulose membranes (GE Healthcare). Membranes were blocked during 1 h at room temperature in PBS 1X containing 0.1% Igepal and 3% BSA.

Membranes were analysed using the following antibodies: anti-HA rat monoclonal antibody (Roche, 1:2,500); anti-Nsr1p mouse monoclonal antibody (Abcam, 1:5,000), anti-NCL rabbit polyclonal antibody (Abcam, 1:5,000), anti-GAPDH (Sigma, 1:5,000), anti-EBNA1 mouse monoclonal antibody (OT1X, 1:2,000), anti-OVA rabbit polyclonal antibody (Sigma, 1:2,500), anti-actin (Sigma, 1/5,000). The membranes were then washed with fresh PBS 1X + 0.1% Igepal and incubated for 45 min with swine anti-rabbit or goat anti-mouse secondary antibodies (Dako) conjugated to horseradish peroxidase at a 1:3,000 dilution, and analysed by enhanced chemiluminescence (ECL, GE Healthcare) using a Vilbert-Lourmat Photodocumentation Chemistart 5000 imager. All the experiments were repeated at least three times. Relative protein levels for each sample were normalized to GAPDH or Actin protein levels as indicated, using Fusion-Capt Advance software.

Cell culture and transfection. H1299 cells are derived from metastatic lymph node from lung carcinoma. Raji cells are type III latency Burkitt's lymphoma. HCT116 cells are derived from colorectal carcinoma. B95.8 cells are derived from cotton-top Tamarin Monkey peripheral blood lymphocyte. Mutu-1 cells are derived from an EBV-positive Burkitt's lymphoma biopsy specimen from a Kenyan patient. NPC-6661 cell line was established from a xenografted NPC in the early 1990s (ref. 36) and was

kindly provided by Prof. Kwok-Wai Lo from the Chinese University of Hong Kong. H1299, Raji, B95.8 and Mutu-1 cells were cultured in RPMI-1640 media supplemented with 10% fetal bovine serum (FBS) and 2 mM L-glutamine. HCT116 cells were cultured in McCoy's 5A Glutamax media supplemented with 10% FBS, and NPC-6661 cells in RPMI-1640 media supplemented with 25 mM HEPES (Gibco) and 2 mM L-glutamine and 10% FBS. All cells were cultured at 37 °C with 5% CO_2. Transient transfections were performed using Genejuice reagent (Merck Bioscience) according to the manufacturer's protocol or electroporation using Gene PulserXL system (Biorad).

RNA extraction and quantitative real-time PCR. Total yeast, H1299 or Mutu-1 cellular RNA was extracted using RNAeasy and RNAase-free, DNase kits (Qiagen). cDNA synthesis was carried out using 1 µg of DNA-free RNA using M-MLV reverse transcriptase (invitrogen) and Oligo-dT primer. Triplicated cDNA samples were analysized by quantitative PCR using PERFECTA SYBR fastmix (Quanta Bioscience). The relative abundance of target mRNA was normalized using Actin as an endogenous control. Quantification of gene expression was determined using the $-2^{\Delta\Delta Ct}$ method. The primers used for PCR were *ADE2*-forward: 5′-ATTGTGCAAATGCCTAGAGGTG-3′, *ADE2*-reverse: 5′-AATCATAA - GCGCCAAGCAGTC-3′; Actin-forward: 5′-ATGGTNGGNATGGGNCARAAR-3′, Actin-reverse: 5′-CTCCATRTCRTCCCAGTTGGT-3′; *EBNA1*-forward: 5′-GGCAGTGGACCTCAAAGAAGAG-3′; *EBNA1*-reverse: 5′-CAATGCAACTTG-GACGTTTTT-3′; OVA-forward: 5′-GAGGAGGCTTGGAACCTAT-3′; OVA-reverse: 5′-CAGTTTGAGAATCCACGGAG-3′. All the experiments were performed in triplicates and were repeated at least three times.

NCL siRNA downregulation. 1.75×10^5 H1299 cells were transfected with 0.75 µg of EBNA1, EBNA1ΔGAr, 235GAr-OVA or OVA vectors using standard procedures and incubated at 37 °C for 8 h. Cells were then transfected either with 40 nM of control siRNA or FlexiTube GeneSolution for NCL (Qiagen). siRNA transfection were performed using HiPerFect transfection reagent (Qiagen) following the manufacturer's protocol. Forty hours after siRNA transfection, cells were collected for western blot or flow cytometry analyses.

Mutu-1 cells were electroporated using SG Cell Line 4D-Nucleofector X Kit from Lonza (V4XC-3012) following manufacturer's instructions and 300 nM of control siRNA or FlexiTube GeneSolution for NCL (Qiagen). Forty hours after siRNA transfection, cells were collected for western blot analyses.

Flow cytometry analysis. Forty-eight hours after the transfection, cells were collected using trypsin and washed twice with 1X PBS. Cells were suspended in 50 µl of 1X PBS and incubated with 0.4 µg of anti-mouse OVA257–264 (SIIN-FEKL) peptide antibody bound to H-2 Kb PE or anti-mouse MHC Class I (H-2 Kb) antibody bound to PE (Ebioscience) for 30 min at room temperature. Cells were then washed with 1X PBS and analysed by FACS on a CANTO II flow cytometer (BD Biosciences, USA).

RNA pulldown experiments. For the preparation of whole cell extracts, confluent H1299 cells were collected after trypsin treatment and washed twice with 1X PBS (Gibco). Cells were suspended in 500 µl of lysis buffer (20 mM Tris-HCl pH 7.5; 200 mM NaCl and 0.1% Igepal) containing 1X protease inhibitor cocktail (Roche). Cell lysis was performed by five series of vortex followed by 10 min incubation on ice, and three series of 3 s sonication at 20% amplitude. After lysis cells were centrifuged at 4 °C for 15 min at 16,000*g*, and the supernatant was quantified by Bradford. The whole cell extracts or recombinant GST-NCL (Abnova) were used for pulldown assays with the following G-quadruplex forming oligonucleotides: GQ- 5′-GGGGCAGGAGCAGGAGGA-3′Biotin TEG, ARPC2- 5′ AGCCGGGGGCUGGGCGGGGACCGGGCUUGU-3′Biotin TEG. The negative control for EBNA1 G4 was the GM- 5′ GAGGCAGUAGCA-GUAGAA-3′Biotin TEG oligonucleotide which, according to the GQRS-H predictor software[30], is unable to form G4 structures. To avoid unspecific binding, high-affinity streptavidin sepharose beads (GE Healthcare) were incubated in 1 ml blocking buffer containing 10 mM Tris-HCl pH 7.5; 100 mM KCl; 0.1 mM EDTA; 1 mM DTT; 0.01% Triton X-100; 0.1% BSA; 0.02% *S. cerevisiae* tRNAs (Sigma), for 1 h at 4 °C on a rotating wheel. An amount of 10 pg of each folded biotinylated RNA oligos was incubated with 50 µl of solution containing the streptaviding sepharose beads for 90 min at 4 °C on a rotating wheel. Five hundred micrograms of cell extract or 200 ng of recombinant GST-NCL (Abnova) was incubated with the RNA oligonucleotides bound to the streptavidin beads during 90 min at room temperature. Beads were washed with increasing KCl concentration (200–800 mM). Protein still bound to beads after the washes were eluted using 2X SDS loading buffer and analysed by western blotting against NCL, as previously described. In the input lane of the western blots was loaded a quantity of extract which corresponds to half of the quantity that was incubated with the beads for each condition.

Proximity ligation assay. Cells were fixed with 4% paraformaldehyde in PBS 1X for 20 min and permeabilized with 0.4% Triton X-100, 0.05% CHAPS for 5 min at room temperature. A quantity of 50 ng of EBNA1-digoxigenin mRNA probe (5′ CTTTCCAAACCACCCTCCTTTTTTGCGCCTGCCTCCATCAAAAA 3′) or control sense probe was denaturated 5 min at 80 °C and the hybridization reaction was carried out overnight at 37 °C in 40 µl hybridization buffer (10% formamide; 2X SSC, 0.2 mg ml^{-1} *E. coli* tRNAs, 0.2 mg ml^{-1} sheared salmon sperm DNA and 2 mg ml^{-1} BSA. A blocking solution of 3% BSA 0.1% saponine in 1X PBS was added for 30 min followed by 2 h incubation at room temperature with the primary antibodies (anti-digoxigenin 1/200 -Sigma- and anti-NCL 1/1000 -Abcam-) diluted in PBS 1X, 0.3% BSA, 0.1% saponine. The PLA was carried out using the Duolink PLA *in situ* kit, PLA probe anti-rabbit plus, the Duolink *in situ* PLA probe anti-mouse MINUS and the *in situ* detection reagent FarRed (all from Sigma) following the manufacturer's protocol. PLA results were visualized using a Zeiss LSM780 confocal microscope. All the PLA experiments were performed at least three times independently and, each time, PLA dots were counted in 50–100 cells. For each PLA experiment, the following controls were used: w/o mRNA probe, w/o antibodies and with the control sense probe.

^{35}S methionine pulse-labeling. 8×10^5 cells were transiently transfected with 4 µg of 235GAr-OVA or OVA vectors and, 8 h later, NCL silencing was performed using 40 nM of NCL siRNA or control siRNA (as previously described). Forty hours after the transfection, cells were incubated 30 min in a methionine-free medium. After incubation, 25 µM of MG132 proteasome inhibitor was added to the medium and cells were incubated for 45 min. Cells were then cultured in a medium containing 0.15 mCi ml^{-1} ^{35}S-methionine (Perkin Elmer, Boston, USA) for 1 h and collected. Cell pellets were suspended in 20 mM Tris-HCl, pH 7.5, 150 mM NaCl, 1% Igepal and treated as described above. Lysates were precleared with 1 µg normal rabbit serum (Dako) bound to protein G-Sepharose magnetic beads (GE Healthcare) for 30 min at 4 °C and further immunoprecipitated with 1 µg of anti-OVA polyclonal antibody (Sigma) or IgG-rabbit (Dako), prebound to protein G-Sepharose magnetic beads overnight at 4 °C. Beads were then washed and proteins eluted using 2X SDS loading buffer. Immunoprecipitates were analysed by SDS-PAGE using 10% precast NUPAGE gels (invitrogen). The amount of radiolabelled proteins was visualized using a Storm Phosphorimager (GE Healthcare).

T-cell proliferation assay. Naive $OVA_{257-264}$ specific CD8+ T cells were isolated by negative selection from peripheral and mesenteric lymph-nodes of 12-week-old female OT1 mice using the CD8$^+$ T-cell isolation kit (Miltenyi Biotec, Germany). Afterwards, CD8$^+$ T cells were stained with CellTraceTM Violet (Thermo Fisher Scientific, USA) according to the manufacturer's protocol and mixed with H1299 cells cotransfected with mouse k^b expression vector and OVA or GAr-OVA constructs. For all the assays, 10^5 H1299 cells were collected 48 h after transfection and co-incubated with 4×10^5 stained T cells at 37 °C in humidified air/CO_2 atmosphere in 1 ml of RPMI medium containing 10% FBS, 4 mM L-glutamine, 100 U ml^{-1} penicillin, 100 µg ml^{-1} streptomycin, 5 mM HEPES and 0.05 mM 2-mercaptoethanol (Sigma-Aldrich). After 3 days, cells were collected, stained with hamster anti-mouse CD3-APC (Miltenyi Biotec) and fixable viability dye eFluor 780 (eBioscience, USA) and analysed by FACS on a CANTO II flow cytometer (BD Biosciences, USA). Cells were gated for live CD3$^+$ cells (10,000 events collected) and data were analysed using BD FACSDiva software version 8.0.1. The percentage of proliferating T cells was considered for statistical analysis.

MTT assay. A total of 30,000 Mutu-1 cells were plated in 0.1 ml in 96-well flat bottom plates and exposed to PhenDC3 at the indicated concentrations or DMSO (vehicle). After 24 h, 10 µl of 5 mg ml^{-1} MTT solution (CT01-5, Merck Millipore) in PBS pH 7.4 was added to each well and incubated for 4 h. A volume of 0.1 ml of isopropanol-HCl 0.1 N-Triton X-100 10% was added to each well to dissolve the formazan crystals. The absorbance was then measured at 540 nm.

Statistical analyses. Data shown are mean ± s.d. of minimum three independent experiments. Two-tailed unpaired Student's *t*-test was performed by comparing data to the corresponding reference point or as indicated and *P* values are shown. $^*P<0.05$; $^{**}P<0.01$; $^{***}P<0.001$; NS: not significant.

Fluorescence displacement assay for G4 ligands. G4-fluorescence displacement (FID) assay is performed in a 96-well non-binding surface black with black bottom polystyrene microplates (Corning). Every ligand is tested on a line of the microplate, in duplicate (in other plate). The microplate is filled with (a) K^+100 solution (qs for 200 µL) (b) 10 µl of a solution of prefolded oligonucleotides (5 µM) and TO (10 µM—2 molar equiv.) and (c) an extemporaneously prepared 5 µM ligand solution in K^+100 buffer (0–100 µl along the line of the microplate, that is, from column A to column H: 0, 0.125, 0.25, 0.375, 0.5, 0.625, 0.75, 1.0, 1.25, 1.5, 2.0 and 2.5 µM). After 5 min of orbital shaking at 500 r.p.m., fluorescence is measured using the following experimental parameters; positioning delay: 0.5 s, 20 flashes per well, emission/excitation filters for TO: 485/520, gain adjusted at 80% of the fluorescence from the most fluorescent well (that is, a well from column A). The percentage of TO displacement is calculated from the fluorescence intensity (*F*), using: % TO displacement = $1-F/F_0$ (F_0 being the fluorescence from the fluorescent probe bound to DNA without added ligand. The percentage of displacement is then plotted as a function of the concentration of added ligand. The DNA affinity is evaluated by the concentration of ligand required to decrease the fluorescence of the probe by 50%, noted DC_{50}, and determined after nonlinear fitting of the displacement curve.

Data availability. The authors declare that data supporting the findings of this study are available within the article and the Supplementary Information, or available from the corresponding author upon reasonable request.

References

1. Ozoya, O. O., Sokol, L. & Dalia, S. EBV-related malignancies, outcomes and novel prevention strategies. *Infect. Disord. Drug. Targets* **16,** 4–21 (2016).
2. Thorley-Lawson, D. A. & Allday, M. J. The curious case of the tumour virus: 50 years of Burkitt's lymphoma. *Nat. Rev. Microbiol.* **6,** 913–924 (2008).
3. Young, L. S. & Rickinson, A. B. Epstein-Barr virus: 40 years on. *Nat. Rev. Cancer* **4,** 757–768 (2004).
4. Blake, N. Immune evasion by gammaherpesvirus genome maintenance proteins. *J. Gen. Virol.* **91,** 829–846 (2010).
5. Frappier, L. Ebna1. *Curr. Top Microbiol. Immunol.* **391,** 3–34 (2015).
6. Daskalogianni, C. *et al.* Epstein-Barr virus-encoded EBNA1 and ZEBRA: targets for therapeutic strategies against EBV-carrying cancers. *J. Pathol.* **235,** 334–341 (2015).
7. Tellam, J. *et al.* Endogenous presentation of CD8 + T cell epitopes from Epstein-Barr virus-encoded nuclear antigen 1. *J. Exp. Med.* **199,** 1421–1431 (2004).
8. Yin, Y., Manoury, B. & Fahraeus, R. Self-inhibition of synthesis and antigen presentation by Epstein-Barr virus-encoded EBNA1. *Science* **301,** 1371–1374 (2003).
9. Apcher, S., Daskalogianni, C., Manoury, B. & Fahraeus, R. Epstein Barr virus-encoded EBNA1 interference with MHC class I antigen presentation reveals a close correlation between mRNA translation initiation and antigen presentation. *PLoS Pathog.* **6,** e1001151 (2010).
10. Levitskaya, J. *et al.* Inhibition of antigen processing by the internal repeat region of the Epstein-Barr virus nuclear antigen-1. *Nature* **375,** 685–688 (1995).
11. Apcher, S. *et al.* mRNA translation regulation by the Gly-Ala repeat of Epstein-Barr virus nuclear antigen 1. *J. Virol.* **83,** 1289–1298 (2009).
12. Murat, P. & Balasubramanian, S. Existence and consequences of G-quadruplex structures in DNA. *Curr. Opin. Genet. Dev.* **25,** 22–29 (2014).
13. Beaudoin, J. D. & Perreault, J. P. 5′-UTR G-quadruplex structures acting as translational repressors. *Nucleic Acids Res.* **38,** 7022–7036 (2010).
14. Didiot, M. C. *et al.* The G-quartet containing FMRP binding site in FMR1 mRNA is a potent exonic splicing enhancer. *Nucleic Acids Res.* **36,** 4902–4912 (2008).
15. Gomez, D. *et al.* Telomerase downregulation induced by the G-quadruplex ligand 12459 in A549 cells is mediated by hTERT RNA alternative splicing. *Nucleic Acids. Res.* **32,** 371–379 (2004).
16. Marcel, V. *et al.* G-quadruplex structures in TP53 intron 3: role in alternative splicing and in production of p53 mRNA isoforms. *Carcinogenesis* **32,** 271–278 (2011).
17. Siddiqui-Jain, A., Grand, C. L., Bearss, D. J. & Hurley, L. H. Direct evidence for a G-quadruplex in a promoter region and its targeting with a small molecule to repress c-MYC transcription. *Proc. Natl Acad. Sci. USA* **99,** 11593–11598 (2002).
18. Hanakahi, L. A., Sun, H. & Maizels, N. High affinity interactions of nucleolin with G-G-paired rDNA. *J. Biol. Chem.* **274,** 15908–15912 (1999).
19. Maizels, N. & Gray, L. T. The G4 genome. *PLoS Genet.* **9,** e1003468 (2013).
20. Rhodes, D. & Lipps, H. J. G-quadruplexes and their regulatory roles in biology. *Nucleic Acids. Res.* **43,** 8627–8637 (2015).
21. Abdelmohsen, K. & Gorospe, M. RNA-binding protein nucleolin in disease. *RNA Biol.* **9,** 799–808 (2012).
22. Abdelmohsen, K. *et al.* Enhanced translation by Nucleolin via G-rich elements in coding and non-coding regions of target mRNAs. *Nucleic Acids Res.* **39,** 8513–8530 (2011).
23. Tosoni, E. *et al.* Nucleolin stabilizes G-quadruplex structures folded by the LTR promoter and silences HIV-1 viral transcription. *Nucleic Acids Res.* **43,** 8884–8897 (2015).
24. Gonzalez, V., Guo, K., Hurley, L. & Sun, D. Identification and characterization of nucleolin as a c-myc G-quadruplex-binding protein. *J. Biol. Chem.* **284,** 23622–23635 (2009).
25. Lista, M. J. *et al.* The long-lasting love affair between the budding yeast *Saccharomyces cerevisiae* and the Epstein-Barr virus. *Biotechnol. J.* **10,** 1670–1681 (2015).
26. Voisset, C. *et al.* A yeast-based assay identifies drugs that interfere with immune evasion of the Epstein-Barr virus. *Dis. Model Mech.* **7,** 435–444 (2014).
27. Chen, Y. L. *et al.* Nucleolin is important for Epstein-Barr virus nuclear antigen 1-mediated episome binding, maintenance, and transcription. *Proc. Natl Acad. Sci. USA* **111,** 243–248 (2014).
28. von Hacht, A. *et al.* Identification and characterization of RNA guanine-quadruplex binding proteins. *Nucleic Acids Res.* **42,** 6630–6644 (2014).
29. Murat, P. *et al.* G-quadruplexes regulate Epstein-Barr virus-encoded nuclear antigen 1 mRNA translation. *Nat. Chem. Biol.* **10,** 358–364 (2014).
30. Frees, S., Menendez, C., Crum, M. & Bagga, P. S. QGRS-Conserve: a computational method for discovering evolutionarily conserved G-quadruplex motifs. *Hum. Genom.* **8,** 8 (2014).
31. Bugaut, A. & Balasubramanian, S. 5′-UTR RNA G-quadruplexes: translation regulation and targeting. *Nucleic Acids Res.* **40,** 4727–4741 (2012).
32. Monchaud, D. & Teulade-Fichou, M. P. A hitchhiker's guide to G-quadruplex ligands. *Org. Biomol. Chem.* **6,** 627–636 (2008).
33. Piazza, A. *et al.* Genetic instability triggered by G-quadruplex interacting Phen-DC compounds in *Saccharomyces cerevisiae*. *Nucleic Acids Res.* **38,** 4337–4348 (2010).
34. Muller, S. & Rodriguez, R. G-quadruplex interacting small molecules and drugs: from bench toward bedside. *Expert Rev. Clin. Pharmacol.* **7,** 663–679 (2014).
35. Largy, E., Hamon, F. & Teulade-Fichou, M. P. Development of a high-throughput G4-FID assay for screening and evaluation of small molecules binding quadruplex nucleic acid structures. *Anal. Bioanal. Chem.* **400,** 3419–3427 (2011).
36. Hui, A. B., Cheung, S. T., Fong, Y., Lo, K. W. & Huang, D. P. Characterization of a new EBV-associated nasopharyngeal carcinoma cell line. *Cancer Genet. Cytogenet.* **101,** 83–88 (1998).
37. Murat, P. & Tellam, J. Effects of messenger RNA structure and other translational control mechanisms on major histocompatibility complex-I mediated antigen presentation. *Wiley Interdiscip. Rev. RNA* **6,** 157–171 (2015).
38. Blondel, M., Galan, J. M. & Peter, M. Isolation and characterization of HRT1 using a genetic screen for mutants unable to degrade Gic2p in *Saccharomyces cerevisiae*. *Genetics* **155,** 1033–1044 (2000).
39. Blondel, M. *et al.* Degradation of Hof1 by SCF(Grr1) is important for actomyosin contraction during cytokinesis in yeast. *EMBO J.* **24,** 1440–1452 (2005).
40. Ito, H., Fukuda, Y., Murata, K. & Kimura, A. Transformation of intact yeast cells treated with alkali cations. *J. Bacteriol.* **153,** 163–168 (1983).
41. Longtine, M. S. *et al.* Additional modules for versatile and economical PCR-based gene deletion and modification in *Saccharomyces cerevisiae*. *Yeast* **14,** 953–961 (1998).

Acknowledgements

We thank all group members for valuable discussion and G. Friocourt, L. Meijer and B. Abiven for critical proofreading of the manuscript. We are indebted to F. Lacroute for the kind gift of the pFL44L-based yeast genomic DNA library, to K.W. Lo for the kind gift of NPC-661 cell line, to F. Mahuteau-Betzer for helpful discussions and for having seeded our collaborative network and to the imaging platform of the Brest University for the use of the confocal microscope. The work on EBV in the teams of M.B. and R.F. was supported by the following grant agencies: 'La Ligue contre le cancer', 'La Ligue contre le cancer CSIRGO', CREATE from the Région Bretagne, 'Fondation ARC', 'Institut National du cancer (INCa)' and IBSAM. M.J.L. is a recipient of a joint PhD grant from 'La Ligue contre le cancer Bretagne' and Région Bretagne and of a 6 month-extension from 'Fondation ARC'.

Author contributions

M.J.L., C.V. and M.B. conceived and designed the experiments. M.J.L., R.P.M., O.B., M.-A.C., S.F., P.P., C.D. and C.B. performed the experiments. M.J.L., R.P.M., M.-A.C., S.F., P.P., C.D., C.B., C.J., M.-P.T.-F., R.F., C.V. and M.B. analysed the data. C.G., M.-P.T.-F., R.P.M. and R.F. contributed reagents. M.J.L., R.F. and M.B. wrote the first draft of the paper. M.J.L., R.P.M., C.D., M.-P.T.-F., C.V., R.F. and M.B. reviewed and edited the manuscript. R.F., C.V. and M.B. supervised the work. M.J.L., C.V., M.-P.T.-F., R.F. and M.B. revised the manuscript.

Additional information

Supplementary Information accompanies this paper at http://www.nature.com/naturecommunications

Competing interests: The authors declare no competing financial interests.

Reprints and permission information is available online at http://npg.nature.com/reprintsandpermissions/

How to cite this article: Lista, M. J. *et al.* Nucleolin directly mediates Epstein-Barr virus immune evasion through binding to G-quadruplexes of EBNA1 mRNA. *Nat. Commun.* **8,** 16043 doi: 10.1038/ncomms16043 (2017).

Publisher's note: Springer Nature remains neutral with regard to jurisdictional claims in published maps and institutional affiliations.

molecules

MDPI

Communication

In Cellulo Protein-mRNA Interaction Assay to Determine the Action of G-Quadruplex-Binding Molecules

Rodrigo Prado Martins [1], Sarah Findakly [1], Chrysoula Daskalogianni [1,2], Marie-Paule Teulade-Fichou [3], Marc Blondel [4,*] and Robin Fåhraeus [1,2,5,6,*]

1 Université Paris 7, Inserm, UMR 1162, 75013 Paris, France; rodrigo.prado-martins@inserm.fr (R.P.M.); sarah.findakly@inserm.fr (S.F.); chrysoula.daskalogianni@inserm.fr (C.D.)
2 ICCVS, University of Gdańsk, Science, ul. Wita Stwosza 63, 80-308 Gdańsk, Poland
3 Chemistry, Modelling and Imaging for Biology, CNRS UMR9187-Inserm U1196, Institut Curie, Université Paris-Sud, F-91405, Orsay, France; mp.teulade-fichou@curie.fr
4 GGB, Université de Brest, Inserm, CHRU Brest, EFS, UMR 1078, F-29200 Brest, France
5 Department of Medical Biosciences, Umeå University, 90187 Umeå, Sweden
6 RECAMO, Masaryk Memorial Cancer Institute, Zluty kopec 7, 65653 Brno, Czech Republic
* Correspondence: marc.blondel@univ-brest.fr (M.B.); robin.fahraeus@inserm.fr (R.F.); Tel.: +33-142-499-269 (R.F.)

Academic Editor: Sara N. Richter
Received: 8 November 2018; Accepted: 26 November 2018; Published: 29 November 2018

Abstract: Protein-RNA interactions (PRIs) control pivotal steps in RNA biogenesis, regulate multiple physiological and pathological cellular networks, and are emerging as important drug targets. However, targeting of specific protein-RNA interactions for therapeutic developments is still poorly advanced. Studies and manipulation of these interactions are technically challenging and in vitro drug screening assays are often hampered due to the complexity of RNA structures. The binding of nucleolin (NCL) to a G-quadruplex (G4) structure in the messenger RNA (mRNA) of the Epstein-Barr virus (EBV)-encoded EBNA1 has emerged as an interesting therapeutic target to interfere with immune evasion of EBV-associated cancers. Using the NCL-EBNA1 mRNA interaction as a model, we describe a quantitative proximity ligation assay (PLA)-based in cellulo approach to determine the structure activity relationship of small chemical G4 ligands. Our results show how different G4 ligands have different effects on NCL binding to G4 of the *EBNA1* mRNA and highlight the importance of in-cellulo screening assays for targeting RNA structure-dependent interactions.

Keywords: structure-activity relationship; protein-mRNA interactions; G-quadruplexes; PhenDC3; pyridostatin; EBNA1; Epstein-Barr virus (EBV)

1. Introduction

Accumulating evidence indicates an ever-expanding role for RNAs in regulating most aspects of cell biology that range from small non-coding RNAs to messenger RNAs (mRNAs). The more traditional role of mRNAs as "only messengers" is changing and new knowledge is emerging showing how the encoding sequences are taking on more diverse functions and can influence the activity of the encoded proteins. Most, if not all aspects of mRNAs, and this is presumably true also for non-coding RNAs, are governed by interactions with cellular proteins. These ribonucleoproteins (RNP) complexes control RNA metabolism and form scaffolds to orchestrate and organize protein networks and complex functional units [1]. Thus, interfering with specific protein-RNA complexes holds promise for new therapeutic developments as well as furthering our understanding of cell biological process. However,

it is challenging to specifically target protein-RNA interactions (PRIs) for several reasons. One reason is that the interactions between proteins and RNAs, in particular mRNAs, are often dependent on RNA structures. However, the folding of RNAs, the chaperones involved, and how RNA-binding protein (RBP) specifically recognize certain RNA structures are still relatively unknown. New evidence that follows technical developments together with studies on disease-related single synonymous mutations have highlighted that folding of RNAs into 3D structures that serve as a protein-binding platform is a regulated and dynamic process encompassing relatively large sequences [2–6]. Thus, RNA structures from the same RNA sequence can be different in vitro as compared to in vivo, making it difficult to set up in vitro-based drug screening assays to identify compounds that interfere with specific PRIs.

G-quadruplexes (G4) are non-canonical nucleic acid structures based on the stacking of several G-quartets, further stabilized by cations positioned in the central channel of the G4 helix [7,8]. These structures are frequently found in eukaryotic transcripts [8] and their formation has been implicated in several steps of gene expression. Indeed, a relevant number of disease-related genes have been shown to be regulated by G4 structures and their RBP [9]. We have recently reported that nucleolin (NCL) directly binds G4 formed in the GAr-encoding sequence of the Epstein Barr virus (EBV) *EBNA1* mRNA (Figure 1A,B, see also Reference [10]). This interaction is critical for minimizing *EBNA1* mRNA translation and thereby the production of EBNA1-derived antigenic peptides for the major histocompatibility (MHC) class I pathway, allowing EBV-infected cells to evade the immune system [11]. As EBV is associated with several human cancers and as all EBV-infected cells express EBNA1, the *EBNA*1 mRNA-NCL interaction represents an interesting target for developing drugs that aim to induce an immune response against EBV-related diseases. It also serves as a broader model for developing techniques required to study structured RNA-protein interactions. Here, we use the NCL-*EBNA1* mRNA interaction to illustrate how different compounds binding to the same G4 have specific effects on the interaction with NCL in cellulo. This illustrates a so far unknown role of G4 structures in mediating specific interactions with proteins, indicating that particular G4-protein interactions can be targeted specifically. We also report how to generate quantitative data using proximity ligation to verify the capacity of different G4 ligands to prevent NCL-*EBNA1* mRNA interactions and their role in controlling *EBNA1* mRNA translation.

2. Materials and Methods

2.1. Cell Culture, Transfection, and Drug Treatments

The human lung carcinoma cell line H1299 and the EBV-producing marmoset B-cell line B95-8 were cultured in RPMI-1640 supplemented with 10% fetal bovine serum (FBS), 2 mM L-glutamine, 100 U/mL penicillin, and 100 µg/mL streptomycin. H1299 transient transfections were performed using Genejuice reagent (Merck Bioscience, Darmstadt, Germany) according to manufacturer's protocol. All cells were cultured at 37 °C with 5% CO_2. For drug treatments, 10^5 B95-8 cells were incubated with 5 µM of PhenDC3 [12] or pyridostatin (PDS, Sigma-Aldrich (now Merck), Darmstadt, Germany) for 36 h. Drug stock solutions were prepared in DMSO (Euromedex, Strasbourg, France).

2.2. RNA In Situ Hybridization-Immunofluorescence (rISH-IF) and Immunofluorescence (IF)

H1299 cells were plated on 12-mm-diameter coverslips in 24-well plates and transfected with 200 ng of EBNA1 construct [13]. At 24 h post-transfection, cells were fixed with PBS 4% paraformaldehyde for 20 min and then washed with PBS for 10 min. For rISH-IF, samples were overnight incubated in 70% (*v*/*v*) ethanol at 4 °C. After rehydration in PBS for 30 min, samples were permeabilized with PBS 0.4% Triton X-100, 0.05% CHAPS for 10 min at room temperature, and pre-treated with hybridization buffer (10% formamide, 2X SSC, 0.2 mg/mL *E. coli* 522 tRNAs, 0.2 mg/mL sheared salmon sperm DNA and 2 mg/mL BSA) for 30 min at room temperature. Samples were then incubated overnight with 50 ng of an EBNA1-digoxigenin DNA probe (5′ CTTTCCAAACCACCCTCCTTTTTTGCGCCTGCCTCCATCAAAAA-digoxigenin 3′) in a

humidified chamber at 37 °C. To avoid secondary structures, the probe was diluted in 5 µL of water, denaturated at 80 °C for 5 min, chilled on ice for 5 min, and resuspended in 35 µL of hybridization buffer. After hybridization, samples were serially washed for 20 min with 2X SSC 10% formamide, hybridization buffer (twice), 2X SSC, and PBS. Washes were carried out at room temperature, except with hybridization buffer (37 °C). Samples were saturated with PBS 3% BSA for 30 min and incubated with a mouse anti-digoxigenin (1/200, clone DI-22, Sigma) for 2 h at room temperature. A goat anti-mouse immunoglobulin G (IgG) secondary antibody conjugated to Alexa Fluor® 568 (Sigma) was used to detect immunocomplexes (1 h at 37 °C) and DAPI was used for nuclear counterstaining under standard conditions. For IF, fixed samples were saturated with PBS 3% BSA for 30 min, incubated with rabbit polyclonal antibody anti-NCL (1/1000, ab22758-Abcam) for 2 h and goat anti-rabbit Ig secondary antibody conjugated to Alexa Fluor® 488 (Sigma) for 1 h at 37 °C. DAPI was used for nuclear counterstaining.

2.3. Sequence of EBNA1 cDNA

The sequence of EBNA1 cDNA (GenBank: MG021311.1) is as follows (the GAr-encoding sequence which forms G4 is highlighted in cyan):

ATGTCTGACGAGGGACCAGGTACAGGACCTGGAAATGGCCTAGGACAGAAGGAAGACAC
ATCTGGACCAGACGGCTCCAGCGGCAGTGGACCTCAAAGAAGAGGGGGGGATAACCATGGAC
GAGGACGGGGAAGAGGACGAGGACGAGGAGGCGGAAGACCAGGAGCTCCGGGCGGCTCAG
GATCAGGGCCAAGACATAGAGATGGTGTCCGGAGACCCCAAAAACGTCCAAGTTGCATTGGC
TGCAAAGGGGCCCACGGTGGAACAGGAGCAGGAGGAGGGGCAGGAGCAGGAGGGGCAGGA
GCAGGAGGAGGGGCAGGAGCAGGAGGAGGGGCAGGAGCAGGAGGAGCAGGAGGAGGGGC
AGGAGCAGGAGGAGGGGCAGGAGCAGGAGGAGGGGCAGGAGCAGGAGGAGGGGCAGGAG
CAGGAGGAGGGGCAGGAGCAGGAGGAGGGGCAGGAGGAGGAGGAGGGGCAGGAGCAGGA
GGAGGGGCAGGAGCAGGAGGAGGGGCAGGAGCAGGAGGAGGGGCAGGAGGGGCAGGAGC
AGGAGGAGGGGCAGGAGCAGGAGGAGGGGCAGGAGCAGGAGGAGGGGCAGGAGCAGGAG
GGGCAGGAGCAGGAGGAGGGGCAGGAGCAGGAGGGGCAGGAGCAGGAGGAGGGGCAGGA
GCAGGAGGAGGGGCAGGAGCAGGAGGGGCAGGAGCAGGAGGGGCAGGAGCAGGAGGGGC
AGGAGCAGGAGGGGCAGGAGGAGGAGGAGCAGGAGGGGCAGGAGGGGCAGGAGCAGGAG
GGGCAGGAGGGGCAGGAGCAGGAGGAGGGGCAGGAGGGGCAGGAGCAGGAGGAGGGGCA
GGAGGGGCAGGAGCAGGAGGGGCAGGAGGGGCAGGAGCAGGAGGGGCAGGAGGGGCAGG
AGCAGGAGGGGCAGGAGGGGCAGGAGCAGGAGGAGGGGCAGGAGCAGGAGGGGCAGGAG
CAGGAGGTGGAGGCCGGGGTCGAGGAGGCAGTGGAGGCCGGGGTCGAGGAGGTAGTGGA
GGCCGGGGTCGAGGAGGTAGTGGAGGCCGCCGGGGTAGAGGACGTGAAAGAGCCAGGGGG
GGAAGTCGTGAAAGAGCCAGGGGGAGAGGTCGTGGACGTGGTGAAAAGAGGCCCAGGAGT
CCCAGTAGTCAGTCATCATCATCCGGGTCTCCACCGCGCAGGCCCCCTCCAGGTAGAAGGCC
ATTTTTCCACCCTGTAGGGGAAGCCGATTATTTTGAATACCACCAAGAAGGTGGCCCAGATGG
TGAGCCTGACATGCCCCCGGGAGCGATAGAGCAGGGCCCCGCAGATGACCCAGGAGAAGGC
CCAAGCACTGGACCCCGGGGTCAGGGTGATGGAGGCAGGCGCAAAAAAGGAGGGTGGTTT
GGAAAGCATCGTGGTCAAGGAGGTTCCAACCAGAAATTTGAGAACATTGCAGAAGGTTTAAG
AACTCTCCTGGCTAGGTGTCACGTAGAAAGGACTACCGATGAAGGAACTTGGGTCGCCGGTG
TGTTCGTATATGGAGGTAGTAAGACCTCCCTTTACAACCTCAGGCGAGGAATTGCCCTTGCTAT
TCCACAATGTCGTCTTACACCATTGAGTCGTCTCCCCTTTGGAATGGCCCCTGGACCCGGCCCA
CAACCTGGCCCACTAAGGGAGTCCATTGTCTGTTATTTCATTGTCTTTTTACAAACTCATATATTT
GCTGAGGGTTTGAAGGATGCGATTAAGGACCTTGTTATGCCAAAGCCCGCTCCTACCTGCAATA
TCAAGGCGACTGTGTGCAGCTTTGACGATGGAGTAGATTTGCCTCCCTGGTTTCCACCTATGGT
GGAAGGGGCTGCCGCGGAGGGTGATGACGGAGATGACGGAGATGAAGGAGGTGATGGAG
ATGAGGGTGAGGAAGGGCAGGAGTGA

2.4. Proximity Ligation Assay (PLA)

H1299 cells were plated and fixed as previously described. For experiments using B95-8, 12-mm-diameter coverslips were coated with poly-L-lysine 0.01% (Sigma) for 30 min and air-dried for 5 min in 24-well plates. B-cells were then resuspended in PBS, plated on pre-treated coverslips and incubated for 2 h at room temperature. After a wash with PBS for 5 min, cells were fixed with PBS 4% paraformaldehyde for 20 min and re-washed with PBS for 10 min. Following fixation, both cell lines were processed for in situ hybridization according to the rISH-IF protocol. Samples were then saturated with PBS 3% BSA for 30 min and incubated for 2 h at room temperature with a mix of primary antibody containing the mouse anti-digoxigenin and the rabbit anti-nucleolin previously described. Subsequently, PLA was carried out using the Duolink PLA in situ kit (Sigma), anti-rabbit plus and anti-mouse minus probes (Sigma) following the manufacturer's protocol.

2.5. Microscopy and Image Analysis

Samples were examined with an LSM 800 confocal laser microscope (Carl Zeiss MicroImaging, Jena, Germany). ImageJ [14] was used for analysis of images. PLA signals were quantified in 100 cells per sample according to the protocol provided as Supplementary materials. Data analysis was carried out by ANOVA with Tukey HSD test using GraphPad Prism 5 for Windows (GraphPad Software, San Diego, CA, USA). Data shown are mean ± SD of three independent experiments.

3. Results and Discussion

3.1. Detection of EBNA1 mRNA and NCL by rISH-IF and IF

EBNA1 is essential for EBV genome maintenance and, as such, is expressed in all EBV-carrying cells, including cancers. Because EBNA1 is highly antigenic, EBV has evolved a sophisticated strategy to evade the immune detection of latently infected cells by limiting *EBNA1* mRNA translation and, as a consequence, by minimizing the production of antigenic peptides for the major histocompatibility (MHC) class I pathway [13]. Nucleolin (NCL) directly binds G4 structures in the GAr (the glycine-alanine rich domain of EBNA1)-coding sequence of the *EBNA1* mRNA and this is essential for suppressing the translation of the *EBNA1* mRNA and the production of antigenic peptides (Figure 1A,B). A small G4 ligand, PhenDC3, can displace NCL from the *EBNA1* message and augment its translation, thereby increasing the production of antigenic peptides and triggering $CD8^+$ T cell response [11]. Interestingly, another study based on in vitro translation showed that pyridostatin (PDS), another G4-binding compound frequently used as benchmark, instead further suppressed *EBNA1* mRNA translation [15]. This observation is surprising, as it has previously not been appreciated that G4 ligands can have different effects on the function of the G4 or on their interaction with cellular factors. In this context, G4 structures might be targeted in a specific way by therapeutic intervention, opening a so far unknown field of drug target validation in cellulo. In order to shed light on the apparent discrepancy between how different G4 ligands act on the NCL-*EBNA1* mRNA interaction and thus their potential use as compounds that can trigger an immune reaction against EBV-carrying cancers, we developed a protocol based on proximity ligation (Figure 1C,D). This approach allows us to overcome difficulties with RNA folding in vitro to quantitatively study endogenous protein-mRNA interactions in cellulo and to avoid using large tags and overexpression system. By combining in-cellulo data with in vitro assays, this approach has the advantage of providing a straightforward and easy confirmation of the relevance of in vitro studies based on recombinant proteins and synthetic RNAs with in vivo data. In addition, we developed a method to quantify protein-mRNA interactions, which could allow structure-activity relationship (SAR) studies in cellulo to be carried out on a specific RNA-protein interaction.

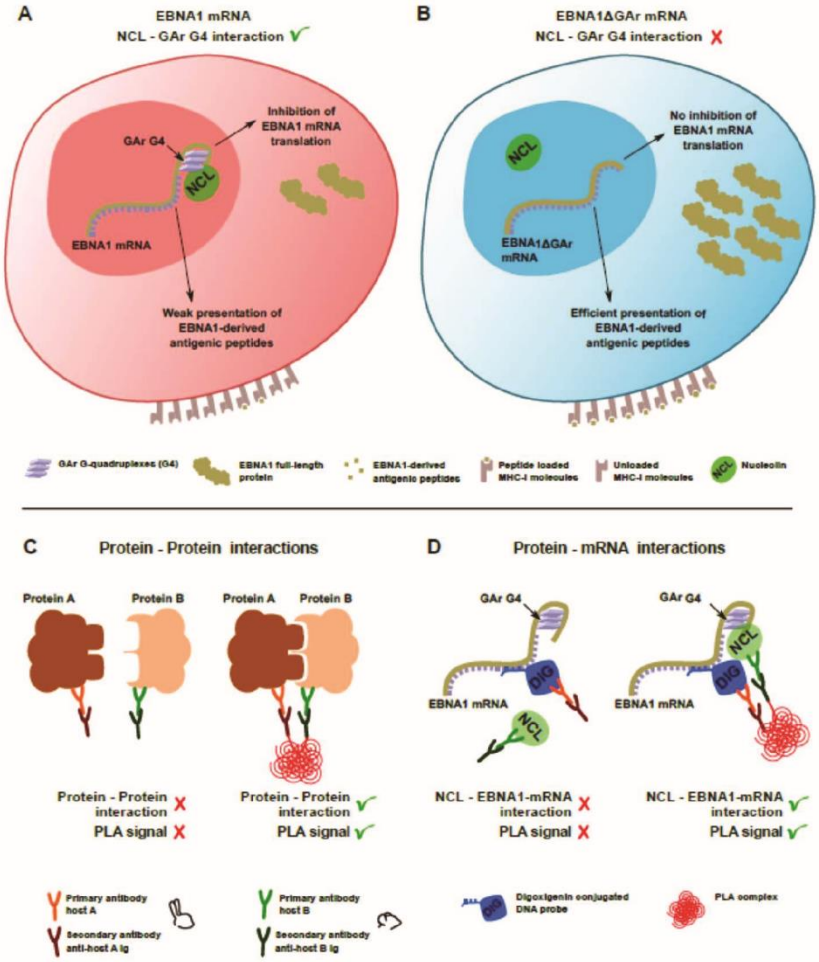

Figure 1. (**A**) cartoon depicting the interaction between nucleolin (NCL) and the G4 formed in the GAr-encoding sequence of *EBNA1* mRNA. This interaction is crucial for EBNA1/Epstein-Barr virus (EBV) immune evasion as it inhibits both *EBNA1* mRNA translation and the production of EBNA1-derived antigenic peptides, hence limiting the production of EBNA1 to the minimal level to fulfill its essential role in maintenance and replication of the viral genome and, at the same time, allowing EBNA1 to evade the immune system. (**B**) If the interaction between EBNA1 G4 and NCL is compromised or lost (e.g., when EBNA1ΔGAr, a form of EBNA1 deleted for its GAr domain, is expressed), then full length EBNA1ΔGAr protein as well as EBNA1-derived antigenic peptides are expressed at a higher level, leading to recognition of EBV-infected cells by the immune system of the host. (**C**) Schematic depicting the principle of the proximity ligation assay (PLA) between two proteins (or two epitopes of the same protein). (**D**) Schematic depicting the adaptation of the PLA to visualize protein/mRNA interactions in cellulo.

The proximity ligation assay (PLA) was originally conceived to detect proteins in close proximity. For this, one pair of primary antibodies raised in two different species is used to target the two proteins of interest (Figure 1C). Afterwards, DNA strand-conjugated secondary antibodies and enzymatic reactions are employed to generate fluorescent reporter molecules [16]. Since we aimed to explore a protein-mRNA interaction, a hybridization step was added in order to tag the mRNA of interest with a complex recognizable by antibodies (Figure 1D). A similar approach has been reported for DNA-protein interactions [17]. Therefore, as an initial step, EBV negative cells transfected, or not, with an EBNA1 construct were analyzed by RNA in situ hybridization coupled to immunofluorescence (rISH-IF). This enabled us to first validate the hybridization conditions using the digoxigenin-labelled EBNA1 probe and the mouse anti-digoxigenin primary antibody to be employed in the PLA (Figure 2A).

IF was also performed to determine the appropriate conditions for detecting endogenous NCL using a rabbit anti-NCL antibody (Figure 2B). Altogether, these assays demonstrated an accumulation of NCL and *EBNA1* mRNA in the nucleus.

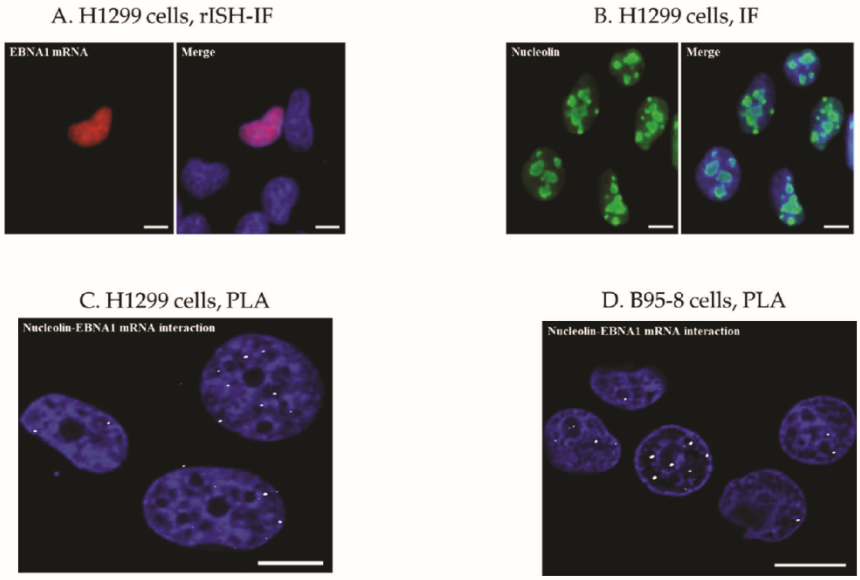

Figure 2. Use of PLA for the study of a protein-mRNA interaction. (A) H1299 cells were transfected with *EBNA1* and analyzed by RNA in situ hybridization-immunofluorescence (rISH-IF) to verify the specificity of the *EBNA1*-digoxigenin probe and to validate the detection of probe-mRNA complexes using a mouse anti-digoxigenin antibody. Immunocomplexes were detected using an anti-mouse Alexa Fluor® 568-conjugated secondary antibody, revealing the accumulation of *EBNA1* mRNA in the nucleus. *EBNA1* mRNA is depicted in red. (**B**) Immunofluorescence (IF) was performed in H1299 cells using a rabbit anti-nucleolin antibody to set up the appropriate conditions for detection of endogenous NCL. The expected labelling of NCL in the nucleolus was confirmed. (**C**) PLA in *EBNA1*-transfected H1299 cells using mouse anti-digoxigenin and rabbit anti-nucleolin tested in (A) and (B). Anti-rabbit and anti-mouse Ig PLA probes were used following the manufacturer's protocol to generate PLA complexes depicted as white dots. Each dot represents an interaction between NCL and *EBNA1* mRNA. (**D**) The EBV-transformed B-cell line B95-8 was tested for endogenous NCL-*EBNA1* mRNA interaction under the same conditions used in (**C**). PLA uncovered this interaction in the nuclear compartment as in *EBNA1*-transfected H1299 cells shown in (**C**). Scale bars represent 10 μm.

3.2. Analysis of NCL-EBNA1 mRNA Interactions by Proximity Ligation

PLA was then carried out to detect the NCL-*EBNA1* mRNA interactions in situ using either transfected cells or EBV-infected cells. PLA complexes are depicted as white dots and each dot represents an interaction between NCL and *EBNA1* mRNA. In line with rISH-IF and IF results, interactions were uncovered in or at the close vicinity of the nuclear compartment of EBNA1-transfected cells (Figure 2C) and EBV-transformed lymphoblastic B95-8 cells (Figure 2D), confirming that NCL binds EBNA1 mRNA in the nucleus of virus-carrying cells. During and after transcription, mRNAs undergo a complex maturation process relying on a large repertoire of RBP and indeed, protein-mRNA interactions control pivotal steps of mRNA biogenesis and function [18]. In addition, evidence is accumulating that these interactions play a broader role in cellular processes, regulating multiple enzymatic and metabolic activities [19]. Hence, these results denote that EBV exploits host cell mRNA maturation process/es in order to hamper translation and thus immune responses.

3.3. Use of Quantitative PLA to Evaluate the Effect of RNA-Binding Drugs on NCL-EBNA1 mRNA Interactions

An estimated 2–3% of cancers are associated with EBV, making GAr-based EBNA1 immune evasion an important target for therapeutic approaches against EBV-related cancers [20,21]. Therefore, the binding of NCL to G4 in *EBNA1* mRNA represents a promising target for novel therapeutic strategies aimed at stimulating immune recognition of EBV-carrying cancers. This, and the fact that different compounds bind the G4 of the *EBNA1* mRNA, makes this an interesting model system for the identification of compounds that interfere with a specific RNA-protein interaction. Since NCL binds specifically G4 within EBNA mRNA [11], we treated, or not, B95.8 cells with the G4 ligands PDS or PhenDC3 (Figure 3) and evaluated the effect of treatments on this interaction using PLA. Of note, PhenDC3, but not PDS, reduced the NCL-*EBNA1* mRNA interaction (Figure 4A). This is surprising as both compounds bind strongly the *EBNA1* mRNA G4 structure in vitro [11,22]. In addition, a previous report has shown that PDS suppresses EBNA1 synthesis in vitro [15], while PhenDC3 increases the levels of EBNA1 in cellulo [11]. Altogether, these contrasting results indicate that different G4 ligands may induce distinct biological responses and complementary assays are required to determine the activity of these compounds in the cellular context. To refine this finding, we developed a protocol to quantify PLA results using the public domain image processing program ImageJ (Figure 4B and Supplementary materials). As advantages, quantitative PLA generates information suitable for statistical tests, avoids subjective data interpretation, and enables the estimation of differences less evident by the comparison of single images. This approach revealed a remarkable difference between the ability of PDS and PhenDC3 in preventing the NCL-*EBNA1* mRNA interaction (Figure 4C). It has been reported that by binding to an RNA fold, small molecules can alter RNA structure, inhibiting or enhancing protein-RNA associations [23]. Therefore, one could speculate that PDS and PhenDC3 may modify G4 structure in a different way, thereby preventing, or not, the binding of NCL, which can help to explain the discrepancy between these two G4 ligands. Alternatively, the difference between these two compounds in their ability to prevent NCL binding to G4 of *EBNA1* mRNA may be due to differential affinities for these G4. In line with this hypothesis, we have previously observed that PDS binding affinity for EBNA1 G4 is significantly weaker when compared to PhenDC3 as evaluated by G4-FID assay: DC_{50} (PDS) $\approx$ 0.47 μM); DC_{50} (PhenDC3) $\approx$ 0.26 μM. This was further confirmed by the thermal stabilization values (ΔTm) measured by the FRET-melting assay on EBNA1 G4 (ΔTm PDS = 14.3 °C; ΔTm PhenDC3 = 20.5 °C [11]. Although the two assays are calibrated for selecting high affinity binders, the difference is nonetheless significant. Thus, it is tempting to deduce that the higher affinity of PhenDC3 for the EBNA1 G4 might give it an advantage when placed in a complex cellular milieu, thereby allowing this compound, and not PDS, to prevent NCL binding by a competitive mechanism (Figure 4D). In support of this we have previously shown that PhenDC3 is able to inhibit the pulldown of NCL by EBNA1 G4-coated beads, whereas PDS has no effect in the same conditions [11]. However, one can consider this last possibility quite unlikely, as the affinity of PDS for the *EBNA1* mRNA G4 structure is quite high per se, at least in vitro. Hence, PDS should also prevent NCL binding, although less efficiently than PhenDC3. Finally, another possibility is that PDS and PhenDC3 may have different binding sites on *EBNA1* mRNA G4. In particular, a ternary interaction could exist between PDS/NCL/*EBNA1* mRNA G4 as has been observed in the case of TERRA G4, the G4 ligand carboxypyridostatin (cPDS, a chemical derivative of PDS), and anti-G4 antibodies [24], whereas PhenDC3 and NCL may share the same, or overlapping, binding site(s). The number of binding sites may also strongly differ from one G4 ligand to another, especially with long G4-forming domains like the GAr-encoding sequence of *EBNA1* mRNA [25]. All these possibilities highlight the importance of methods enabling the study of RNA-protein interactions and the control of these interactions by candidate molecules in presence of the multiple biological entities within the cell.

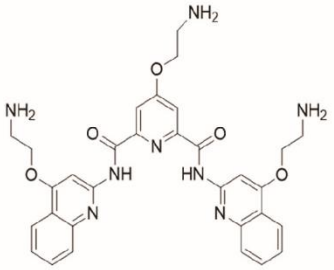

pyridostatin (PDS)

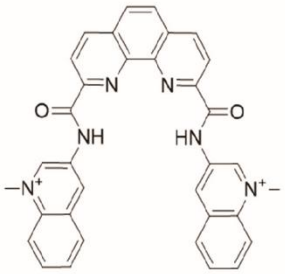

PhenDC3

Figure 3. Molecular structures of the G-quadruplex (G4) ligands pyridostatin (PDS) and PhenDC3.

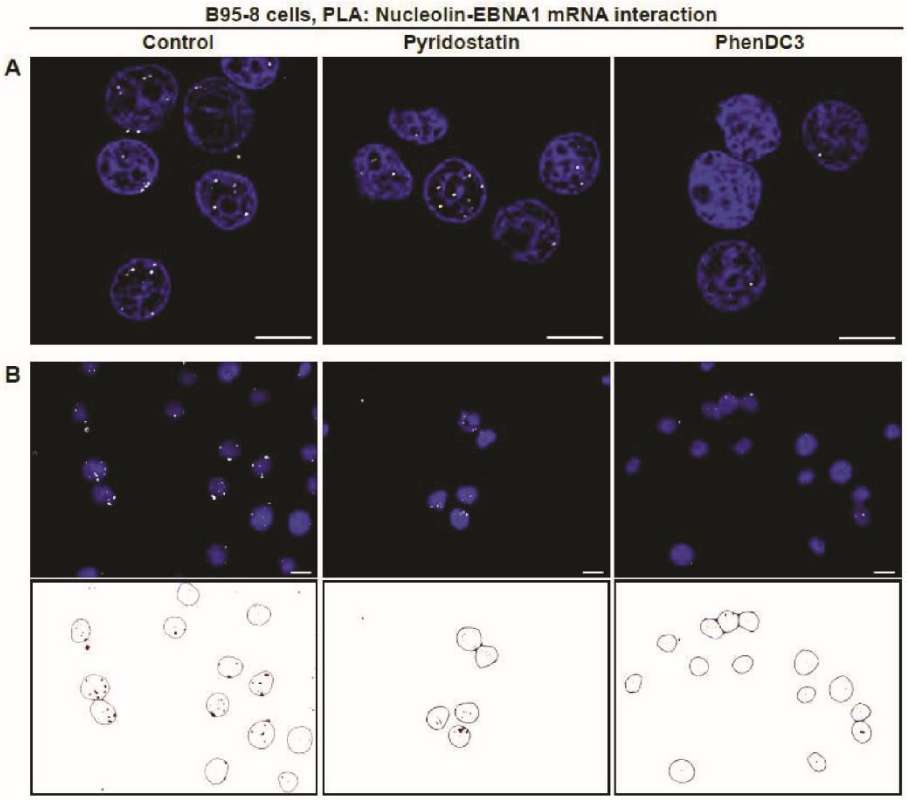

Figure 4. *Cont.*

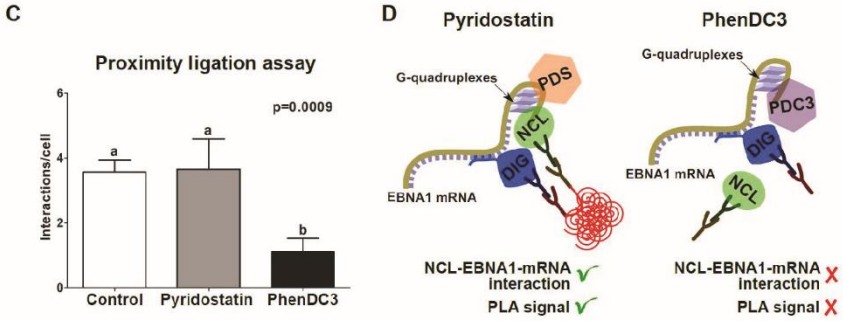

Figure 4. PLA as a tool for the characterization of RNA-binding drugs. (**A**) B95-8 cells treated with the G-quadruplex (G4) ligands pyridostatin (PDS) or PhenDC3 were tested for the NCL-*EBNA1* mRNA interaction using PLA. PhenDC3, but not PDS, was shown to prevent the interaction, denoting that PhenDC3 competes specifically with NCL for binding *EBNA1* mRNA G4. (**B**) Quantitative PLA was performed to quantify the effect of PDS and PhenDC3 on NCL-*EBNA1* mRNA interactions. One hundred cells from control (DMSO)-, PDS-, and PhenDC3-treated groups were imaged and the number of interactions per cell was estimated using a customized protocol in ImageJ. Upper and lower lanes depict images before and after analysis, respectively. Open circles represent the nucleus included in the analysis and red dots depict PLA complexes. Cells located in the border of images and dots found outside filtered nucleus were excluded from the analysis. (**C**) Histogram displaying the number of NCL-*EBNA1* mRNA interactions per cell from control (DMSO)-, PDS-, and PhenDC3-treated groups. Data shown are mean ± SD of three independent experiments performed as described in (**B**). (**D**) Schematic depicting the use of PLA to evaluate the effect of PDS and PhenDC3 on the NCL-*EBNA1* mRNA interactions in EBV-infected B95-8 cells. PhenDC3, but not PDS, competes with NCL for binding *EBNA1* mRNA G4. One possible explanation for this difference (differential binding sites for PhenDC3 and PDS, the latter forming a ternary complex EBNA1 mRNA/NCL/PDS, whereas PhenDC3 and NCL would share a common binding site) is shown. By preventing this interaction, PhenDC3 stimulates the translation of the *EBNA1* mRNA and the production of EBNA1-derived antigenic peptides for the MHC class I pathway. PDS and PDC3 mean pyridostatin and PhenDC3, respectively. Scale bars represent 10 μm.

4. Concluding Remarks

Protein-mRNA interactions influence multiple aspects of cellular function. However, in spite of progress experienced over the last decades, the study of these interactions has been restricted to assays technically demanding and unable to provide accurate information at subcellular levels. In this context, PLA represents an attractive alternative to overcome these limitations, opening new avenues for the study of protein-mRNA interactions in cellulo. We provided evidences that PLA can be coupled to quantitative analysis and be successfully employed to screen molecules interfering with target protein-mRNA interactions. Additionally, the approach described here can be adapted to other technologies, like flow cytometry, for medium to high throughput drug screening. This highlights the potential of mRNA-protein PLA as a tool for efforts focused not only on targeting specific G4 structures, but more generally for drug development based on disruption of specific protein-RNA structure complexes.

Supplementary Materials: The supplementary materials are available online.

Author Contributions: Conceptualization, R.P.M., M.B. and R.F.; Methodology, R.P.M., S.F. and C.D.; Software, R.P.M.; Validation, R.P.M., M.-P.T.-F., M.B. and R.F.; Formal Analysis, R.P.M., M.-P.T.-F., M.B. and R.F.; Resources, M.-P.T.-F. and R.F.; Writing-Original Draft Preparation, R.P.M., M.-P.T.-F., M.B. and R.F.; Writing-Review & Editing, R.P.M., M.-P.T.-F., M.B. and R.F.; Supervision, M.-P.T.-F., M.B. and R.F.; Funding Acquisition, R.F., M.B. and M.-P.T.-F.

Funding: This work was supported by the following grant agencies: La Ligue contre le cancer, La Ligue contre le cancer CSIRGO, Fondation ARC, Institut National du cancer (INCa), Cancerfonden (16059), Cancerforskningsfondedn Norr and Vetenskapsradet. This work was partially supported by the project MEYS-NPS

I-L01413. RF was partially supported by P206/12/G151. The International Centre for Cancer Vaccine Sciences is within the International Agendas program of the FNP co-financed by the European Union under the European Regional Development Fund.

Conflicts of Interest: The authors declare no commercial or financial conflict of interest.

References

1. Beckmann, B.M.; Castello, A.; Medenbach, J. The expanding universe of ribonucleoproteins: Of novel RNA-binding proteins and unconventional interactions. *Pflugers Arch.* **2016**, *468*, 1029–1040. [CrossRef] [PubMed]
2. Bao, H.L.; Ishizuka, T.; Sakamoto, T.; Fujimoto, K.; Uechi, T.; Kenmochi, N.; Xu, Y. Characterization of human telomere RNA G-quadruplex structures in vitro and in living cells using 19F NMR spectroscopy. *Nucleic Acids Res.* **2017**, *45*, 5501–5511. [CrossRef] [PubMed]
3. Bao, H.L.; Xu, Y. Investigation of higher-order RNA G-quadruplex structures in vitro and in living cells by (19)F NMR spectroscopy. *Nat. Protoc.* **2018**, *13*, 652–665. [CrossRef] [PubMed]
4. Haeusler, A.R.; Donnelly, C.J.; Periz, G.; Simko, E.A.; Shaw, P.G.; Kim, M.S.; Maragakis, N.J.; Troncoso, J.C.; Pandey, A.; Sattler, R.; et al. C9orf72 nucleotide repeat structures initiate molecular cascades of disease. *Nature* **2014**, *507*, 195–200. [CrossRef] [PubMed]
5. Taylor, J.P. Neurodegenerative diseases: G-quadruplex poses quadruple threat. *Nature* **2014**, *507*, 175–177. [CrossRef] [PubMed]
6. Wolfe, A.L.; Singh, K.; Zhong, Y.; Drewe, P.; Rajasekhar, V.K.; Sanghvi, V.R.; Mavrakis, K.J.; Jiang, M.; Roderick, J.E.; Van der Meulen, J.; et al. RNA G-quadruplexes cause eIF4a-dependent oncogene translation in cancer. *Nature* **2014**, *513*, 65–70. [CrossRef] [PubMed]
7. Largy, E.; Granzhan, A.; Hamon, F.; Verga, D.; Teulade-Fichou, M.P. Visualizing the quadruplex: From fluorescent ligands to light-up probes. *Top Curr. Chem.* **2013**, *330*, 111–177. [PubMed]
8. Mendoza, O.; Bourdoncle, A.; Boule, J.B.; Brosh, R.M., Jr.; Mergny, J.L. G-quadruplexes and helicases. *Nucleic Acids Res.* **2016**, *44*, 1989–2006. [CrossRef] [PubMed]
9. Song, J.; Perreault, J.P.; Topisirovic, I.; Richard, S. RNA G-quadruplexes and their potential regulatory roles in translation. *Translation (Austin)* **2016**, *4*. [CrossRef] [PubMed]
10. Lista, M.J.; Martins, R.P.; Angrand, G.; Quillevere, A.; Daskalogianni, C.; Voisset, C.; Teulade-Fichou, M.P.; Fahraeus, R.; Blondel, M. A yeast model for the mechanism of the Epstein-Barr virus immune evasion identifies a new therapeutic target to interfere with the virus stealthiness. *Microb. Cell.* **2017**, *4*, 305–307. [CrossRef] [PubMed]
11. Lista, M.J.; Martins, R.P.; Billant, O.; Contesse, M.A.; Findakly, S.; Pochard, P.; Daskalogianni, C.; Beauvineau, C.; Guetta, C.; Jamin, C.; et al. Nucleolin directly mediates Epstein-Barr virus immune evasion through binding to G-quadruplexes of EBNA1 mRNA. *Nat. Commun.* **2017**, *8*. [CrossRef] [PubMed]
12. De Cian, A.; Delemos, E.; Mergny, J.L.; Teulade-Fichou, M.P.; Monchaud, D. Highly efficient G-quadruplex recognition by bisquinolinium compounds. *J. Am. Chem. Soc.* **2007**, *129*, 1856–1857. [CrossRef] [PubMed]
13. Yin, Y.; Manoury, B.; Fahraeus, R. Self-inhibition of synthesis and antigen presentation by Epstein-Barr virus-encoded EBNA1. *Science* **2003**, *301*, 1371–1374. [CrossRef] [PubMed]
14. Schneider, C.A.; Rasband, W.S.; Eliceiri, K.W. NIH Image to ImageJ: 25 years of image analysis. *Nat. Methods* **2012**, *9*, 671–675. [CrossRef] [PubMed]
15. Murat, P.; Zhong, J.; Lekieffre, L.; Cowieson, N.P.; Clancy, J.L.; Preiss, T.; Balasubramanian, S.; Khanna, R.; Tellam, J. G-quadruplexes regulate Epstein-Barr virus-encoded Nuclear Antigen 1 mRNA translation. *Nat. Chem. Biol.* **2014**, *10*, 358–364. [CrossRef] [PubMed]
16. Soderberg, O.; Gullberg, M.; Jarvius, M.; Ridderstrale, K.; Leuchowius, K.J.; Jarvius, J.; Wester, K.; Hydbring, P.; Bahram, F.; Larsson, L.G.; et al. Direct observation of individual endogenous protein complexes in situ by proximity ligation. *Nat. Methods* **2006**, *3*, 995–1000. [CrossRef] [PubMed]
17. Gomez, D.; Shankman, L.S.; Nguyen, A.T.; Owens, G.K. Detection of histone modifications at specific gene loci in single cells in histological sections. *Nat. Methods* **2013**, *10*, 171–177. [CrossRef] [PubMed]
18. de Klerk, E.; t Hoen, P.A. Alternative mRNA transcription, processing, and translation: Insights from RNA sequencing. *Trends Genet.* **2015**, *31*, 128–139. [CrossRef] [PubMed]

19. Mitchell, S.F.; Parker, R. Principles and properties of eukaryotic mRNPs. *Mol. Cell.* **2014**, *54*, 547–558. [CrossRef] [PubMed]
20. Daskalogianni, C.; Pyndiah, S.; Apcher, S.; Mazars, A.; Manoury, B.; Ammari, N.; Nylander, K.; Voisset, C.; Blondel, M.; Fahraeus, R. Epstein-Barr virus-encoded EBNA1 and ZEBRA: Targets for therapeutic strategies against EBV-carrying cancers. *J. Pathol.* **2015**, *235*, 334–341. [CrossRef] [PubMed]
21. Wilson, J.B.; Manet, E.; Gruffat, H.; Busson, P.; Blondel, M.; Fahraeus, R. EBNA1: Oncogenic activity, immune evasion and biochemical functions provide targets for novel therapeutic strategies against Epstein-Barr virus-associated cancers. *Cancers (Basel)* **2018**, *10*, 109. [CrossRef] [PubMed]
22. Biffi, G.; Di Antonio, M.; Tannahill, D.; Balasubramanian, S. Visualization and selective chemical targeting of RNA G-quadruplex structures in the cytoplasm of human cells. *Nat Chem* **2014**, *6*, 75–80. [CrossRef] [PubMed]
23. Hermann, T. Strategies for the design of drugs targeting RNA and RNA-protein complexes. *Angew. Chem. Int. Ed. Engl.* **2000**, *39*, 1890–1904. [CrossRef]
24. Yangyuoru, P.M.; Di Antonio, M.; Ghimire, C.; Biffi, G.; Balasubramanian, S.; Mao, H. Dual binding of an antibody and a small molecule increases the stability of terra G-quadruplex. *Angew. Chem. Int. Ed. Engl.* **2015**, *54*, 910–913. [CrossRef] [PubMed]
25. Gabelica, V.; Maeda, R.; Fujimoto, T.; Yaku, H.; Murashima, T.; Sugimoto, N.; Miyoshi, D. Multiple and cooperative binding of fluorescence light-up probe thioflavin T with human telomere DNA G-quadruplex. *Biochemistry* **2013**, *52*, 5620–5628. [CrossRef] [PubMed]

Sample Availability: Samples of the compound PhenDC3 are available from the authors. PDS is commercially available (Sigma-Aldrich, now Merck).

3086–3100 *Nucleic Acids Research, 2019, Vol. 47, No. 6* *Published online 9 January 2019*
doi: 10.1093/nar/gky1296

Nuclear processing of nascent transcripts determines synthesis of full-length proteins and antigenic peptides

Rodrigo Prado Martins[1], Laurence Malbert-Colas[1], María José Lista[2], Chrysoula Daskalogianni[1,3], Sebastien Apcher[4], Marika Pla[5], Sarah Findakly[1], Marc Blondel[2] and Robin Fåhraeus[1,3,6,7,*]

[1]Université Paris 7, Inserm, UMR 1162, Paris, France, [2]Université de Brest, Inserm, EFS, UMR 1078, GGB, F-29200 Brest, France, [3]ICCVS, University of Gdańsk, Science, ul. Wita Stwosza 63, 80-308 Gdańsk, Poland, [4]Institut Gustave Roussy, Université Paris Sud, UMR 1015, Villejuif, France, [5]Université Paris 7, IUH, Inserm, UMR-S-1131, Paris, France, [6]Department of Medical Biosciences, Umeå University, Umeå, Sweden and [7]RECAMO, Masaryk Memorial Cancer Institute, Zluty kopec 7, 656 53 Brno, Czech Republic

Received July 11, 2018; Revised November 23, 2018; Editorial Decision December 14, 2018; Accepted December 18, 2018

ABSTRACT

Peptides presented on major histocompatibility (MHC) class I molecules form an essential part of the immune system's capacity to detect virus-infected or transformed cells. Earlier works have shown that pioneer translation peptides (PTPs) for the MHC class I pathway are as efficiently produced from introns as from exons, or from mRNAs targeted for the nonsense-mediated decay pathway. The production of PTPs is a target for viral immune evasion but the underlying molecular mechanisms that govern this non-canonical translation are unknown. Here, we have used different approaches to show how events taking place on the nascent transcript control the synthesis of PTPs and full-length proteins. By controlling the subcellular interaction between the G-quadruplex structure (G4) of a gly-ala encoding mRNA and nucleolin (NCL) and by interfering with mRNA maturation using multiple approaches, we demonstrate that antigenic peptides derive from a nuclear non-canonical translation event that is independently regulated from the synthesis of full-length proteins. Moreover, we show that G4 are exploited to control mRNA localization and translation by distinguishable mechanisms that are targets for viral immune evasion.

INTRODUCTION

Viral interference with the host cell provides windows of opportunities to disclose cell biological processes. Viral evasion of the immune system is no exception and the different steps of antigen presentation on major histocompatibility (MHC) class I molecules have largely been characterized using viral factors (1). Previous works by our and other teams have focused on how the Epstein-Barr virus (EBV)-encoded EBNA1 employs a *cis*-acting mechanism to suppress translation of its own mRNA in order to minimize the production of antigenic peptide substrates and thereby avoid host immune response (2,3).

Full-length proteins are poor substrates for the MHC class I pathway, at least in experimental conditions, and alternative sources of antigenic peptide substrates have been suggested (4–6). Previous works have shown little difference in antigen presentation if the antigenic peptide is derived from introns or exons, from 3′ UTRs or from mRNAs targeted for nonsense-mediated decay (NMD) (7–9). Transfected capped ovalbumin (OVA) mRNAs produce full-length proteins as long as the mRNA is present for at least eight hours, whereas antigenic peptide substrates from the same mRNAs are synthesized up to 2 h post-transfection (7). Furthermore, intron-derived nascent peptides can be detected in the nuclear compartment (8). These different observations implicate a non-canonical nuclear mRNA translation event producing pioneer translation products (PTPs) for the MHC class I pathway.

Canonical mRNA translation is initiated at the m^7Cap-structure by the binding of the eIF4E, which normally leads to translation initiation at the first downstream AUG codon (10). Alternatively, the ribosome can bypass the m^7Cap and initiate directly on the message via internal ribosome entry sites (IRES) that are normally located in the 5′ UTRs (11,12). The requirement for initiating at AUG is not absolute and it has been proposed that a large amount of small

*To whom correspondence should be addressed. Tel: +33 172639366; Email: robin.fahraeus@inserm.fr

peptide products detected by mass spectrometry are initiated from non-AUG codons (13).

The newly synthesized pre-mRNAs engage with the splicing machinery and with RNA quality control mechanisms. Following splicing, mRNAs bind nuclear export factors such as the export factor 1 (NFX1) for transport through the nuclear pore complex (14). However, some cellular and viral RNAs, like those exported by the HIV-1 Rev machinery, instead use the chromosome region maintenance 1 protein homologue (CRM1) for cytoplasmic transport (15). So far, little is known of how alternative mRNA processing pathways affect nuclear export and translation.

Nucleolin (NCL) is a multifunctional protein that interacts with RNAs, DNAs and proteins. It plays a major role in ribosomal biogenesis but is also implicated in various processes such as replication, transcription, cell cycle control and apoptosis (16). As an RNA binding protein (RBP), NCL displays a preference for endogenous and exogenous G-rich sequences, including G-quadruplexes (G4), found in transcripts untranslated and coding regions (17,18). This protein is reported to stabilize G4 structures in viruses such as HIV (19) and in mRNAs encoding cancer proteins (20). A *cis*-mediated translation control of EBNA1 involves NCL binding to the G4 structure formed by the gly-ala repeat (GAr)-encoding sequence in EBNA1 transcript. Consequently, NCL binding is necessary for the GAr-mediated inhibition of antigen presentation (21,22). G4 RNA structures are also implicated in controlling gene regulation by affecting splicing, polyadenylation, mRNA translation and stability (20,23–25).

In this study, we took advantage of the unique properties of the NCL-GAr mRNA interactions to control translation and used different tools as intronless and intron-bearing constructs, IRES structures and alternative RNA export to show that events taking place on nascent transcripts determine the synthesis of neoantigens and full-length proteins. These results further demonstrate the existence of different mRNA translation events for the production of peptide products with alternative functions and will help to design future vaccine strategies against virus-infected or transformed cells.

MATERIALS AND METHODS

Plasmid constructions

The sets of splicing reporters described in Figure 1 were constructed as described in Supplementary Figure S1. Briefly, full-length Globin intron-bearing and OVA exon 5–7 fragment were amplified by PCR from the Glob-exon-SL8 construct (8) and chicken genomic DNA, respectively. The amplicons were cloned into pcDNA3 to create the control constructs or replaced the OVA ORF of the pcDNA3-GAr-OVA construct (26) to generate plasmids with the GAr domain upstream and in the same frame of the inserts. Afterwards, RNA from H1299 cells transfected with the resulting intron-bearing constructs was used to produce cDNA employing M-MLV reverse transcriptase and oligo-dT (Invitrogen). The resulting cDNAs were employed in a second round of cloning using the same primers and pcDNA3 or pcDNA3-GAr-OVA construct as vectors to produce the corresponding intronless constructs. Globin intronless-RRE, GAr-Globin-intron-bearing-RRE and GAr-Globin intronless-RRE constructs were cloned following the same method using the plasmid Glob-exon-SL8-RRE (8), herein Globin intron-bearing-RRE, as template. C-myc-IRES-OVA construct was described elsewhere (2) and for generating HCV-IRES-OVA construct, IRES was PCR amplified from HCV genomic DNA and cloned into the 5′ UTR of pcDNA3-OVA (2). The HA-NCLΔNLS plasmid was created by replacing the NLS sequence KKRA of a pcDNA3-HA-NCL construct (21) with AARA by site-directed mutagenesis. The Rev expression vector was a gift from Ali Saïb, Saint-Louis Hospital, Paris. All constructs were amplified in DH5α *Escherichia coli* and sequenced by Sanger method. The list of plasmids, primers and restriction enzymes used in this study is provided in Supplementary Table S1.

Cell culture, transfection and drug treatments

The human lung carcinoma cell line H1299 was cultured in RPMI-1640 supplemented with 10% fetal bovine serum (FBS), 2 mM L-glutamine, 100 U/ml penicillin and 100 μg/ml streptomycin. Transient transfections were performed using Genejuice reagent (Merck Bioscience) according to manufacturer's protocol. All cells were cultured at 37°C with 5% CO_2. For cell treatments with isoginkgetin (Sigma) and PhenDC3 (27), cells were incubated with 30 and 5 μM of drug for 24 and 40 h after transfection, respectively. Drug stock solutions were prepared in DMSO (Euromedex).

RNA extraction, RT-PCR and qRT-PCR

H1299 cells were plated in six-well plates and transfected with the indicated constructs. At 48 h post transfection, cells were washed with cold PBS and RNA was purified using the RNeasy Mini Kit and on-column DNase treatment (Qiagen) following the manufacturer's protocol. Nuclear/cytoplasmic RNA extractions were carried out as described elsewhere (8) employing transfected H1299 cells. RT was carried out using M-MLV reverse transcriptase and random hexamers or oligo(dT) primers (Invitrogen). RT-PCR was performed using Phusion high-fidelity PCR master mix (Thermo Scientific) and a set of primers described in Figure 1A and Supplementary Table S2. qRT-PCR was performed as previously described (8) using specific primer pairs for each gene fragment of interest (see Supplementary Table S2).

Western blot analysis

Whole cell lysates were prepared 48 h post-transfection and protein concentration was measured using a Bradford assay. Samples were electrophoretically separated in NuPAGE® Bis-Tris gels 10% (Invitrogen), transferred onto 0.45 μm nitrocellulose membranes (GE) and blotted under standard conditions using the following antibodies: mouse monoclonal anti-HBB antibody (2H3, Sigma), rabbit polyclonal anti-OVA antibody (C6534 Sigma), mouse monoclonal anti-actin (AC-15 Sigma), mouse polyclonal anti-HA antibody (a kind gift from Borek Vojtesek, Masaryk Memorial Cancer Institute, Brno, Czech Republic) and chicken

polyclonal anti-HIV-1 Rev (ab36623, Abcam). Anti-mouse (Dako), anti-rabbit (Dako) or anti-chicken (Sigma) secondary antibodies conjugated to horseradish peroxidase were used to generate immunocomplexes revealed with enhanced chemiluminescence (Thermo Scientific). Membranes were scanned in a MyECL imager (Thermo Scientific) and signal intensity was determined using My Image software (Thermo Scientific).

Immunofluorescence and RNA-FISH

H1299 cells were plated on 12-mm-diameter coverslips in 24-well plates, and transfected with the indicated constructs or pCDNA3. At 24 h post-transfections cells were fixed with 4% paraformaldehyde for 20 min, permeabilized with PBS 0.4% Triton X-100, 0.05% CHAPS for 10 min at room temperature and saturated with PBS 3% BSA for 30 min. Samples were incubated overnight at 4°C with rabbit polyclonal antibody anti-NCL (ab22758, Abcam) or mouse monoclonal anti-HA-Tag conjugated to Alexa Fluor® 488 (6E2, Cell Signaling). A goat anti-rabbit Ig antibody conjugated to Alexa Fluor® 647 (Sigma) was used as secondary antibody when necessary. RNA-FISH assays were performed employing Globin and OVA probes obtained from Biosearch Technologies according to the manufacturer's protocol. For nucleolar co-staining, samples were incubated with anti-nucleolin conjugated to Alexa Fluor® 488 (ab154028, Abcam) after probes hybridization. For immunofluorescence coupled to RNA-FISH, samples were incubated with chicken polyclonal anti-HIV-1 Rev antibody (ab36623, Abcam) after hybridization and immunocomplexes were detected under standard conditions using goat anti-chicken IgY conjugated to Alexa Fluor® 568 (Abcam). Samples were examined in an LSM 800 confocal laser microscope (Carl Zeiss MicroImaging GmbH, Jena, Germany).

Proximity ligation assay (PLA) for mRNA - protein interactions

H1299 cells were grown, fixed and permeabilized as described for immunofluorescence. Samples were overnight hybridized with 50 ng of a Globin DNA probe (5′-GGCCTCACCACCAACTTCATCCACGTTCACC TTGCAAAAA-3′) conjugated to digoxigenin in the 3′ end. Afterwards, samples were saturated with PBS 3% BSA, 0.1% saponine and incubated for 2 h with mouse monoclonal anti-digoxigenin (DI-22, Sigma) and rabbit polyclonal anti-NCL (ab22758, Abcam) primary antibodies diluted in blocking solution. The proximity ligation assay (PLA) was carried out using the Duolink PLA *in situ* kit (Sigma) following the manufacturer's protocol. For co-staining of HIV-1 Rev protein in PLA samples, chicken polyclonal anti-HIV-1 Rev antibody (ab36623, Abcam) and goat anti-chicken IgY conjugated to Alexa Fluor® 568 (Abcam) were added to primary antibodies and Duolink secondary antibodies mixes, respectively. For co-staining of NCLΔNLS or nucleolus, samples were incubated for 45 min with mouse monoclonal anti-HA-Tag antibody conjugated to Alexa Fluor® 488 (6E2, Cell Signaling) or anti-Fibrillarin antibody conjugated to Alexa Fluor® 488 (EPR10823B, Abcam) after the PLA amplification step.

In vivo and *in vitro* protein–RNA co-immunoprecipitation

In vivo protein–RNA co-immunoprecipitation was carried out as described elsewhere (28) using a rabbit polyclonal anti-NCL (ab22758, Abcam). For *in vitro* assays, 1 μg of total RNA from transfected cells were co-incubated under agitation with 100 ng of recombinant NCL (MyBioSource) in binding buffer (50 mM Tris pH 7.5, 150 mM NaCl, 0.02 mg/ml yeast tRNA, 0.2 mg/ml BSA) at 4°C. After incubation, NCL–RNA complexes were pulled down using protein B-coated sepharose beads according to standard conditions and purified using the TRIzol (Life Technologies). Precipitated RNAs were analyzed by RT-qPCR using the primers pairs described in the Supplementary Table S2.

Antigen presentation assays

Naive $OVA_{257–264}$ specific $CD8^+$ T cells were isolated by negative selection from peripheral and mesenteric lymph-nodes of 12 weeks old female OT-I mice using the $CD8^+$ T cell isolation kit (Miltenyi Biotec, Germany). Afterwards, $CD8^+$ T cells were stained with CellTrace™ Violet (Thermo Fisher Scientific, USA) according to the manufacturer's protocol and mixed with H1299 cells co-transfected with mouse Kb expression vector and the indicated constructs. For all the assays, 10^5 H1299 cells were harvested 48 h after transfection or after treatment and co-incubated with 4×10^5 stained $CD8^+$ T cells at 37°C in humidified air/CO_2 atmosphere in RPMI medium containing 10% FBS, 4 mM L-glutamine, 100 U/ml penicillin, 100 μg/ml streptomycin, 5 mM HEPES and 0.05 mM 2-mercaptoethanol (Sigma-Aldrich). After 3 days, cells were harvested, stained with hamster anti-mouse CD3-APC (Miltenyi Biotec) and fixable viability dye eFluor® 780 (eBioscience, USA) and analyzed on a CANTO II flow cytometer (BD Biosciences, USA). Cells were gated for live $CD3^+$ cells (10 000 events collected) and data were analyzed using FlowJo software version 8 (Tree Star). The percentage of proliferating T cells was considered for statistical analysis (29). For IL-2 release analysis, supernatants were collected after 3 days of co-incubation and IL-2 levels were measured employing the IL-2 ELISA MAX™ Standard kit (Biolegend, USA) according to manufacturer's instructions.

Polysome profiling

Five–fifty percent (w/v) linear sucrose gradients were freshly casted on SW41 ultracentrifuge tubes (Beckmann) using the Gradient master (BioComp instruments) following the manufacturer's instructions. Forty-eight hours post transfection, H1299 cells (with 80% confluency) were treated with cycloheximide 100 μg/ml for 5 min at 37°C and washed twice with 1× PBS (Dulbecco modified PBS, GIBCO) containing cycloheximide 100 μg/ml. Cells were then scraped and lysed with polysome lysis buffer (100 mM KCl, 50 mM HEPES–KOH, 5 mM $MgCl_2$, 0.1% NP-40, 1 mM DTT, cycloheximide 100 μg/ml, pH 7.4). Lysates were loaded on a sucrose gradient and centrifuged at 222 228 × g for 2 h at 4°C in a SW41 rotor. Samples were fractionated using Foxy R1 fraction collector (Teledyne ISCO) at 0.5 min intervals (30). RNA purifications from fractions were performed using ethanol precipitation

combined with RNeasy Mini Kit (Qiagen). RT and qRT-PCR were performed as described above using primers described in Supplementary Table S2. The relative distribution of target mRNA was calculated using fraction 1 as reference according to Panda *et al.* (31).

Statistical analysis

Data were analyzed by ANOVA in conjunction with Tukey's test or two-tailed unpaired Student's t-test using GraphPad Prism 5 for Windows (GraphPad Software). Data shown are mean ± s.d. of minimum three independent experiments. $*P < 0.05$; $**P < 0.01$; $***P < 0.001$; ns, not significant.

RESULTS

A gly-ala repeat (GAr) of EBNA1 suppresses mRNA translation and antigen presentation in the context of intronless, but not intron-bearing, sequences

Accumulating evidence show that antigenic peptides for the MHC class I pathway are derived from alternative mRNA translation products (2,7,8). To better understand the processes producing antigenic peptide substrates, we took advantage of the unique properties of a gly-ala (GAr)-encoding sequence that, when fused to the 5′ coding sequence of any mRNA, suppresses translation *in cis* and impedes the production of antigenic peptide substrates for the MHC class I pathway (26,32). We set up different strategies to modify the way GAr-carrying mRNAs are processed, trafficked and interact with specific proteins and how this affects the synthesis of full-length proteins and antigenic peptide substrates. We first created two sets of constructs in which mRNAs encoding β-Globin (Globin) or chicken ovalbumin (OVA) are expressed *via* splicing of intron-bearing sequences (Globin intron-bearing and OVA intron-bearing) or from intronless sequences (Globin intronless and OVA intronless). The same constructs were further used to include the GAr-encoding sequence in their 5′ coding sequences (GAr-Globin intron-bearing, GAr-OVA intron-bearing, GAr-Globin intronless and GAr-OVA intronless). Subsequently, the SL8 epitope from chicken OVA was inserted into the first exon of Globin constructs (Figure 1A and Supplementary Figure S1).

Using the indicated forward (F) and reverse (R) primers and RT-PCR we could confirm that the presence of the SL8 epitope, or the GAr, did not affect pre-mRNA splicing and that the mRNAs derived from spliced or intronless sequences are the same (Figure 1B). In line with previous reports (33), intron-bearing sequences gave rise to higher mRNA levels, as compared to the corresponding intronless messages, independently of the presence of the GAr (Figure 1C). Interestingly, the presence of introns overcame the translation inhibitory effect of the GAr in both the OVA and the Globin context (Figure 1D). Estimated protein:RNA ratios indicated that intron-bearing mRNAs are less efficiently translated than intronless transcripts, except for the GAr-carrying constructs (Figure 1E). Of note, polysome fractionation of cells expressing globin intron-bearing or intronless constructs also showed that mRNAs from intronless sequences are more prevalent in heavy polysomes than their counterparts from intron-bearing sequences, indicating that the former are more efficiently translated. Furthermore, the analysis of polysome fractions also revealed a higher accumulation of GAr-intronless mRNA in light ribosomes, as compared to GAr-carrying mRNAs from intron-bearing sequences. This observation further confirms that the GAr-mediated inhibition of mRNA translation is disrupted in the context of intron-bearing sequences (Supplementary Figure S2A and B).

We next tested if the effect of introns on preventing GAr-mediated suppression of protein synthesis also affected its capacity to inhibit the production of antigenic peptide substrates. OT-1 cells are TCR transgenic $CD8^+$ T lymphocytes from the OT-1 mice, which specifically target OVA SL8 epitopes presented on murine MHC class I molecules (Kb). Cell-trace Violet-labelled OT-1 cells were incubated with H1299 cells expressing the Kb and the indicated SL8-encoding constructs. Production of antigenic peptide substrates was estimated by determining OT-1 cell proliferation using FACS analysis (Figure 1F) (29). In both the context of OVA and Globin, we observed that the GAr suppressed the production of antigenic peptide substrates only in the context of intronless, and not intron-bearing, mRNAs.

Splicing alters GAr mRNA trafficking and prevents the NCL – GAr mRNA interaction

We next set out to investigate the mechanisms whereby splicing affects GAr-mediated translation control and the interaction with NCL by evaluating mRNA localization. RNA-FISH was carried out using probes against OVA or Globin mRNAs revealing that RNAs encoded from intron-bearing or intronless RNAs without the GAr were predominantly detected in the cytoplasmic compartment, with a smaller fraction in the nucleus (Figure 2A, upper panels). Similarly, the corresponding intron-bearing GAr-carrying mRNAs were predominantly detected in the cytoplasm. On the contrary, GAr intronless messages were mainly observed in the nucleoplasm (Figure 2A, lower panels and Supplementary Figure S3). Quantification of Globin or OVA mRNAs in the cytoplasmic and nuclear fractions by RT-qPCR confirmed that the GAr-carrying intronless mRNAs are predominantly located in the nuclear compartment (Figure 2B, left and right graphs).

The GAr-encoding RNA sequence forms G4 that act as a platform for NCL binding (21). Using the proximity ligation assay (PLA) adapted to protein-mRNA interactions (34), we uncovered that NCL binds GAr-Globin intronless mRNAs in the nucleoplasm and no interactions were detected in the cytoplasm. This interaction was not observed using the GAr-Globin intron-bearing RNA, or RNAs without the GAr sequence (Figure 2C, Supplementary Figures S4 and S5). NCL binding to intronless GAr mRNAs was further confirmed by an *in vivo* RNA-CoIP assay, where NCL was immunoprecipitated (IPed) and the presence of Globin RNAs was determined using RT-qPCR (Figure 2D). Next, we tested if the GAr G4 structure was still present in the intron-bearing transcript. RNA from cells transfected with indicated constructs was subjected to an *in vitro* RNA-CoIP assay using recombinant NCL and similar interaction levels were observed between NCL and

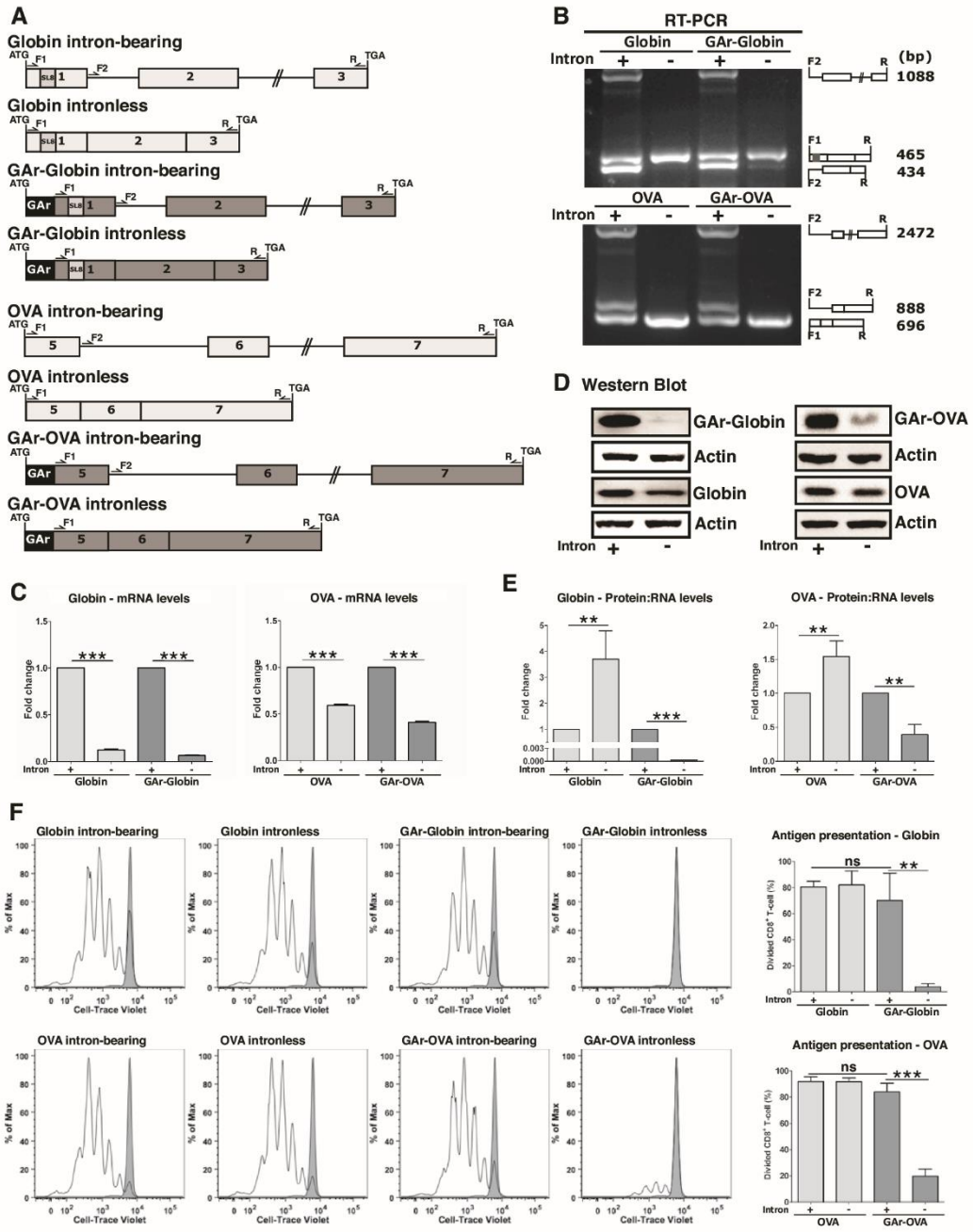

Figure 1. mRNA splicing prevents GAr-mediated suppression of canonical translation and antigen presentation. (**A**) Cartoon illustrating Globin and Ovalbumin (OVA) constructs. Intron-bearing and intronless constructs were generated with, or without, the coding sequence of the gly-ala repeat (GAr) in their 5′ end. OVA-derived SIINFEKL antigenic peptide (SL8) was inserted into the exon 1 of Globin constructs. (**B**) RT-PCR from Globin (upper panel) and OVA (lower panel) mRNAs. cDNA from indicated constructs was analyzed by multiplex PCR using F1, F2 and R primers (represented in A), revealing that the GAr does not affect splicing. Cartoons (right) represent primers and the corresponding RT-PCR products. (**C**) Graphs show the relative mRNA levels by qPCR from cells transfected with indicated constructs. (**D**) Western blots show that the GAr-mediated translation suppression is disrupted in intron-bearing mRNAs. Intron-bearing and intronless constructs without the GAr show similar protein levels. One of three independent experiments using Globin (left) and OVA (right) constructs is shown. (**E**) Data from (C) and (D) were used to calculate the relative protein:mRNA ratios. mRNAs from intronless constructs without the GAr are more efficiently translated than corresponding intron-bearing constructs except for GAr-carrying constructs. Graphs show the mean of intronless:intron-bearing ratios from three independent experiments. (**F**) H1299 cells transiently expressing murine MHC-I (Kb) and the indicated constructs were co-incubated with OT-1 $CD8^+$ T-cells labelled with Cell-trace Violet. The levels of OT-1 cells proliferation were analyzed by FACS. Open peaks in the histogram represent successive generations of T-cells indicating T cell activation. Grey peaks denote unstimulated controls. Cells expressing GAr-intronless constructs failed to stimulate OT-1 cells. Graphs (right) depict the mean percentage of dividing $CD8^+$ T-cell from three independent experiments. $^{**}P < 0.01$, $^{***}P < 0.001$, ns: not significant.

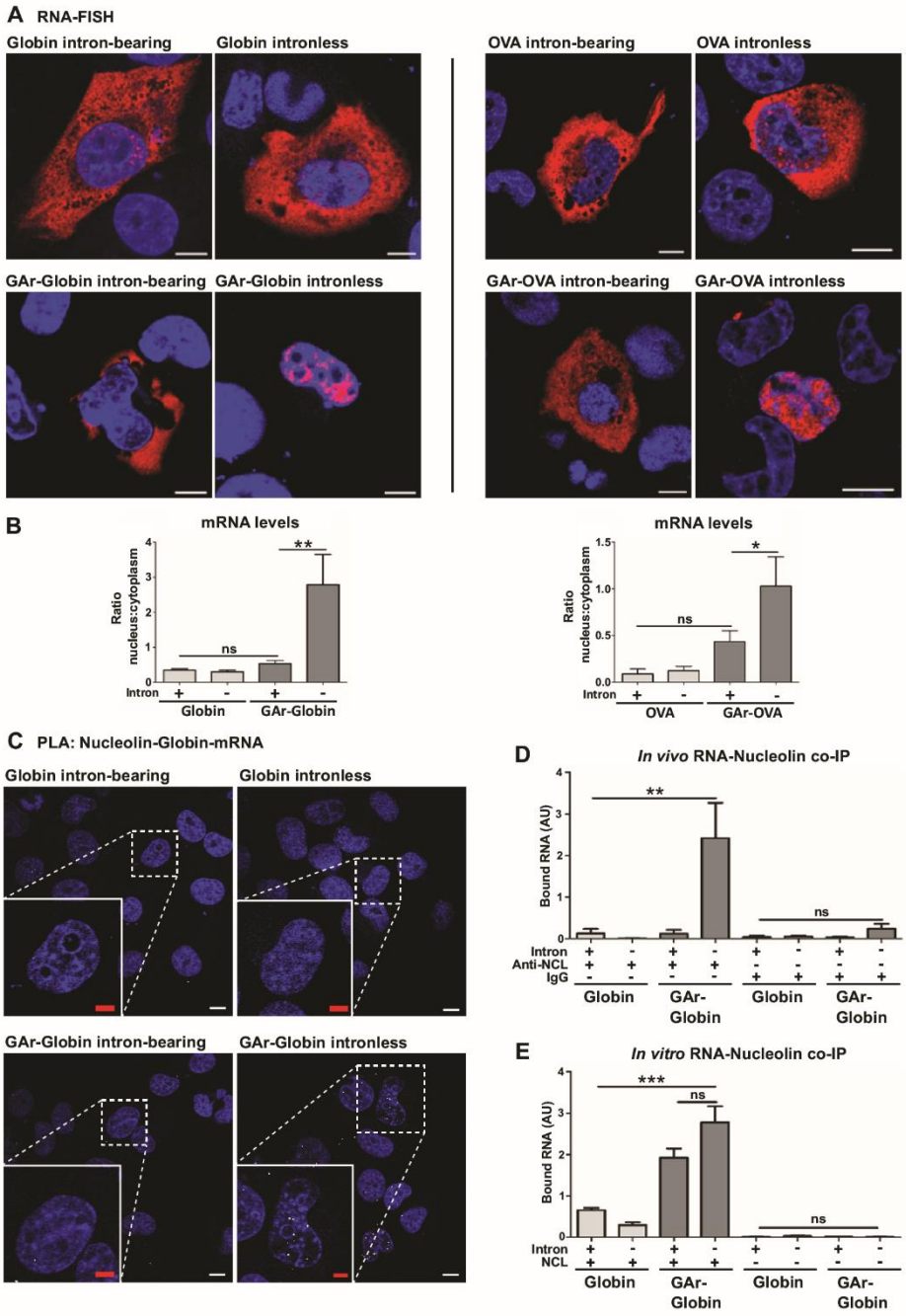

Figure 2. Splicing modifies mRNA localization and prevents nucleolin (NCL) - GAr mRNA interaction. (**A**) Cells expressing the indicated constructs were analyzed by RNA-FISH using probes against Globin or OVA mRNA. Fusion of the GAr to intronless Globin or OVA shifts the localization of mRNA from predominantly cytoplasmic to predominantly nuclear. The GAr does not affect export of corresponding intron-bearing constructs. Red and blue represent mRNAs and DAPI, respectively (see also Supplementary Figure S3). Scale bar = 10 μm. (**B**) Graphs show the relative ratio of nuclear to cytoplasmic mRNA levels from cells as in (A) using RT-qPCR. Histograms represent the mean of three independent experiments. $*P < 0.05$, $**P < 0.01$, ns: not significant. (**C**) Proximity Ligation Assay (PLA) showing the interaction between NCL and GAr-carrying mRNAs. PLA complexes are depicted as white dots and blue represents DAPI (for PLA controls see Supplementary Figure S4). NCL interacts with the G4 structure of the GAr-Globin intronless mRNA (lower right) predominantly in the nucleus. No interactions are observed in cells transfected with the GAr-Globin intron-bearing or constructs without the GAr. White and red scale bars denote 20 and 10 μm, respectively. (**D**) Cells expressing the indicated constructs were subjected to *in vivo* RNA co-immunoprecipitation (RNA-coIP) using an antibody against NCL. Bound RNA was analyzed by RT-qPCR, confirming that NCL interacts only with GAr intronless RNA. Graphs represent the mean of three independent experiments. $**P < 0.01$, ns: not significant. (**E**) Total RNA from transfected cells was incubated with recombinant NCL *in vitro* and analyzed as in (D). NCL interacts *in vitro* with GAr-intronless and GAr-intron-bearing RNAs. Graphs represent the mean of three independent experiments. $***P < 0.001$, ns: not significant.

intronless or intron-bearing GAr-Globin mRNAs *in vitro* (Figure 2E). Hence, the intron-bearing constructs retain their G4 structure and the capacity to bind NCL, showing that targeting GAr-carrying mRNAs for splicing makes the RNA non-accessible for NCL.

Splicing inhibition restores NCL – GAr mRNA interaction and stimulates antigenic peptide production

Next, we employed the NCL–GAr mRNA interaction to differentiate between synthesis of full-length proteins and antigenic peptide substrates. This interaction is prevented by the G4 ligand PhenDC3 (21). As expected, treatment of cells expressing the intronless GAr-Globin mRNAs with this compound prevented NCL binding (Figure 3A, upper panels) and increased the synthesis of both full-length protein and antigenic peptide substrates from the GAr-Globin intronless mRNA (Figure 3B and C). These effects were associated with an accumulation of GAr-intronless mRNAs in the cytoplasm (Figure 3A, lower panels). PhenDC3 had no effect on antigen presentation in cells expressing GAr-intron-bearing mRNAs, in line with the fact that these transcripts do not interact with NCL (Figure 3C).

Since targeting GAr-carrying mRNAs for splicing prevents NCL binding (see Figure 2), we next tested if splicing inhibition can restore the interaction. Treatment of cells expressing GAr-Globin intron-bearing mRNAs with the splicing inhibitor Isoginkgetin resulted in an accumulation of pre-mRNAs in the nuclear compartment and a high number of NCL – GAr mRNA interactions in the nucleus (Figure 3D, upper and lower panels, 3E and Supplementary Figure S6A). Of note, while splicing inhibition prevented the synthesis of full-length proteins (Figure 3F), it increased the synthesis of antigenic peptide substrates, despite inducing the NCL – mRNA interaction (Figure 3G). Isoginkgetin treatment had no effect on antigen presentation from the GAr-Globin intronless mRNA, confirming that the observed results are attributed to splicing inhibition and not to off-target effects of the drug (Figure 3G, Supplementary Figure S6B). These data support the idea that antigenic peptide substrates for the MHC class I pathway are produced by a mechanism independent from full-length protein synthesis. Moreover, they indicate that NCL interaction with GAr-intron-bearing RNAs upon splicing inhibition does not suppress the production of antigenic peptide substrates.

Cytoplasmic NCL – mRNA interactions prevent canonical translation but not synthesis of antigenic peptides

Previous data show that PhenDC3 treatment disrupts the NCL interaction, interferes with the localization of intronless mRNAs and increases full-length protein levels and antigen presentation. Interestingly, when the nuclear retention of intron-bearing RNAs is caused by splicing inhibition, the binding of NCL does not affect the production of antigenic peptide substrates. To clarify how these different observations are inter-linked and if the effect of NCL to suppress mRNA translation is related to nuclear retention, we analyzed the effect of NCL on intron-bearing RNAs once the mRNAs had reached the cytoplasm. Spliced GAr mRNAs are typically localized in the cytoplasm (Figure 2A and B). Since NCL is found in the nucleus (Figure 4A, upper left), we created a cytoplasmic NCL construct by disrupting the nuclear localization sequence of an HA-tagged NCL (HA-NCLΔNLS) (Figure 4A, upper right). When we performed PLA in cells expressing HA-NCLΔNLS together with GAr-Globin intron-bearing RNAs, we observed the HA-NCLΔNLS – GAr mRNA interaction in the cytoplasm (Figure 4A, lower right). As expected, the endogenous NCL did not interact with the intron-bearing GAr-Globin mRNA (Figure 4A, lower left).

The presence of HA-NCLΔNLS hampered the synthesis of full-length proteins from the GAr intron-bearing mRNAs (Figure 4B), but it had no effect on the production of antigenic peptide substrates (Figure 4C). Hence, when NCL interacts with the GAr mRNA in the cytoplasm it only interferes with the canonical translation and not with the production of antigenic peptide substrates. These results support the notion that translation events taking place in the cytoplasm do not affect the production of antigenic peptide substrates for the MHC class I pathway.

Altering the 5′ UTR of GAr-carrying mRNAs affects their ability to interact with NCL

Previous reports have shown that fusing the c-myc IRES to the 5′ UTR of intronless GAr-carrying mRNAs overcomes GAr-mediated translation suppression (2). We added c-myc and HCV IRES structures to the 5′ UTR of GAr-carrying messages (Figure 5A) and RNA-FISH analysis showed that the c-myc IRES had no effect on the localization of the intronless GAr mRNA whereas the HCV IRES stimulated nuclear export (Figure 5B, upper panels). Screening of NCL – GAr mRNA interactions using the PLA showed that both IRESs prevented the binding of NCL (Figure 5B, lower panels). In addition, *in vitro* RNA co-IP using total RNA from transfected cells and recombinant NCL showed that neither the c-myc nor the HCV IRES-carrying mRNAs interacted with NCL (Figure 5C). This shows that IRES sequences in the 5′ UTR of the GAr-carrying mRNAs prevent their interaction with NCL both *in vitro* and *in cellulo*, presumably by interfering with the formation of the G4 structure.

As expected, the c-myc IRES overcame GAr-mediated translation suppression and had no impact on translation efficiency of non GAr-carrying mRNAs. The presence of the HCV IRES, however, further suppressed protein synthesis, which can be explained by the fact that the HCV IRES forms a hairpin structure that prevents cap-dependent translation also in the absence of the GAr (Figure 5D and Supplementary Figure S7). Importantly, both IRESs prevented GAr-mediated suppression of antigen presentation (Figure 5E). Hence, the HCV IRES stimulates antigen presentation while suppressing canonical translation, further supporting the notion that full-length proteins and antigenic peptide substrates are derived from distinguishable translation events.

We have previously shown that NCL suppresses translation when bound to the G4 structures present in GAr-

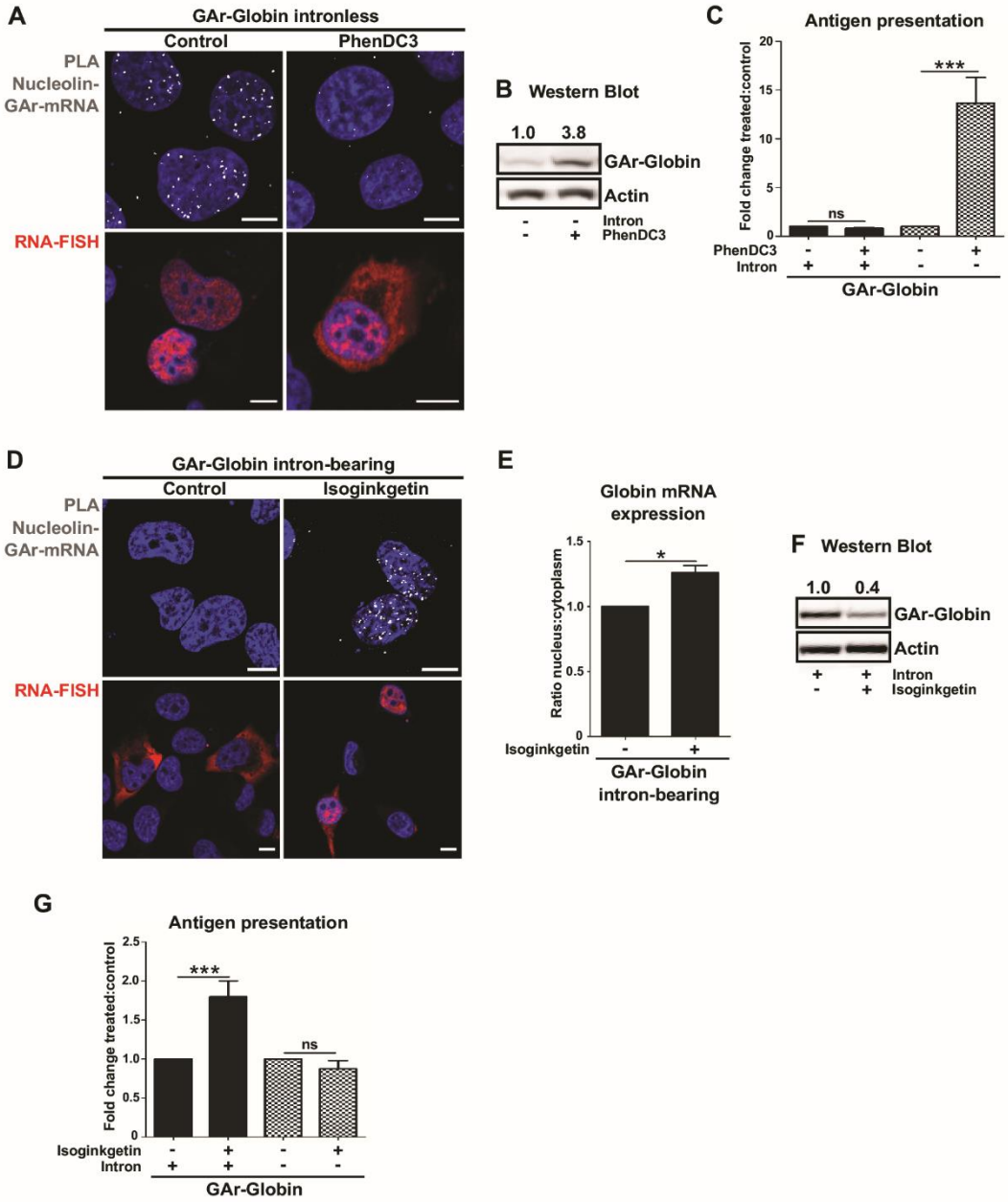

Figure 3. Splicing inhibition induces NCL - GAr mRNA interaction but does not affect the synthesis of antigenic peptides. (**A**) Screening of NCL - GAr mRNA interactions (white dots) by PLA (upper panels) and RNA localization by RNA-FISH (lower panels) in cells expressing intronless GAr-Globin, treated or not with PhenDC3 (5 μM for 40 h). (**B**) Western blot analysis of cells transfected and treated as in (A) show higher GAr-Globin protein levels upon PhenDC3 treatment. One of three independent experiments is shown. (**C**) H1299 cells expressing murine MHC-I (Kb) and the GAr-Globin intron-bearing or intronless constructs were treated with PhenDC3 (5 μM for 40 h) and co-cultured with OT1 $CD8^+$ T cells. The levels of antigen presentation were estimated by measuring the IL-2 release. (**D**) NCL – GAr mRNA interactions by PLA (upper panels) and RNA-FISH (lower panels) in cells expressing the GAr-Globin intron-bearing mRNA, following isoginkgetin treatment (30 μM for 24 h). (**E**) Cells transfected and treated as in (D) were fractionated for analysis of RNA from the nucleus and cytoplasm by RT-qPCR. Histograms represent the mean of three independent experiments. $*P < 0.05$. (**F**) Western blot analysis of cells as in (D) show lower GAr-Globin protein levels upon isoginkgetin treatment. One of three independent experiments is shown. **G**) Cells were transfected and tested for antigen presentation as in (C) after treatment with isoginkgetin (30 μM for 24 h). Isoginkgetin treatment significantly increased the levels of antigen presentation from the GAr-Globin intron-bearing construct whereas no effect was observed upon PhenDC3 treatment. Blue and red represent DAPI and mRNA, respectively. Scale bar = 10 μm.

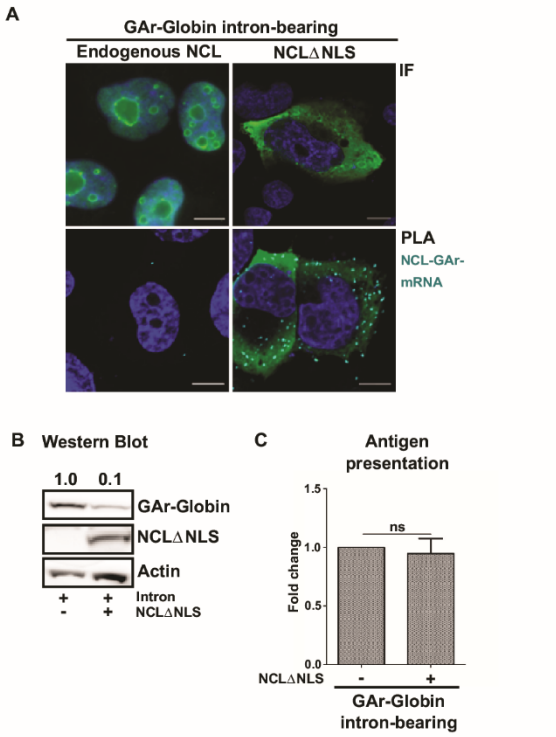

Figure 4. A cytoplasmic NCL suppresses synthesis of full-length protein from GAr-intron-bearing mRNAs but has no effect on antigen presentation. (**A**) Immunofluorescence (IF) shows endogenous NCL predominantly localized in the nucleolus (upper left). An anti-HA antibody shows an HA-tagged NCL lacking the nuclear localization signal (HA-NCLΔNLS) in the cytoplasm (upper right). PLA (lower panels) shows that NCLΔNLS but not endogenous NCL interacts with the GAr-Globin intron-bearing transcript in the cytoplasm. Green, dark blue and light blue represent nucleolin, DAPI and PLA, respectively. Scale bar = 10 μm. (**B**) Cells transfected as in (A) were analyzed by western blot. NCLΔNLS suppresses canonical translation of GAr-Globin intron-bearing. (**C**) Cells expressing MHC-I (Kb) and the indicated constructs were co-incubated with OT1 cells. IL-2 levels show that the expression of NCLΔNLS in the cytoplasm had no effect on the presentation of GAr-Globin intron-bearing-derived antigenic peptides. Graphs represent the mean of three independent experiments. ns: not significant.

encoding mRNA, but we also observed that treating cells with PhenDC3 induced the export of GAr-intronless transcripts to the cytoplasm (see Figure 3A and B). This raised the possibility that NCL might anchor the mRNA in the nucleus. To test this, we treated cells expressing the c-myc IRES-GAr mRNA with PhenDC3 and analyzed RNA location by FISH. In non-treated cells this mRNA remained nuclear in spite of not interacting with NCL, but following PhenDC3 treatment it was predominantly detected in the cytoplasm (Figure 5F). This shows that other G4-binding factor/s prevent mRNA export. Interestingly, the nuclear export of c-myc IRES-GAr mRNA promoted by PhenDC3 was associated with an increased synthesis of both protein and antigenic peptide substrates (Figure 5G and H). These data show that the GAr G4 can act as a hub for different cellular factors that interfere with mRNA processing in varied ways.

Altered mRNA export pathway prevents the interaction between NCL and intronless GAr-carrying mRNAs

Presented results suggest that distinct maturation mechanisms that restrain mRNAs in the nucleus, or drive them to cytoplasm, control the synthesis of full-length protein and antigenic peptide substrates. To test the role of mRNA export pathways, we targeted the nuclear intronless GAr mRNA for the CRM1 export pathway using the HIV-1 RRE-Rev system. RNA-FISH revealed that the insertion of the RRE sequence to the 3′ UTR of GAr-Globin intronless mRNA (GAr-Globin intronless-RRE) did not result in any change in its subcellular localization (Figure 6A, i–ii and see Figure 2A). The RRE itself had no effect on the NCL – GAr mRNA interaction (Figure 6A, vi–vii). In the presence of the Rev protein, intronless GAr-Globin-RRE mRNA was exported to the cytoplasm (Figure 6A, iii-v) and the interaction with NCL was lost (Figure 6A, viii–x). The presence of Rev also enhanced the rate of protein expression from GAr-carrying and non-GAr-carrying RRE mRNAs, with a nearly 25-fold induction of expression from the GAr-Globin intronless-RRE (Figure 6B, upper panels and lower graph). When we looked at the effect of Rev on the production of antigenic peptide substrates, we observed a significant suppression from all mRNAs tested with the clear exception of the intronless GAr-Globin-RRE, for which an ∼5-fold induction was uncovered (Figure 6C). Thus, Rev-mediated export of mRNAs originally located in the cytoplasm improved their rate of translation but at the same time reduced the synthesis of antigenic peptides. Importantly, the forced export of the nuclear-retained intronless GAr-carrying mRNAs prevented NCL binding and promoted a concurrent increase of both canonical translation and antigen presentation. These results support the hypothesis that protein-RNA intereaction taking place on the nascent transcript control the synthesis of full length proteins and antigenic peptide substrates.

DISCUSSION

We have employed multiple approaches to show that the synthesis of full-length proteins and antigenic peptide substrates for the MHC class I pathway are separate events independently regulated on the nascent transcript.

Translation in the nuclear compartment is still clouded in controversy despite several reports suggesting that it indeed can take place (35–42). In support of a nuclear non-canonical translation event for the production of antigenic peptide substrates, we show that (i) splicing inhibition promotes an increase of antigen presentation in spite of reducing protein levels, (ii) the interaction between NCL and mRNAs in the cytoplasm prevents synthesis of full-length proteins but has no effect on the production of antigenic peptide substrates, (iii) the HCV IRES overcomes GAr-mediated inhibition of antigenic peptides production while suppressing the synthesis of full-length proteins and iv) alternative mRNA export via the CRM1-dependent pathway of non-GAr-carrying intronless messages stimulates protein synthesis but suppresses antigen presentation (Figure 7). These results are in line with previous reports showing that mRNAs targeted for the NMD pathway produce antigenic peptides substrates but not full-length proteins and

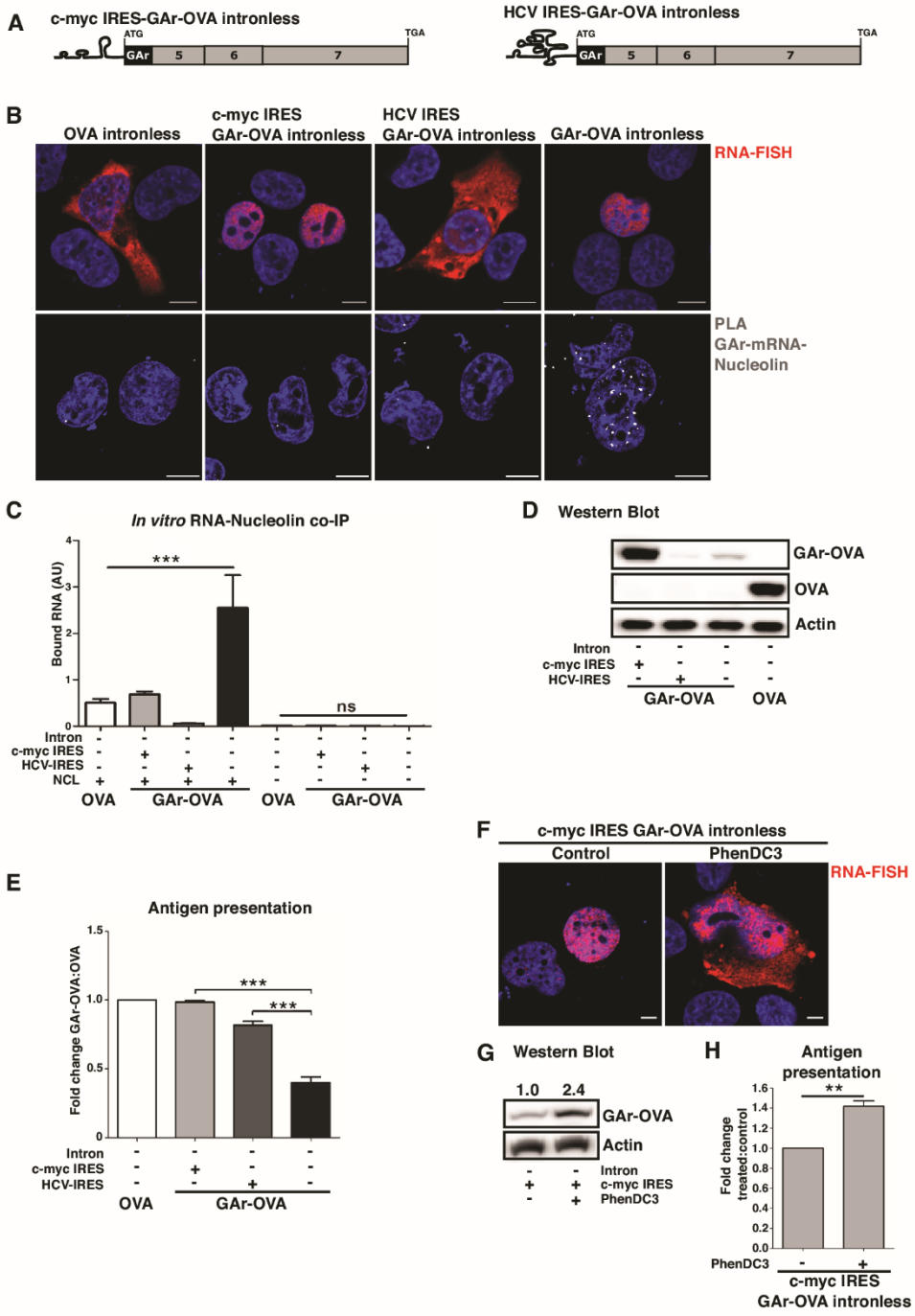

Figure 5. IRES sequences fused to the 5′ UTR of GAr-intronless mRNAs disrupt G4 function and differentiate synthesis of full-length vs antigenic peptide products. (**A**) Cartoon illustrating c-myc IRES-GAr-OVA intronless and HCV IRES-GAr-OVA intronless constructs. (**B**) RNA FISH (upper panels) and PLA analysis (lower panels) of NCL – GAr mRNA interactions (depicted as white dots) in cells expressing the indicated constructs. c-myc IRES GAr-OVA and HCV IRES GAr-OVA intronless mRNAs show different locations (upper panels). The presence of either IRES sequences prevents the interaction with NCL (lower panels). (**C**) *In vitro* RNA co-immunoprecipitation (RNA-coIP) on total RNA derived from cells expressing the indicated constructs. Graphs represent the mean of three independent experiments. ***$P < 0.001$, ns: not significant. (**D**) Western blots show the protein levels from intronless OVA, GAr-OVA and IRES-carrying GAr-OVA constructs (see also Supplementary Figure S7). (**E**) Antigen presentation determined by IL-2 release from OT-1 cells co-incubated with cells expressing murine MHC-I (Kb) and indicated constructs. Graphs represent the mean of three independent experiments. ***$P < 0.001$. (**F**) RNA-FISH on cells expressing intronless c-myc IRES GAr-OVA treated with PhenDC3 (5 μM for 40 h). (**G**) Western blot on cells transfected and treated as in (F). One of three independent experiments is shown. (**H**) Cells expressing murine MHC-I (Kb) and the c-myc IRES GAr-OVA intronless construct were treated with PhenDC3 and tested for antigen presentation as in (E). Blue represents DAPI. Scale bar = 10 μm.

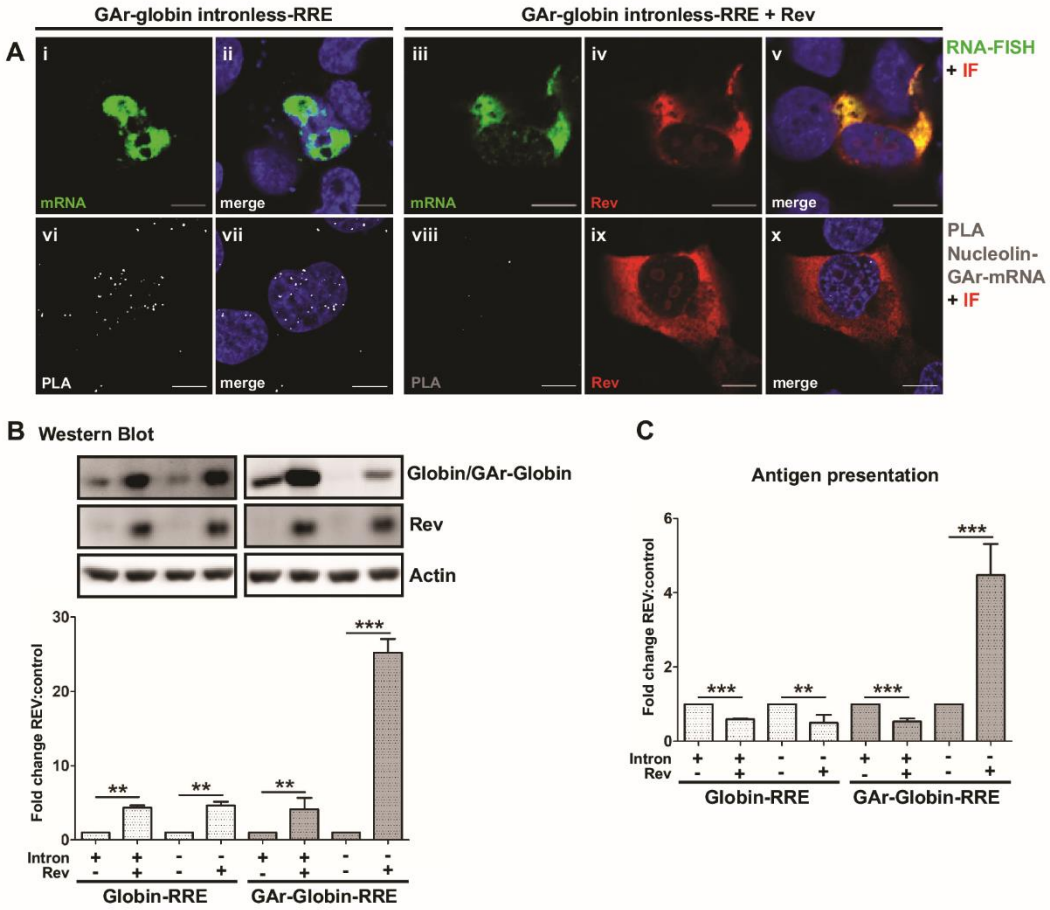

Figure 6. Rev-mediated nuclear-export prevents NCL - GAr-intronless mRNA interaction. (**A**) RNA FISH coupled to IF (upper panels) and PLA analysis of NCL – GAr mRNA interactions coupled to IF (lower panels) in cells expressing indicated constructs. Upper panels: The Rev response element (RRE) sequence was fused to the 3′UTR of GAr-Globin intronless (GAr-Globin intronless-RRE) (see also Supplementary Figure S8A). The GAr-Globin intronless-RRE mRNA is exported to the cytoplasm in a Rev-dependent fashion (iii–v). Lower panels: The GAr intronless mRNA does not interact with NCL following nuclear export by Rev (viii–x). PLA complexes are depicted as white dots and each complex represent an interaction between NCL and GAr-mRNA. Green and red denotes GAr mRNA and Rev, respectively. Blue represents DAPI. Scale bar = 10 μm. (**B**) Western blot analysis (upper panels) of cells expressing Rev or empty vector and indicated intronless or intron-bearing constructs. Nuclear export of mRNAs by Rev results in higher protein expression. Graph (lower) shows fold changes of Globin:actin protein levels relative to controls without Rev and represent three independent experiments. $^{**}P < 0.01$, $^{***}P < 0.001$. (**C**) Antigen presentation levels were determined by measuring the IL-2 release by OT-1 lymphocytes co-incubated with cells expressing murine MHC-I (Kb) and the same constructs as in (**B**). Nuclear export of mRNAs by Rev suppresses the synthesis of antigenic peptide substrates except for the intronless GAr-Globin-RRE construct, which shows an ∼5-fold increase of antigen presentation. Data shown are fold changes relative to controls without Rev and represent three independent experiments. $^{**}P < 0.01$, $^{***}P < 0.001$.

that nascent intron-derived peptides are detected in the nucleus and presented on MHC class I molecules (8). The synthesis of antigenic peptide substrates might relate to previous published observations of ribosomal factors on nascent mRNAs and of coupled transcription-translation in eukaryotic cells (37,41,42). Furthermore, mass spectrometry analyses have also shown that a large proportion of small peptide products are derived from non-canonical translation (13). A non-canonical translation taking place in the nucleus might not require the same translation factors as the synthesis of full-length proteins, which takes the edge off some of the arguments against nuclear translation. Taken together, previous and presented data suggest a model in which a major source of antigenic peptide substrates for the MHC class I pathway are synthesized by a nuclear event taking place on pre-spliced mRNAs (7,8,43). However, this does not rule out other sources of peptide substrates for the MHC class I pathway (44).

Pre-mRNAs are processed and exported to the cytoplasm as translation competent mRNAs (14,45). Nuclear mRNA retention is considered rare in mammalian cells (46) and few RNA sequences promoting nuclear retention have been identified (47). Here, we show that in addition to provide a NCL-binding platform, the G4 structure of the GAr-encoding mRNA also promotes nuclear retention. This supports previous findings that the G4 acts as a protein binding platform (21) and not as an inhibitor of translation elongation (48). The relevance of RNA G4 in the physiological context has been a matter of debate. However, the observation that these structures are thermodynamically very stable

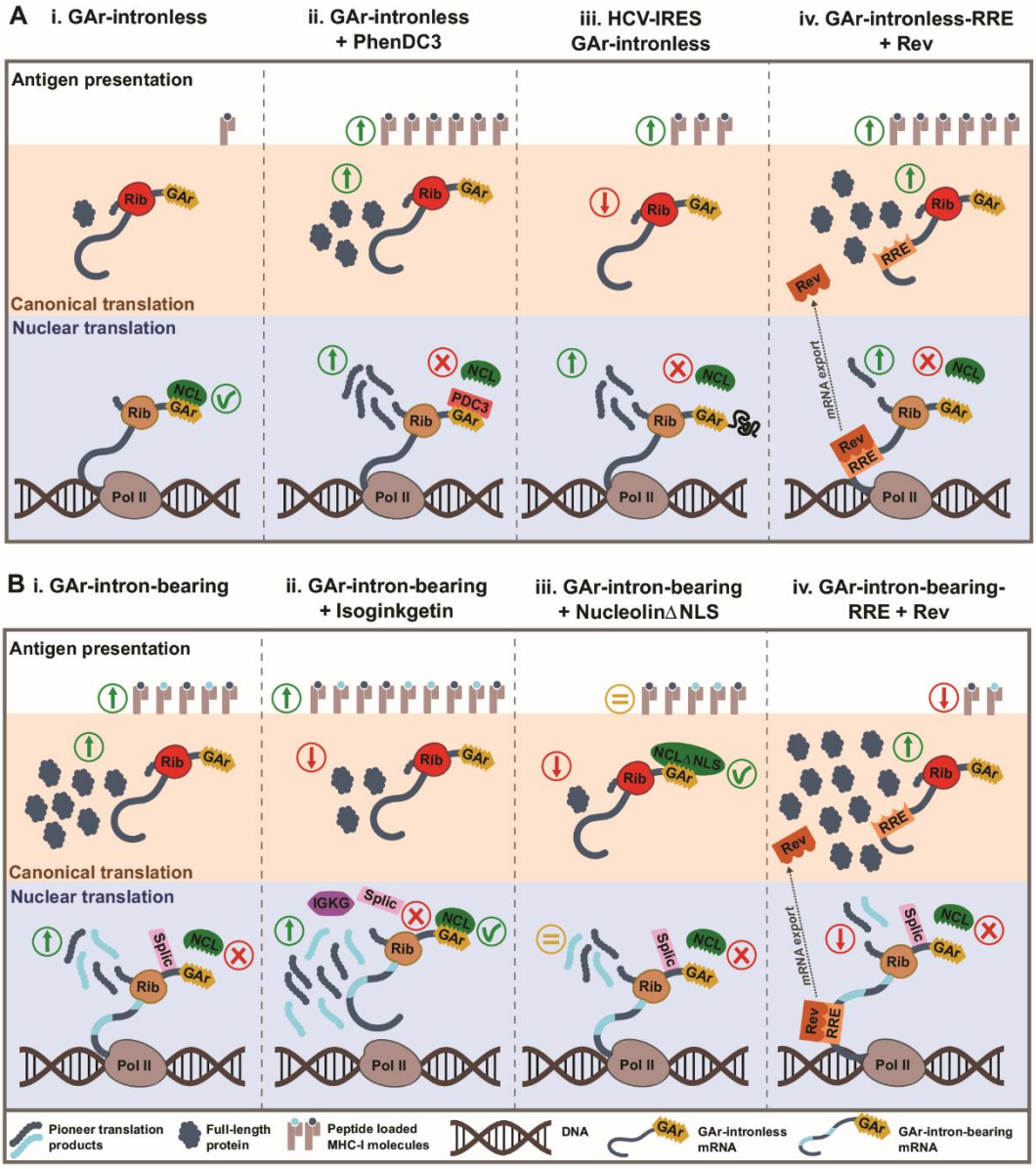

Figure 7. Scheme of the effects of G4 ligands, splicing and alternative mRNA export on the synthesis of full-length proteins and pioneer translation products (PTPs) from intronless and intron-bearing GAr-carrying transcripts. (**A**) GAr-intronless mRNAs. (A.i) GAr-mediated inhibition of full-length proteins and PTPs production depend on the binding of Nucleolin (NCL) to G-quadruplexes (G4) formed by GAr-encoding mRNA in the nucleus. (A.ii) The G4-ligand PhenDC3 prevents the NCL - GAr-mRNA interaction, promoting increased protein and antigen presentation levels. (A.iii) Fusion of the HCV IRES structure to the 5′UTR of GAr-intronless mRNAs hampers NCL - GAr-mRNA interactions resulting in an increase of PTPs production concurrent with reduced full-length protein levels. (A.iv) HIV-1 Rev-mediated mRNA export prevents NCL binding to the GAr mRNA resulting in increased full-length protein and PTPs production. In (A.ii) to (A.iv), changes are illustrated taking (A.i) as reference. (**B**) GAr-intron-bearing mRNAs. (B.i) NCL does not interact with GAr-carrying mRNAs targeted by the splicing machinery (Splic). GAr-mediated control of mRNA translation and antigen presentation is disrupted in the context of intron-bearing messages (changes illustrated taking A.i as reference). (B.ii) Splicing inhibition by Isoginkgetin (IGKG) reduces protein levels but promotes an increase in PTPs production. IGKG prevents mRNA maturation allowing non-spliced pre-mRNAs to interact with NCL after the production of PTPs has taken place. (B.iii) A NCL defective for nuclear localization (NCLΔNLS) interacts with spliced GAr-mRNAs in the cytoplasm, resulting in a strong decrease in full-length protein synthesis without affecting PTPs production. (B.iv) Rev-mediated export of GAr-intron-bearing mRNA prevents the production of PTPs in the nucleus and reduces antigen presentation levels in spite of increasing canonical translation. In B.ii to B.iv, changes are illustrated taking B.i as reference. Green and red arrows denote increased and decreased levels, respectively. Yellow equals signs indicate no significant change. Ribosomes (Rib) translating PTPs and full-length proteins are depicted in brown and red, respectively. Dark and light blue lines denote exonic and intronic RNA sequences, respectively. Pol II: RNA polymerase II.

under near physiological ionic conditions *in vitro* strongly suggests that they are likely to form *in vivo* (25) and accumulating evidence from *in cellulo* experiments demonstrate that RNA G4 play a relevant role in the gene regulation process (20,21,25,48). In accordance with our observations, Serikawa *et al.* (20) showed that NCL binds RNA G4 motifs found in tumor-associated mRNAs *in cellulo.* Moreover, putative quadruplex sequences have been identified in the mRNAs coding other gammaherpesviral maintenance proteins similar to EBNA1 (48). Therefore, it is tempting to infer that NCL - G4 interactions play a relevant role in tumor biology and might be exploited by viruses to control mRNA translation and antigen presentation.

Both capacities of the GAr G4 to interact with NCL and promote mRNA nuclear retention are disrupted by the G4 ligand PhenDC3, but these two functions can also be targeted independently by fusing the c-myc or the HCV IRESs to the 5′ UTR of GAr-carrying mRNAs. Both IRESs disrupt the capacity of the G4 structure to bind NCL *in vitro* and *in vivo* but the c-myc IRES does not interfere with nuclear retention, whereas HCV IRES-carrying mRNAs are exported freely. This indicates that the nuclear retention factor has a different binding affinity for the G4 as compared to NCL, supporting the idea that the folding of G4 RNA structures *in vivo* can take different conformations and is influenced by flanking sequences (49,50). Lago *et al.* (17) observed that NCL modifies the overall structure and steric hindrance of G4 forming sequences. Therefore, modifications of the GAr G4 structure induced by NCL, or factor/s promoting nuclear retention, could represent a mechanosensor governing mRNA maturation. Interestingly, the intron-bearing G4 RNA binds a cytoplasmic NCL (NCLΔNLS) and suppress translation, despite the fact that the mRNA has been scanned during RNA quality control, showing that the G4 structure is refolded after the pioneer round of translation. The RNA helicase RHAU has been shown to bind mRNAs *in cellulo,* unwind G4 structures and function as the main source of tetramolecular RNA G4-resolving activity in HeLa cells lysates (51,52). A similar activity has been described for the human DHX9 helicase (53).

The interaction with NCL was also prevented by placing the GAr in the context of intron-bearing mRNAs. However, in this case the structure of the G4 is not disrupted since GAr-intron bearing transcripts interact with NCL *in vitro* and splicing inhibition allows NCL to access the G4 in the nucleus. Therefore, engaging the mRNA with the splicing machinery prevents NCL access to the nascent transcript. Upon splicing inhibition, NCL binding to intron-containing RNAs in the nucleus does not affect the production of antigenic peptides. This indicates that NCL must interact with nascent transcripts in order to suppress the production of antigenic peptides and reinforces the idea that PTPs are produced co-transcriptionally (8).

As we observed that G4-carrying intron-bearing RNAs are freely exported, it is possible that splicing also prevents the access of a nuclear retention factor/s to G4. It should be noted that EBNA1 has been reported to bind G4-forming RNAs in order to recruit the origin recognition complex (ORC) and modulate EBV DNA replication and episome maintenance (54). Therefore, one cannot exclude the possibility that EBNA1 interferes with translation and antigen presentation by binding G4 structures in its own mRNA.

There is yet little known about alternative and regulated mRNA maturation pathways. However, these results indicate that the formation of specific RNP complexes on the nascent transcripts control mRNA maturation pathways that determine how the messages will be translated in the cytoplasm. In line with this notion, NCL is under normal conditions only bound to GAr-carrying mRNAs in the nucleus but it still prevents canonical translation in the cytoplasm. This notion is also illustrated by Rev-mediated mRNA export via the CRM1 pathway (Supplementary Figure S8A and B). Rev targets pre-spliced mRNAs for nuclear export and this prevents NCL from binding the GAr G4 structure, resulting in an increase in the antigenic peptides production. However, Rev-mediated nuclear export of non-GAr-carrying mRNAs instead results in a sharp loss of antigenic peptides production. This might appear contradictory, but one has to keep in mind that the actual numbers of antigenic peptides derived from GAr intronless mRNAs following Rev-mediated export are far less than the number of peptides derived from non-GAr-carrying messages. Hence, Rev-mediated export of GAr-carrying mRNAs does not restore antigenic peptide production: it merely increases the numbers from very low to low. In this scenario, a Rev-dependent loss of NCL binding is sufficient to allow the production of PTPs before the message is exported. Mature mRNAs are also efficiently exported by Rev, leading to higher levels of full-length proteins. It cannot be ruled out that the minor increase of antigen presentation from GAr fusion proteins observed from Rev-dependent export might be associated to a protein-based source of peptides.

It was surprising to see that the c-myc IRES-carrying mRNAs overcome GAr-mediated suppression of full-length protein synthesis while retaining a mainly nuclear localization. It might have been expected that an increase in synthesis would have been accompanied with nuclear export. Thus, nuclear retention *per se* is not sufficient to inhibit translation and this presumable relates to previous observations that a fraction of mRNAs are engaged with translation. Taken together, we suggest a model whereby GAr is targeting NCL to intronless mRNAs and this suppresses the synthesis of PTPs in the nucleus as well as full-length proteins in the cytoplasm (Figure 7). It is possible that the function of the GAr is to promote an mRNA maturation pathway which allows G4 to engage with NCL and suppress mRNA translation. Additionally, this alternative pathway might enable the binding of other factor/s to the G4 structure, leading to nuclear retention. Further studies will clarify the implication of nuclear retention in the viral strategy to evade the immune system.

NCL is a multifunctional RNA binding protein that suppresses translation of multiple mRNAs (16,24,55). Nevertheless, the underlying molecular mechanism of this inhibitory effect is poorly understood. The presented model for how the GAr governs translation during early mRNA maturation shows some similarities with the alternative mRNA nuclear export (ALREX) concept. ALREX-elements located in the 5′ of mRNAs coding sequences control translation, transcript export and encode a signal sequence, which guides proteins to the endoplasmic reticu-

lum (ER) (56). EBNA1 or the GAr-carrying proteins that we have used are not targeted to the ER. Nevertheless, the fact that the GAr mRNA sequence controls mRNA export and translation suggests a more general concept in which mRNA maturation, export and translation are interlinked. In the case of EBNA1, the interaction between the RNA and nucleolin in the nucleoplasm controls both the production of antigenic peptide substrates and canonical cytoplasmic translation. For the RanBP2/Nup358, the interaction with ALREX-elements takes place at the nuclear membrane. In either case, NCL and RanBP2/Nup358 are likely to affect translation by modifying mRNP complexes that govern translation initiation before the mRNAs reach the cytoplasm. Their respective effects on canonical translation presumably take place before they are displaced by the scanning ribosomes during the first round of pioneer translation.

The design of new vaccines against transformed or virus-infected cells relies on the presentation of neoantigens on MHC class I molecules. Thus, the presented results will lead to a better understanding of the underlying molecular mechanisms that control the synthesis of peptide substrates for the MHC class I pathway and pave the way for the development of new therapeutic approaches aimed at regulating the presentation of antigens in pathological conditions.

SUPPLEMENTARY DATA

Supplementary Data are available at NAR Online.

ACKNOWLEDGEMENTS

We thank the staff of the Plateforme Technologique of the Institut Universitaire d'Hématologie (IUH) - Paris, for their skillful technical assistance.

FUNDING

Institut National Du Cancer (INCa) [10683]; Inserm, Cancerforskningsfonden Norr, Cancerfonden [160598]; Vetenskapsradet, La Ligue contre le Cancer Grand-Ouest (CSIRGO) and RECAMO [GACR P206/12/G151, MYES-NPS I-LO1413]; The 'International Centre for Cancer Vaccine Science' project is carried out within the International Agendas programme of the Foundation for Polish Science co-financed by the European Union under the European Regional Development Fund. Funding for open access charge: INCa [10683].
Conflict of interest statement. None declared.

REFERENCES

1. Hansen,T.H. and Bouvier,M. (2009) MHC class I antigen presentation: learning from viral evasion strategies. *Nat. Rev. Immunol.*, **9**, 503–513.
2. Apcher,S., Daskalogianni,C., Manoury,B. and Fahraeus,R. (2010) Epstein Barr virus-encoded EBNA1 interference with MHC class I antigen presentation reveals a close correlation between mRNA translation initiation and antigen presentation. *PLoS Pathog.*, **6**, e1001151.
3. Tellam,J.T., Lekieffre,L., Zhong,J., Lynn,D.J. and Khanna,R. (2012) Messenger RNA sequence rather than protein sequence determines the level of self-synthesis and antigen presentation of the EBV-encoded antigen, EBNA1. *PLoS Pathog.*, **8**, e1003112.
4. Yewdell,J.W., Anton,L.C. and Bennink,J.R. (1996) Defective ribosomal products (DRiPs): a major source of antigenic peptides for MHC class I molecules? *J. Immunol.*, **157**, 1823–1826.
5. Shastri,N., Schwab,S. and Serwold,T. (2002) Producing nature's gene-chips: the generation of peptides for display by MHC class I molecules. *Annu. Rev. Immunol.*, **20**, 463–493.
6. Starck,S.R. and Shastri,N. (2011) Non-conventional sources of peptides presented by MHC class I. *Cell. Mol. Life Sci.*, **68**, 1471–1479.
7. Apcher,S., Daskalogianni,C., Lejeune,F., Manoury,B., Imhoos,G., Heslop,L. and Fahraeus,R. (2011) Major source of antigenic peptides for the MHC class I pathway is produced during the pioneer round of mRNA translation. *Proc. Natl. Acad. Sci. U.S.A.*, **108**, 11572–11577.
8. Apcher,S., Millot,G., Daskalogianni,C., Scherl,A., Manoury,B. and Fahraeus,R. (2013) Translation of pre-spliced RNAs in the nuclear compartment generates peptides for the MHC class I pathway. *Proc. Natl. Acad. Sci. U.S.A.*, **110**, 17951–17956.
9. Schwab,S.R., Li,K.C., Kang,C. and Shastri,N. (2003) Constitutive display of cryptic translation products by MHC class I molecules. *Science*, **301**, 1367–1371.
10. Jackson,R.J., Hellen,C.U. and Pestova,T.V. (2010) The mechanism of eukaryotic translation initiation and principles of its regulation. *Nat. Rev. Mol. Cell Biol.*, **11**, 113–127.
11. Martinez-Salas,E., Francisco-Velilla,R., Fernandez-Chamorro,J. and Embarek,A.M. (2017) Insights into structural and mechanistic features of viral IRES elements. *Front. Microbiol.*, **8**, 2629.
12. Leppek,K., Das,R. and Barna,M. (2018) Functional 5′ UTR mRNA structures in eukaryotic translation regulation and how to find them. *Nat. Rev. Mol. Cell Biol.*, **19**, 158–174.
13. Kearse,M.G. and Wilusz,J.E. (2017) Non-AUG translation: a new start for protein synthesis in eukaryotes. *Genes Dev.*, **31**, 1717–1731.
14. Martins,R.P. and Fahraeus,R. (2017) A matter of maturity: The impact of pre-mRNA processing in gene expression and antigen presentation. *Int. J. Biochem. Cell Biol.*, **91**, 203–211.
15. Zapp,M.L. and Green,M.R. (1989) Sequence-specific RNA binding by the HIV-1 Rev protein. *Nature*, **342**, 714–716.
16. Jia,W., Yao,Z., Zhao,J., Guan,Q. and Gao,L. (2017) New perspectives of physiological and pathological functions of nucleolin (NCL). *Life Sci.*, **186**, 1–10.
17. Lago,S., Tosoni,E., Nadai,M., Palumbo,M. and Richter,S.N. (2017) The cellular protein nucleolin preferentially binds long-looped G-quadruplex nucleic acids. *Biochim. Biophys. Acta Gen. Subj.*, **1861**, 1371–1381.
18. Abdelmohsen,K., Tominaga,K., Lee,E.K., Srikantan,S., Kang,M.J., Kim,M.M., Selimyan,R., Martindale,J.L., Yang,X., Carrier,F. *et al.* (2011) Enhanced translation by Nucleolin via G-rich elements in coding and non-coding regions of target mRNAs. *Nucleic Acids Res.*, **39**, 8513–8530.
19. Tosoni,E., Frasson,I., Scalabrin,M., Perrone,R., Butovskaya,E., Nadai,M., Palu,G., Fabris,D. and Richter,S.N. (2015) Nucleolin stabilizes G-quadruplex structures folded by the LTR promoter and silences HIV-1 viral transcription. *Nucleic Acids Res.*, **43**, 8884–8897.
20. Serikawa,T., Spanos,C., von Hacht,A., Budisa,N., Rappsilber,J. and Kurreck,J. (2018) Comprehensive identification of proteins binding to RNA G-quadruplex motifs in the 5′ UTR of tumor-associated mRNAs. *Biochimie.*, **144**, 169–184.
21. Lista,M.J., Martins,R.P., Billant,O., Contesse,M.A., Findakly,S., Pochard,P., Daskalogianni,C., Beauvineau,C., Guetta,C., Jamin,C. *et al.* (2017) Nucleolin directly mediates Epstein-Barr virus immune evasion through binding to G-quadruplexes of EBNA1 mRNA. *Nat. Commun.*, **8**, 16043.
22. Lista,M.J., Martins,R.P., Angrand,G., Quillevere,A., Daskalogianni,C., Voisset,C., Teulade-Fichou,M.P., Fahraeus,R. and Blondel,M. (2017) A yeast model for the mechanism of the Epstein-Barr virus immune evasion identifies a new therapeutic target to interfere with the virus stealthiness. *Microb. Cell*, **4**, 305–307.
23. Millevoi,S., Moine,H. and Vagner,S. (2012) G-quadruplexes in RNA biology. *Wiley Interdiscip. Rev. RNA*, **3**, 495–507.
24. Song,J., Perreault,J.P., Topisirovic,I. and Richard,S. (2016) RNA G-quadruplexes and their potential regulatory roles in translation. *Translation (Austin)*, **4**, e1244031.
25. Bugaut,A. and Balasubramanian,S. (2012) 5′-UTR RNA G-quadruplexes: translation regulation and targeting. *Nucleic Acids Res.*, **40**, 4727–4741.

26. Yin,Y., Manoury,B. and Fahraeus,R. (2003) Self-inhibition of synthesis and antigen presentation by Epstein-Barr virus-encoded EBNA1. *Science*, **301**, 1371–1374.
27. De Cian,A., Delemos,E., Mergny,J.L., Teulade-Fichou,M.P. and Monchaud,D. (2007) Highly efficient G-quadruplex recognition by bisquinolinium compounds. *J. Am. Chem. Soc.*, **129**, 1856–1857.
28. Candeias,M.M., Malbert-Colas,L., Powell,D.J., Daskalogianni,C., Maslon,M.M., Naski,N., Bourougaa,K., Calvo,F. and Fahraeus,R. (2008) P53 mRNA controls p53 activity by managing Mdm2 functions. *Nat. Cell Biol.*, **10**, 1098–1105.
29. Lyons,A.B. and Doherty,K.V. (2004) Flow cytometric analysis of cell division by dye dilution. *Curr. Protoc. Cytom.*, doi:10.1002/0471142956.cy0911s27.
30. Gnanasundram,S.V., Pyndiah,S., Daskalogianni,C., Armfield,K., Nylander,K., Wilson,J.B. and Fahraeus,R. (2017) PI3Kdelta activates E2F1 synthesis in response to mRNA translation stress. *Nat. Commun.*, **8**, 2103.
31. Panda,A.C., Martindale,J.L. and Gorospe,M. (2017) Polysome fractionation to analyze mRNA distribution profiles. *Bio. Protoc.*, **7**, e2126.
32. Apcher,S., Komarova,A., Daskalogianni,C., Yin,Y., Malbert-Colas,L. and Fahraeus,R. (2009) mRNA translation regulation by the Gly-Ala repeat of Epstein-Barr virus nuclear antigen 1. *J. Virol.*, **83**, 1289–1298.
33. Shaul,O. (2017) How introns enhance gene expression. *Int. J. Biochem. Cell Biol.*, **91**, 145–155.
34. Lopez,I., Tournillon,A.S., Prado Martins,R., Karakostis,K., Malbert-Colas,L., Nylander,K. and Fahraeus,R. (2017) p53-mediated suppression of BiP triggers BIK-induced apoptosis during prolonged endoplasmic reticulum stress. *Cell Death Differ.*, **24**, 1717–1729.
35. Allfrey,V.G. (1954) Amino acid incorporation by isolated thymus Nuclei. I. The role of desoxyribonucleic acid in protein synthesis. *Proc. Natl. Acad. Sci. U.S.A.*, **40**, 881–885.
36. Goidl,J.A. (1978) Does protein synthesis occur within the nucleus? Good evidence that it does. *Trends Biochem. Sci.*, **3**, N225–N228.
37. Iborra,F.J., Jackson,D.A. and Cook,P.R. (2001) Coupled transcription and translation within nuclei of mammalian cells. *Science*, **293**, 1139–1142.
38. Iborra,F.J., Escargueil,A.E., Kwek,K.Y., Akoulitchev,A. and Cook,P.R. (2004) Molecular cross-talk between the transcription, translation, and nonsense-mediated decay machineries. *J. Cell Sci.*, **117**, 899–906.
39. David,A., Dolan,B.P., Hickman,H.D., Knowlton,J.J., Clavarino,G., Pierre,P., Bennink,J.R. and Yewdell,J.W. (2012) Nuclear translation visualized by ribosome-bound nascent chain puromycylation. *J. Cell Biol.*, **197**, 45–57.
40. Al-Jubran,K., Wen,J., Abdullahi,A., Roy Chaudhury,S., Li,M., Ramanathan,P., Matina,A., De,S., Piechocki,K., Rugjee,K.N. *et al.* (2013) Visualization of the joining of ribosomal subunits reveals the presence of 80S ribosomes in the nucleus. *RNA*, **19**, 1669–1683.
41. Brogna,S., Sato,T.A. and Rosbash,M. (2002) Ribosome components are associated with sites of transcription. *Mol. Cell*, **10**, 93–104.
42. Baboo,S., Bhushan,B., Jiang,H., Grovenor,C.R., Pierre,P., Davis,B.G. and Cook,P.R. (2014) Most human proteins made in both nucleus and cytoplasm turn over within minutes. *PLoS One*, **9**, e99346.
43. Apcher,S., Prado Martins,R. and Fahraeus,R. (2016) The source of MHC class I presented peptides and its implications. *Curr. Opin. Immunol.*, **40**, 117–122.
44. Blum,J.S., Wearsch,P.A. and Cresswell,P. (2013) Pathways of antigen processing. *Annu. Rev. Immunol.*, **31**, 443–473.
45. Hocine,S., Singer,R.H. and Grunwald,D. (2010) RNA processing and export. *Cold Spring Harb. Perspect. Biol.*, **2**, a000752.
46. Bahar Halpern,K., Caspi,I., Lemze,D., Levy,M., Landen,S., Elinav,E., Ulitsky,I. and Itzkovitz,S. (2015) Nuclear retention of mRNA in mammalian tissues. *Cell Rep.*, **13**, 2653–2662.
47. Wegener,M. and Muller-McNicoll,M. (2018) Nuclear retention of mRNAs - quality control, gene regulation and human disease. *Semin. Cell Dev. Biol.*, **79**, 131–142.
48. Murat,P., Zhong,J., Lekieffre,L., Cowieson,N.P., Clancy,J.L., Preiss,T., Balasubramanian,S., Khanna,R. and Tellam,J. (2014) G-quadruplexes regulate Epstein-Barr virus-encoded nuclear antigen 1 mRNA translation. *Nat. Chem. Biol.*, **10**, 358–364.
49. Guedin,A., Gros,J., Alberti,P. and Mergny,J.L. (2010) How long is too long? Effects of loop size on G-quadruplex stability. *Nucleic Acids Res.*, **38**, 7858–7868.
50. Guo,J.U. and Bartel,D.P. (2016) RNA G-quadruplexes are globally unfolded in eukaryotic cells and depleted in bacteria. *Science*, **353**, aaf5371.
51. Chalupnikova,K., Lattmann,S., Selak,N., Iwamoto,F., Fujiki,Y. and Nagamine,Y. (2008) Recruitment of the RNA helicase RHAU to stress granules via a unique RNA-binding domain. *J. Biol. Chem.*, **283**, 35186–35198.
52. Creacy,S.D., Routh,E.D., Iwamoto,F., Nagamine,Y., Akman,S.A. and Vaughn,J.P. (2008) G4 resolvase 1 binds both DNA and RNA tetramolecular quadruplex with high affinity and is the major source of tetramolecular quadruplex G4-DNA and G4-RNA resolving activity in HeLa cell lysates. *J. Biol. Chem.*, **283**, 34626–34634.
53. Chakraborty,P. and Grosse,F. (2011) Human DHX9 helicase preferentially unwinds RNA-containing displacement loops (R-loops) and G-quadruplexes. *DNA Repair (Amst.)*, **10**, 654–665.
54. Norseen,J., Johnson,F.B. and Lieberman,P.M. (2009) Role for G-quadruplex RNA binding by Epstein-Barr virus nuclear antigen 1 in DNA replication and metaphase chromosome attachment. *J. Virol.*, **83**, 10336–10346.
55. Abdelmohsen,K. and Gorospe,M. (2012) RNA-binding protein nucleolin in disease. *RNA Biol.*, **9**, 799–808.
56. Akef,A., Zhang,H., Masuda,S. and Palazzo,A.F. (2013) Trafficking of mRNAs containing ALREX-promoting elements through nuclear speckles. *Nucleus*, **4**, 326–340.

3.4 Recherche au sein de l'UMR ISP

Le développement de nouvelles alternatives à l'antibiothérapie reste un enjeu dans la lutte contre les infections bactériennes. Bien que les vaccins représentent une solution attractive, ces derniers possèdent une efficacité limitée dans le cadre de plusieurs maladies des animaux de rente, notamment les mammites. En plus de leur impact sur la santé des animaux et sur l'économie de l'exploitation laitière, les mammites peuvent engendrer des retombées négatives importantes sur la santé publique et le bien-être animal. Les vaccins contre les mammites actuellement disponibles ciblent principalement la réponse immunitaire humorale. Cependant, les mécanismes de la réponse à médiation cellulaire jouent un rôle essentiel dans la réponse aux pathogènes de la glande mammaire et une approche permettant la stimulation robuste de cette réponse demeure une lacune difficile à combler. Cela est dû, en partie, au manque de connaissances sur les différents aspects de l'immunité adaptative à médiation cellulaire, tout particulièrement chez les ruminants.

Lors des mammites et autres infections, les cellules épithéliales sont les premières cellules exposées aux pathogènes. Certains microorganismes sont capables de pénétrer dans ces cellules et de survivre dans le milieu intracellulaire à l'abri des anticorps et des phagocytes. Cette capacité est souvent évoquée comme un facteur clé pour les infections persistantes, lesquelles limitent le contrôle de nombreuses maladies chez les animaux puisqu'elles facilitent la propagation furtive des pathogènes dans les troupeaux. Des cellules cytotoxiques ciblant les cellules épithéliales infectées pourraient contrecarrer ce phénomène d'échappement aux défenses immunitaires et contribuer à la guérison. La cytotoxicité antigène-spécifique nécessite la présentation de peptides du pathogène en association avec le CMH-I à la surface de la cellule infectée. Cependant, la capacité des cellules épithéliales à présenter des antigènes a été peu étudiée.

La réponse immunitaire cellulaire peut être de type 1, 2 ou 3 selon les médiateurs impliqués, ainsi que leur fonction et leur effet pathophysiologique (**Figure 27**). Les réponses de type 1 (IFNγ-dépendante) et 3 (IL-17-dépendante) sont les plus pertinentes dans le cadre des infections bactériennes. Ces réponses reposent sur les lymphocytes T $CD4^+$ (Th) et $CD8^+$ (Tc) produisant de l'IFNγ, classés comme Th1 et Tc1, et ceux produisant d'IL-17A avec ou sans IFNγ, appelés Th17 et Tc17 [36]. Les voies moléculaires modulant la polarisation et la plasticité des lymphocytes n'ont pas été décryptées chez le bovin. De plus, la fonction d'autres membres de la famille des lymphocytes T ($CD3^+$) comme les lymphocytes double négatifs (DNT, $CD4^-$ et $CD8^-$), double positifs (DPT, $CD4^+$ et $CD8^+$) et les lymphocytes $TCR\gamma\delta^+$ restent peu connus.

Dans le cadre de mes recherches, j'envisage de m'adresser aux différentes étapes de la réponse immunitaire à médiation cellulaire, dans le but d'apporter une vision globale de ce processus qui comprend les bases de la présentation d'antigènes bactériens, les interactions entre les populations cellulaires impliquées et les mécanismes moléculaires entrainant l'activation et la polarisation des lymphocytes.

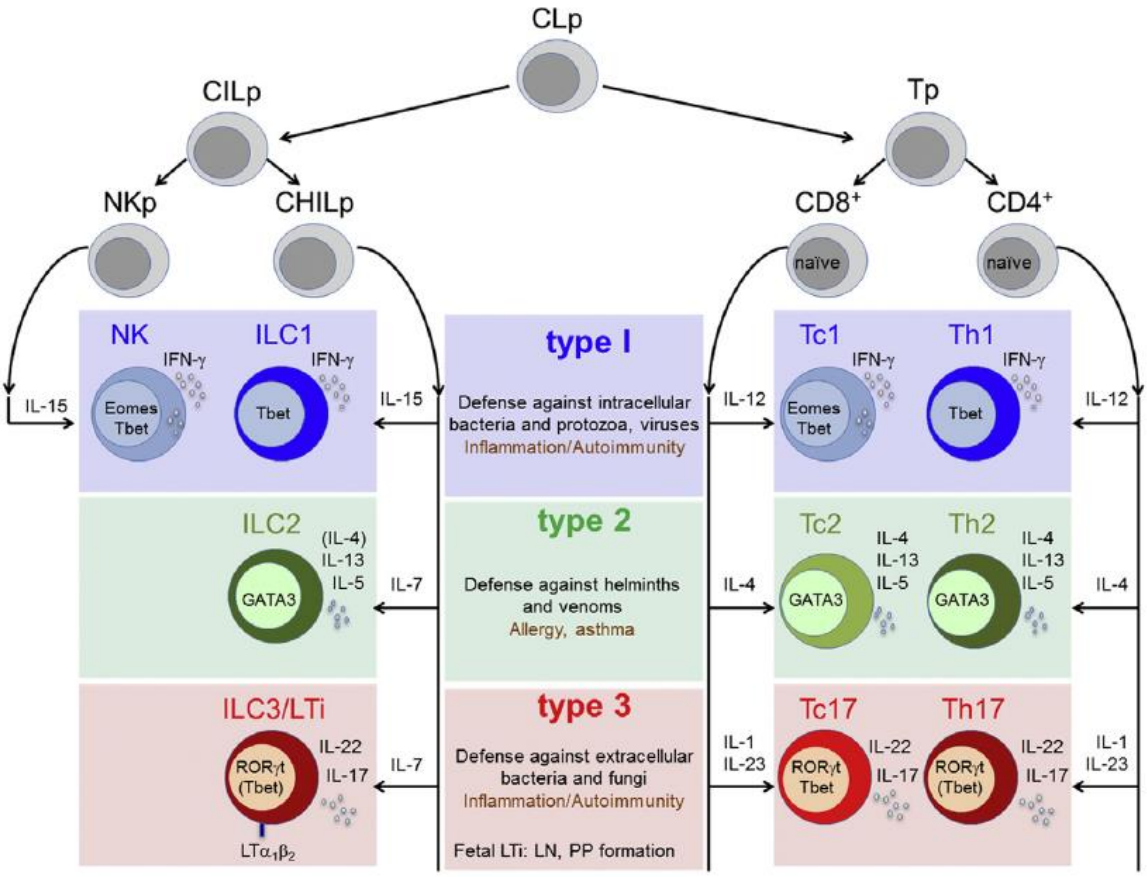

Figure 27 - Les trois types principales d'immunité à médiation cellulaire. L'immunité de type 1 est exécutée par les cellules T-bet$^+$ IFNγ$^+$ suivantes : Th1 (CD4$^+$), ILC1, Tc1 (CD8$^+$, Eomes$^+$) et NK (Eomes$^+$). L'immunité de type 2 est mise en place par des cellules GATA3$^+$ produisant de l'IL-4, IL-5 et IL13 : Th2 (CD4$^+$), ILC2, Tc2 (CD8$^+$). L'immunité de type 3 est assurée par des cellules RORγt$^+$ produisant de l'IL-17 et IL-22 : Th17 (CD4$^+$), ILC3, Tc17 (CD8$^+$). CLp : progéniteur lymphoide commun, CILp : progéniteur lymphoïde commun innée, LN : ganglion lymphatique, PP, plaques de Peyer, Tp, progéniteur des lymphocytes T. D'après Annunziato et al. [36].

3.4.1 Projet LymphoBov : étude de la polarisation et plasticité des lymphocytes T bovins

Les cellules Th17 modulent le recrutement de neutrophiles et la réponse pro-inflammatoire des barrières épithéliales. Notre équipe a mis en évidence que ces cellules jouent un rôle important dans la réponse immunitaire contre les mammites [37, 38]. Néanmoins, des nombreuses études rapportent que les lymphocytes Th17 sont peu abondants au niveau des sites d'inflammation *in vivo* à cause de leur plasticité élevée et de leurs mécanismes d'auto-régulation qui limitent leur expansion. Au cours de diverses

pathologies pro-inflammatoires, les cellules Th17 acquièrent la capacité de produire l'IFNγ, ce qui mène à leur orientation rapide vers le phénotype Th1. Ces cellules Th1 originaires de lymphocytes Th17 (Th1-non classiques) sont supposées être fonctionnellement différentes des Th1 et Th17, étant associées aux inflammations chroniques [39]. Les mécanismes déterminant la plasticité des lymphocytes Th17, ainsi que les différences entre les lymphocytes Th1 et Th1-non classiques restent peu compris et n'ont pas été étudiés chez les bovins.

La polarisation des lymphocytes T vers un phénotype de type 1 ou 3 est régulée par l'enchainement de modifications ayant lieu au niveau du transcriptome. Cependant, les connaissances de ce processus sont basées fondamentalement sur les observations chez la souris et, dans une moindre mesure, chez l'Homme [36]. L'activation de STAT-1 par l'IFNγ et de STAT-4 par l'IL12 sont critiques pour l'induction du facteur de transcription T-bet, le principal médiateur du développement des lymphocytes Th1. D'autre part, la stimulation des lymphocytes Th naïfs par l'IL-6 et TGFβ conduit à l'expression des facteurs de transcription STAT-3 et RORγt et détermine leur orientation vers le phénotype Th17 [40]. Des observations récentes ont mis en évidence l'existence de modifications chimiques post-transcriptionnelles dans les molécules d'ARNm, donnant naissance à un nouveau domaine d'étude nommé épitranscriptomique. En effet, la méthylation de l'adénosine pour former la N6-méthyladénosine (m6A) est la modification épitranscriptomique la plus abondante et joue un rôle majeur dans l'homéostasie et la fonction des cellules du système immunitaire [41]. Cependant, l'impact de cette modification sur la plasticité des lymphocytes Th17 n'a pas été étudiée.

Dans le cadre du projet LymphoBov, nous proposons ainsi d'analyser les modifications transcriptionnelles et post-transcriptionnelles déterminant le phénotype et la plasticité des lymphocytes T CD4$^+$. De plus, nous apporterons la première caractérisation des lymphocytes Th1 "non classiques" chez les bovins. Ce projet s'inscrit dans le cadre d'une collaboration avec l'UE-PAO (Département PHASE, Inra Nouzilly) pour l'obtention du matériel biologique nécessaire et est soutenu par le Département Santé Animale grâce au financement d'une bourse de M2 et d'un crédit accordé aux nouveaux arrivants.

Une approche mise en place par notre équipe [42] nous a permis d'isoler et de multiplier les lymphocytes impliqués dans les réponses de type 1 et 3. Ces lymphocytes ont ensuite été

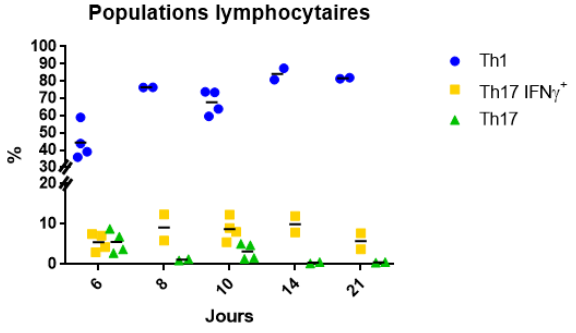

Figure 28 : **Analyse phénotypique des lymphocytes T par cytométrie en flux.** Les pourcentages de trois populations lymphocytaires : Th1, Th17 IFNγ+ et Th17 sont montrés au jours 6, 8, 10, 14 et 21. Les cellules de quatre vaches pour les jours 6 et 10 et de deux vaches pour les jours 8, 14 et 21 ont été analysées.

analysés pour la présence d'IL-17$^-$ IFNγ$^+$ à différents jours de culture après leur tri magnétique et un faible maintien du phénotype Th17 a été observé (**Figure 28**).

Pour mieux comprendre ces résultats, ces cellules ont été triés par cytométrie en flux afin d'isoler les populations d'intérêt et les remettre en culture. Cette stratégie a été répétée deux fois consécutives, dans le but de suivre l'évolution du phénotype des populations étudiées et d'obtenir les échantillons nécessaires pour les études transcriptomique et épitranscriptomique (**Figure 29A**). Nos résultats préliminaires indiquent que les lymphocytes bovins IL-17$^-$ IFNγ$^+$ sont capables de maintenir le phénotype Th1 au fil du temps, tandis que les cellules Th17 (IL-17$^+$ IFNγ$^-$) présentent une plasticité élevée et s'orientent vers le

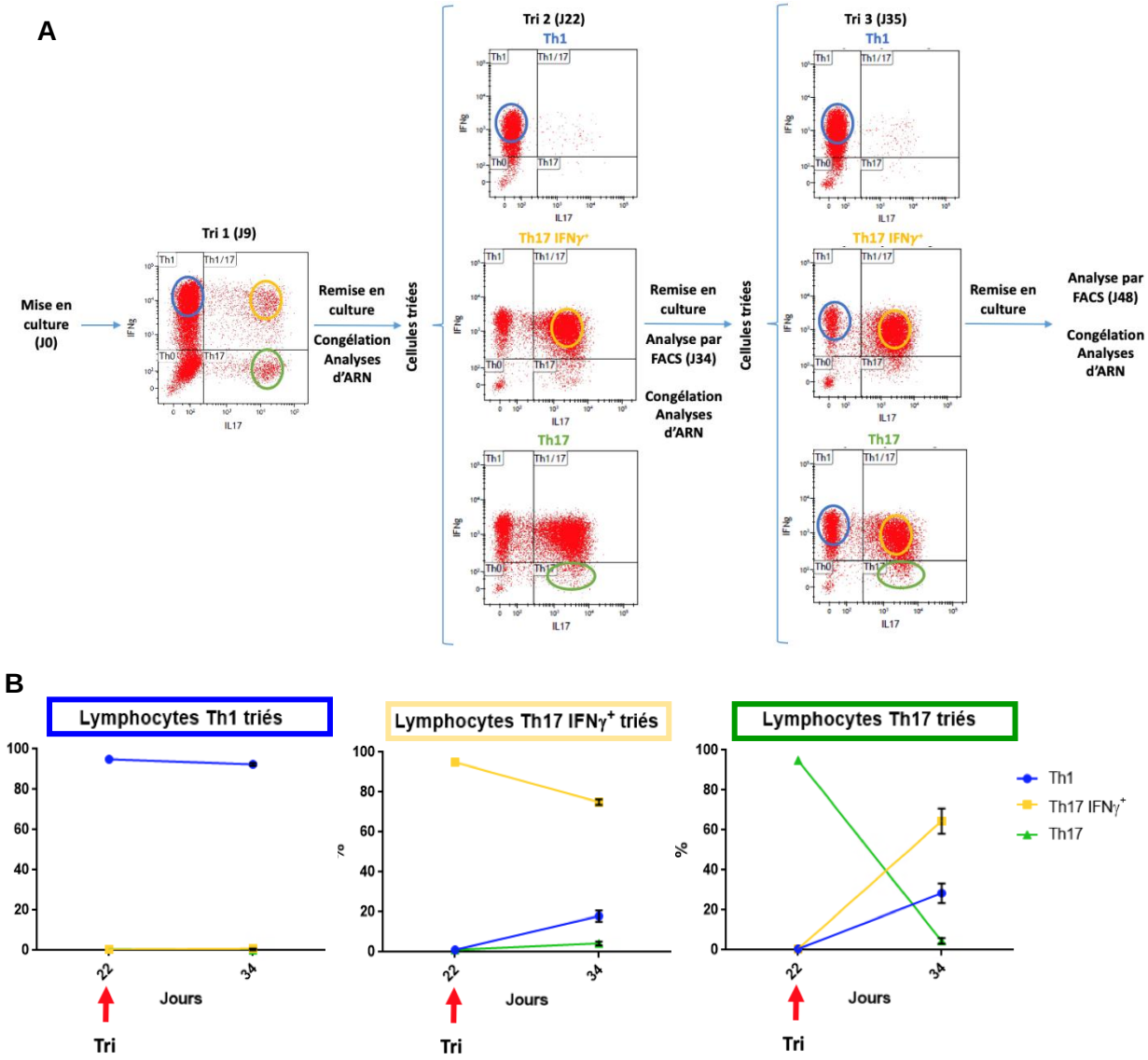

Figure 29 : Analyse et tri de populations lymphocytaires bovines par cytométrie en flux. **A :** Suite à leur isolement et expansion, les lymphocytes ont été triées aux jours 9, 22 et 35. Les cellules correspondant aux régions entourées ont été remises en culture puis retriées ou congelées pour des analyses ARN. **B :** Des lymphocytes triés à J22 ont été remis en culture et leur phénotype a été analysé par cytométrie en flux à J34. Les pourcentages de chaque population étudiée sont montrés. Après 12 jours d'incubation, les lymphocytes Th17 et Th17 IFNγ+ ont graduellement perdu la capacité de produire de l'IL-17, donnant naissance à une population strictement IFNγ+ (ex-Th17 ou Th1-non classiques). D'autre part, les cellules Th1 n'ont pas présenté une modification de leur phénotype. Cunha et al. *Manuscrit en préparation.*

phénotype Th1 (**Figure 29B-C**). A présent, nous mettons en place des analyses qui nous permettront de comprendre les bases moléculaires de ces observations.

Les résultats issus de ce projet nous permettront de mieux comprendre les mécanismes déterminant le phénotype et les fonctions des lymphocytes Th1 et Th17 bovins. Ces connaissances seront essentielles pour la mise en place de nouvelles approches centrées sur la stimulation de la réponse à médiation cellulaire comme piste de prévention des infections bactériennes, notamment par des nouvelles approches vaccinales.

3.4.2 Projet PAgBac : analyse de la présentation d'antigènes bactériens

Comme discuté précédemment, le CMH-I est requis pour la détection d'antigènes provenant de cellules tumorales ou infectées par des virus, mais également pour la "présentation croisée" (*cross-presentation*) de peptides d'origine exogène. Malgré l'abondance de données illustrant l'activation de la voie du CMH-I lors de nombreuses infections bactériennes, la présentation croisée d'antigènes bactériens a été peu étudiée chez les animaux de rente. Récemment, nous avons mis en place une analyse par cytométrie en flux qui nous a permis de détecter la prolifération de lymphocytes T cytotoxiques bovins induite par des cellules dendritiques dérivées de monocytes (moDC) infectées par *Staphylococcus aureus.*

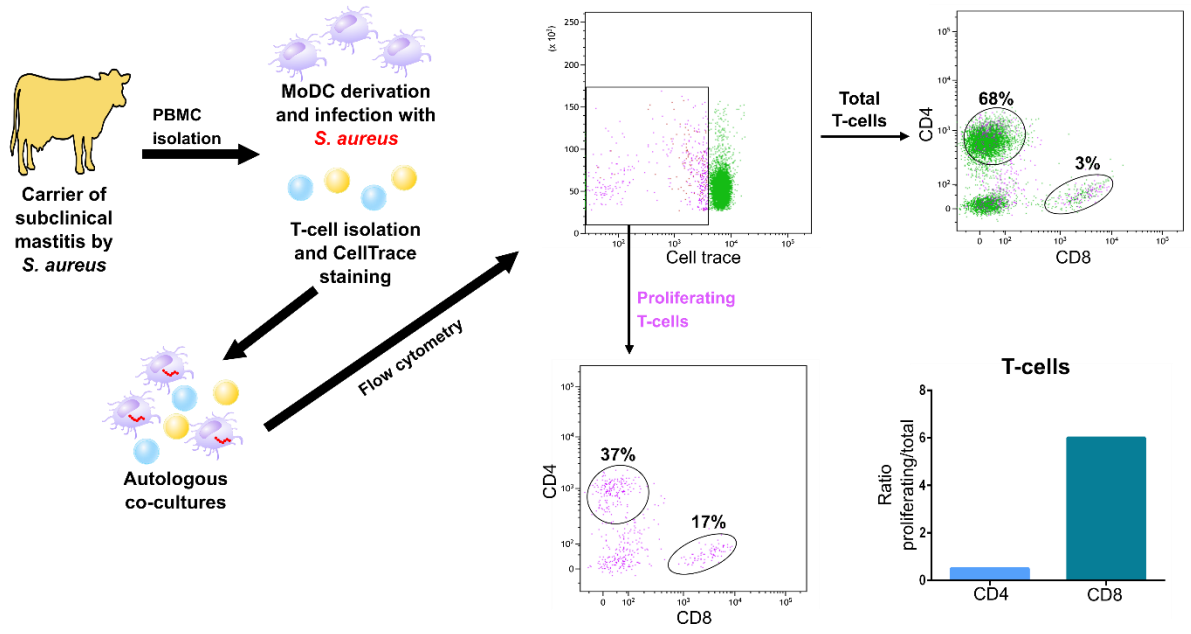

Figure 30 – Etude de la présentation d'antigènes de *Staphylococcus aureus* par cytométrie en flux. Des cellules mononuclées du sang (PBMC) d'un animal atteint de mammite à *S. aureus* ont été utilisées pour la production de cellules dendritiques dérivées du sang (moDC) et pour l'isolement de lymphocytes T. Les lymphocytes ont été marqués avec *Cell Trace* (CT) et mis en co-cultures autologues avec des moDC préalablement infectées avec *S. aureus.* La réponse lymphocytaire a été évaluée par cytométrie en flux selon la présence de marqueurs de surface et la perte du marquage (CT). L'infection par *S. aureus a* davantage stimulé les lymphocytes T $CD8^+$. *Données non publiées.*

Dans différentes infections, les cellules épithéliales sont la première barrière exposée aux pathogènes, certains étant capables de pénétrer ces cellules et d'y survivre à l'abri des anticorps et des cellules phagocytaires. La capacité des certains pathogènes à survivre dans le milieu intracellulaire est souvent évoquée comme un facteur clé dans l'apparition des infections persistantes. Ces infections limitent le contrôle de nombreuses maladies chez les animaux puisqu'elles facilitent la propagation furtive des pathogènes dans les troupeaux. Des cellules cytotoxiques ciblant les cellules épithéliales infectées pourraient contrecarrer ce phénomène d'échappement aux défenses immunitaires et contribuer à la guérison.

La cytotoxicité antigène-spécifique nécessite la présentation de peptides du pathogène en association avec le CMH-I à la surface de la cellule infectée. Cependant, la capacité des cellules épithéliales à présenter des antigènes reste méconnue, particulièrement chez les animaux d'élevage. Dans le cadre du projet PAgBac, j'envisage d'explorer la capacité des cellules épithéliales bovines à induire une réponse cytotoxique en activant les lymphocytes T $CD8^+$. Pour cela, un modèle *ex vivo* pour l'étude de la présentation croisée chez le bovin sera mis en place en collaboration avec Sébastien Holbert (ISP, équipe SPVB), en adaptant à cette espèce un système rapporteur murin (Kb-B3Z) amplement utilisé pour l'étude de la réponse antigène-spécifique via le CMH-I (**Figure 31**).

En effet, l'hybridome murin B3Z possède les mêmes activités qu'un lymphocyte T $CD8^+$, avec la particularité de reconnaitre spécifiquement le peptide rapporteur SIINFEKL de l'ovalbumine, présenté dans le contexte du CMH-1 murin (Kb). La fusion du peptide SIINFEKL à une protéine de n'importe quel pathogène permet ainsi l'étude de la présentation d'antigènes en utilisant les cellules B3Z, sans les inconvénients liés à la production de lymphocytes T $CD8^+$ spécifiques. Suite à leur activation, les cellules B3Z prolifèrent en sécrétant de l'IL2 dans le milieu. Étant donné que l'hybridome B3Z reconnait uniquement le CMH-I d'origine murine, l'expression de cette molécule sera induite chez une lignée épithéliale mammaire bovine par transfection transitoire. Les cellules transfectées seront infectées avec une souche d'un pathogène extracellulaire (*Escherichia coli*) exprimant le peptide SIINFEKL, transformée (invasive) ou pas (non-invasive) avec le gène *Rck* de *Salmonella,* qui confère la capacité de pénétrer dans les cellules épithéliales. Les cellules infectées seront ensuite co-incubées avec l'hybridome murin B3Z. La réponse spécifique des B3Z au peptide exprimé par les souches *d'E. coli* nous permettra de montrer la présentation croisée d'antigènes bactériens par des cellules épithéliales bovines. Comme contrôle, les mêmes expériences seront mises en place en parallèle avec des MoDCs. Cette stratégie expérimentale nous donnera la possibilité d'étudier les mécanismes fondamentaux de la présentation d'antigènes chez les animaux de rente suite aux infections par des différents pathogènes d'intérêt.

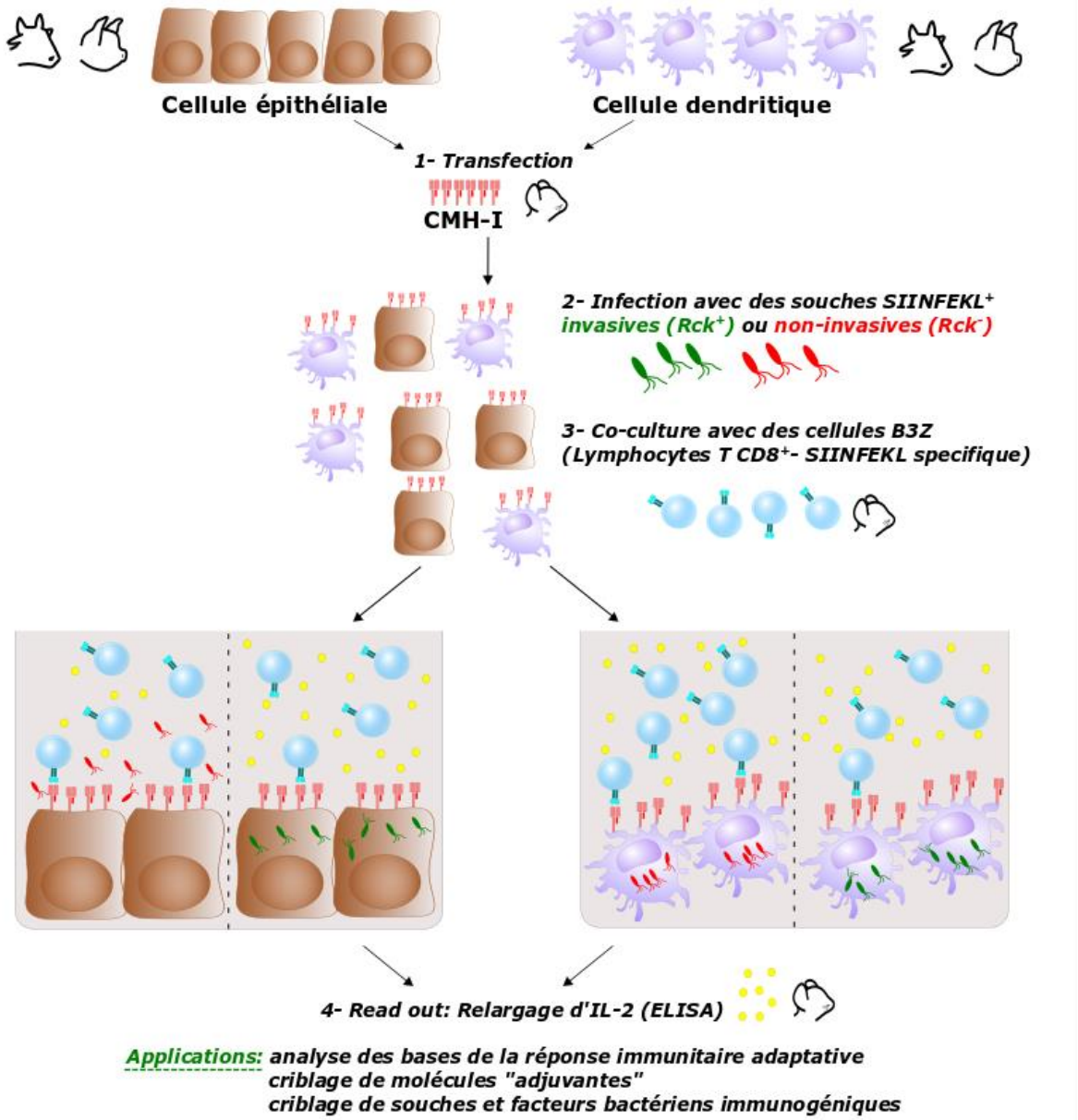

Figure 31 – Modèle *ex vivo* pour l'étude de la présentation croisée chez les animaux de rente. Cette approche pourra être utilisée pour étudier la mécanistique de la présentation de peptides antigéniques des bactéries et d'autres pathogènes par la voie du CMH-I. De plus, cette stratégie expérimentale pourra être appliquée au criblage de molécules chimiques, de facteurs d'un même pathogène ou de différents pathogènes interférant dans ce processus.

Plus concrètement, ce modèle sera développé et validé pour analyser l'influence du devenir de *Salmonella* Typhimurium dans la niche intracellulaire sur le déclenchement de la réponse immunitaire. Ensuite, nous envisageons la mise en place d'une plateforme pour le criblage de molécules, de souches et de facteurs microbiens stimulant la réponse cytotoxique, dans le but d'apporter des nouvelles cibles pour la lutte contre les infections persistantes. Nous croyons que ce projet nous permettra d'acquérir les compétences et les données préliminaires nécessaires à la mise en place des nouvelles approches pour l'analyse des réponses antigène-spécifiques nécessitant, pour ce faire, uniquement de cellules de nos espèces cibles.

3.4.3 Encadrement

Pendant l'année 2019/2020, j'ai eu l'opportunité de débuter mes activités d'encadrement chez ISP grâce au financement d'une bourse de M2 par le Département Santé Animale d'INRAE. Les travaux menés par Jennifer Bodin s'inscrivent dans le cadre du projet Lymphobov, présenté dans la section 3.4.1. Jennifer a manifesté son intérêt pour la carrière d'ingénieur d'études et a récemment décroché un CDD au sein de l'équipe AIM (INRAE Centre Val de Loire) en tant qu'assistant ingénieur.

Pour la suite, ma proposition de sujet de M2 pour l'année 2020/2021 a été validée et sera cofinancée par l'unité ISP. Ce sujet porte sur le développement d'un modèle *ex vivo* pour l'étude de la réponse des cellules de la glande mammaire aux infections bactériennes. J'envisage de proposer un sujet de thèse pendant le prochain appel de co-financement par le Département Santé Animal. Ce sujet s'adressera à la thématique et les objectifs de ma demande de financement ANR jeune chercheuses jeunes chercheurs (JCJC), récemment sélectionné pour la deuxième phase d'évaluation (Projet CelBoVax, AAPG 2020). Mes activités en tant qu'encadrant incluent également la direction des activités scientifiques de Patricia Cunha, technicienne de laboratoire au sein de l'équipe ISP.

3.4.4 Collaborations et participation à la vie de l'unité

Je collabore avec des collègues de différentes équipes de l'unité ISP, d'autres unités de l'Inra Centre Val de Loire et d'autres institutions pour la mise en place des projets décrits anterieurement et d'autres dans lesquels je suis impliqué en tant que responsable de *work-package.* Le projet Masticells, coordonné par Pierre Germon (IBIR-ISP, Inra), porte sur la caractérisation des cellules somatiques du lait impliquées dans la clairance bactérienne. Je suis co-responsable des work-packages centrés sur les interactions entre deux pathogènes majeurs de la glande mammaire et les macrophages et sur la mise au point d'un modèle murin de mammite. Le projet Animalt, coordonné par Sonia Lamandé (AIM-ISP, Inra), propose de nouveaux modèles d'étude *ex vivo* pour répondre aux questions scientifiques en lien avec l'alimentation ou l'infectiologie dans les tissus cibles de différents pathogènes des animaux de rente. Nous utiliserons des explants de mamelle comme alternative aux approches *in vivo* pour étudier la modulation de la réponse immunitaire innée et adaptative pendant un processus infectieux. De plus, je continue à collaborer avec les équipes qui m'ont accueilli pendant mon doctorat et mon post-doctorat (**Figure 32**).

En outre, je participe aux activités collectives de l'unité ISP en tant que membre du comité d'organisation du PhD day. Cet évènement a pour but de donner à nos doctorants une première opportunité de présenter leurs travaux dans le contexte d'une réunion scientifique organisée en anglais. Je contribue aussi au déroulement du Master 1 Sciences, Technologie et Santé de l'Université de Tours en tant que membre du jury de soutenances.

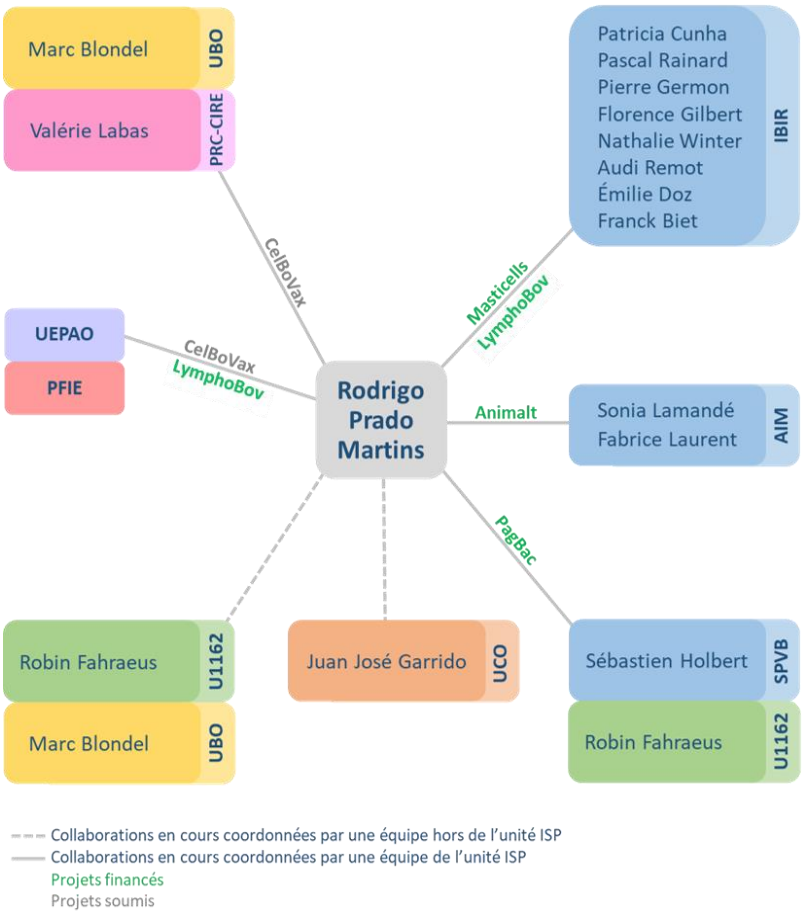

Figure 32 – Réseau de collaborations et projets en cours.

AIM : Apicomplexes et Immunité Mucosale, UMR ISP, INRAE Nouzilly.
IBIR : Infections Bactériennes et Immunité des Ruminants Inrae, UMR ISP, INRAE Nouzilly.
PFIE : Plateforme d'Infectiologie Expérimentale, , INRAE Nouzilly.
PRC-CIRE : Plateforme de Chirurgie et d'Imagerie pour la Recherche et l'Enseignement, UMR PRC, , INRAE Nouzilly.
SPVB : Signalisation, Portage et Virulence Bactérienne, UMR ISP, INRAE Nouzilly.
UBO : Université Bretagne Occidentale, Inserm, EFS - U1078. Brest.
UCO : Universidad de Córdoba, Équipe AGR231. Córboda, Espagne
UEPAO : Unité Expérimentale Physiologie Animale de l'Orfrasière. , INRAE Nouzilly.
U1162 – Université Paris 7, Inserm. Paris.

3.4.5 Perpectives

Récemment, j'ai soumis une lettre d'intention en réponse à l'appel à projets génériques 2020 de l'ANR, instrument Jeunes Chercheuses-Jeunes Chercheur (JCJC). **CelBoVax**, sélectionné pour l'étape 2 d'évaluation, a pour but de mettre en place une approche innovante pour la production de vaccins bovins de dernière génération. Comme preuve de concept, nous ciblerons *Staphylococcus aureus,* un pathogène majeur impliqué dans les infections intramammaires des vaches laitières. En utilisant une stratégie multidisciplinaire, ce projet abordera chaque étape de la production d'un vaccin prototype qui inclura : le développement et la sélection de vecteurs d'antigène, l'identification d'antigènes d'intérêt par des analyses protéomiques et *in silico* et la mise en place de stratégies simples et abordables pour l'analyse *in vivo* de l'activité des vaccins candidats (**Figure 33**). Le financement demandé pour ce projet est de 380 k€ et inclut le financement d'une bours de thèse. Son acceptation faciliterait mon évolution vers le statut de Directeur de recherche et une position de leadership dans le domaine de la vaccinologie vétérinaire.

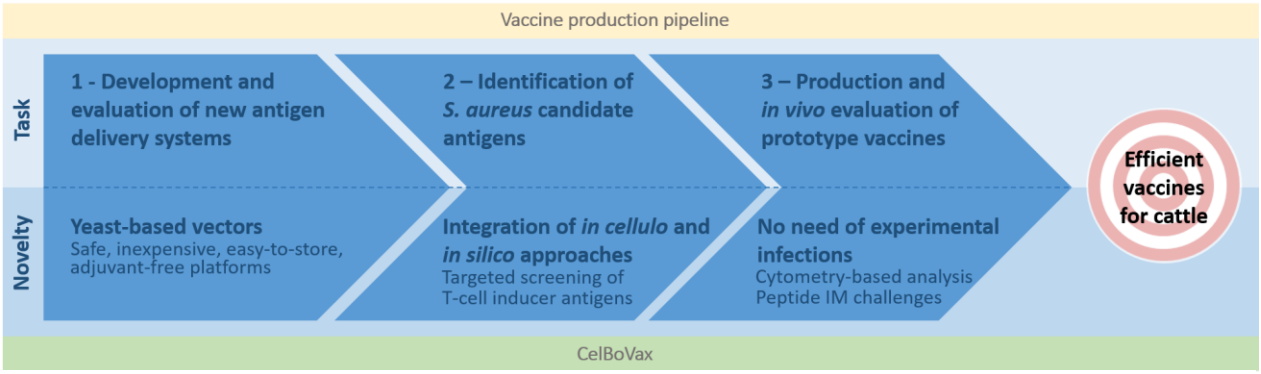

Figure 33 – Programme, objectifs et livrables de CelBoVax

J'envisage de mettre à profit les compétences et l'expérience acquises dans le cadre de mes différents projets pour développer des stratégies innovantes pour la prévention et le contrôle des infections bactériennes chez le bétail. Mon ambition est d'animer une équipe centrée sur ces enjeux pour contribuer à la mise en place de systèmes d'élevage durables (**Figure 34**).

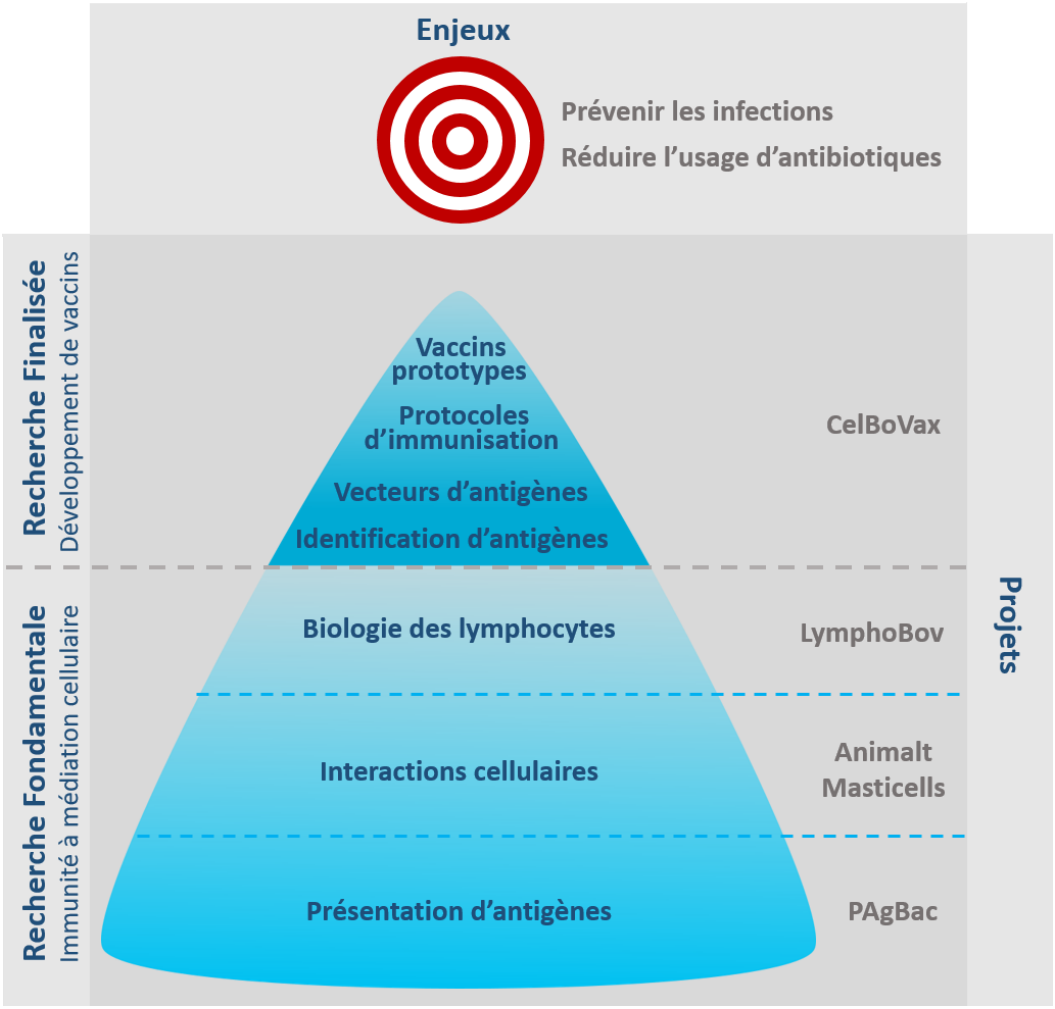

Figure 34 – Plan stratégique et enjeux de mon projet de recherche

4. Références

1. De Vliegher, S., et al., *Invited review: Mastitis in dairy heifers: nature of the disease, potential impact, prevention, and control.* J Dairy Sci, 2012. **95**(3): p. 1025-40 http://doi.org/10.3168/jds.2010-4074

2. Martins, R.P., Silva, JAG, Nakazato, L., Dutra, V., Almeida Filho, ES, *PREVALÊNCIA E ETIOLOGIA INFECCIOSA DA MASTITE BOVINA NA MICRORREGIÃO DE CUIABÁ, MT.* Ciencia Animal Brasileira, 2010. **11**(1): p. 181-187 http://doi.org/10.5216/cab.v11i1.5085

3. Caramori Júnior, J., Viana, C., Nakazato, L., Jardim, L., Martins, R. P., Oliveira Filho, J., Dutra, V., *Prevalência de lesões pulmonares características da infecção por Mycoplasma hyopneumoniae em suínos abatidos na Baixada Cuiabana*, in *Revista do Conselho Regional de Medicina Veterinária do Estado de Mato Grosso*. 2006. p. 29.

4. Martins, R.P., Cunha Neto, A. , *Detecção de vacas com mastite subclínica no rebanho de uma queijaria em Nossa Senhora do Livramento.*, in *Produtor Rural*. 2004: Brazil. p. 65-66.

5. Marques, M.R.H., Martins, R. P., Cunha Neto, A, *Ocorrência de Staphylococcus coagulase positiva em leite e queijo: identificação, perfil enzimático e biotipagem. .* Higiene Alimentar, 2006. **21**(140): p. 86-94,

6. Martins, R.P., Cunha Neto, A., Marques , M. , *Etiologia da mastite subclínica em vacas do rebanho de uma queijaria em Nossa Senhora do Livramento, MT.* Higiene Alimentar, , 2006(139): p. 104-110,

7. Martins, R.P., Nakazato, L., Dutra, V., Leite, D. S., *Analysis of virulence genes in Escherichia coli isolated from grated cheese. .* Food Science and Technology 2011. **31**(1): p. 106-108,

8. Martins, R.P., et al., *Prevalence of enterotoxigenic and Shiga toxin-producing Escherichia coli in pigs slaughtered in Mato Grosso, Brazil.* J Infect Dev Ctries, 2011. **5**(2): p. 123-7 http://doi.org/10.3855/jidc.1217

9. Martins, R.P., et al., *Preliminary virulence genotyping and phylogeny of Escherichia coli from the gut of pigs at slaughtering stage in Brazil.* Meat Sci, 2013. **93**(3): p. 437-40 http://doi.org/10.1016/j.meatsci.2012.10.007

10. Silva, M.C., Faria, G. S., Paula, D. A. J., Martins, R. P., Caramori Junior, J. G., Kich, J. D., Colodel, E. M., Nakazato, L., Dutra, V., *Prevalência de Salmonella sp. em suínos abatidos no Estado de Mato Grosso. .* Ciência Rural 2008. **39**(1): p. 266-268,

11. European Food Safety, A., P. European Centre for Disease, and Control, *The European Union One Health 2018 Zoonoses Report.* EFSA J, 2019. **17**(12): p. e05926 http://doi.org/10.2903/j.efsa.2019.5926

12. Boyen, F., et al., *Non-typhoidal Salmonella infections in pigs: a closer look at epidemiology, pathogenesis and control.* Vet Microbiol, 2008. **130**(1-2): p. 1-19 http://doi.org/10.1016/j.vetmic.2007.12.017

13. Baptista, F.M., et al., *Modelling food safety and economic consequences of surveillance and control strategies for Salmonella in pigs and pork.* Epidemiol Infect, 2011. **139**(5): p. 754-64 http://doi.org/10.1017/S0950268810001767

14. Tam, M.A., et al., *Early cellular responses to Salmonella infection: dendritic cells, monocytes, and more.* Immunol Rev, 2008. **225**: p. 140-62 http://doi.org/10.1111/j.1600-065X.2008.00679.x

15. Tsolis, R.M., et al., *How to become a top model: impact of animal experimentation on human Salmonella disease research.* Infect Immun, 2011. **79**(5): p. 1806-14 http://doi.org/10.1128/IAI.01369-10

16. Bearson, B.L. and S.M. Bearson, *Host specific differences alter the requirement for certain Salmonella genes during swine colonization.* Vet Microbiol, 2011. **150**(3-4): p. 215-9 http://doi.org/10.1016/j.vetmic.2010.12.026

17. Martins, R.P., et al., *Exploring the immune response of porcine mesenteric lymph nodes to Salmonella enterica serovar Typhimurium: an analysis of transcriptional changes, morphological alterations and pathogen burden.* Comp Immunol Microbiol Infect Dis, 2013. **36**(2): p. 149-60 http://doi.org/10.1016/j.cimid.2012.11.003

18. Martins, R.P., et al., *Proteomic analysis of porcine mesenteric lymph-nodes after Salmonella typhimurium infection.* J Proteomics, 2012. **75**(14): p. 4457-70 http://doi.org/10.1016/j.jprot.2012.03.045
19. Martins, R.P., et al., *Pyroptosis and adaptive immunity mechanisms are promptly engendered in mesenteric lymph-nodes during pig infections with Salmonella enterica serovar Typhimurium.* Vet Res, 2013. **44**: p. 120 http://doi.org/10.1186/1297-9716-44-120
20. Fink, S.L. and B.T. Cookson, *Apoptosis, pyroptosis, and necrosis: mechanistic description of dead and dying eukaryotic cells.* Infect Immun, 2005. **73**(4): p. 1907-16, http://www.ncbi.nlm.nih.gov/entrez/query.fcgi?cmd=Retrieve&db=PubMed&dopt=Citation&list_uids=15784530
21. Miao, E.A., et al., *Caspase-1-induced pyroptosis is an innate immune effector mechanism against intracellular bacteria.* Nat Immunol, 2010. **11**(12): p. 1136-42 http://doi.org/10.1038/ni.1960
22. Martins, R.P., et al., *Innate and adaptive immune mechanisms are effectively induced in ileal Peyer's patches of Salmonella typhimurium infected pigs.* Dev Comp Immunol, 2013. **41**(1): p. 100-4 http://doi.org/10.1016/j.dci.2013.04.020
23. Matsuno, K., et al., *The microstructure of secondary lymphoid organs that support immune cell trafficking.* Arch Histol Cytol, 2010. **73**(1): p. 1-21 http://doi.org/10.1679/aohc.73.1
24. Meurens, F., et al., *Early immune response following Salmonella enterica subspecies enterica serovar Typhimurium infection in porcine jejunal gut loops.* Vet Res, 2009. **40**(1): p. 5 http://doi.org/10.1051/vetres:2008043
25. Morel, C., et al., *Mycobacterium bovis BCG-infected neutrophils and dendritic cells cooperate to induce specific T cell responses in humans and mice.* Eur J Immunol, 2008. **38**(2): p. 437-47, http://www.ncbi.nlm.nih.gov/entrez/query.fcgi?cmd=Retrieve&db=PubMed&dopt=Citation&list_uids=18203135
26. Collado-Romero, M., et al., *An in vivo proteomic study of the interaction between Salmonella Typhimurium and porcine ileum mucosa.* J Proteomics, 2012. **75**(7): p. 2015-26 http://doi.org/10.1016/j.jprot.2012.01.001
27. Aguilar, C., et al., *Interaction between Campylobacter and intestinal epithelial cells leads to a different proinflammatory response in human and porcine host.* Vet Immunol Immunopathol, 2014. **162**(1-2): p. 14-23 http://doi.org/10.1016/j.vetimm.2014.09.003
28. Kobayashi, K.S. and P.J. van den Elsen, *NLRC5: a key regulator of MHC class I-dependent immune responses.* Nat Rev Immunol, 2012. **12**(12): p. 813-20 http://doi.org/10.1038/nri3339
29. Apcher, S., et al., *Major source of antigenic peptides for the MHC class I pathway is produced during the pioneer round of mRNA translation.* Proc Natl Acad Sci U S A, 2011. **108**(28): p. 11572-7 http://doi.org/10.1073/pnas.1104104108
30. Apcher, S., et al., *Translation of pre-spliced RNAs in the nuclear compartment generates peptides for the MHC class I pathway.* Proc Natl Acad Sci U S A, 2013. **110**(44): p. 17951-6 http://doi.org/10.1073/pnas.1309956110
31. Duvallet, E., M. Boulpicante, and S. Apcher, *[Synthesis of MHC class I antigenic peptides in the nucleus: a role for the nuclear translation at last?].* Med Sci (Paris), 2014. **30**(3): p. 229-31 http://doi.org/10.1051/medsci/20143003002
32. Yin, Y., B. Manoury, and R. Fahraeus, *Self-inhibition of synthesis and antigen presentation by Epstein-Barr virus-encoded EBNA1.* Science, 2003. **301**(5638): p. 1371-4 http://doi.org/10.1126/science.1088902
33. Lista, M.J., et al., *Nucleolin directly mediates Epstein-Barr virus immune evasion through binding to G-quadruplexes of EBNA1 mRNA.* Nat Commun, 2017. **8**: p. 16043 http://doi.org/10.1038/ncomms16043
34. Prado Martins, R., et al., *In Cellulo Protein-mRNA Interaction Assay to Determine the Action of G-Quadruplex-Binding Molecules.* Molecules, 2018. **23**(12) http://doi.org/10.3390/molecules23123124

35. Martins, R.P., et al., *Nuclear processing of nascent transcripts determines synthesis of full-length proteins and antigenic peptides.* Nucleic Acids Res, 2019. **47**(6): p. 3086-3100 http://doi.org/10.1093/nar/gky1296

36. Annunziato, F., C. Romagnani, and S. Romagnani, *The 3 major types of innate and adaptive cell-mediated effector immunity.* J Allergy Clin Immunol, 2015. **135**(3): p. 626-35 http://doi.org/10.1016/j.jaci.2014.11.001

37. Porcherie, A., et al., *IL-17A Is an Important Effector of the Immune Response of the Mammary Gland to Escherichia coli Infection.* J Immunol, 2016. **196**(2): p. 803-12 http://doi.org/10.4049/jimmunol.1500705

38. Roussel, P., et al., *Investigating the contribution of IL-17A and IL-17F to the host response during Escherichia coli mastitis.* Vet Res, 2015. **46**: p. 56,

39. Basdeo, S.A., et al., *Ex-Th17 (Nonclassical Th1) Cells Are Functionally Distinct from Classical Th1 and Th17 Cells and Are Not Constrained by Regulatory T Cells.* J Immunol, 2017. **198**(6): p. 2249-2259 http://doi.org/10.4049/jimmunol.1600737

40. Peck, A. and E.D. Mellins, *Plasticity of T-cell phenotype and function: the T helper type 17 example.* Immunology, 2010. **129**(2): p. 147-53 http://doi.org/10.1111/j.1365-2567.2009.03189.x

41. Li, H.B., et al., *m(6)A mRNA methylation controls T cell homeostasis by targeting the IL-7/STAT5/SOCS pathways.* Nature, 2017. **548**(7667): p. 338-342 http://doi.org/10.1038/nature23450

42. Cunha, P., et al., *Expansion, isolation and first characterization of bovine Th17 lymphocytes.* Sci Rep, 2019. **9**(1): p. 16115 http://doi.org/10.1038/s41598-019-52562-2

5. Annexes

5.1 Liste de publications et produits

5.1.1 Articles scientifiques

Articles à destination des communautés scientifiques validés par les pairs et publiés dans une revue à comité de lecture ou dans un entrepôt de documents en accès libre

- Depuis le recrutement en tant que CR

24- [Review article] Angrand, G., Quillévéré, Loaëc, Daskalogianni, C., Granzhan, A., Teulade-Fichou, Fahraeus, Martins, R. P., Blondel, M. (2019). Sneaking Out for Happy Hour: Yeast-Based Approaches to Explore and Modulate Immune Response and Immune Evasion. Genes, 10 (9), 22 p. , DOI : 10.3390/genes10090667 http://prodinra.inra.fr/record/482602 Auteur de correspondance, écriture du manuscrit, author de correspondence. Citations : 3

- Activé post-doctorale

23- [Research article] Bellido-Carreras, N., Argüello, H., Zaldívar-López, S., Jiménez-Marín, Á., Martins, R. P., Arce, C., Morera, L., Carvajal, A., Garrido, J. J. (2019). Salmonella Typhimurium Infection Along the Porcine Gastrointestinal Tract and Associated Lymphoid Tissues. Veterinary Pathology, 56 (5), 681-690. , DOI : 10.1177/0300985819843682 http://prodinra.inra.fr/record/479647 Conception et mise en place des expériences. Citations : 2

22- [Research article] Martins, R. P., Malbert-Colas, L., Lista, M. J., Daskalogianni, C., Apcher, S., Pla, M., Findakly, S., Blondel, M., Fåhraeus, R. (2019). Nuclear processing of nascent transcripts determines synthesis of full-length proteins and antigenic peptides. Nucleic Acids Research, 47 (6), 3086-3100. , DOI : 10.1093/nar/gky1296 http://prodinra.inra.fr/record/468442 Conception et mise en place des expériences, écriture du manuscrit. Citations : 10

21- [Research article] Reznichenko, O., Quillévéré, A., Martins, R. P., Loaëc, Kang, Lista, Beauvineau, González-García, Guillot, R., Voisset, Daskalogianni, Fåhraeus, Teulade-Fichou, M.-P., Blondel, M., Granzhan, A. (2019). Novel cationic bis(acylhydrazones) as modulators of Epstein–Barr virus immune evasion acting through disruption of interaction between nucleolin and G-quadruplexes of EBNA1 mRNA. European Journal of Medicinal Chemistry, 178, 13-29. , DOI : 10.1016/j.ejmech.2019.05.042 http://prodinra.inra.fr/record/479649 Conception et mise en place des expériences, écriture du manuscrit. Citations : 10

20- [Research article] Martins, R. P., Findakly, S., Daskalogianni, C., Teulade-Fichou, M.-P., Blondel, M., Fåhraeus, R. (2018). In cellulo protein-mRNA interaction assay to determine the action of G-quadruplex-binding molecules. Molecules, 23 (12), 1-11. , DOI :10.3390/molecules23123124 http://prodinra.inra.fr/record/468443 Conception et mise en place des expériences, écriture du manuscrit. Citations : 5

19- [Review article] Lista, M. J., Martins, R. P., Angrand, G., Quillévéré, A., Daskalogianni, C., Voisset, C., Teulade-Fichou, M.-P., Fåhraeus, R., Blondel, M. (2017). A yeast model for the mechanism of the Epstein-Barr virus immune evasion identifies a new therapeutic target to interfere with the virus stealthiness. Microbial Cell , 4 (9), 305-307. , DOI : 10.15698/mic2017.09.590 http://prodinra.inra.fr/record/468448 Écriture du manuscrit. Citations : 14

18- [Research article] Lista, M. J., Martins, R. P., Billant, O., Contesse, M.-A., Findakly, Pochard, Daskalogianni, Beauvineau, Guetta, Jamin, Teulade-Fichou, Fåhraeus, Voisset, Blondel, M. (2017). Nucleolin directly mediates Epstein-Barr virus immune evasion through

binding to G-quadruplexes of EBNA1 mRNA. Nature Communications, 8, 1-13. , DOI : 10.1038/ncomms16043 http://prodinra.inra.fr/record/468456 Conception et mise en place des expériences, écriture du manuscrit. Citations : 37

17- [Research article] López, I., Tournillon, A.-S., Martins, R. P., Karakostis, K., Malbert-Colas, L., Nylander, K., Fåhraeus, R. (2017). p53-mediated suppression of BiP triggers BIK-induced apoptosis during prolonged endoplasmic reticulum stress. Cell Death and Differentiation, 24 (10), 1717-1729. , DOI : 10.1038/cdd.2017.96 http://prodinra.inra.fr/record/468512 Conception et mise en place des expériences, écriture du manuscrit. Citations : 26

16- [Review article] Martins, R. P., Fåhraeus, R. (2017). A matter of maturity: The impact of pre-mRNA processing in gene expression and antigen presentation. International Journal of Biochemistry and Cell Biology, 91, 203-211. , DOI : 10.1016/j.biocel.2017.05.023 http://prodinra.inra.fr/record/468513 Auteur de correspondance, conception et mise en place des expériences, écriture du manuscrit. Citations : 2

15- [Review article] Apcher, S., Martins, R. P., Fåhraeus, R. (2016). The source of MHC class I presented peptides and its implications. Current Opinion in Immunology, 40, 117-122. , DOI : 10.1016/j.coi.2016.04.002 http://prodinra.inra.fr/record/468516 Écriture du manuscrit. Citations : 15

14- [Research article] Duvallet, E., Boulpicante, M., Yamazaki, T., Daskalogianni, C., Martins, R. p., Baconnais, S., Manoury, B., Fahraeus, R., Apcher, S. (2016). Exosome-driven transfer of tumor-associated Pioneer Translation Products (TA-PTPs) for the MHC class I cross-presentation pathway. Oncoimmunology, 5 (9), 1-16. , DOI : 10.1080/2162402X.2016.1198865 http://prodinra.inra.fr/record/468515 Conception et mise en place des expériences, écriture du manuscrit. Citations : 13

- Doctorat en Biosciences

13- [Research article] Aguilar, C., Jiménez-Marín, Á., Martins, R. P., Garrido, J. J. (2014). Interaction between Campylobacter and intestinal epithelial cells leads to a different proinflammatory response in human and porcine host. Veterinary Immunology and Immunopathology, 162 (1-2), 14-23. , DOI : 10.1016/j.vetimm.2014.09.003 http://prodinra.inra.fr/record/468517 Conception et mise en place des expériences, écriture du manuscrit. Citations : 11

12- [Research article] Martins, R. P., Collado-Romero, M., Arce, C., Lucena, C., Carvajal, A., Garrido, J. J. (2013). Exploring the immune response of porcine mesenteric lymph nodes to Salmonella enterica serovar Typhimurium: an analysis of transcriptional changes, morphological alterations and pathogen burden. Comparative Immunology, Microbiology and Infectious Diseases, 36 (2), 149-160. , DOI : 10.1016/j.cimid.2012.11.003 http://prodinra.inra.fr/record/468522 Conception et mise en place des expériences, écriture du manuscrit. Citations : 20

11- [Research article] Martins, R. P., Lorenzi, V., Arce, C., Lucena, C., Carvajal, A., Garrido, J. J. (2013). Innate and adaptive immune mechanisms are effectively induced in ileal Peyer's patches of Salmonella typhimurium infected pigs. Developmental and Comparative Immunology, 41 (1), 100-104. , DOI : 10.1016/j.dci.2013.04.020 http://prodinra.inra.fr/record/468519 Conception et mise en place des expériences, écriture du manuscrit. Citations : 11

10- [Research article] Martins, R. P., Aguilar, C., Graham, JE., Carvajal, A., Bautista, R., Claros, MG., Garrido, J. J. (2013). Pyroptosis and adaptive immunity mechanisms are promptly engendered in mesenteric lymph-nodes during pig infections with Salmonella enterica serovar Typhimurium. Veterinary Research, 44, 1-14. , DOI : 10.1186/1297-9716-44-120

http://prodinra.inra.fr/record/468518 Conception et mise en place des expériences, écriture du manuscrit. Citations : 18

09- [Research article] Collado-Romero, M., Martins, R. P., Arce, C., Moreno, Á., Lucena, C., Carvajal, A., Garrido, J. J. (2012). An in vivo proteomic study of the interaction between Salmonella Typhimurium and porcine ileum mucosa. Journal of Proteomics, 75 (7), 2015-2026. , DOI : 10.1016/j.jprot.2012.01.001 http://prodinra.inra.fr/record/468524 Conception et mise en place des expériences, écriture du manuscrit. Citations : 29

08- [Research article] Martins, R. P., Collado-Romero, M., Martínez-Gomáriz, M., Carvajal, A., Gil, C., Lucena, C., Moreno, Á., Garrido, J. J. (2012). Proteomic analysis of porcine mesenteric lymph-nodes after Salmonella typhimurium infection. Journal of Proteomics, 75 (14), 4457-4470. , DOI : 10.1016/j.jprot.2012.03.045 http://prodinra.inra.fr/record/468523 Conception et mise en place des expériences, écriture du manuscrit. Citations : 24

- Doctorat vétérinaire

07- [Research article] Martins, R. P., da Silva, M. C., Dutra, V., Nakazato, L., da Silva Leite, D. (2013). Preliminary virulence genotyping and phylogeny of Escherichia coli from the gut of pigs at slaughtering stage in Brazil. Meat Science, 93 (3), 437-440. , DOI : 10.1016/j.meatsci.2012.10.007 http://prodinra.inra.fr/record/468521 Auteur de correspondance, conception et mise en place des expériences, écriture du manuscrit, auteur de correspondance. Citations : 10

06- [Research article] Martins, R. P., Nakazato, L., Dutra, V., Leite, D. d. S. (2011). Analysis of virulence genes in Escherichia coli isolated from grated cheese. Food Science and Technology (Brésil), 31 (1), 106-108. , DOI : 10.1590/S0101-20612011000100014 http://prodinra.inra.fr/record/468525 Conception et mise en place des expériences, écriture du manuscrit. Citations : 4

05- [Research article] Martins, R. P., da Silva, M. C., Dutra, V., Nakazato, L., Leite, D. d. S. (2011). Prevalence of enterotoxigenic and Shiga toxin-producing Escherichia coli in pigs slaughtered in Mato Grosso, Brazil. Journal of Infection in Developing Countries, 5 (2), 123-126. , DOI : 10.3855/jidc.1217 http://prodinra.inra.fr/record/468526 Auteur de correspondance, conception et mise en place des expériences, écriture du manuscrit. Citations : 19

04- [Research article] Martins, R. P., Da Silva, J. A. G., Nakazato, L., Dutra, V., De Almeida Filho, E. S. (2010). Prevalencia e etiologia infecciosa de mastite bovina na microrregiao de Cuiaba-MT. Ciencia Animal Brasileira, 11 (1), 181-187. http://prodinra.inra.fr/record/468528 Auteur de correspondance, conception et mise en place des expériences, écriture du manuscrit. Citations : 47

03- [Short article] Silva, M. C. d., Faria, G. S., Paula, D. A. J. d., Martins, R. P., Caramori Junior, J. G., Kich, J. D., Colodel, E. M., Nakazato, L., Dutra, V. (2008). Prevalência de Salmonella sp. em suínos abatidos no Estado de Mato Grosso. Ciência Rural, 39 (1), 266-268. http://prodinra.inra.fr/record/468529 Conception et mise en place des expériences, écriture du manuscrit. Citations : 25

02- [Research article] Marques, M. R. H., Martins, R. P., Cunha Neto, A. (2006). Ocorrência de Staphylococcus coagulase positiva em leite e queijo: identificação, perfil enzimático e biotipagem. Higiene Alimentar, 21 (140), 86-94. http://prodinra.inra.fr/record/468530 Conception et mise en place des expériences, écriture du manuscrit. Citations : 8

01- [Research article] Martins, R. P., Cunha Neto, A., Marques , M. (2006). Etiologia da mastite subclínica em vacas do rebanho de uma queijaria em Nossa Senhora do Livramento, MT.

Higiene Alimentar, 20 (139), 104-110. http://prodinra.inra.fr/record/468533 Auteur de correspondance, conception et mise en place des expériences, écriture du manuscrit. Citations : 6

5.1.2 Produits, documents et publications destinés à des utilisateurs de la recherche

5.1.2.1 Brevets

- Activé post-doctorale

01- Martins, R. P., Fahraeus, R., Daskalogianni, C., Teulade-Fichou, M.-P., Granzhan, A., Reznichenko, O., Voisset, C., Lista, M. J., Quillévéré , A., Blondel, M. (2018). Novel hydrazone derivatives for preventing or treating EBV-related cancers (Brevet N° 18305392.5 – 1110). http://prodinra.inra.fr/record/468592

5.1.2.2 Articles dans des revues à visées professionnelles ou techniques

- Doctorat vétérinaire

02- [Short article] Caramori Júnior, J., Viana, C., Nakazato, L., Jardim, L., Martins, R. P., Oliveira Filho, J., Dutra, V. (2006). Prevalência de lesões pulmonares características da infecção por Mycoplasma hyopneumoniae em suínos abatidos na Baixada Cuiabana . Revista do Conselho Regional de Medicina Veterinária do Estado de Mato Grosso, 38, 29. http://prodinra.inra.fr/record/479774

01- [Short article] Martins, R. P., Cunha Neto, A. (2004). Detecção de vacas com mastite subclínica no rebanho de uma queijaria em Nossa Senhora do Livramento. Produtor Rural, 137, 65-66. http://prodinra.inra.fr/record/479775

5.1.3 Ouvrages, chapitres d'ouvrages, rapports diplômants

5.1.3.1 Chapitres d’ouvrages

- Depuis le recrutement en tant que CR

01- [Book chapter] Granzhan, A., Martins R.P., Fåhraeus, R., Blondel, M. (Auteur de correspondance), Teulade-Fichou, M-P. (Auteur de correspondance) (2020). Quadruplex-interacting compounds for regulating the translation of the Epstein–Barr virus nuclear antigen 1 (EBNA1) mRNA: A new strategy to prevent and treat EBV-related cancers. Annual Reports in Medicinal Chemistry. *In press.* DOI : 10.1016/bs.armc.2020.05.001

5.1.3.2 Thèse

01- Martins, R. P. (2013). Swine immune response to Salmonella enterica serovar Typhimurium. A functional genomics approach (Thèse de doctorat, Universidad de Córdoba (Cordoba), ESP). 230 http://prodinra.inra.fr/record/468534

5.1.4 Communications à des congrès et colloques

5.1.4.1 Communications invitées

- Activé post-doctorale

03- [Présentation orale] Martins, R. P. (2018). Production of antigenic peptides for the MHC-I pathway is tightly regulated by the mRNA maturation process. Presented at 8. Jornadas de divulgación de la investigación en Biología Molecular, Celular Genética y Biotecnología. Cordoue, Cordoue, ESP. http://prodinra.inra.fr/record/468582

- Doctorat en Biosciences

02- [Présentation orale] Martins, R. P. (Auteur de correspondance), Santiago, R. B., Moreno, A., Garrido-Pavon, J. J., Nally, J. E. (2013). Detection of Salmonella antigens expressed in swine gut by Hydrophobic Antigen Tissue Triton Extraction (HATTREX). In: Farm animal proteomics 2013 : Proceedings of the 4th Management Committee Meeting and 3rd Meeting of Working Groups 1, 2 & 3 of COST Action FA1002 (p. 116-119). Kosice, SVK (2013-04-25 - 2013-04-26). http://prodinra.inra.fr/record/468586

01- [Présentation orale] Martins, R. P. (Auteur de correspondance), Collado-Romero, M., Arce , C., Garrido-Pavon, J. J. (2011). Aplicación de la genómica funcional al estudio de la respuesta intestinal porcina frente a la infección por *Salmonella enterica* serovar Typhimurium. Presented at La investigación en Veterinaria y Ciencia y Tecnología de Alimentos, Cordoue, ESP (2011-11-07 - 2011-11-11). http://prodinra.inra.fr/record/468590

5.1.4.2 Communications avec actes

- Activé post-doctorale

09- [Présentation orale] Martins, R. P. (Auteur de correspondance), Fahraeus, R. (2016). Pre-mRNA events decide translation initiation efficacy. International Journal of Biochemistry and Cell Biology, 91, part B. Presented at 1st International Caparica Conference in Splicing, Caparica, PRT (2016-09-12 - 2016-09-14). http://prodinra.inra.fr/record/468583

- Doctorat en Biosciences

08- [Poster] Martins, R. P., Lorenzi, V., Lucena, C., Claros, M. G., Bautista, R., Garrido-Pavon, J. J. (2012). Laser capture microdissection coupled to microarray analysis to explore the transcriptomic response of porcine Peyer's patches to Salmonella Typhimurium. Presented at 4. European Veterinary Immunology Workshop (EVIW), Edinburgh, GBR (2012-09-02 - 2012-09-05). http://prodinra.inra.fr/record/468593

07- [Présentation orale] Martins, R. P., Moreno, A., Bautista, R., Claros, M. G., Carvajal, A., Garrido-Pavon, J. J. (Auteur de correspondance) (2012). Conjunctive analysis of genomics and proteomics data: an innovative approach to screen targets for the genetic improvement of resistance to salmonellosis in pigs. In: XVI Reunión de Mejora Genética Animal (p. 6 p). Presented at 16. Reunión de Mejora Genética Animal, Menorca, ESP (2012-05-31 - 2012-06-02). http://prodinra.inra.fr/record/468587

06- [Poster] Martins, R. P. (Auteur de correspondance), Collado-Romero, M., Arce, C., Bautista, R., Claros, M. G., Carvajal, A., Garrido, J. J. (2011). Respuesta transcripcional de nódulos linfáticos mesentéricos porcinos a la infección con Salmonella enterica serovar Typhimurium . Presented at 38. Congreso de la Sociedad Española de Genética, Murcia, ESP (2011-09-21 - 2011-09-23). http://prodinra.inra.fr/record/468594

05- [Présentation orale] Martins, R. P., Martinez-Gomariz, M., Gutierrez, M., Carvajal, A., Garrido-Pavon, J. J. (Auteur de correspondance) (2011). Proteome analysis of porcine mesenteric lymph-nodes after Salmonella Typhimurium infection. In: Farm Animal Proteomics. Presented at COST-Farm Animal Proteomics Spring Meeting, Glasgow, GBR (2011-03-31 - 2011-04-01). GBR : Almeida, A.M. ; McLaughlin, M. ; Eckersall D. http://prodinra.inra.fr/record/468589

04- [Poster] Martins, R. P., Collado-Romero, M., Arce, C., Garrido, J. J. (2010). Transcriptional profiling of porcine mesenteric lymph-nodes from an experimental infection with Salmonella Typhimurium: a time course analysis. Presented at International Symposium on Animal Genomics for Animal Health (AGAH 2010), Paris, FRA (2010-05-31 - 2010-06-02). http://prodinra.inra.fr/record/468595

03- [Short paper] Martins, R. P. (Présentateur), Collado-Romero, M., Arce, C., Garrido-Pavon, J. J. (2010). Pathogen load and expression of immune-related genes in mesenteric lymph-nodes of pigs experimentally infected with Salmonella typhimurium. New Biotechnology, 27 (supplément 1). Presented at 4. ESF Conference on Functional Genomics and Disease, Dresden, DEU (2010-04-14 - 2010-04-17). 1p, DOI : 10.1016/j.nbt.2010.01.077 http://prodinra.inra.fr/record/468536

02- [Présentation orale] Martins, R. P., Garrido-Pavon, J. J. (2009). Caracterización genómica de la respuesta inmune de nódulos linfáticos mesentéricos porcinos a la infección con Salmonella Typhimurium. In: I Congreso Científico de Investigadores en Formación (p. 40-42). Presented at 1. Congreso Científico de Investigadores en Formación, Cordoue, ESP (2009-10-15 - 2009-10-16). Cordoba, ESP : Universidad de Cordoba. http://prodinra.inra.fr/record/468591

01- [Poster] Martins, R. P., Collado-Romero, M., Arce, C., Garrido, J. J. (2009). Analysis of the mesenteric lymph nodes and intestinal mucosa immune response to an experimental infection with Salmonella typhimurium in pigs. Presented at 3rd ASM Conference on Salmonella: Biology, Pathogenesis & Prevention, Aix-en-Provence, FRA (2009-10-05 - 2009-10-09). http://prodinra.inra.fr/record/468596

5.2 Liste de contrats de recherche

5.2.1 Acceptés

2. UMR ISP, INRAE, Nouzilly (France). Étude de la polarisation et plasticité des lymphocytes bovins. Financement Jeune Chercheur, Département Santé Animale, INRAE, France. Coordinateur, depuis 01/2020. 10 k€.

1. UMR ISP, INRAE, Nouzilly (France). Présentation croisée d'antigènes : une nouvelle piste pour lutter contre les infections bactériennes persistantes – PagBac. Crédit à projets collaboratifs, UMR ISP, INRAE, France. Coordinateur, depuis 10/2019. 15 k€.

5.2.2 Soumis

1. UMR ISP, INRAE, Nouzilly (France). CelBoVax: Novel comprehensive approach to shape cattle cell-mediated immunity. Financement ANR Jeune Chercheuse Jeune Chercheur, France. 2020. Coordinateur, sélectionné pour l'étape 2 d'évaluation. 380 k€.

5.3 Responsabilités collectives

5.3.1 Encadrement

UMR ISP, INRAE

9 – Patricia CUNHA, Technicienne de laboratoire, UMR ISP, INRAE, Nouzilly. Depuis 01/2020

8 - Jennifer BODIN, Étudiante de M2 (stage) – Université de Tours, Nouzilly. 01-06/2020

UMR1162, Inserm

7- Petter BROHAGEN, Étudiant de Médecine (stage) - Linkoping University, Suède. 09-12/2018

6 - Natividad BELLIDO, Doctorante (mission) - Université de Cordoue, Espagne. 11/2018

5 - Maria do Rosario CAMPOS FERNANDES, Doctorante (stage) - UNL, Portugal. 06/2018

4 - Aikaterini THERMOU, Programme Erasmus (stage) - University of Patras, Grèce. 12/2017 – 05/2018

3 - María José LISTA, Doctorante (mission) - Inserm UMR1078, Brest. 10-12/2015 et 07-08/2016

2 - Alicia QUILLÉVÉRÉ, IE (mission) - Inserm UMR1078, Brest. 10-11/2017 et 11/2018

1 - Laurence MALBERT-COLAS, IE - Inserm UMR1162, Paris. 01/2016 – 12/2018

5.3.2 Co-encadrement

UMR1162, Inserm

4 - Ewa SROKA, Doctorante - University of Gdansk, Pologne. 10/2017 – 12/2018

3 - Iolanda ALVES, Doctorante - University of Gdansk, Pologne. 10/2017 – 12/2018

2 - Alice ZHENG, Doctorante - Université Paris Diderot, Paris. 10/2017 – 12/2018

1 - Maria Camila TOVAR, Étudiante en M2 - Université Paris Descartes, Paris. 01-06/2018

5.4 Participation aux jurys et comités

5.4.1 Master 1 – Sciences, technologie et santé, Université de Tours

4 – Aicha DEMBELE, promotion 2019/2020

3 – Fouad LAHMER, promotion 2019/2020

2 – Lise GODRY, promotion 2019/2020

1 – Eglantine SIRET, promotion 2018/2019

5.4.2 Comités de suivi de thèses

4 – Ronan LE SENECHAL, 1ère année, dirigé par Pr. Marc Blondel, Université Bretagne Loire. Brest, 2020.

3 – Maria Camila TOVAR, 2ème année, dirigée par Dr. Robin Fahraeus, Université de Paris. Paris, 2020.

2 – Maria Camila TOVAR, 1ère année, dirigée par Dr. Robin Fahraeus, Université de Paris. Paris, 2019.

1 – Justine HABAULT, 3ème année, dirigée par Dr. Jean-Luc Poyet, Université de Paris. Paris, 2019.

5.5 Résumés des publications

premières pages mises en ordre chronologique